Comparative study of the proteome of S. coelicolor M145 and S. lividans TK24, two phylogenetically closely related strains with very different abilities to accumulate TAG and produce antibiotics

Aarón Millán Oropeza

NNT : 2017SACLS160

THESE DE DOCTORAT
DE
L'UNIVERSITE PARIS-SACLAY
PREPAREE A
L'UNIVERSITE PARIS-SUD

ECOLE DOCTORALE N° 581
Agriculture, alimentation, biologie, environnement et santé (ABIES)

Spécialité de doctorat : Microbiologie

Par

M. Aarón Millán Oropeza

Comparative study of the proteome of *S. coelicolor* M145 and *S. lividans* TK24, two phylogenetically closely related strains with very different abilities to accumulate TAG and produce antibiotics

Thèse présentée et soutenue à Orsay, le 23 juin 2017 :

Composition du Jury :

Mme Fabienne Malagnac	Prof. Université Paris-Saclay	Présidente
M. Sébastien Rigali	Prof. Université de Liège	Rapporteur
M. Bertrand Aigle	Prof. Université de Lorraine	Rapporteur
Mme Warren Albertin	MCF. ENSCP de Bordeaux	Examinatrice
M. Ivan Mijakovic	Prof. Chalmers University of Technology	Examinateur
Mme Marie-Jöelle Virolle	DR. Université Paris-Saclay	Directrice de thèse
Mme Céline Henry	IE. Université Paris-Saclay- INRA	Co-encadrante de thèse

Dedicated to our little angel Ian

ACKNOWLEDGMENTS

Je tiens à remercier à la France pour m'avoir accueilli pendant ma formation Doctorale dans un environnement international et unique, c'était une toute première expérience à l'étranger très enrichissante. Également je remercie à CONACyT et à l'Ambassade de France au Mexique pour le support économique tout au long de mes études à l'Université Paris-Sud.

J'exprime ma gratitude aux membres du jury qui m'ont fait l'honneur de juger ce travail de thèse ainsi pour les échanges très enrichissantes lors de ma soutenance que je n'oublierai jamais.

Je suis très reconnaissant à ma directrice de thèse Marie-Jöelle Virolle pour m'avoir accueilli dans son laboratoire de recherche. Cette opportunité m'a permis d'apprendre beaucoup des choses du milieu professionnel et surtout du développement personnel. Je vous remercie pour vos recommandations, votre soutien pendant la thèse et votre passion pour les *Streptomyces*.

Un grand merci à ma co-encadrante de thèse Céline Henry pour sa gentillesse, complicité et soutien tout au long de mon séjour en France. Les expériences vécues dans les réunions, formations et congrès ont été des apprentissages significatifs pour mon projet professionnel et personnel. Merci Céline pour être une formidable encadrante et une excellente personne.

C'était un grand plaisir de travailler en collaboration avec les tous les gens de PAPPSO et du bâtiment 526, une expérience exceptionnelle au niveau scientifique, technique et culturel. Merci beaucoup! Spécialement à Mélisande Blein-Nicolas pour m'avoir encouragé et formé au monde de la bio-informatique où je suis toujours motivé.

Je remercie à mes collègues du laboratoire pour les moments vécus ensemble. À Michelle pour m'avoir formé à la manipulation des *Streptomyces* et aussi pour ta gentillesse et support inconditionnel. À Marc pour les conseils pragmatiques dans les situations les plus invraisemblables au labo. À Clara pour avoir toujours un sourire et une histoire drôle à raconter, Euro2016 inclus. Également, je remercie aux autres

membres qui ont fait partie du groupe MES : Anthony, Chlöe, Maxime, Ahmed, Imen, Ines, Catherine, Esma, Jade, Benjamin, Marc-Antoine et Morgane. C'était un plaisir de travailler à côte de vous. Également, je remercie aux voisins du couloir pour son agréable compagnie jour après jour et pour les *afterworks* « Picon-bière ». Merci à Jean-Luc, Sylvie, Armel, Emmanuelle, Soumaya, Laura, Luisa, Laetitia, Sylvain, Florence, Jerzy, Drago, Mathieu, Mauro, Babil, Brittany, Céline, Antoine et Christiane.

Je remercie également aux gens du LCP, du LETIAM pour son agréable compagnie et collaboration pendant une partie importante de ma thèse. Merci énormément Jean Bleton pour ton soutien et ton aide, tu es un chercheur et une personne formidable. Merci à Fathi, Naira, Philippe, Aurélien, Sanaz, Doura, Marine, Myriam, Ariane, Alex et Rolando. Grâce à cette collaboration j'ai trouvé des personnes très importantes pour moi.

Thanks to my good friends Rolando and Nga for the great moments spent together including running to catch a night bus in the middle of Palaiseau or falling from the "easier" and scarier ski station ;-P

Muito obrigado ao meu amor, à minha paixão, Diana, pelos momentos juntos nesta etapa profissional e pessoal. Estou muito contente de ter tido a sorte de conhecer o urso mais jeitoso e lindíssimo do mundo... Nossa!

Gracias especiales al club de los "sabrosos" Leticia, Marta, Karen, Adriana, Nicolas, Edgar, David, Elodie, Proxy, Romain, Antoine y Robin por las noches en Paris que hicieron mi estancia más feliz.

Muchas gracias a Abuelo, Alan, Pakún, J-Lu, Pablo, Pam, Angie y Sr. Tavo por llenar de memes mi móvil y de alegría mis tardes.

Gracias a mi linda familia por apoyarme en todas mis decisiones así como en ésta etapa de mi vida. Los amo mamá, papá, Emi, Maga, Geraldine e Ian.

TABLE OF CONTENTS

LIST OF FIGURES

LIST OF TABLES

LIST OF ABBREVIATIONS

1,3PG:	1,3-bisphosphoglycerate
2PG:	2-phosphoglycerate
3PG:	3-phosphoglycerate
6PGL:	6-phosphoglucono-lactone
αKG:	α-ketoglutarate
ACC:	Acetyl-CoA Carboxylase
ACN:	Acetonitrile
ACP:	Acyl Carrier Protein
ACT:	Actinorhodin
AGPAT:	1-acylglycerol–3-phosphate acyltransferase
ANOVA:	Analysis of variance
AT:	Acyltransferase
ATBH:	Aminotrihydroxybacteriohopane
ATR:	Attenuated Total Reflection
BSA:	Bovine serum albumin
CCR:	Carbon Catabolite Repression
CIT:	Citrate
CDA:	Calcium-Dependent Antibiotics
CDI:	Collision-induced dissociation
CRP:	Cyclic AMP receptor protein
CSR:	Cluster-situated regulators
CPK:	Cryptic Polyketide Coelimycin P1
DAG:	Diacylglycerol
DGAT:	Diacylglycerol acyltransferase
DH:	Dehydratase
DHA:	Dihydroxyacetone
DHAP:	Dihydroxyacetone phosphate
DMAPP:	Dimethylallyl diphosphate
E4P:	Erythrose-4-phosphate
EI:	Electron ionization

emPAI	Exponentially modified Protein Abundance Index
ER:	Enoyl reductase
ESI:	Electrospray ionization
ETF:	Electron transfer flavoproteins
E-value	Expectation value
F1,6P:	Fructose-1,6-biphosphate
F6P:	Fructose-6-phosphate
FAME:	Fatty Acid Methyl Esters
FAS:	Fatty acid synthetase
FDR:	False discovery rate
FID:	Flame ionization detector
FTIR:	Fourier Transform Infrared
FUM:	Fumarate
G1P:	Glucose-1-phosphate
G6P:	Glucose-6-phosphate
GAP:	Glyceraldehyde-3-phosphate
GC-MS:	Gas Chromatography coupled to Mass Spectrometry
GDH:	Glutamate dehydrogenase
GL6P:	6-phosphogluconate
GlcP:	Glucose permeases
Glk:	Glucose kinase
GLM:	Generalized linear mixed model
Gly3P:	Glycerol-3-phosphate
GPAT:	Gly3P-acyltransferase
GS:	Glutamine synthetase
GOGAT:	Glutamate synthase
GXL:	Glyoxylate
HCD:	Higher-energy collisional dissociation
HILIC:	Hydrophilic interaction chromatography
HPr:	Histidine-containing protein
HS:	Hyperscore
iCIT:	Isocitrate
iTRAQ:	Isobaric Tag for Relative and Absolute Quantitation

IPP: Isoprenyl diphosphate

IR: Infrared

KR: Ketoreductase

KS: Ketosynthase

LC: Liquid Chromatography

LIT: Linear Ion Trap

MAL: Malate

MALDI: Matrix-Assisted Laser Desorption / Ionization

MDR: Multi-drug resistant

MRSA: Methicillin resistant *Staphylococcus aureus*

MS: Mass Spectrometry

NGS: Next-Generation Sequencing

NRP: Non-ribosomal peptides

NRPS: Non-ribosomal peptides synthetase

OAA: Oxaloacetate

ORF: Open read frame

P: Phosphate

PA: Phosphatidic acid

PAF: Protein Abundance Factor

PAP: Phosphatidic acid phosphatase

PCA: Principal component analysis

PCD: Programmed cell death

PCP: Peptidyl carrier protein

PEP: Phosphoenolpyruvate

Pi: Inorganic phosphate

Pfk: Phosphofructokinase

PK: Polyketides

PKS: Polyketide synthases

PL: Phospholipids

PLS: Partial least square

PolyP: Inorganic polyphosphate

ppb: Parts per billion

PPDK: Pyruvate phosphate dikinase

ppGpp: Guanosine pentaphosphate

PPK: Polyphosphate kinase

ppm: Parts per million

PPP: Pentose phosphate pathway

PTMs: Post-translational modifications

PTS: Phosphotransferase systems

Q: Quadrupole

R5P: Ribose-5-phosphate

RED: Undecylprodigiosin

RiPP: Ribosomally synthesized and Posttranslationally modified Peptides

RL5P: Ribulose-5-phosphate

ROS: Reactive oxygen specie

S7P: Sedoheptulose-7-phosphate

SAM: S-adenosylmethionine

SC: Spectral counting

SCX: Strong cation exchange

SDS-PAGE: Sodium Dodecyl Sulfate-Polyacrylamide Gel Electrophoresis

SEM: Standard error of the mean

SUC: Succinate

SucCoA: succinyl-CoA

TAG: Triacylglycerol

TCA: Tricarboxylic acid cycle

TE: Thioesterase

TEFA: Total esterified fatty acids

TFA: Trifluoroacetic acid

ToF: Time of flight

Tpi: Triosephosphate isomerase

UPS: Universal stress protein

VRSA: Vancomycin resistant *Staphylococcus aureus*

X5P: Xylulose-5-phosphate

XIC: Extracted Ion Current

INTRODUCTION

The beginning of the modern "antibiotic era" goes back in 1928, when Alexander Fleming (1881 – 1955), a Scottish biologist and botanist accidentally observed an inhibition halo of seed cultures of *Staphylococcus aureus* caused by a contaminant mold. This mold, eventually identified as *Penicillium notatum*, produced an active agent named penicillin and proved to be effective against Gram-positive bacteria such as *Staphylococcus* or *Streptococcus* that are causing of septicemia and scarlet fever, respectively. Later penicillin was isolated, produced at large-scale and used as a life-saver antibacterial compound during World War II (Hopwood, 2007; Demain and Sanchez, 2009).

However, penicillin was not effective against Gram-negative pathogenic bacteria like *Salmonella, Vibrio cholerae* or other bacteria responsible for urinary tract infections. This hurdle coupled with the start of World War II mobilized the research of new active compounds against disease-producing bacteria. One of the pioneers on this field was the Ukrainian-American microbiologist Selman Waksman (1888 – 1973), supervisor of the graduated studies of Albert Schatz that led to the discovery of an antibiotic produced by *Streptomyces griseus*: streptomycin (ACS, 2005), in 1943. Streptomycin was capable of killing gram-negative pathogens and tubercle bacillus without causing lethal or side-effects to humans. Eventually, streptomycin and penicillin were commercialized at large-scale by pharmaceutical companies during the 1940's (Woodruff, 1981). These successful breakthroughs also released the quest for new antibacterial compounds. Many antibiotics were identified between 1940 and 1960 in what is commonly known as the "golden age" of antibiotics discovery (Figure A).

Approximately two-thirds of all known antibiotics used in modern medicine are produced by Actinomycetes, from which the large majority are synthesized by the *Streptomyces* genus (Barka *et al.*, 2016). *Streptomyces* are saprophytic, soil-dwelling microorganisms with complex life cycle that play key roles in soil ecology due to their ability to scavenge nutrients and to hydrolyze a wide range of polysaccharides and other natural macromolecules (Chater *et al.*, 2010). The life cycle of *Streptomyces* starts with the germination of a spore that grows out to form a branched vegetative mycelium.

Then, under adverse conditions, such as nutrient depletion, an aerial mycelium arises from the vegetative mycelium. The tip ends of these aerial hyphae will then generate spores. Interestingly, antibiotics biosynthesis is usually concomitant to aerial mycelium development (Bibb, 2005; Chater *et al.*, 2010).

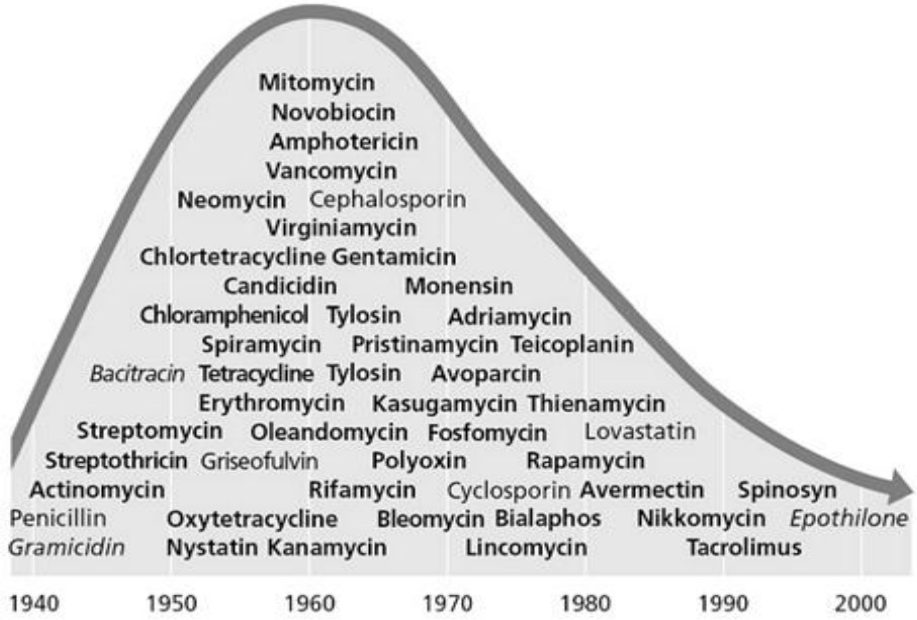

Figure A. Discovery of important antibiotics and other natural products over the years (Hopwood, 2007).
Bold type indicates Actinomycete products; normal type indicates fungal products; italic type indicates products from non-actinomycete bacteria.

After this ‘golden age’, scientific and economic situations changed. In the 1990’s the efficiency of the classical screening methods decreased and antibiotic resistance of pathogenic bacteria increased as a result of the extensive and uncontrolled use/consumption of antibiotics resulting in their spreading in the environment (Berdy, 2012). In the same decade, resistant gram positive bacteria emerged as a major health threats with methicillin (MRSA) and vancomycin (VRSA) resistant *Staphylococcus aureus*, penicillin resistant *Streptococcus pneumonia*, and multi-drug resistant (MDR) *Clostridium difficile* (Fair and Tor, 2014). In the United States, at least 2 million people become infected with bacteria that are resistant to antibiotics and at least 23,000 people die each year as a direct result of these infections (Center for Disease Control and Prevention, 2017). This reappearing of ‘old’ pathogens that became antibiotic-resistant could potentially bring us back to the pre-antibiotic era.

Fortunately, the research of novel bioactive natural products from actinobacteria re-emerged at the beginning of the 21st century with the sequencing of the genome of numerous *Streptomyces* species starting that of the historical model strain *Streptomyces coelicolor* (Bentley *et al.*, 2002). *In silico* analysis of *S. coelicolor* (Challis and Hopwood, 2003), revealed that this strain contains pathways directing the biosynthesis of more than 20 secondary metabolites whereas only four were previously identified. This clearly evidenced that the metabolic potential of *Streptomyces*, and actinobacteria in general, was largely underestimated and that they possess a cryptic potential for the production of novel antimicrobials.

The development of faster and less-expensive next-generation sequencing (NGS) technologies and the establishment of bioinformatic tools led to the development of genetic engineering strategies to discover needed novel bioactive secondary metabolites (Figure B). In this regard, it was speculated that only 1-3% of the Streptomycete antibiotics have been discovered and finding the remaining 97–99% will require high-throughput screening by modern technologies (Clardy *et al.*, 2006).

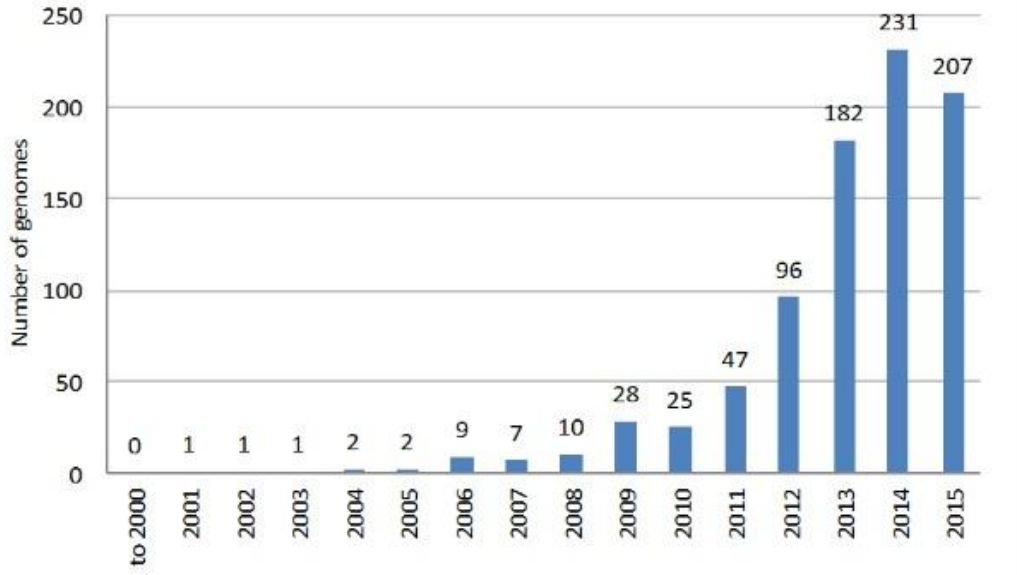

Figure B. Number of genomes of actinobacteria species relevant to natural products deposited at NCBI databases per year (Gomez-Escribano *et al.*, 2016).

Most of the secondary metabolites are distributed in three major classes: polyketides (PK), non ribosomal peptides (NRP), or hybrids thereof (PK-NRP). For PK, the elongation chain starters comprise malonyl-CoA and methylmalonyl-CoA monomer

units; while, for NRP proteinogenic or non-proteinogenic amino acids are the monomer units used for chain elongation (Fischbach and Walsh, 2006). In both cases, the precursors of these building-blocks required for secondary metabolite biosynthesis are generated from primary metabolism. Tremendous efforts have been made to understand the molecular basis underlying the links between primary and secondary metabolism in *Streptomyces* (Alam *et al.*, 2010; Nieselt *et al.*, 2010; Thomas *et al.*, 2012). However, the metabolic features accompanying the transition between primary to secondary metabolism remain to be unraveled.

To contribute to the elucidation of these links, I conducted a shotgun proteomic strategy using last cutting-edge mass spectrometry technology applied to the model, sequenced and phylogenetically closely-related *Streptomyces* species *S. coelicolor* and *S. lividans* in order to determinate the nature of the metabolic features underlying the biosynthesis of secondary metabolites. Both strains possess the same pathways for the biosynthesis of well-characterized secondary metabolites of the polyketide (actinorhodin, ACT) or peptidyl (calcium-dependent antibiotics CDA, undecylprodigiosin, RED) families but the expression of these pathways is high in *S. coelicolor* and relatively low in *S. lividans*. The better understanding of these processes would foster new strategies to enhance production of known as well as cryptic antibiotics.

The present thesis work is described in five chapters:

- In the first chapter, the state of the art concerning primary and secondary metabolism in *Streptomyces* is introduced. The advances of central carbon, nitrogen, phosphate and energetic metabolism are described. Afterwards, a description of the secondary metabolites biosynthesis and its regulation is presented in the historically antibiotic-producing model specie *S. coelicolor*. What is currently known on the relationships between primary and secondary metabolism in *S. coelicolor* and *S. lividans* is also described.

- In the second chapter, the label-free proteomic strategies are presented including the recent and efficient shotgun approach. The methods of relative-quantitation used in

proteomics are also mentioned. And, a section is dedicated to high-throughput proteomic studies conducted in *Streptomyces*.

- In the third chapter, a simple and fast method to quantify total fatty acids methyl esters in *Streptomyces* is described. This method is based on Fourier Transform Infrared (FTIR) Spectroscopy using Attenuated Total Reflection mode (ATR). The validity of this method was assessed using the classical approaches of Gas Chromatography coupled to Mass Spectrometry (GC-MS) and FTIR in transmission mode with the help of KBr pellets. The proposed method was tested with various *Streptomyces* species and proved to be suitable for screening purposes.

- The fourth chapter describes a comparative label-free proteomic study of the model species *S. coelicolor* and *S. lividans* cultivated in liquid R2YE medium supplemented with glucose under oxygen-limiting conditions. A total of 2024 proteins were identified and quantified, from them 360 showed significant differences in abundance between the species. The contrasted reaction to oxygen limitation of these two species is discussed. This study confirmed the previously observed oxidative and glycolytic metabolism of *S. coelicolor* and *S. lividans*, respectively.

- In the fifth chapter, a comparative and quantitative proteomic analysis of *S. coelicolor* and *S. lividans* was conducted in solid R2YE medium supplemented with glucose or glycerol as main carbon sources. This study allowed the identification of 4372 proteins which represents the largest proteome dataset of any *Streptomyces* specie until now. The spatio-temporal analysis showed 1040 proteins with significant variation. The unprecedented depth of this study allowed to precisely define the metabolic features underlying the contrasted abilities of these two species to produce antibiotics and to accumulate storage lipids.

Finally, an integrated discussion and conclusion are presented. This part sums up the studies conducted during this thesis and details possible perspectives for potential evolution of the project.

CHAPTER I. BIBLIOGRAPHIC STUDY

1.1. The genus *Streptomyces*

The phylum Actinobacteria is one of the largest taxonomic units among the 18 major lineages within the domain of bacteria, including 5 subclasses, 6 orders, and 14 suborders (Ludwig *et al.*, 2012). The analysis based on sequencing the 16S rRNA gene, DNA-DNA hybridization and chemical composition allowed to classify the order of Actinomycetales into 14 suborders, including: Actinomycineae, Actinopolysporineae, Catenulisporineae, Corynebacterineae, Frankineae, Glycomycineae, Jiangellineae, Kineosporineae, Micrococcineae, Micromonosporineae, Propionibacterineae, Pseudonocardineae, Streptomycineae, and Streptosporangineae (Sen *et al.*, 2014) (Figure 1. 1). It is precisely in the Streptomycineae suborder where is classified the family Streptomycetaceae that includes the important genus of *Streptomyces*.

Streptomyces are saprophytic, soil-dwelling, Gram-positive bacteria with high G+C content (69-78%) of their genome. They have a complex morphological and metabolic differentiation cycle. These bacteria are of great importance for mankind due to their ability to synthesize antibiotics and other bio-active molecules useful in medicine or agriculture (Challis and Hopwood, 2003; Barka *et al.*, 2016).

Streptomyces live in the superficial layers of terrestrial or marine soils, where they play key ecological roles in the recycling of C, N and P present in organic debris originated from plant, fungi or insects. They are capable of hydrolyze a wide range of polysaccharides (cellulose, chitin, xylan, and agar) and other natural macromolecules (proteins, lipids, nucleic acids, etc.) (Chater *et al.*, 2010). Furthermore, *Streptomyces* can also colonize the rhizosphere to control the spread of fungal pathogens by creating a symbiosis with the plants (Hopwood, 2007).

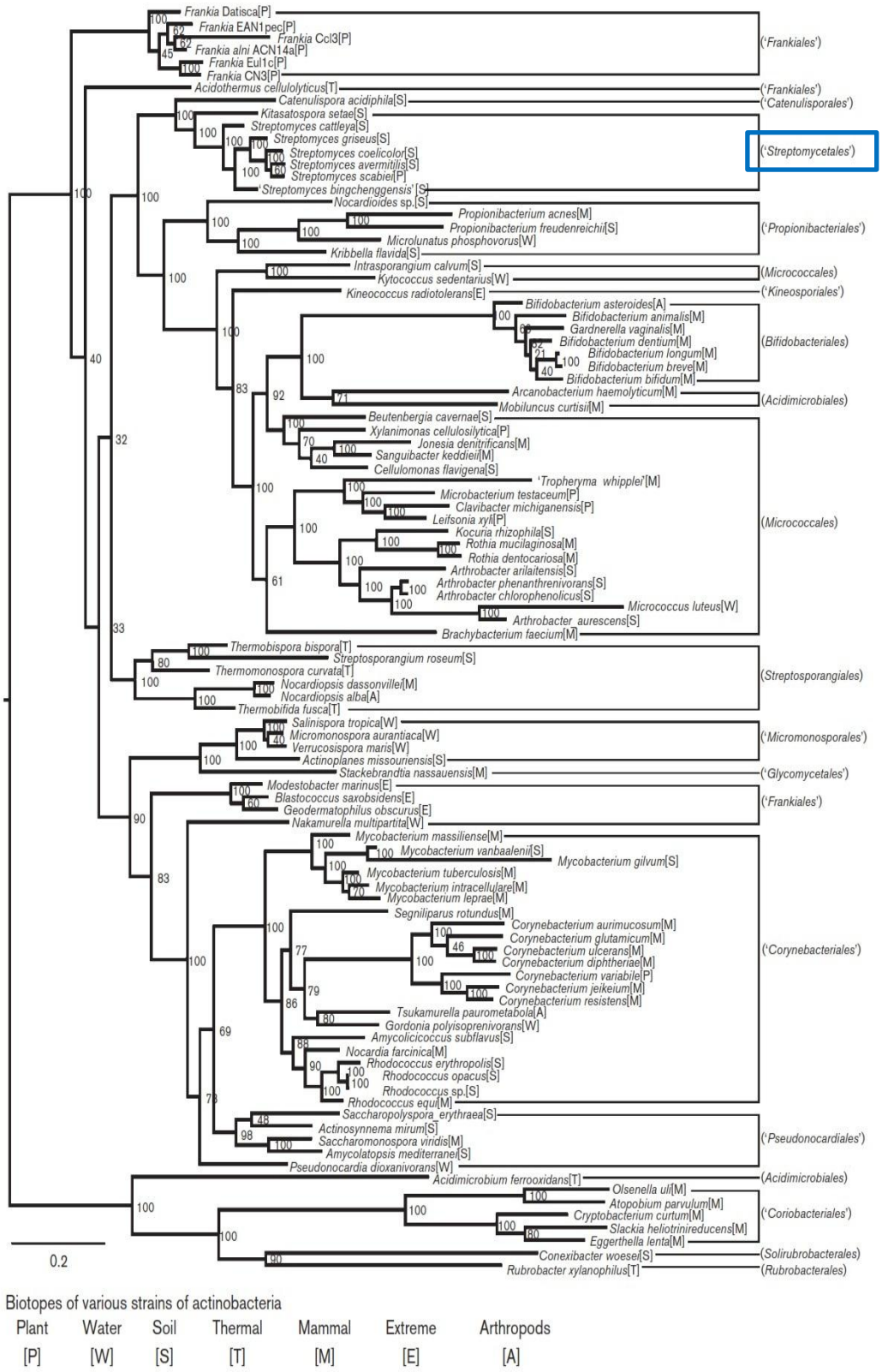

Figure 1. 1. Phylogenetic tree reconstructed with 100 actinobacterial species (Sen *et al.*, 2014).

1.2. Development cycle of *Streptomyces*

The life cycle of *Streptomyces* on solid surfaces is more complex than that of other bacteria (Figure 1. 2). The asexual cycle starts with the germination of a spore which is dormant until the suitable conditions occur for growth, including water availability, presence of nutriments (C, P, N) and the presence of divalent cations (Ca^{2+}, Mg^{2+} and Fe^{2+}) (Yagüe *et al.*, 2013; Bobek *et al.*, 2014). The spores allow *Streptomyces* to survive for long periods under adverse conditions (i.e. desiccation, poor nutrient availability, oxygen limitation or competition with other soil microorganisms). Germination is regulated by the cyclic AMP receptor protein (Crp) encoded by *SCO3571*. The deletion of this gene leads to a drastic delay of germination and cell growth as well as premature sporulation (Derouaux *et al.*, 2004; Piette *et al.*, 2005). Another gene involved at the germination stage is *nepA* (SCO4002), a structural cell wall protein that regulates spore dormancy under unfavorable environmental conditions (de Jong *et al.*, 2009).

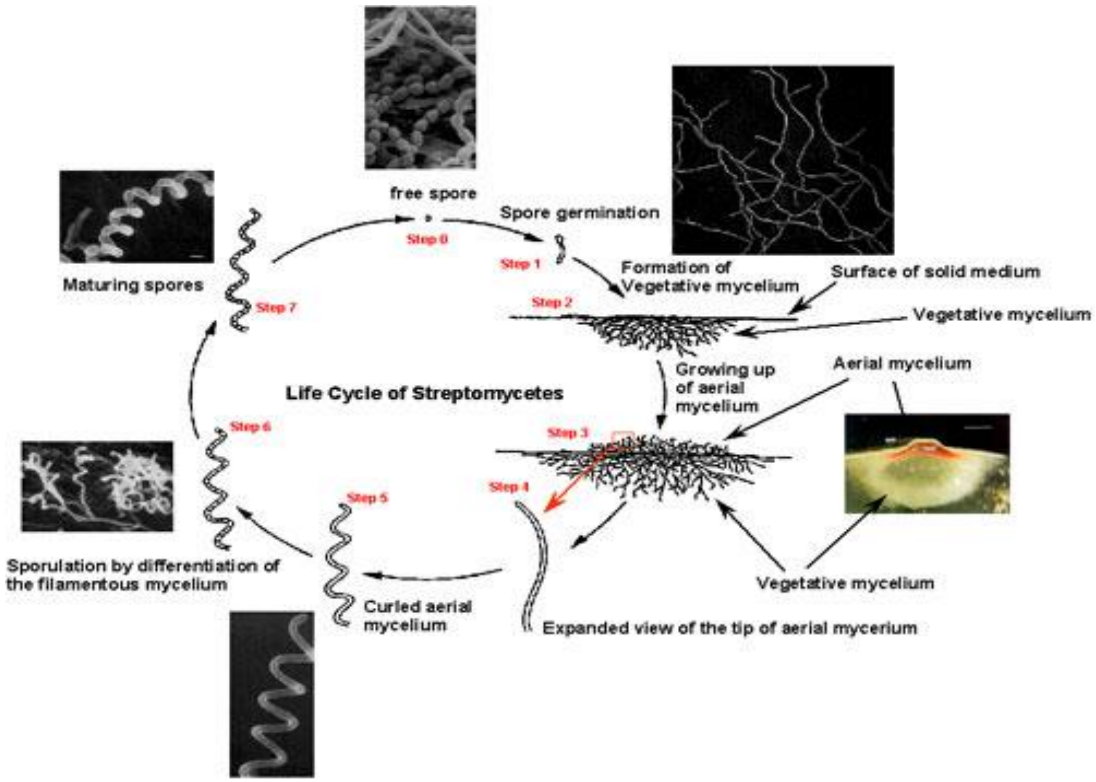

Figure 1. 2. Developmental cycle of *Streptomyces* on solid cultures of *Streptomyces*. Image from the website of Laboratory of Cell Biochemistry, Hiroshima University, http://home.hiroshima-u.ac.jp/~mbiotech/hosenkin_lab/Front-e.html , accessed on April 8th, 2017.

Once the germination is triggered, the spore swells and a germ tube emerges that will grow and branch to form the compartmentalized vegetative mycelium (Yague *et al.*, 2016). After growth of the vegetative mycelium, and in condition of nutriments depletion *Streptomyces* must switch into survival and dispersal mode. To do so, aerial hyphae is induced from vegetative mycelium. The vegetative mycelium is autolytically degraded by a programmed cell death (PCD) mechanism in order to recycle the necessary nutriments to erect a second mass of aerial mycelium (Miguelez *et al.*, 1999; Manteca *et al.*, 2006). The tip ends of hyphae will differentiate into chains of unigenomic spores where gene exchange takes place (Claessen *et al.*, 2006). The production of antibiotics is often concomitant of the late steps of this developmental process (Bibb, 2005). These new spores are dispersed by wind or animals to give rise of new colonizing mycelia.

Early aerial hyphal formation is regulated by an extracellular signaling cascade dependent on the *bld* genes, for bald, whose deletion/mutation results in species unable to form aerial hyphae (Claessen *et al.*, 2006). Moreover, the processes of sporulation septation, spore maturation and the synthesis of grey spore pigment are regulated by the *whi* genes (Kelemen *et al.*, 1998; Chater, 2001). *Whi* mutants are capable to form aerial mycelium but they cannot achieve the sporulation process properly (Figure 1. 3).

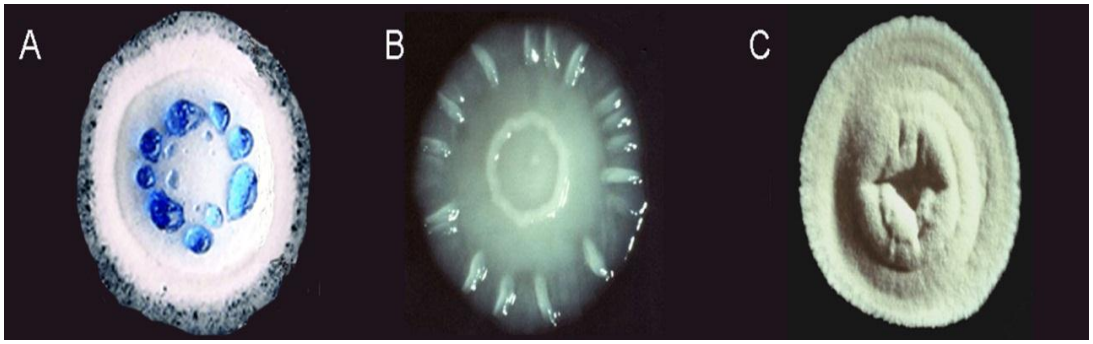

Figure 1. 3. Optical pictures of isolated colonies of wild-type *S. coelicolor* (A), a *bldH* mutant with no aerial hyphae (B), and a *whi* mutant with white colour of the aerial hyphae (C) The blue drops are the antibiotic actinorhodin produced by *S. coelicolor*.
Image obtained from Dr Paul Hoskinsson's laboratory website http://spider.science.strath.ac.uk/sipbs/staff/Paul_Hoskisson.html , accessed on April 8th, 2017.

In liquid cultures, cell development of *Streptomyces* shows similar features than on solid medium but usually does not undergoes sporulation (Manteca *et al.*, 2008). This is important for industrial purposes since large-scale production of antibiotics is conducted in liquid cultures in large bioreactors. A first phase of active growth begins with the development of a compartmentalized mycelium that forms pellets and is followed by a transient growth arrest being correlated with the death of mycelial cells presents in the center of the pellets (Manteca *et al.*, 2008). Then, the formation of a second multinucleated differentiated mycelium emerges after the death process of the first compartmentalized mycelium (Figure 1. 4). The secondary metabolites are generally produced at this late stage (Takano *et al.*, 1992; Huang *et al.*, 2001).

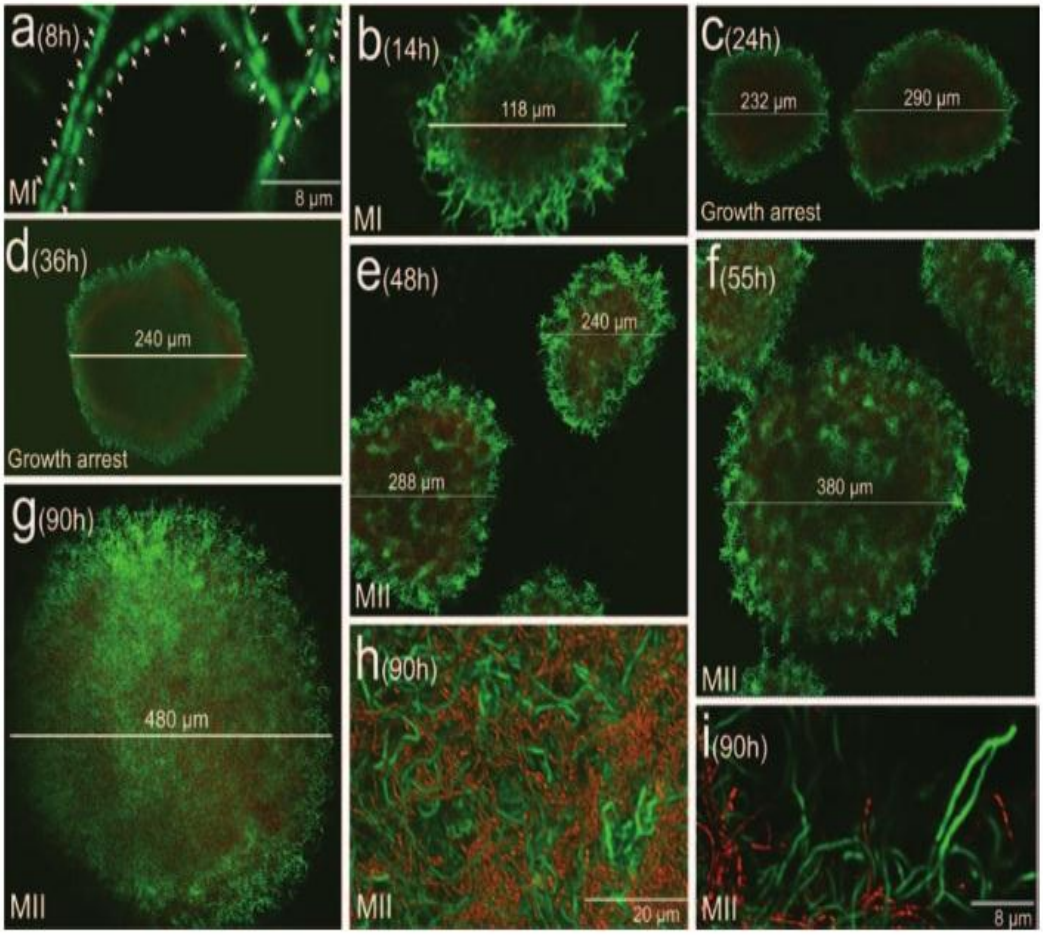

Figure 1. 4. Confocal laser scanning fluorescence microscopy of the development cell death processes of *S. coelicolor* in liquid cultures (Manteca *et al.*, 2008).
Culture time points (hours), pellet diameters (micrometers), and the growth arrest phase are indicated. Arrows in panel indicate septa. MI = first mycelium. MII = second mycelium.

1.3. Genome architecture of *Streptomyces*

The specie *S. coelicolor* is the most largely studied *Streptomyces* specie mainly due to its capacity to produce the red-pigmented undecylprodigiosin (RED) and blue-pigmented actinorhodin (ACT) antibiotics which are easy to detect visually at different stages of development. In 2002, the sequencing of the genome of *S. coelicolor* was a major achievement that contributed to a better knowledge of the molecular basis underlying antibiotics production in *Streptomyces* (Bentley *et al.*, 2002). Since then, the improvements on NGS technologies helped to sequence genomes more efficiently and at lower expenses than at the beginning of the 21st century (Gomez-Escribano *et al.*, 2016). Nowadays, it is possible the access to more than 30 completed genomes of different *Streptomyces* species (Harrison and Studholme, 2014). The genome characteristics of three model species, *S. coelicolor*, *S. lividans* and *S. griseus* are indicated in Table 1. 1 (Bentley *et al.*, 2002; Ohnishi *et al.*, 2008; Ruckert *et al.*, 2015).

Table 1. 1. Genome characteristics of the model species *S. coelicolor*, *S. lividans* and *S. griseus*.

Features	***S. coelicolor***	***S. lividans***	***S. griseus***
Length (bp)	8 667 507	8 345 283	8 545 929
Coding sequences	7 825	7360	7 138
Cytoplasmic (%) *	71.5	72.1	71.2
Membrane (%) *	24.5	24.2	25.4
Extracellular (%) *	4.0	3.7	3.4
G + C content (%)	72.1	72.2	72.2
rRNA genes	18	13	18
tRNA genes	63	64	66
GenBank number	AL645882	ACEY00000000	AP009493

* Sub-cellular distribution from LocateP database (Zhou *et al.*, 2008)

Streptomyces genome size remains among the largest in bacteria. The 8-9 Mb genomes are linear and constituted by a central “core” as well as by a left and right "arms" or terminal regions (1.5-Mb left and 2.3-Mb right) that are more variable than the core region (Figure 1. 5).

The central core constitutes approximately half of the total size of the chromosome. It contains essential genes necessary for growth such as those controlling DNA replication, transcription, translation, and central metabolism. The terminal regions contain repeated terminal sequences as well as a large number of transposable elements that renders highly variable and instable this part of the chromosome (Leblond and Decaris, 1994; Lin and Chen, 1997).

More than two-thirds of the proteins involved in biosynthesis of secondary metabolites tend to be located in the terminal regions. The latter are thought to be the siege of incorporation of foreign genes via horizontal transfer. This process is likely to be involved in the large diversity of secondary metabolites produced by the Streptomyces species.

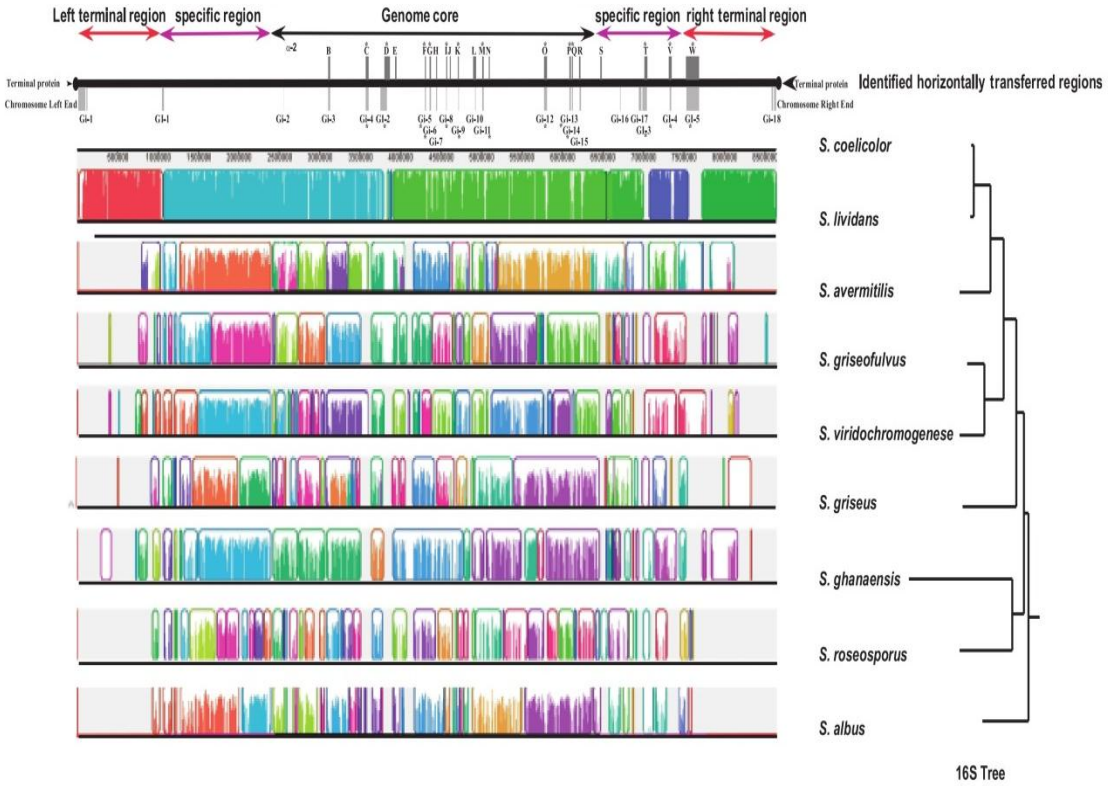

Figure 1. 5. The genomes of various *Streptomyces* were aligned with the 8.67 Mb genome of *S. coelicolor* using MAUVE software (Kirby, 2011).
The colored blocks represent syntenous regions. These were then compared with a 16S phylogenetic tree of the same species. At the top of the alignment are indicated the horizontally transferred regions within the *S. coelicolor* genome.

1.4. Primary metabolism in *Streptomyces*

Primary metabolism involves the catabolic and anabolic reactions of the cell. The catabolic reactions generate building-blocks, energy and reducing power for further utilization of the anabolism that includes proteins, nucleic acids, lipids and storage substances biosynthesis (Figure 1. 6). In bacteria, genes of primary metabolism are usually clustered in operons; however, it should be stressed that *Streptomyces* often possess multiple paralogs genes located at different chromosomal positions that encode proteins with similar function involved in primary metabolism (Siebring, 2010). This feature clearly makes more complex the analysis of the functioning of primary metabolism of *Streptomyces.*

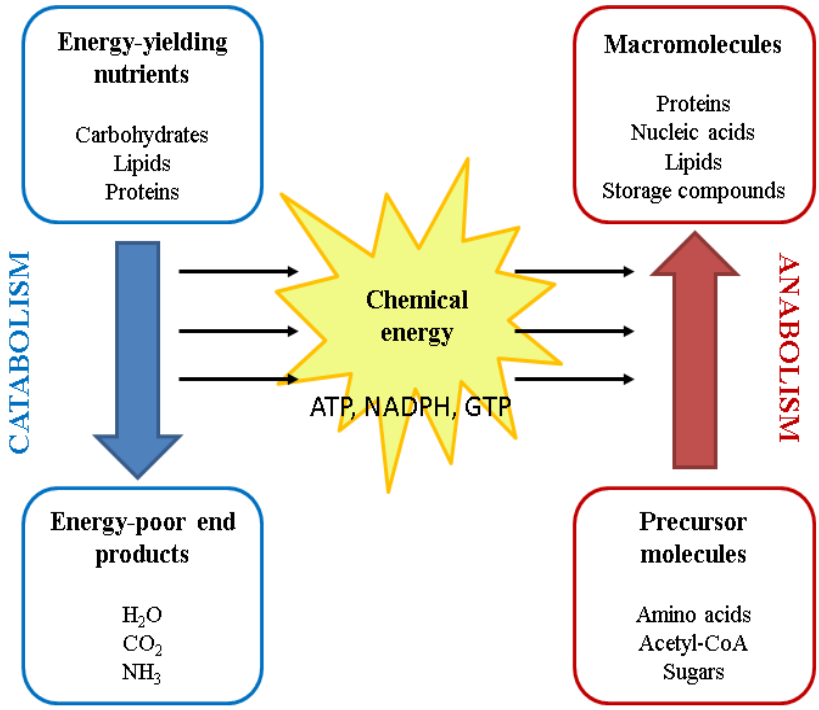

Figure 1. 6. Schematic representation of catabolic and metabolic reactions.

1.4.1. Central carbon metabolism

In many bacteria, the transport of glucose, the preferred carbon substrate, into the cell is conducted by phosphotransferase systems (PTS) that uses phosphoenolpyruvate

as phosphoryl donor. PTS consists of sugar-specific PTS permeases, also referred to as enzymes II (EII), and two general PTS proteins, enzyme I (EI) and histidine-containing protein (HPr), that participate in the phosphorylation of all PTS-transported carbohydrates (Bruckner and Titgemeyer, 2002). The genome of *S. coelicolor* encodes the complete PTS machinery that includes the genes: *ptsI* (EI), *ptsH* (HPr), *crr* (EII), two fructose/mannitol EII permeases, and four glucose/sucrose EII permeases (Parche *et al.*, 2000). However, the major glucose transport system in *S. coelicolor* is not the PTS, the latter is required for fructose (Nothaft *et al.*, 2003) and N-acetylglucosamine (Parche *et al.*, 2000) transport; instead, it is the glucose permeases (GlcP). Two *glcP* gene copies have been discovered in different parts of the chromosome of *S. coelicolor*: *glcP1* (SCO5578) and *glcP2* (SCO7153)(van Wezel *et al.*, 2005).

Like other bacteria, *Streptomyces* assimilates selectively the different carbon sources in preferential order; once the preferred carbon source is depleted the assimilation of secondary substrates is activated. This type of regulation is known as Carbon Catabolite Repression (CCR) (Gorke and Stulke, 2008). In *S. coelicolor*, glucose kinase (Glk) represents the main glucose phosphorylating enzyme thought to act also as a regulatory protein in CCR (Kwakman and Postma, 1994). Deletion mutants of the *glkA* gene have shown to be incapable of growing on glucose as sole carbon source (Angell *et al.*, 1994). Furthermore, *glk* is thought to interact with *glcP* to form a complex required for the efficient transport of glucose into the cell (van Wezel *et al.*, 2007). This interaction might be facilitated by the gene product SCO2127 which has been associated with the glucose CCR phenomenon (Guzman *et al.*, 2005; Forero *et al.*, 2012). The protein SCO2127, located next to a Glk (SCO2126), was proposed to be a regulatory protein of CCR and mycelium differentiation by modulating the lipoprotein ABC-type permease (BldKB, SCO5113) in cultures grown in presence of glucose (Chavez *et al.*, 2011). Still the functioning of CCR in *Streptomyces* remains enigmatic.

1.4.1.1. Glycolysis and gluconeogenesis

The Embden-Meyerhof-Parnas pathway, also known as glycolysis, is the sequence of reactions catabolizing glucose which is highly conserved in bacteria including *Streptomyces* (Figure 1. 7).

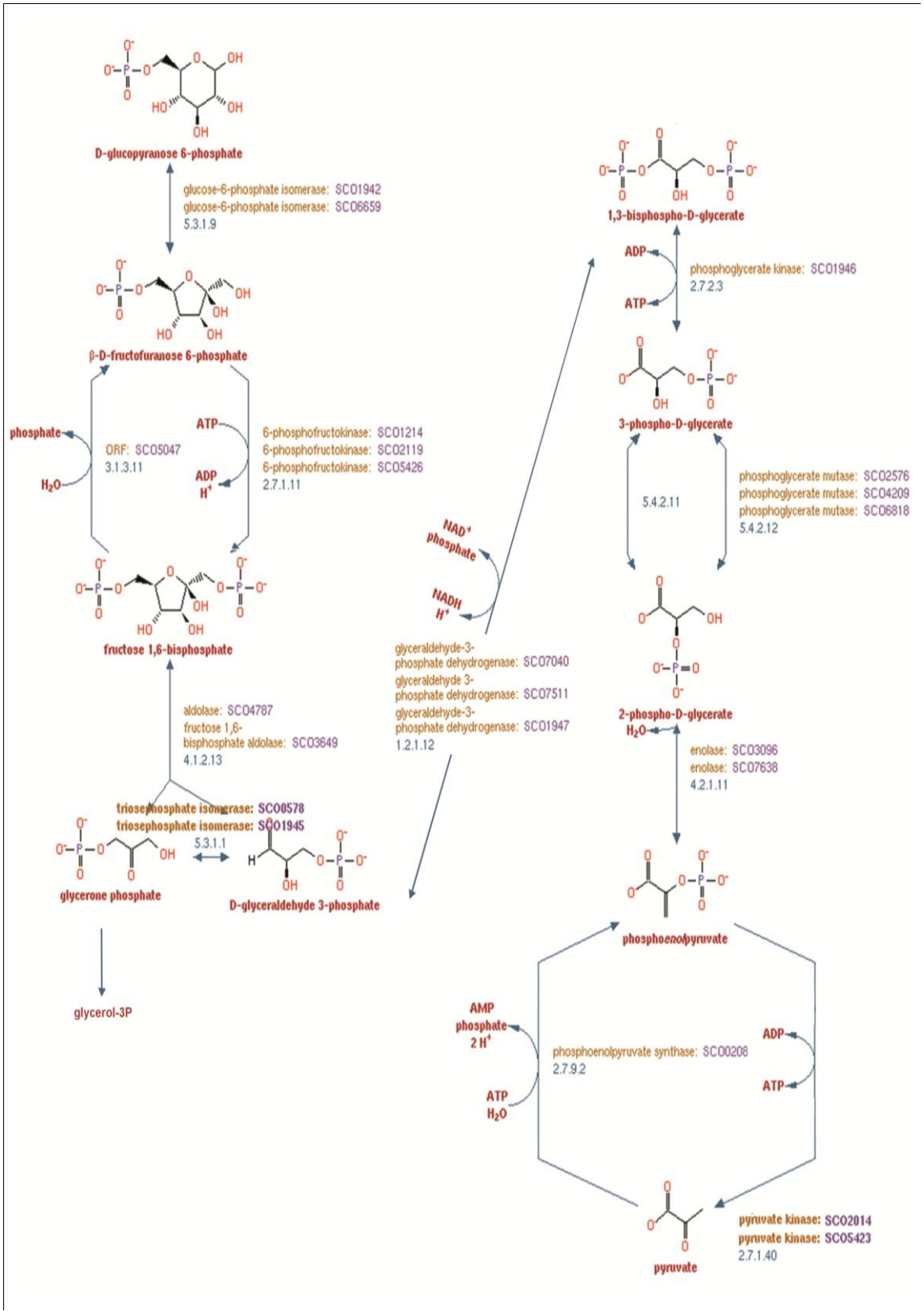

Figure 1. 7. Glycolysis/gluconeogenesis pathway in *S. coelicolor* (BioCyc Database Collection).

Glycolysis occurs in two main stages, the first stage catalyzes the splitting of one molecule of glucose into one molecule of glyceraldehyde-3-phosphate (GAP) and one molecule of dihydroxyacetone phosphate (DHAP, also called glycerone phosphate) that are inter-convertible; while the second stage catalyzes the oxidation of GAP into pyruvate and DHAP into glycerol-3-phosphate (Gly3P). Overall, one mole of glucose generates two moles of pyruvate, two moles of ATP and two moles of NADH (Berg *et al.*, 2002). At first, glucose is phosphorylated by the glucose kinase (Glk). The product, glucose-6-phosphate (G6P), is isomerized into fructose-6-phosphate (F6P) in a reaction catalyzed by G6P isomerase. F6P is the substrate of phosphofructokinase (Pfk) that adds a second phosphate to the sugar in order to form fructose-1,6-biphosphate (F1,6P). Then, F1,6P is divided into GAP and glycerone phosphate or dihydroxyacetone (DHA) by the enzyme F1,6P aldolase. Eventually, the reversible conversion between DHA and GAP is catalyzed by the enzyme triosephosphate isomerase (Tpi). Until this step, 2 moles of ATP are consumed; in the following steps oxidation of GAP will produce 2 moles of ATP and 2 moles of NADH. The enzyme GAP dehydrogenase catalyzes the conversion of GAP into 1,3-bisphosphoglycerate (1,3PG). The next reaction, catalyzed by phosphoglycerate kinase, involves the addition of phosphate to 1,3PG at phosphate level phosphorylation generating 3-phosphoglycerate (3PG) and ATP. The 3PG is then isomerized into 2-phosphoglycerate (2PG) by the phosphoglycerate mutase. The enzyme enolase catalyzes the conversion of 2PG into phosphoenolpyruvate (PEP). The last step of glycolysis, the enzyme pyruvate kinase catalyzes the conversion of PEP into pyruvate and generates ATP.

As observed in Figure 1. 7, the genome of *S. coelicolor* contains multiple paralogs genes encoding similar related enzymes for a given step of the glycolysis. The function of this redundancy is poorly understood. For instance, the enzyme Pfk presents three isoforms, SCO1214, SCO2119 and SCO5426, the latter being the more expressed during growth (Siebring, 2010). Interestingly, deletion mutants of SCO5426, that are likely to have a reduced glycolytic flux, showed an enhanced capacity to produce the pigmented antibiotics ACT and RED (Borodina *et al.*, 2008).

In absence of glycolytic carbon sources, *Streptomyces* possess the machinery to grow on gluconeogenic carbon sources such as glutamine, glutamate (Borodina *et al.*, 2005; van Wezel *et al.*, 2006) or form acetyl-CoA originated from storage lipid degradation

(Olukoshi and Packter, 1994). Gluconeogenesis operates in the opposite direction of glycolysis. In gluconeogenesis, PEP can be generated from pyruvate by the pyruvate phosphate dikinase (PPDK, SCO0208) and the conversion of F1,6P into F6P is catalyzed by the enzyme fructose-1,6-biphosphatase (SCO5047).

1.4.1.2. Pentose phosphate pathway

The pentose phosphate pathway (PPP) is a pathway branched on glycolysis (Figure 1. 8). There are two phases in the PPP, the first one is oxidative and generates NADH/NADPH and pentoses for nucleotide biosynthesis, while the second is non-oxidative and generates glycolytic intermediates such as F6P and GAP.

In the oxidative phase, the first step is catalyzed by G6P dehydrogenase that converts G6P into 6-phosphoglucono-lactone (6PGL) generating NADPH. Then, 6PGL is converted into 6-phosphogluconate (GL6P) by 6-phosphogluconolactonase. Afterwards, GL6P is converted into ribulose-5-phosphate (RL5P) by GL6P dehydrogenase. The RL5P is an important precursor for ATP, coenzyme A, NAD, FAD, DNA and RNA generation. Eventually RL5P is isomerized into ribose-5-phosphate (R5P) or into xylulose-5-phosphate (X5P) by the enzymes R5P isomerase and ribulose phosphate-3-epimerase, respectively.

The non-oxidative phase of PPP involves the reactions catalyzed by transketolase and transaldolase. The transketolase catalyzes the reaction that transfers a C2 fragment from X5P to R5P in order to form sedoheptulose-7-phosphate (S7P) and GAP. While the transketolase transfers a C3 fragment from S7P to GAP to form erythrose-4-phosphate (E4P) and F6P. Some transketolases can also transfer a C2 moiety from X5P to E4P in order to form F6P and GAP (Berg *et al.*, 2002). Transaldolases and transketolases interconnect PPP and glycolysis.

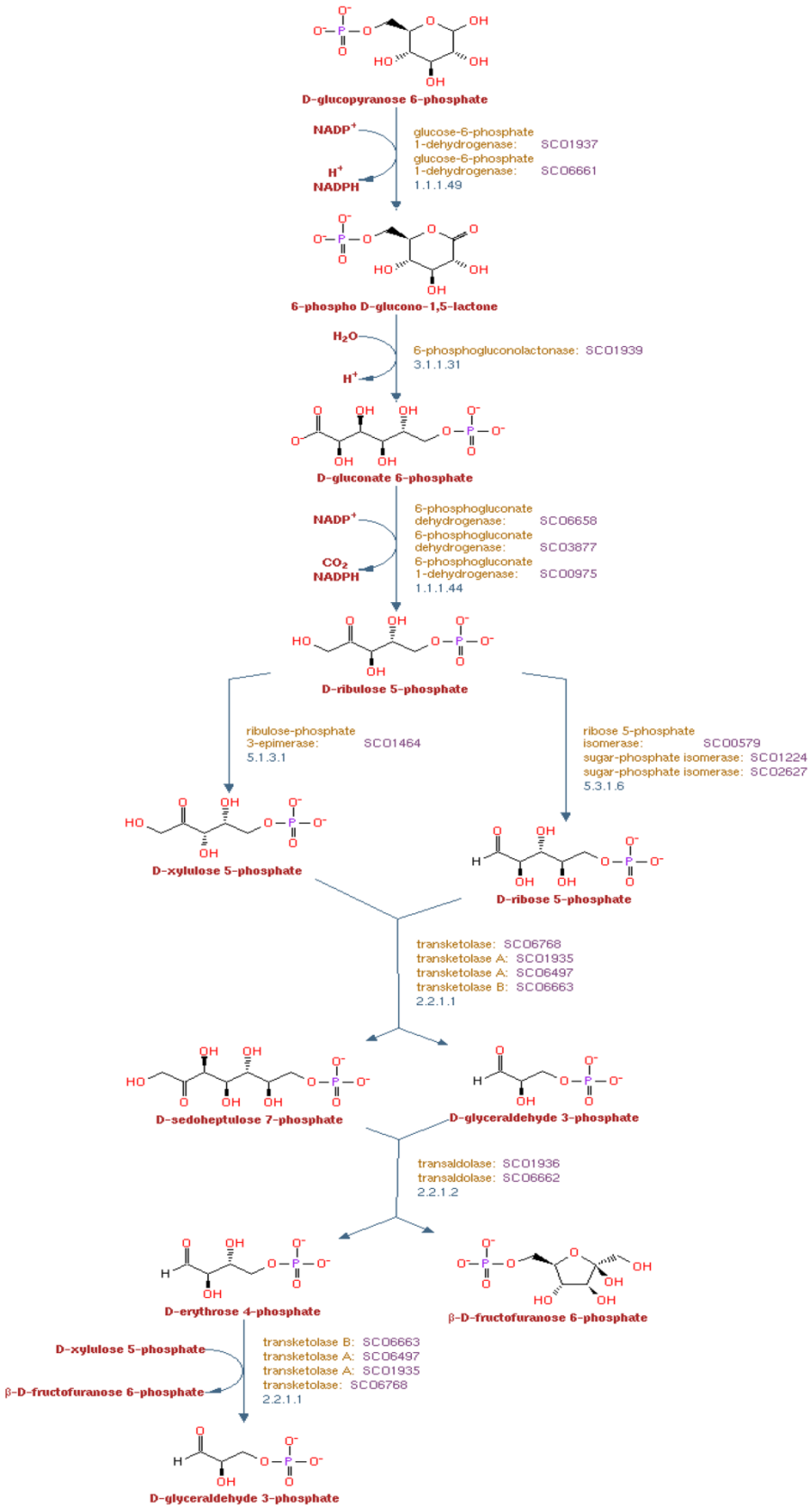

Figure 1. 8. Pentose phosphate pathway in *S. coelicolor* (BioCyc Database Collection).

Two major clusters encoding enzymes involved in the PPP have been identified in *S. coelicolor*, SCO1935-SCO1942 and SCO6658-SCO6663. The latter was shown to be highly active during glucose catabolism (Romero-Rodríguez *et al.*, 2016). In *S. coelicolor* and in *S. lividans*, the PPP is mainly active during the exponential growth phase indicating that it is involved in the synthesis of biomass precursors (Obanye *et al.*, 1996; Rossa *et al.*, 2002; Gubbens *et al.*, 2012). However, PPP should be also active during stationary phase in *S. coelicolor* M145 (antibiotic-producing) and in *S. coelicolor* M1146 (non-antibiotic producing strain) in order to supply NADPH for antibiotics (ACT and RED) or lipids biosynthesis (Coze *et al.*, 2013). It was shown that deletion mutants of the genes involved in the two initial steps of PPP (*zwf1*, *zwf2* and *devB*) in *S. coelicolor* produced reduced levels of ACT and RED suggesting the utilization of NADPH for antibiotic biosynthesis (Butler *et al.*, 2002).

1.4.1.3. Krebs cycle

The Krebs cycle, also known as citric acid cycle or tricarboxylic acid cycle (TCA), transforms the energy stored in acetyl-CoA derived from pyruvate, into high-energy intermediate molecules such as: NAD, NADPH, $FADH_2$, and GTP (Berg *et al.*, 2002). The overall reaction from 1 mole of acetyl-CoA and 1 mole of oxaloacetate (OAA) results in the formation of 1 mole of GTP, 1 mole of $FADH_2$, 2 moles of NADH, 1 mole of NADPH and 2 moles of CO_2 (Figure 1. 9).

The cycle condenses acetyl-CoA (C2), generated from pyruvate by the action of pyruvate dehydrogenase, with OAA (C4) to yield citrate (CIT, C6) in a reaction catalyzed by citrate synthase. Afterwards, CIT is dehydrated by a lyase to form cis-aconitate (C6) which will be converted into isocitrate (iCIT, C6) by the enzyme aconitase. The catalysis of iCIT into α-ketoglutarate (αKG, C5) is achieved by the enzyme iCIT dehydrogenase. The next reaction is conducted by the αKG dehydrogenase that catalyzes the conversion of αKG into succinyl-CoA (SucCoA, C4) which is then converted into succinate (SUC, C4) by the SucCoA synthetase. The succinate is converted into fumarate (FUM, C4) by the enzyme SUC dehydrogenase. FUM is then transformed into malate (MAL, C4) by fumarate dehydratase. At last, malate dehydrogenase closes the cycle by converting MAL into OAA (C4).

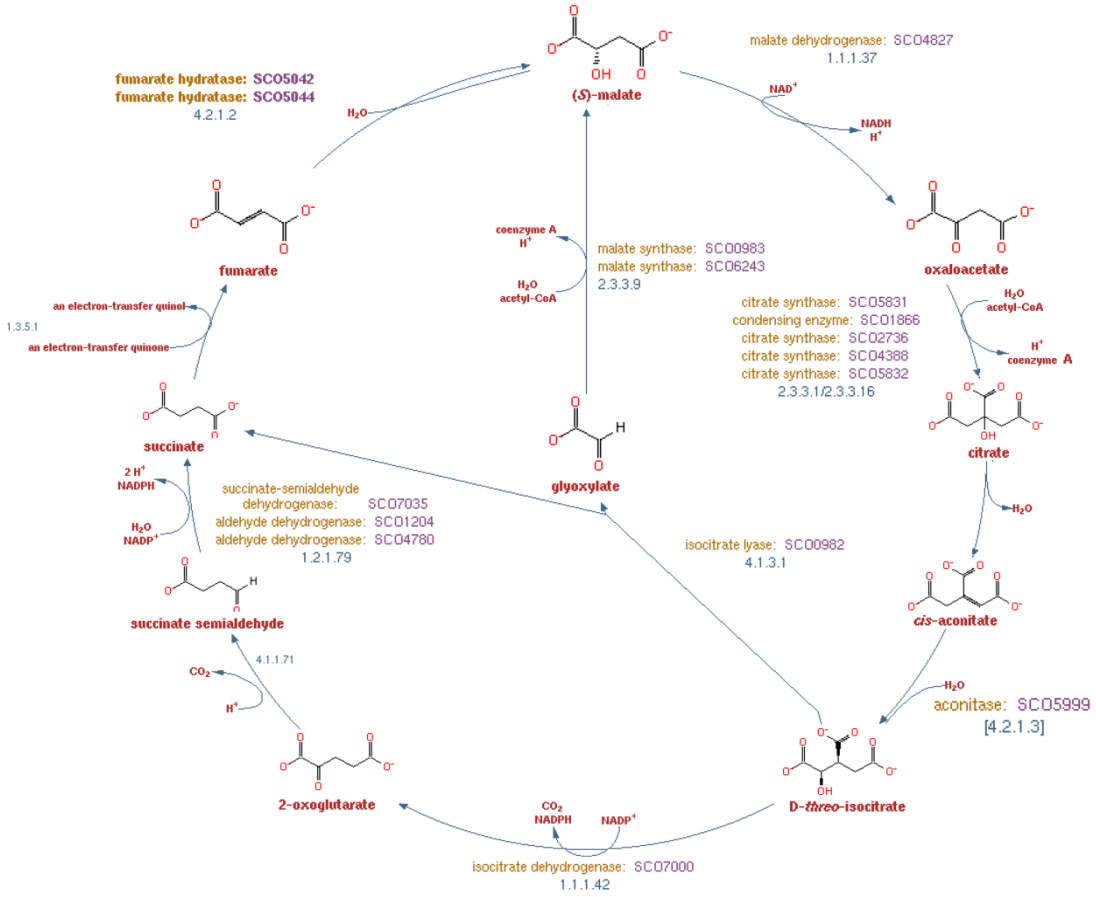

Figure 1. 9. Krebs cycle pathway in *S. coelicolor* (BioCyc Database Collection).

The enzymes of TCA are fundamental for cell growth in *Streptomyces* since the αKG is combined with NH_4 to form glutamine and glutamate. The latter is a nitrogen donor used for the synthesis of other amino acids. The deletion of aconitase and citrate synthase encoding genes in *S. coelicolor* resulted in acidogenesis, glutamate auxotrophy and important growth defects (Viollier *et al.*, 2001; Viollier *et al.*, 2001). Another study indicates that the enzyme isocitrate dehydrogenase (SCO7000) is essential for *S. coelicolor* growth since deletion mutants were unviable (Takahashi-Iniguez *et al.*, 2014).

The reactions, carried out by isocitrate lyase and malate synthase, are a variation of the TCA pathway that is known as the glyoxylate bypass. A comparative *in silico* analysis between the genomes of *S. coelicolor* and *S. lividans*, two phylogenetically closely-related species, revealed the absence of isocitrate lyase (SCO0982) and malate synthase (SCO0983) in *S. lividans* suggesting the lack of glyoxylate bypass in this

specie (Lewis *et al.*, 2010). Furthermore, it has a role in gluconeogenesis yielding glucose from acetyl-CoA generated by the degradation of fatty acids.

1.4.1.4. Anaplerotic reactions

TCA is the main source of metabolic intermediates that in combination with N is used for the biosynthesis of most amino acids as well as nucleotides. Since the intermediates are withdrawn from the TCA cycle for the synthesis of these molecules, the cycle has to be replenished through anaplerotic/re-filling reactions (Figure 1. 10). There are four major anaplerotic reactions, where: i) pyruvate carboxylase catalyzes the conversion of pyruvate into OAA, ii) the malic enzyme generates malate from pyruvate, iii) PEP carboxylase converts PEP into OAA, and iv) PEP carboxykinase converts OAA into PEP.

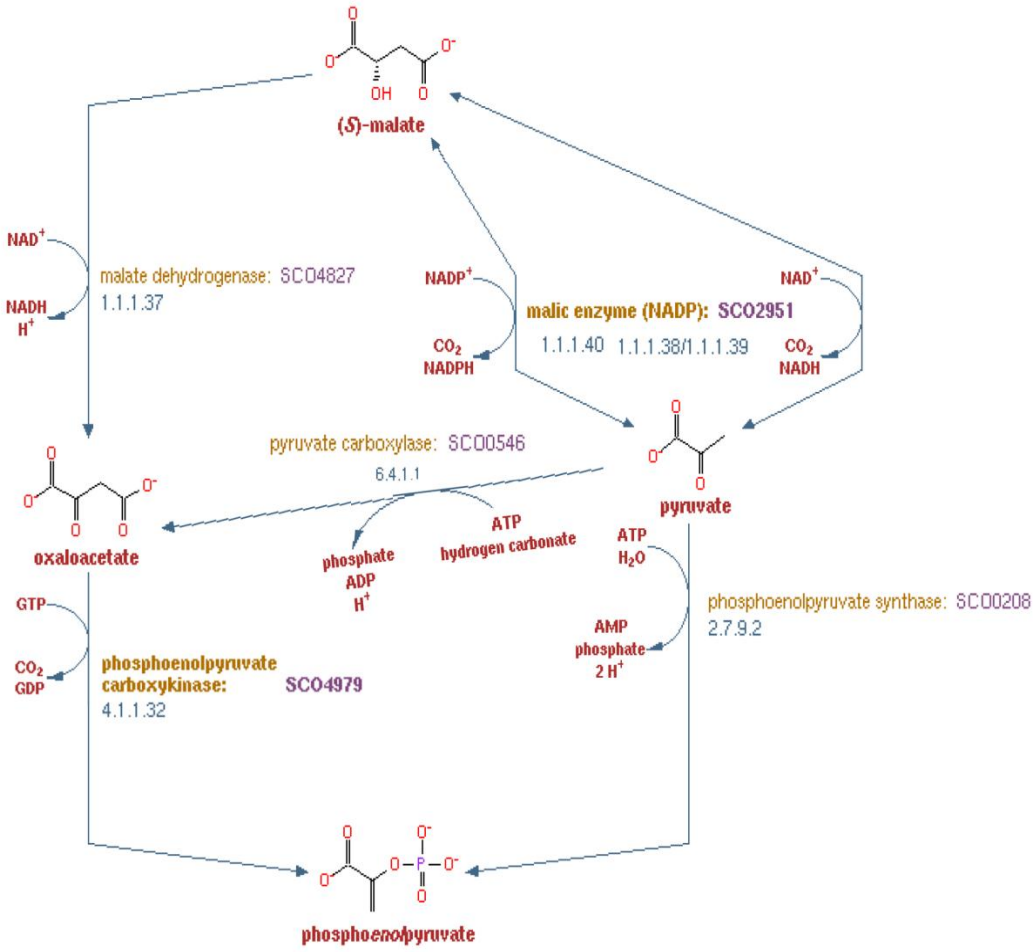

Figure 1. 10. Anaplerotic pathways in *S. coelicolor* (BioCyc Database Collection).

1.4.1.5. Glycerol metabolism

The catabolism of glycerol in *S. coelicolor* is mediated by enzymes encoded by operon the *glyICABX* (SCO1659 - SCO1662). It includes a probable glycerol uptake facilitator protein, a glycerol kinase, a glycerol-3-phosphate (Gly3P) dehydrogenase and a conserved hypothetical protein ParJ (Smith and Chater, 1988). The expression of these genes is under negative control of *glyR* (SCO1660) which is unhooked from its targets by the inducer Gly3P (Hindle and Smith, 1994).

Glycerol uptake is mediated by a facilitator protein that promotes diffusion across the membrane; then, intracellular glycerol is subsequently converted into Gly3P by glycerol kinase (Darbon *et al.*, 1999). The Gly3P is then converted into DHAP by the Gly3P dehydrogenase and join glycolysis. It is noteworthy to mention that Gly3P constitutes the backbone of most cellular lipids.

1.4.1.6. Fatty acids biosynthesis

Fatty acids and their derivatives are essential components of membranes and storage lipids of the triacylglycerol family (TAG) that are crucial source of carbon and metabolic energy. In *Streptomyces*, fatty acids are synthesized by the fatty acid synthetase (FAS) type II systems (Gago *et al.*, 2011). The first step in fatty acid biosynthesis (Figure 1. 11) is the carboxylation of acetyl-CoA by acetyl-CoA carboxylase (ACC), to form malonyl-CoA, which is then converted into malonyl-ACP by malonyl-CoA:ACP transacylase (FabD). The chain elongation steps consist in iterative reactions leading to successive addition of a two-carbon unit to an acyl group. The intermediates are covalently attached to the acyl carrier protein (ACP) through a thioester linkage to the terminal sulphydryl of the 4´-phosphopanteine prosthetic group.

The first elongation step is the condensation of malonyl-ACP with an acyl-CoA, catalyzed by β-ketoacyl-ACP synthase III (FabH), to form β -ketoacyl-ACP. Additional cycles of elongation are catalyzed by the FabF/FabB condensing enzymes. These proteins condense malonyl-ACP with acyl-ACP to extend the acyl chain by two carbons. Then, the NADPH-dependent β-ketoacyl-ACP reductase (FabG) reduces the β-keto group to a β-hydroxyl intermediate. The latter is dehydrated by the β-hydroxyacyl-

ACP dehydratase (FabZ or FabA), to a *trans*-2-enoyl-ACP. At last, the enoyl chain is reduced by the NADPH-dependent (FabI or FabL) enoyl-ACP reductase (Singh and Reynolds, 2015). On completion of each cycle of condensation and chain reduction, the growing acyl chain is transferred back to the ketosynthase to initiate the next cycle (Arabolaza *et al.*, 2008; Gago *et al.*, 2011).

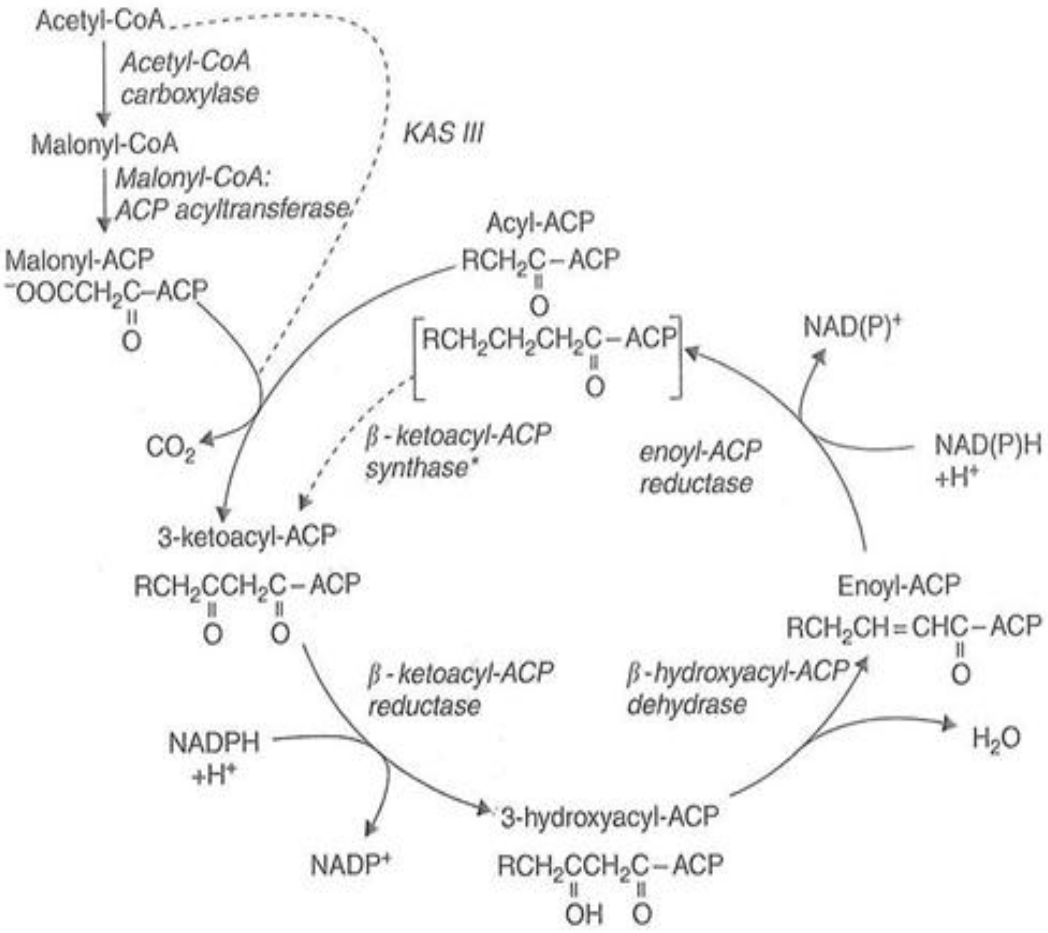

Figure 1. 11. Representation of Fatty Acids Synthetase (Hardwood, 2010).

The regulation fatty acids metabolism is modulated by the FasR regulator that is part of a highly conserved cluster among Actinomycetes: the *fab* operon (Arabolaza *et al.*, 2010). This cluster comprises the genes encoding the FAS II system: *fabD, fabH, acpP* and *fabF* (Figure 1. 12). FasR is essential for cell growth since deletion mutants show severe growth defects and altered physiological differentiation in *S. coelicolor* (Arabolaza *et al.*, 2010).

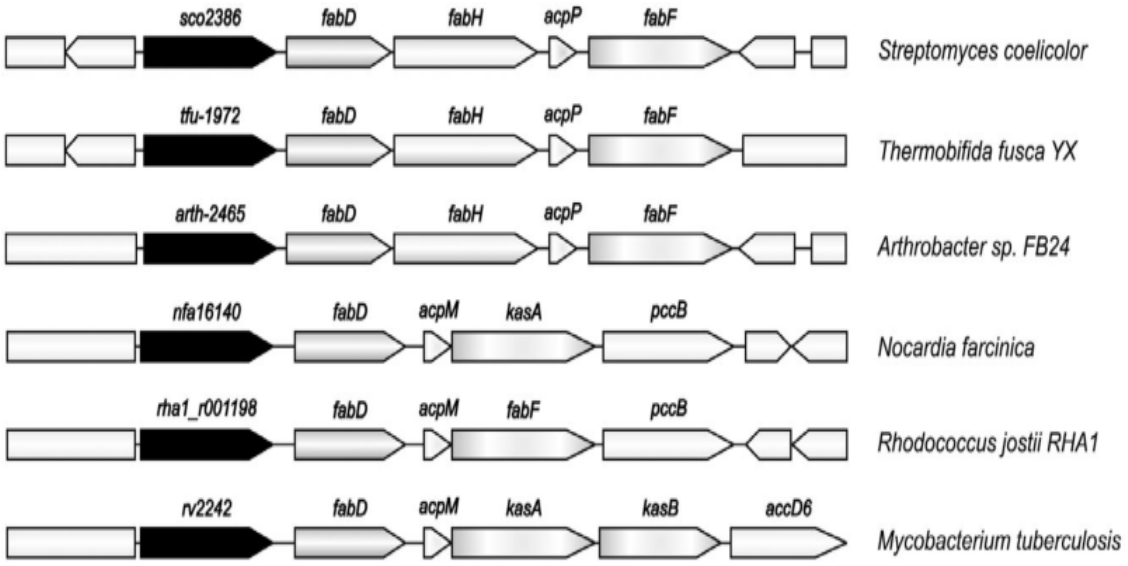

Figure 1. 12. Synteny of *fab* genes clusters in Actinomycetes (Arabolaza *et al.*, 2010).

1.4.2. Nitrogen metabolism

Streptomyces are soil-living bacteria that have to face nitrogen scarcity commonly found in their usual environmental conditions. Ammonium is their preferred nitrogen source but urea and nitrate can also be assimilated (Tiffert *et al.*, 2008). In *S. coelicolor*, ammonium is transported by the ammonium transporter *AmtB* (SCO5583). It can also be generated by deamination of amino acids (glutamine and glutamate catabolism) and by nitrate reduction *via* nitrite to ammonium by the enzymes nitrate reductase and nitrite reductase, respectively (Fink *et al.*, 1999; Moir and Wood, 2001). A summary of the genes involved in nitrogen metabolism of the *S. coelicolor* is shown in Table 1. 2.

Table 1. 2. Genes involved in nitrogen metabolism in S. coelicolor. Adapted from Reuther and Wohlleben (2007) and StrepDB database.

Gene	SCO name	Protein	Function
narG2	SCO0216	Nitrate reductase	Nitrate assimilation
narH2	SCO0217	Nitrate reductase	Nitrate assimilation
narJ2	SCO0218	Nitrate reductase	Nitrate assimilation

narI2	SCO0219	Nitrate reductase	Nitrate assimilation
ORF0518	SCO0518	Possible nitrate reductase	Nitrate assimilation
nasA	SCO2473	Nitrate reductase	Nitrate assimilation
narG3	SCO4947	Nitrate reductase	Nitrate assimilation
narH3	SCO4948	Nitrate reductase	Nitrate assimilation
narJ3	SCO4949	Nitrate reductase	Nitrate assimilation
narI3	SCO4950	Nitrate reductase	Nitrate assimilation
narI	SCO6532	Possible nitrate reductase	Nitrate assimilation
narJ	SCO6533	Possible nitrate reductase	Nitrate assimilation
narH	SCO6534	Possible nitrate reductase	Nitrate assimilation
narG	SCO6535	Possible nitrate reductase	Nitrate assimilation
narB	SCO7374	Nitrate reductase	Nitrate assimilation
nirB	SCO2486 *	Nitrite reductase	Nitrite assimilation
nirB	SCO2487	Nitrite reductase	Nitrite assimilation
nirC	SCO2488	Nitrite reductase	Nitrite assimilation
ORF6102	SCO6102	Nitrite/sulphite reductase	Nitrite assimilation
gdhA	SCO4683 *	NADP-dependent glutamate dehydrogenase (GDH)	Ammonium assimilation
glnA	SCO2198 *	Glutamine synthetase (GS) I	Ammonium assimilation
glnA2	SCO2241	GS-like	Unknown
glnA3	SCO6962	GS-like	Unknown
glnA4	SCO1613	GS-like	Unknown
glnII	SCO2210 *	Glutamine synthetase (GS) II	Ammonium assimilation
gltD	SCO1977	Glutamate synthase (GOGAT)	Glutamine catabolism
gltD	SCO2025	GOGAT	Glutamine catabolism

gltB	SCO2026	GOGAT	Glutamine catabolism
glnR	SCO4159	OmpR-like regulator	Transcriptional regulator
glnRII	SCO2213	OmpR-like regulator	Transcriptional regulator
amtB	SCO5583 *	Ammonium transporter	Ammonium uptake
glnK	SCO5584 *	Nitrogen-regulatory PII protein	Possible post-translational regulation
glnD	SCO5585 *	Adenylyltransferase	Post-translational regulation of PII
glnE	SCO2234	Adenylyltransferase	post-translational regulation of GS
ORF1863	SCO1863	Arginine-rich protein	Unknown
ureD	SCO1231	Urease accessory protein	Urea assimilation
ureG	SCO1232	Urease accessory protein	Urea assimilation
ureF	SCO1233	Urease accessory protein	Urea assimilation
ureC	SCO1234	Urease	Urea assimilation
ureB	SCO1235	Urease	Urea assimilation
ureA	SCO1236 *	Urease	Urea assimilation
ureAB	SCO5525	Urease	Urea assimilation
ureC	SCO5526	Urease	Urea assimilation

* Indicates those genes controlled by *glnR*

The transcriptional regulator *glnR* (SCO4159) is a major regulator of nitrogen metabolism in *Streptomyces*. *S. coelicolor* mutants lacking *glnR* are unable to reduce nitrite to ammonium resulting in lower growth rates than in wild-type strain (Tiffert *et al.*, 2008). The *glnR* master regulator controls positively the expression of the glutamine synthetases (GS) *glnA* and *glnII* but also represses the transcription of *ureA* and *gdhA*. The expression of *glnR* is up-regulated in conditions of nitrogen limitation (Tiffert *et al.*, 2008). It is important to mention that nitrogen limitation is widely known to trigger

fatty acids accumulation in various bacteria as well as antibiotics production in *Streptomyces* (Voelker and Altaba, 2001). In this regard, a recent study demonstrated that *glnR* activates RED production while it represses ACT production in *S. coelicolor;* in the same study, similar behavior was observed in *S. avermitilis*, avermectin production is enhanced while oligomycin production is down-regulated in a Δ*glnR* mutant of this specie (He *et al.*, 2016).

The enzyme glutamate dehydrogenase (GDH) converts αKG and ammonium into glutamate. Then, the incorporation of another molecule of ammonium into glutamate catalyzed by glutamine synthetase (GS) yields glutamine. Another enzyme, glutamate synthase (GOGAT) catalyzes the synthesis of glutamate from glutamine and αKG (Figure 1. 13) (Reuther and Wohlleben, 2007).

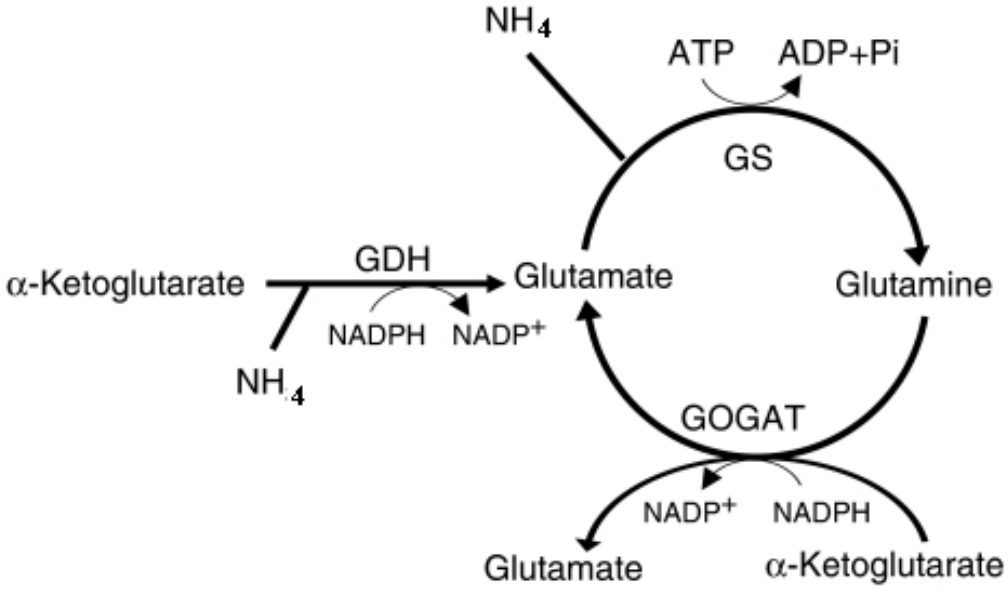

Figure 1. 13. Ammonium assimilation pathways.

1.4.3. Phosphate metabolism

Phosphorous (P) is an essential nutriment for growth in all living organisms since it is a constitutive part of crucial components of the living cells (nucleic acids, phospholipids, lipopolysaccharides, etc.). In *Streptomyces*, the phosphate-limiting condition is known to induce secondary metabolites production (Doull and Vining, 1990; Lounes *et al.*, 1996; Santos-Beneit, 2015; Martin *et al.*, 2017). The enzymes

involved in scavenging and transport of phosphate are various phosphatases and specific high affinity phosphate transporters which are under the positive control of the two component system phosphate regulator *PhoR-PhoP* (Sola-Landa *et al.*, 2003). The PhoR sensor kinase auto-phosphorylates under phosphate limitation and transfers its phosphate group to PhoP. Phosphorylated PhoP has enhanced affinity for specific sequences (PHO boxes) present in the promoter regions of genes of the *pho* regulon, the expression of the latter is either induced or repressed by PhoP (Allenby *et al.*, 2012; Santos-Beneit, 2015).

The master phosphate regulator PhoP performs a major positive regulatory role of phosphate metabolism but also a negative role of other biological processes, including nitrogen metabolism, oxidative phosphorylation, nucleotide biosynthesis, glycogen catabolism as well as secondary metabolite biosynthesis (Figure 1. 14). A PhoP Chip on chip experiment expanded considerably the number of PhoP targeted regions up to 417 (Allenby *et al.*, 2012).

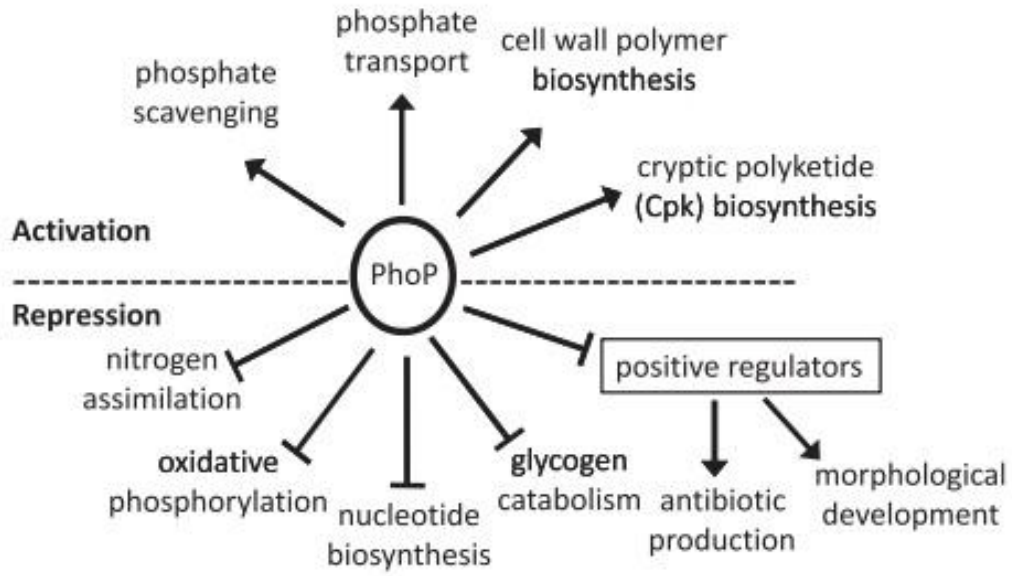

Figure 1. 14. Pathways and biological processes controlled by the two-component system PhoR/PhoP in condition of phosphate limitation (Allenby *et al.*, 2012).

Comparative proteomic and transcriptomics analysis of *PhoP* mutant and wild-type *S. coelicolor* cultures revealed the up-regulation of phosphate-scavenging and specific transport systems under phosphate limitation (Rodriguez-Garcia *et al.*, 2007; Santos-

Beneit *et al.*, 2008). These genes included phosphatases like *phoA*, *phoC*, *phoD* and a phythase as well as the phosphate transporters *pstA*, *pstB*, *pstC* and *pstS*. (Rodriguez-Garcia *et al.*, 2007). Furthermore, PhoP exerts a negative impact on nitrogen metabolism since it represses the expression of the master regulator GlnR in *S. coelicolor* as well as other specific regulatory genes of nitrogen metabolism (Sola-Landa *et al.*, 2013). PhoP represses also the expression of AfsR-AfsS, a regulatory complex that positively activates the biosynthesis of ACT and RED by targeting *actII-ORF4* and *redD*, respectively (Umeyama *et al.*, 2002).

1.4.4. Respiratory chain

The process known as respiratory chain or oxidative phosphorylation takes place in the cytoplasmic membrane of bacteria. The respiratory function generates an electrochemical gradient across the inner membrane via the translocation of protons derived from the oxidation of NADH and succinate. This proton motive force may then be used by the ATP synthase to synthesize ATP. This gradient is achieved depending on environmental and genetic factors. In this regard, respiratory metabolism in bacteria is modular and enables the utilization of the respiratory components in different combinations to optimize respiration and energy conservation under variable conditions (Berg *et al.*, 2002; Shepherd and Poole, 2013).

In *Streptomyces*, the protein complexes involved in oxidative phosphorylation usually include: NADH dehydrogenase I (complex 1), succinate dehydrogenase (complex II), cytochrome bc1 complex (complex III), cytochrome c oxidase (complex IV) and ATP synthase (complex V) (Figure 1. 15). The overall respiration relies on menaquinones as sole lipid-soluble electron and proton carriers (Collins and Jones, 1981).

S. coelicolor genome contains two different types of NADH dehydrogenases, one is a proton or sodium-pumping system (NADH-1) encoded by two putative operons and several orphan genes (SCO4562-SCO4575, SCO4599-SCO4608, SCO6954, SCO 6956), and the other is a non-proton pumping system (NADH-2) encoded by *ndh* genes (SCO4119, SCO3092, SCO6496 and SCO7101) (Bentley *et al.*, 2002; Melo *et al.*, 2004; Schneider *et al.*, 2008).

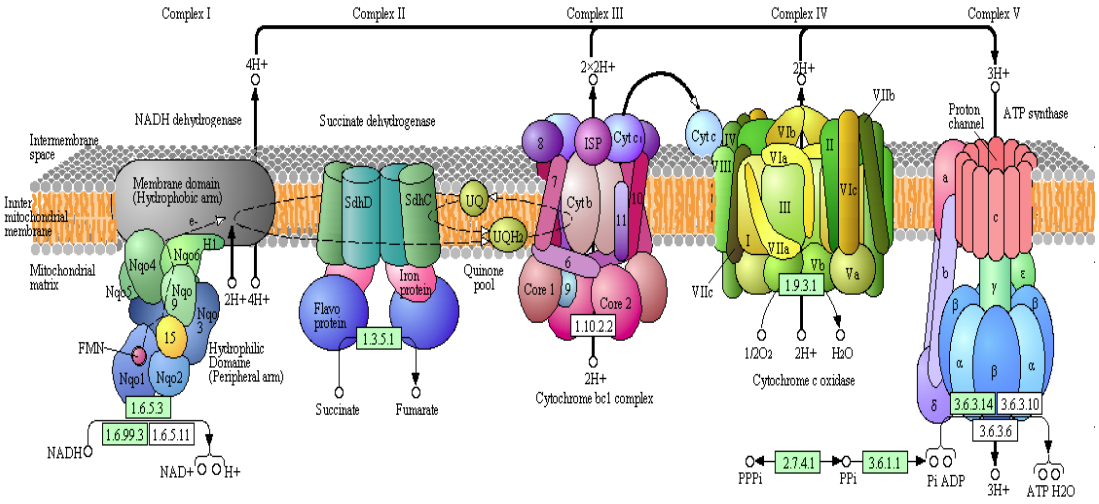

Figure 1. 15. Oxidative phosphorylation representation (Kegg Pathways Database, http://www.kegg.jp/)

The respiratory chain can accept electrons from different substrates (Figure 1. 16), including: electron transfer flavoproteins (ETF), NADH, pyruvate, succinate and *a priori* lactate could also be used as electron transfer system under fermentative conditions (Bentley *et al.*, 2002).

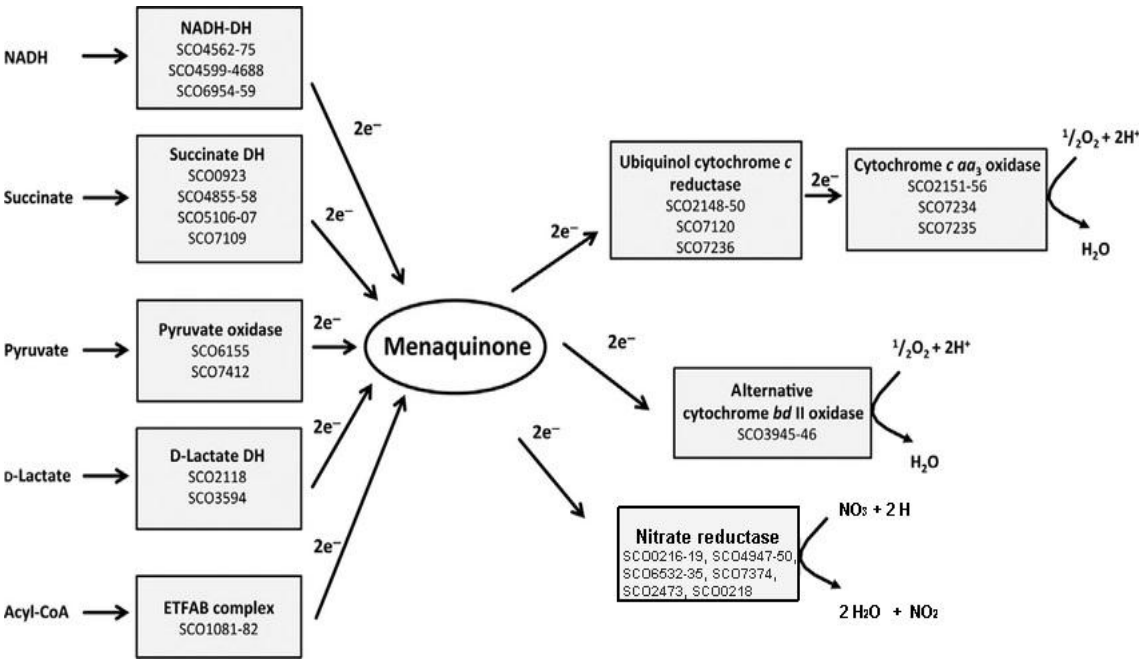

Figure 1. 16. Possible electron donors and cytochrome oxidases encoded in the genome of *S. coelicolor*. Adapted from Sawers *et al.* (2016).

Even if it considered as obligate aerobic bacteria, *Streptomyces* can also survive under oxygen-limiting conditions using nitrogen as final electron acceptor *via* nitrate reductases (Fischer *et al.*, 2010; Fischer *et al.*, 2014). Interestingly, some genes involved in oxidative phosphorylation (cytocrome C and B oxidase complexes, NADH dehydrogenase, succinate dehydrogenase, and nitrate reductase) are under the negative control of the phosphate master regulator PhoP (Figure 1. 14). This indicates that in condition of P limitation, respiration and ATP synthesis slows down. A temporal comparative analysis of *S. coelicolor* wild-type and PhoP deletion-mutants, carried out in conditions of phosphate limitation revealed that the genes encoding enzymes of oxidative phosphorylation are repressed whereas those encoding nitrate reductases are induced (Rodriguez-Garcia *et al.*, 2007; Allenby *et al.*, 2012). These results evidence the ability of *Streptomyces* to switch from aerobic respiration to nitrate respiration.

1.4.5. Storage compounds

Streptomyces cells can store carbon, phosphate and energy for later use in different forms including: glycogen, trehalose, triacylglycerol and/or polyphosphate.

1.4.5.1. Glycogen and trehalose

Glycogen is an α-glucan polymer widespread among living organisms that serves as carbon storage and is commonly synthesized when there is an excess of carbon source (Preiss, 2006). Its biosynthesis from glucose-1-phosphate (G1P) involves the activation of glucose as UDP-glucose by the nucleotide diphosphoglucose pyrophosphorylase (GlgC), UDP-glucose is then polymerized by the glycogen synthase (GlgA) to form a glucan that is transformed into glycogen by the branching enzyme (GlgB). Eventually, glycogen catabolism results in G1P and is carried out by the enzymes glycogen phosphorylase (GlgP) and the debranching enzyme (GlgX). (Preiss, 2006).

Glycogen accumulation in *Streptomyces* occurs transiently in two distinct phases, the first one occurs in the substrate mycelium where aerial branches emerge and the second phase occurs in the tips of aerial hyphae that are undergoing sporulation (Braña *et al.*, 1986; Yeo and Chater, 2005).

Other important storage carbohydrate is trehalose. This disaccharide is present in spores and also functions as stress-protectant, helping to overcome desiccation, cold and osmotic stress (Martín *et al.*, 1986). Trehalose is synthesized in bacteria from glucose phosphate intermediates via trehalose 6-phosphate, using the *GalU-OtsA-OtsB* system (Figure 1. 17). A new *GlgE* pathway, interconnecting threalose and glycogen biosynthetic pathways, has been identified in *Mycobacterium tuberculosis* (Kalscheuer *et al.*, 2010), a close relative of *Streptomyces*, whose key enzymes are also present in the chromosome of *S. coelicolor* (Schneider *et al.*, 2000). In this pathway, trehalose is isomerized into maltose by trehalose isomerase (TreS) and maltokinase Pep2 that phosphorylates maltose using ATP. Afterwards, a novel maltosyltransferase (GlgE) uses α-maltose 1-phosphate as the building block to extend the glucan chains of glycogen (Figure 1. 17).

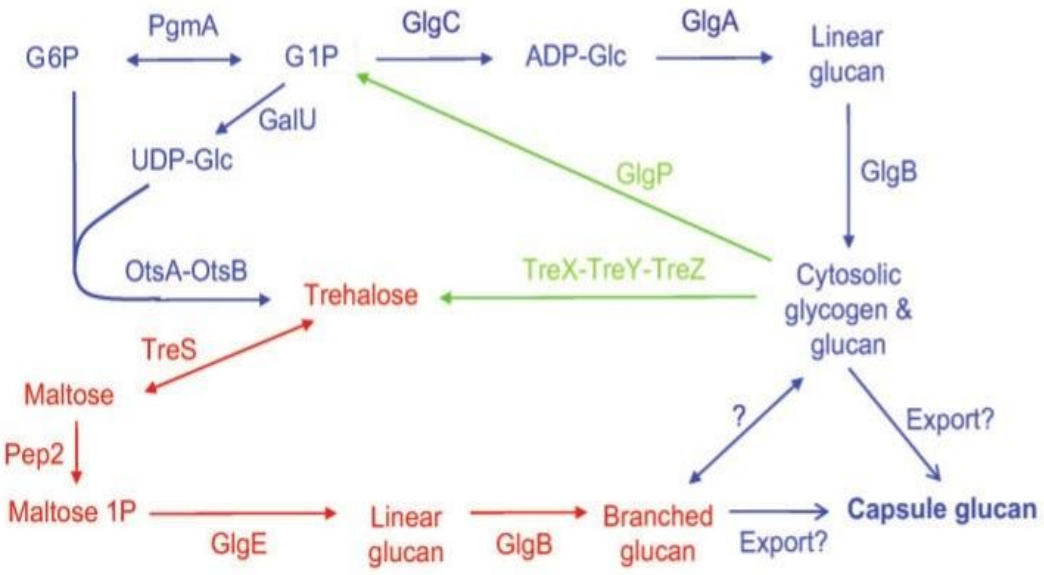

Figure 1. 17. Glucan pathways in *Streptomyces* (Chandra *et al.*, 2011). Classical glycogen pathway (blue). Newly identified *GlgE* pathway (red). Catabolism pathway (green).

1.4.5.1. Triacylglycerols

Triacylglycerols (TAG) consist of a esterified glycerol backbone with three long-chain fatty acids structures and are the most common carbon-based energy reserve in living organisms (Alvarez and Steinbuchel, 2002). Some *Streptomyces* species are able

to store large amounts of TAG (5-41% of dry cell weight) mainly during stationary phase of growth (Olukoshi and Packter, 1994; Arabolaza *et al.*, 2008; Rottig *et al.*, 2016). The biosynthesis of TAG and that of the membranous phospholipids (PL) share common biosynthetic steps. The third position of the glycerol backbone is esterified by a third fatty acid in the case of TAG (also called neutral lipids) and by a polar group linked by a phosphate in the case of PL (Heath *et al.*, 2002).

Both TAG and PL are synthesized *de novo* via the gly3P pathway (Figure 1. 18). In this pathway, gly3P is sequentially acylated with fatty acyl-CoAs by gly3P-acyltransferase (GPAT) and 1-acylglycerol–3-phosphate acyltransferase (AGPAT) to yield phosphatidic acid (PA). PA is then dephosphorylated into diacylglycerol (DAG) by phosphatidic acid phosphatase (PAP). DAG is used in the subsequent biosynthetic pathways for membrane PL or storage lipids (TAG) biosynthesis. In the final step, DAG is acylated into TAG by a DAG acyltransferase (DGAT) (Arabolaza *et al.*, 2008).

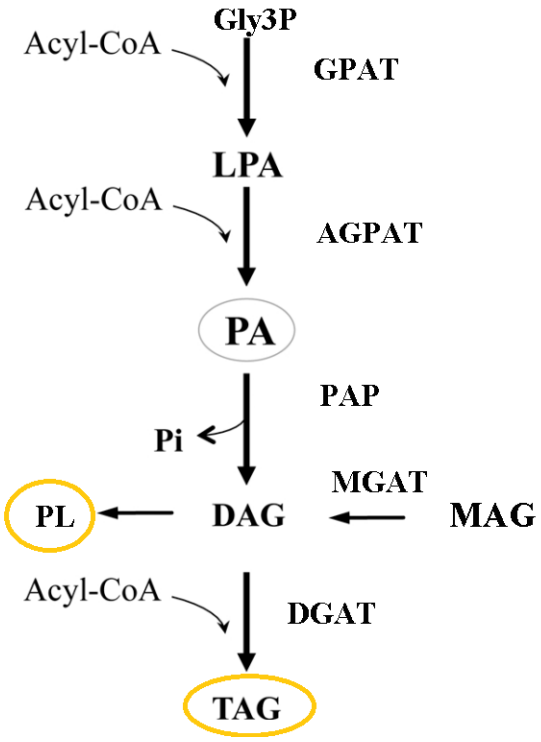

Figure 1. 18. Triacylglycerols and phospholipids biosynthetic pathways.

1.4.5.2. Polyphosphates

The polyphosphate (polyP) is a linear polymer of a few to many hundreds of phosphate (P) residues linked by high-energy phosphoanhydride bond (Figure 1. 19) (Kulaev *et al.*, 2005). This polymer constitutes a reservoir of phosphate and energy. It can also be used by some enzymes in replacement of ATP (Van Dien and Keasling, 1999).

In cells the content of polyP results from the action of enzymes that catalyze the synthesis (polyP kinases (Ppk), enzymatic system linked to oxidative phosphorylation) and degradation (endo and exo-polyphosphatase) of this polymer (Smirnov *et al.*, 2015). Bacteria express two polyP kinases PPK1 and PPK2 that catalyzes the reversible polymerization of γ-phosphate of ATP or GTP, respectively, into polyP (Zhang *et al.*, 2002).The PPK1 or adenosine diphosphate kinase (ADPK) activity of these enzymes depends on the ATP/ADP ratio *in vivo* or in the reaction mix *in vitro*.

In *Streptomyces*, the polyphosphate kinase gene (*ppk*, SCO4145) is a member of the *pho* regulon (Ghorbel *et al.*, 2006) and participates in polyP degradation via its ADPK activity in order to regenerate ATP from ADP and polyP (Esnault *et al.*, 2017). Moreover, some studies have shown that disruption of *ppk* gene in *S. lividans* induces antibiotic production in conditions of P limitation suggesting that energetic stress is a strong trigger factor for antibiotics biosynthesis (Chouayekh and Virolle, 2002; Diaz *et al.*, 2013; Esnault *et al.*, 2017).

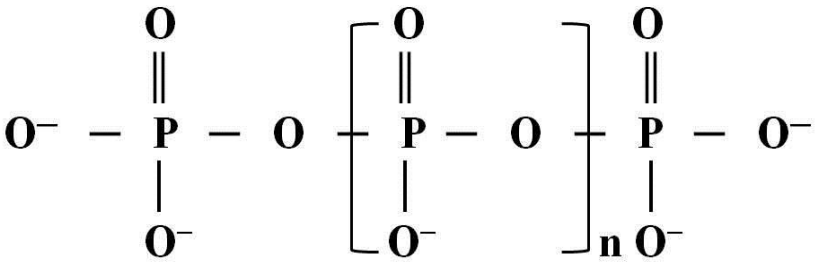

Figure 1. 19. Polyphosphate structure.

1.5. Secondary metabolism in the model specie *Streptomyces coelicolor* and its regulation

Secondary metabolism consists of metabolic pathways and products that are not directly involved in growth of an organism. In this concern, many secondary metabolites are bioactive compounds that are not involved directly on growth, development or reproduction of an organism. The *Streptomyces* genus represent an important source of natural bioactive compounds useful in modern medicine and in agriculture, these compounds include: antibacterial, antifungals, immuno-suppressants, anticancer agents, anti-inflamatory agents, anthelmintics, insecticides and herbicides (Challis, 2014). Precursor molecules for production of secondary metabolites are generated from primary metabolism, it is therefore rational that changes in primary metabolism subsequently impact secondary metabolism (Figure 1. 20).

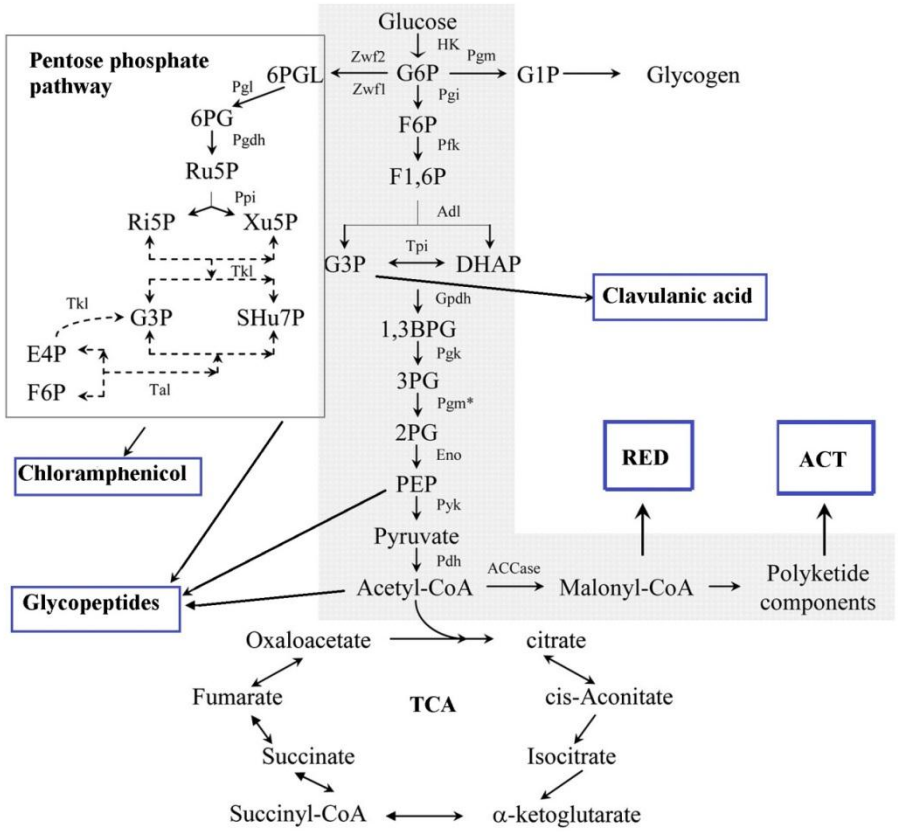

Figure 1. 20. Relationship between primary metabolism and some precursors of Actinomycete-derived antibiotics.

After the 1940's to 1960's, period known as the "golden age" of antibiotics discovery (Figure A), research was committed to unravel the molecular mechanisms involved in secondary metabolites biosynthesis and its regulation. Historically, the specie *S. coelicolor* M145 (lacking of the two plasmids SCP1 and SCP2) was chosen as a model organism since it produces pigmented antibiotics that are visually noticeable, the red-pigmented undecylprodigiosin (RED) and the pH-dependent blue-pigmented actinorhodin (ACT) antibiotics (Hopwood, 2007). The production of these colored molecules greatly facilitated the use of classical genetic approaches (isolation of non- or hyper-producing mutants) to study the regulation of antibiotics production.

The name of *S. coelicolor* means "sky color" in Latin and refers to the production of the blue-pigmented ACT antibiotic. The genome of this specie was the first of the *Streptomyces* genus to be fully sequenced and annotated. Unexpectedly, the genome sequence revealed that *Streptomyces* genus was largely underestimated concerning its capacity to produce secondary metabolites (Bentley *et al.*, 2002). Indeed, *S. coelicolor* was known to synthesize five secondary metabolites with antibiotic activities, including: methylenomycin (cluster carried by the plasmid SCP1 (Hayes *et al.*, 1997)), *whiE* gray-colored spore pigment, calcium-dependent antibiotics (CDA), RED and ACT, ordered by their production at the different stages of growth (Figure 1. 21).

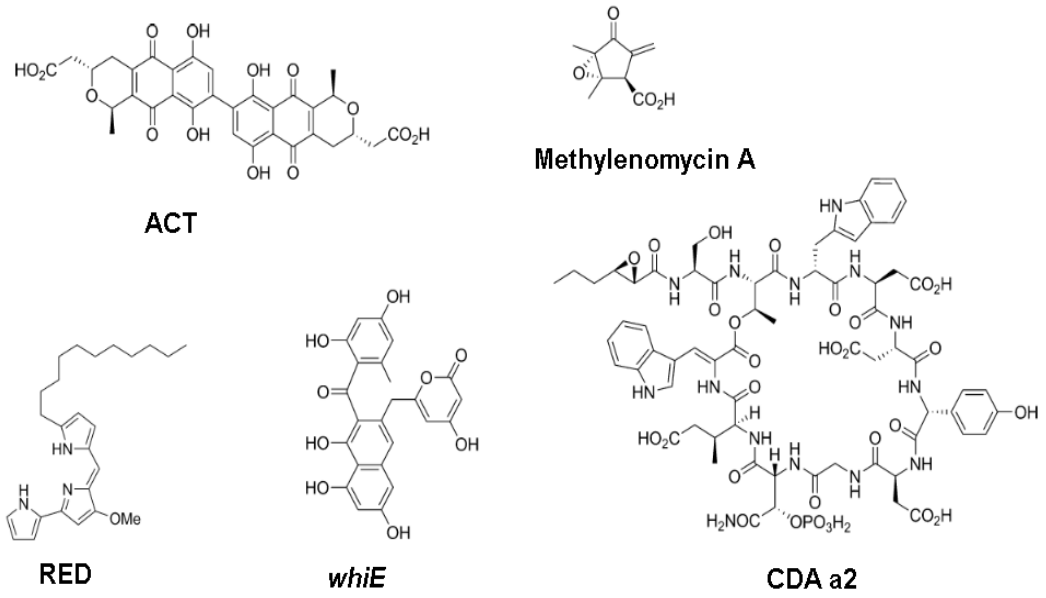

Figure 1. 21. Some secondary metabolites synthesized by *S. coelicolor*.

Indeed the use of automated scanning bioinformatic tools to detect specialized metabolite gene clusters (Medema *et al.*, 2011; Medema *et al.*, 2015) revealed that *S. coelicolor* harbors gene clusters likely to direct the synthesis of at least 20 different secondary metabolites. These include polyketides, non-ribosomal peptides (NRP), γ-butyrolactones, terpenoids, and oligopyrroles (Table 1. 3). However, the expression of most of these secondary metabolites biosynthetic pathways detected *in silico* is very weak so they are qualified of "cryptic" or "silent". This means that specific and usually non-conventional cultivation conditions are necessary to trigger their biosynthesis and that novel strategies to enhance their expression should be conceived and implemented.

Table 1. 3. Gene clusters of secondary metabolites produced by *S. coelicolor* (van Keulen and Dyson, 2014).

Class	Sub class	Metabolite	SCO number
Polyketides	Type I	CPK, coelimycin A/P1	SCO6265 - SCO6288
	Type I	Unknown polyketide	SCO6826 - SCO6827
	Type II	ACT	SCO5071 - SCO5092
	Type II	*WhiE*, gray spore pigment TW95a	SCO5314 - SCO5321
	Type III	Flaviolin	SCO1206 - SCO1208
	Type III	Germicidin A	SCO7221
	Type III	Triketide pyrones	SCO7669 - SCO7671
Fatty acids	Type I PKS/FAS	Ecosapentaenoic acids	SCO0124 - SCO0129
	Type II	Unknown fatty acid	SCO1265 - SCO1273
Terpenoids	Tetraterpenoid	Isorenieratene, β-carotene	SCO0185 - SCO0191
	Triterpenoid	Hopene	SCO6759 - SCO6771
	Sesquiterpenoid	Albaflavenone	SCO5222 - SCO5223
	Sesquiterpenoid	Geosmin	SCO6073
	Monoterpenoid	2-Methylisoborneol	SCO7700 - SCO7701
Peptides	Non-ribosomal	CDA	SCO3210 - SCO3249

	lipopeptide		
	NRP	Unknown peptide	SCO6429 - SCO6438
	NRP	Coelibactin	SCO7676 - SCO7792
	Ribosomally synthesized and Posttranslationally modified Peptides (RiPP)	Unknown bacteriocin	SCO0753 - SCO0756
	RiPP	Unknown Class I lanthipeptide	SCO0256 - SCO0270
	RiPP	SapB Class I lanthipeptide	SCO6681 - SCO6685
	RiPP	Unknown Class I lanthipeptide	SCO6929 - SCO6932
	RiPP	Unknown bacteriocin ?	SCO6045
	NRP hydroxamate	Siderophore coelichelin	SCO0484 - SCO0499
Hybrids and other	NRPS independent siderophore	Desferrioxamine B, E, G_1 , amphiphilic D_1 like	SCO2782 - SCO2785
	NRPS independent siderophore	Unknown siderophore	SCO5799 - SCO5801
	NRPS independent siderophore	Unknown siderophore	SCO6226 - SCO6227
	Olygopyrrole	Prodigiosins, streptorubin, RED	SCO5877 - SCO5898
	γ-Butyrolactone	SCB1, *scbA*	SCO6266
	Carbohydrate	Unknown deoxysugar	SCO0381 - SCO0401
	Monophenolic compound	Unknown melanin	SCO2700 - SCO2701

1.5.1. Polyketides and fatty acids

Polyketides belong to a large class of bioactive compounds used in a wide range of applications in medicine and agriculture. Polyketides are synthesized by a family of enzyme complexes named polyketide synthases (PKS). PKS are evolutionary related to FAS machinery responsible for the *de novo* synthesis of fatty acid (Cronan and Thomas, 2009). Simple carboxylic acid derivatives (acetyl-CoA, malonyl-CoA and methylmalonyl-CoA) are concatenated into linear chains by iterative Claisen condensation, followed in some cases by reductive modification of the resulting β-ketone groups (Weissman, 2009). PKSs have been classified as type I, II, and III according to the modularity (Type II and II) or not (Type I) of their structure (Figure 1. 22).

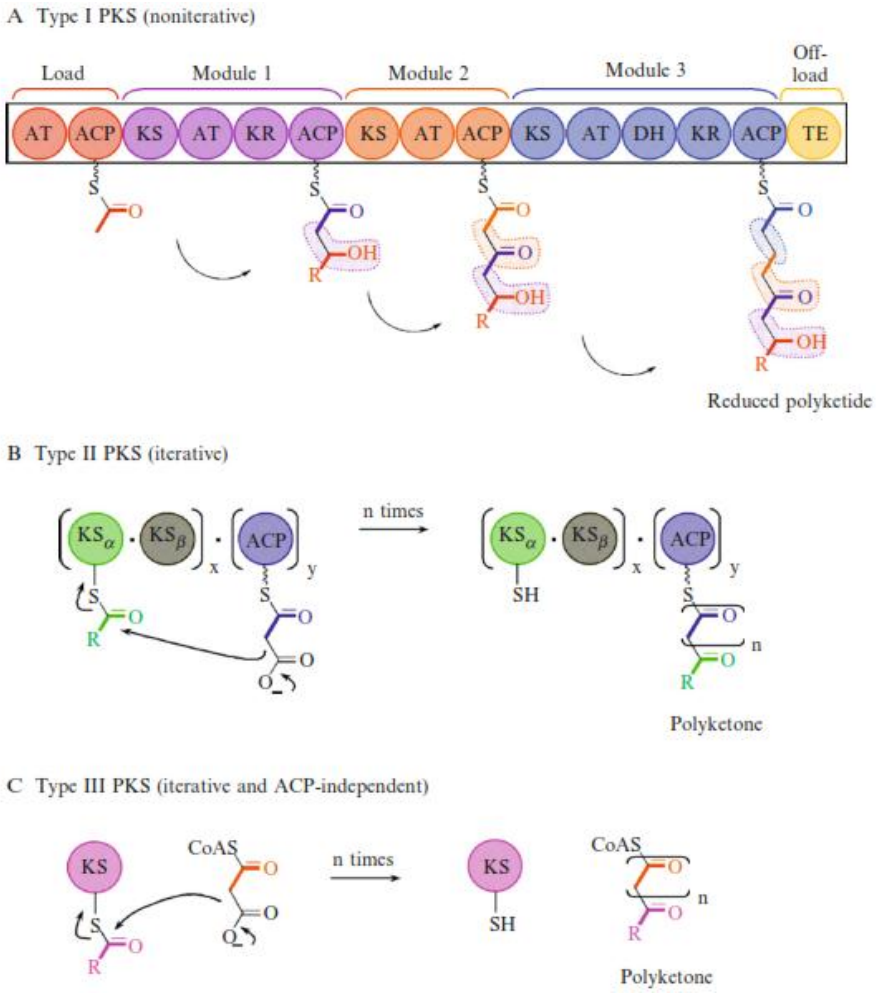

Figure 1. 22. Representation of different types of PKS (Weissman, 2009).

Type I PKSs are multifunctional proteins with individual functional domains necessary for one cycle of β-keto chain elongation and processing, and can be sub-classified into modular and iterative. In modular PKS, each polypeptide contains one or multiple modules, and each module is responsible for one round of condensation and β-keto chain processing. Each catalytic domain of modular type I PKSs is used only once during the biosynthetic process. In contrast, iterative type I PKSs are monomodular and conduct multiple rounds of chain elongation and β-keto chain processing using their catalytic domains multiple times (Keatinge-Clay, 2012). In *Streptomyces*, type I modular PKS are the most common megasynthases where each module contains the three domains required to catalyze one cycle of chain extension: ketosynthase (KS), acyltransferase (AT) and acyl carrier protein (ACP). In addition, three domains associated to keto group modification are also part of type I modular PKS, including ketoreductase (KR), dehydratase (DH) and enoyl reductase (ER) (Staunton and Weissman, 2001). Genome mining approaches helped to identify the biosynthetic cluster of the "silent" yellow pigment (CPK) in *S. coelicolor* that encodes a hexamodular type I PKS responsible for the synthesis of a reduced polyketide by decarboxylative condensation of six malonyl groups (Gomez-Escribano *et al.*, 2012).

Type II PKS are iterative PKS that consist of complexes of individual monofunctional proteins. The chain initiation and elongation are achieved by two ketosynthase-like condensing enzymes and an ACP to which the growing chain is covalently attached as a thioester link. Additional enzymes are involved in the extender and folding pattern of the polyketide chain, including: malonyl-CoA:ACP transferase, KR, cyclases and aromatases (Weissman, 2009). The biosynthetic gene clusters of two aromatic polyketides, the blue-pigmented ACT and the grey spore pigment *whiE*, are the most representative type II PKS in *S. coelicolor* (Yu *et al.*, 1998; Hopwood, 2007).

Type III PKS, also known as chalcone and stilbene synthases, use a single KS-like active site to catalyze the repetitive condensation of acetate units to a CoA-derivatized starter molecule and typically yield mono- and bi-cyclic aromatic products. Acyl groups supply is not dependent on ACP domains. Instead type III PKS use acyl-CoA substrates for chain extension that is often followed by intramolecular condensation and aromatization of the linear intermediates within the same PKS active site cavity (Austin and Noel, 2003). The genome sequence of *S. coelicolor* harbors three type III PKS

responsible for the biosynthesis of flaviolin (SCO1206 – SCO1208), germicidin A (SCO7221) and triketide pyrones (SCO7669 – SCO7671) (Challis, 2014; van Keulen and Dyson, 2014).

1.5.2. Non-ribosomal Peptides (NRP) biosynthesis

Another class of secondary metabolites produced by Streptomycetes is the Nonribosomal Peptides (NRP), commonly synthesized by NRP synthetases (NRPS). The NRPS are modular enzymes that catalyze the synthesis of peptide products from standard and non-proteinogenic amino acids and are frequently modified by the addition of a number of functional prosthetic groups such as methyl, acetyl, or hydroxyl groups (Strieker *et al.*, 2010). This feature of NRPS represents a large number of possibilities to synthesize complex and biologically active molecules. The genome of *S. coelicolor* contains gene clusters capable to synthesize a large amount of NRP such as: coelibactin, siderophores (coelichelin, desferrioxamine), lipopeptides (CDA) and lanthipeptides (SapB, Table 1. 3).

The organization of modules from NRPS consists of at least three core domains catalyzing a specific reaction that incorporates a monomer (Figure 1. 23).

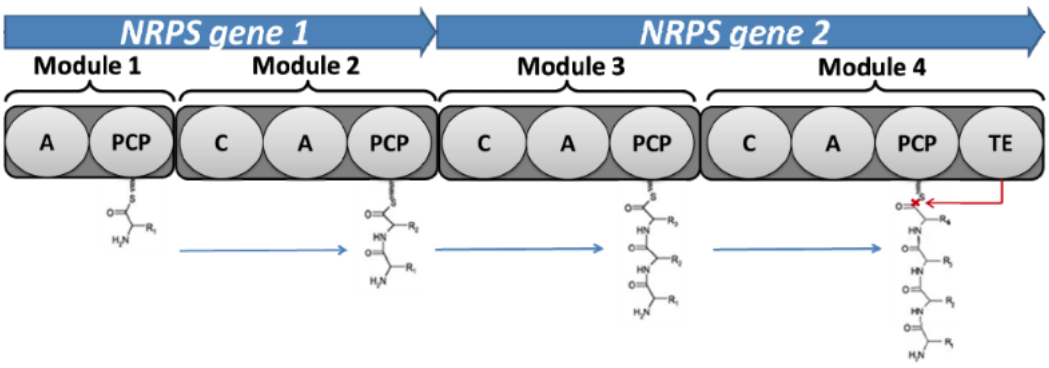

Figure 1. 23. Representation of a NRPS composed of four modules encoded by two genes (Argüelles Arias *et al.*, 2011).

These domains are: the adenylation (A) domain that selects the cognate amino acid that it activates by transforming it into an amino acyl adenylate; the thiolation or peptidyl carrier protein (PCP) domain that covalently binds the activated monomer to the synthetase by a phosphopantetheinyl arm; and, the condensation (C) domain that

catalyzes the formation of a peptide bond between the amino acids linked into two adjacent modules. The first module, a loading module, contains only A and PCP domains, and the termination module contains also a thioesterase (TE) domain, which is in charge of releasing the peptide from the synthetase (Finking and Marahiel, 2004; Argüelles Arias *et al.*, 2011).

1.5.3. Terpenoids

Terpenoids are a vast and diverse group of secondary metabolites derived from the five-carbon monomer isoprenyl diphosphate (IPP) and its isomer dimethylallyl diphosphate (DMAPP). The isoprenyl substrates can be cyclized by terpene cyclase into single-ring or multi-ring products, which can be further diversified by subsequent modification reactions, such as hydroxylation and glycosylation (Cane and Ikeda, 2012; Kuzuyama, 2017).

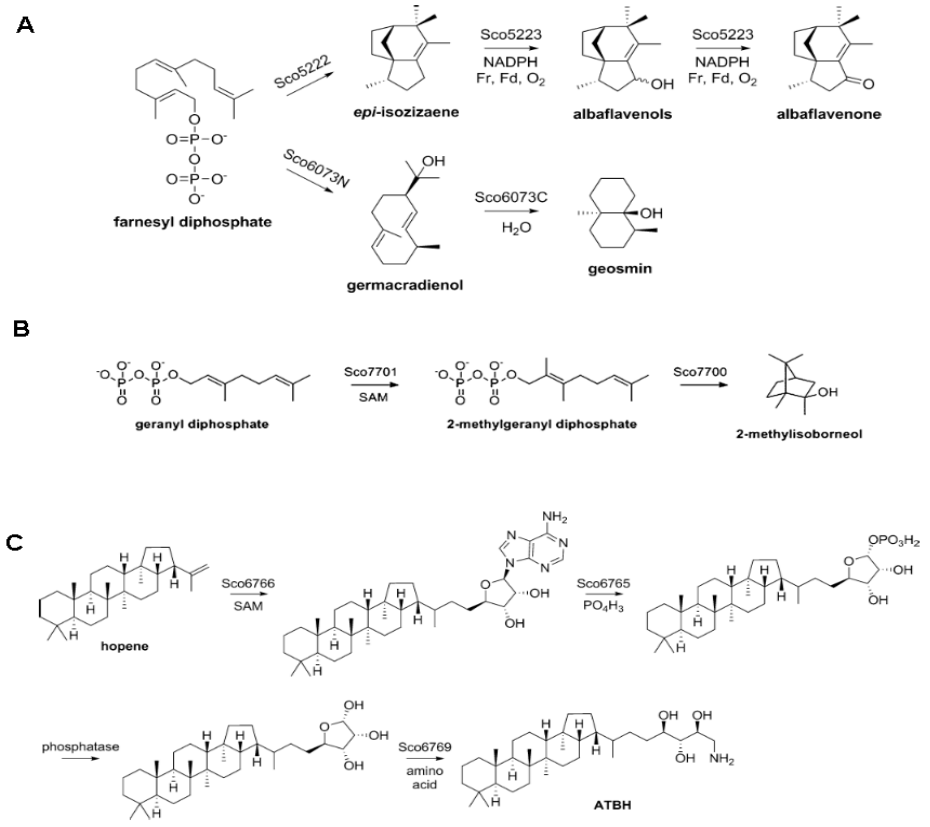

Figure 1. 24. Proposed biosynthetic pathways of albaflavenone, geosmin (A), 2-methylisoborneol (B) and aminotrihydroxybacteriohopane (ATBH) in *S. coelicolor* (Challis, 2014).

The chemical diversity of terpenoids results in a large variety of bioactive compounds. In the case of *S. coelicolor*, five terpenoid biosynthetic clusters have been identified on its genome (Figure 1. 24 and Figure 1. 25), including those that synthesize: the tetraterpenoids isorenieratene and β-carotene (SCO0185 – SCO0191), the triterpenoids hopene and aminotrihydroxybacteriohopane (ATBH) (SCO6759 – SCO6771), the esquiterpenoids albaflavenone and farnesene (SCO5222 – SCO5223), the earthy odor sesquiterpenoid geosmin (SCO6073) and the monoterpenoid 2-methylisoborneol (SCO7700 – SCO7701) (Bentley *et al.*, 2002; van Keulen and Dyson, 2014).

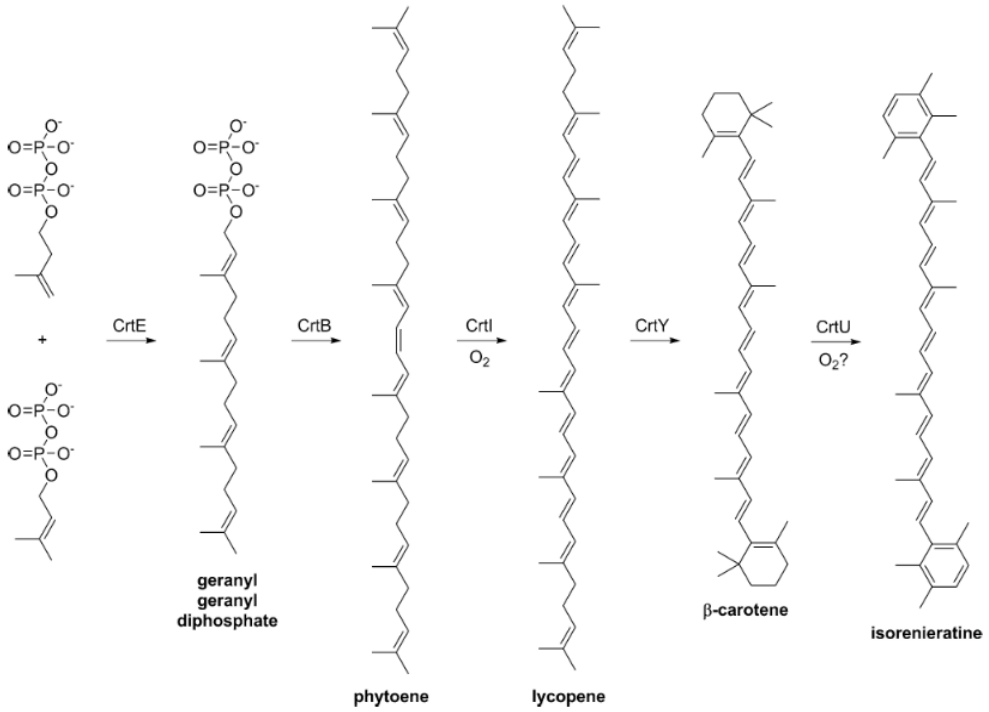

Figure 1. 25. Proposed pathway of isorenieratine and β-carotene biosynthesis in *S. coelicolor* (Challis, 2014).

1.5.4. Regulation of secondary metabolites in *S. coelicolor*

Secondary metabolites production is generally activated under nutriment-starving or stress conditions that occur at the end of vegetative growth of *Streptomyces*. These conditions are accompanied with cell growth arrest that induces complex changes in regulatory gene expression related to secondary metabolites production (Nieselt *et al.*,

2010). The expression of secondary metabolites is controlled by regulators that are classified in two main groups: the cluster-situated regulators (CSR) and the global or pleiotropic regulators (Bibb, 2005; Huang *et al.*, 2005). CRS are present in the biosynthetic pathway of a given secondary metabolite and control the expression of genes of the same cluster, whereas global regulators control, directly or indirectly, the expression of one or more pathways and/or genes of primary metabolism.

The regulation of secondary metabolites production in the model specie *S. coelicolor* has been reviewed in detail by Bibb (2005), Liu *et al.* (2013) and van Wezel and McDowall (2011). A brief summary of the main regulators involved in secondary metabolite production is presented below (Table 1. 4).

Table 1. 4. Regulatory genes involved in secondary metabolites biosynthesis in *S. coelicolor*.

Gene (SCO name)	**Function**	**Reference**
	Cluster-situated regulators	
actII-ORF4 (SCO5085)	Activator of ACT biosynthetic cluster	(Fujii *et al.*, 1996; Arias *et al.*, 1999)
redD (SCO5877)	Activator of RED biosynthetic cluster	(Fujii *et al.*, 1996)
redZ (SCO5881)	Transcriptional activator of *redD*	(Wang *et al.*, 2009)
cdaR (SCO3217)	Regulator of CDA biosynthetic cluster	(Ryding *et al.*, 2002)
absA1/2 (SCO3225, SCO3226)	Two-component system located in CDA biosynthetic cluster. This system represses ACT, RED and CDA production by binding to specific sites upstream of genes encoding regulators of these secondary metabolites.	(McKenzie and Nodwell, 2007)

kasO (SCO6280)	Activator of the silent polyketide CPK cluster	(Takano *et al.*, 2005)
scbR (SCO6265)	Transcriptional repressor of *kasO*. DNA-binding activity impaired by the presence of bacterial hormones γ-butyrolactones.	(Takano *et al.*, 2001; Li *et al.*, 2015)
scbA (SCO6266)	Synthesize γ-butyrolactone hormones and is activated by *scbR*. Inactivation of *scbA* enhances production of ACT and RED.	(Takano *et al.*, 2001)
Pleiotropic regulators		
dasR (SCO5231)	Pleiotropic transcriptional repressor of *actII-ORF4*. Master regulator of genes involved in N-acetylglucosamine transport and catabolism as well as in chitin catabolism, secondary metabolism and stress responses.	(Rigali *et al.*, 2008; Nazari *et al.*, 2013)
rok7B7 (SCO6008)	Transcriptional activator of *actII-ORF4*. It represses *redD* expression.	(Park *et al.*, 2009)
ramR (SCO6685)	Orphan regulator member of the NarL/FixJ family regulators. Binds to the *ramC* promoter and activates the transcription of the *ramCSAB* operon, responsible of the biosynthesis of the lantipeptide SapB.	(Nguyen *et al.*, 2002; O'Connor and Nodwell, 2005)
afsS (SCO4425)	Regulator required for ACT biosynthesis. Modulates stress response to phosphate, nitrogen and sulfate limitation.	(Horinouchi, 2003; Lian *et al.*, 2008; Allenby *et al.*, 2012)
afsR (SCO4426)	Activates *afsS* and competes for its activation with the phosphate master regulator PhoP. DNA-binding activity is blocked by phosphorylation events.	(Santos-Beneit *et al.*, 2011; Allenby *et al.*, 2012)
afsK (SCO4423)	Serine/threonine kinase that phosphorylates AfsR.	(Lee *et al.*, 2002)

pkaG (SCO4487) and *afsL* (SCO4377)	AfsR-like kinases that phosphorylates AfsR. It impacts indirectly on ACT biosynthesis.	(Sawai *et al.*, 2004)
SCO0608 and SCO6808	Binds promoters of *actII-ORF4* and *redD* to repress antibiotic production.	(Yang *et al.*, 2008)
nsdA (SCO5582)	Tetratricopeptide repeat (TPR) protein that represses ACT biosynthesis.	(Li *et al.*, 2006)
nsdB (SCO7252)	TPR protein that represses ACT and CDA production.	(Zhang *et al.*, 2007)
absB (SCO5572)	Pleiotropic gene regulator of ACT, RED and CDA biosynthesis. Deletion mutant affects sporulation maturation.	(Huang *et al.*, 2005)
absC (SCO5405)	MarR-like regulator whose deletion affects RED production and has an impact on pH due to over-production of pyruvate and α-ketoglutarate.	(Yang *et al.*, 2010)
	Sigma-AntiSigma-Anti/Anti sigma	
sigQ (SCO4908)	Putative sigma factor whose deletion induces precocious hyperproduction of ACT, RED and CDA. Deletion mutants exert delayed aerial spores formation.	(Shu *et al.*, 2009)
	WhiB-like regulators	
wblA (SCO3579)	WhiB-like regulator whose over-expression inhibits CDA, RED and ACT biosynthesis. Controls major developmental transitions. Exerts response to oxidative stress.	(Kang *et al.*, 2007; Fowler-Goldsworthy *et al.*, 2011)
wblI (SCO3201)	The over-expression in *S. lividans* TK24 enhances the synthesis of RED and ACT. It exerts a negative impact on the biosynthesis of CPK.	(Yan *et al.*, 2017)
	TetR regulators	
atrA	TetR family regulator responsible for activation	(Uguru *et al.*,

(SCO4118)	of *actII-ORF4* and the NagE2 permease, the latter responsible of N- acetylglucosamine transport. Controls SsgR, protein involved in cell division.	2005; Nothaft *et al.*, 2010; Kim *et al.*, 2015)
SCO3201	TetR-like regulator that represses CDA, ACT and RED biosynthesis. It also binds the promoter region of *scbA*.	(Xu *et al.*, 2010)
SCO1712	TetR family transcriptional regulator. Deletion of SCO1712 induces precocious aerial hypha formation as well as up-regulation of ACT and RED.	(Lee *et al.*, 2010)
rrdA (SCO1104)	TetR family transcriptional regulator that negatively regulates expression of *redD* and positively regulates ACT production.	(Ou *et al.*, 2009)
	γ-Butyrolactone receptor protein	
cprB (SCO6071)	ArpA-like family regulator that is a γ-butyrolactone reception protein. Potentially modulating γ-butyrolactone biosynthesis.	(Bhukya *et al.*, 2014)
cprA (SCO6312)	Arp-like regulator whose disruption reduces ACT and RED biosynthesis as well as delaying sporulation.	(Onaka *et al.*, 1998)
ndgR (SCO5552)	An IcIR-like regulator that binds *scbR-scbA* divergent promoter region and is involved in indirect regulation of glutamine assimilation. Deletion mutants showed up-regulation of proteins involved in ACT biosynthesis.	(Yang *et al.*, 2009)
adpA (SCO2329)	A key regulator of development that negatively regulates transcription of *wblA*.	(Wolanski *et al.*, 2011; Lee *et al.*, 2013)
	Iron metabolism	
dmdR1 (SCO4394)	Regulator of iron metabolism. Deletion of *dmdR1/adm* represses desferrioxamine, ACT and RED biosynthesis.	(Tunca *et al.*, 2009)
	Guanosine pentaphosphate (ppGpp)	

relA (SCO1513)	Catalyzes the synthesis of ppGpp that represses translational apparatus. ppGpp induces ACT and CDA biosynthesis.	(Hesketh *et al.*, 2007; Ryu *et al.*, 2007)
rshA (SCO5794)	Synthesizes ppGpp under carbon and nitrogen limitation. Disruption of *rshA* abolishes ACT biosynthesis and increases RED biosynthesis.	(Ryu *et al.*, 2007)
eshA (SCO7699)	Protein involved in accumulation of ppGpp that directly impacts on ACT biosynthesis.	(Saito *et al.*, 2006)
	Two-component system regulator	
cutR/S (SCO5862, SCO5863)	Two-component system that represses ACT biosynthesis.	(Chang *et al.*, 1996)
rapA1/2 (SCO5403, SCO5404)	Two-component system that positively regulates ACT production as well as *kasO* from CPK biosynthetic cluster.	(Lu *et al.*, 2007)
ecrE1/E2 (SCO6421, SCO6422)	Two-component system that modulates RED biosynthesis by activating transcription of *redD* and *redZ*.	(Wang *et al.*, 2007)
gluRK (SCO5778, SCO5779)	Two-component system regulator involved in glutamate sensing and uptake. Disruption of *gluRK* enhances ACT biosynthesis and reduces RED and CPK production.	(Li *et al.*, 2017)
phoRP (SCO4229, SCO4230)	Master regulator of phosphate assimilation. This two-component system represses ACT and RED biosynthesis but positively regulates CPK. In addition, PhoP binds AfsS to block its activation. PhoP also represses *glnR*, a major nitrogen assimilation regulator.	(Sola-Landa *et al.*, 2005; Santos-Beneit *et al.*, 2011; Allenby *et al.*, 2012; Sola-Landa *et al.*, 2013)
draRK (SCO3062, SCO3063)	Two-component system that positively regulates ACT and negatively regulates the antibiotics RED and CPK.	(Yu *et al.*, 2012)
afsQ1/2	Two-component system important for ACT,	(Shu *et al.*, 2009;

(SCO4906, SCO4907)	RED and CDA production as well as for morphological development. AfsQ1 functions as nitrogen assimilation repressor by competing with GlnR, the nitrogen major regulator, for the binding-promoter regions.	Wang *et al.*, 2013)
	Nitrogen regulation	
glnR (SCO4159)	OmpR-like master regulator of nitrogen assimilation, it is directly involved in positive regulation of ACT and negative regulation of RED.	(He *et al.*, 2016)
	Large ATP-binding regulators of the LuxR family (LAL)	
SCO0877 and *SCO7173*	Both LAL regulators act as negative modulators of the expression of the two-component system PhoR-PhoP and as positive regulators of actinorhodin biosynthesis.	(Guerra *et al.*, 2012)

1.6. Towards the understanding of links between primary and secondary metabolism

The production of antibiotics usually occurs in conditions of growth slowdown and is triggered by nutrimental and/or energetic deficit (Doull and Vining, 1990; Santos-Beneit *et al.*, 2011; Esnault *et al.*, 2017). The processes underlying the biosynthesis of secondary metabolites in *Streptomyces* are highly complex. Indeed, large scale transposition mutagenesis of *S. coelicolor* identified hundreds of genes influencing antibiotics biosynthesis (Xu *et al.*, 2017). The access to the genome sequence of the model specie *S. coelicolor* (Bentley *et al.*, 2002) has led to unravel novel cryptic secondary metabolites biosynthetic pathways besides the "classic" secondary metabolites (i.e. ACT, RED, CDA methylenomycin and *whiE* gray-colored spore pigment, Table 1. 3).

S. coelicolor shares a high similarity with *S. lividans*, since 91% of the ORF encoded by *S. lividans* have orthologs in *S. coelicolor*, including ORF belonging to secondary metabolites biosynthetic clusters (Lewis *et al.*, 2010). However, these two

species showed contrasting abilities to produce antibiotics and to accumulate storage lipid of the triacylglycerol (TAG) family (Le Marechal *et al.*, 2013). Upon growth in the classical R2YE medium supplemented with glucose, *S. coelicolor* produces the three well characterized antibiotics CDA, RED and ACT and its total lipid content is low (< 7 % of dry cell weight). In contrast, *S. lividans* produces weakly these antibiotics and its total lipid content is 3-fold higher (20% of dry cell weight) indicating that it was able to accumulate TAG (Le Marechal *et al.*, 2013). This confirmed the existence of intricate links between TAG metabolism and ACT biosynthesis, since both pathways require acetyl-CoA as common precursor. Indeed, the partial inhibition of fatty acid degradation upon disruption of the *fadD1* gene was shown to correlate with the reduction of ACT and RED production (Banchio and Gramajo, 2002; Arabolaza *et al.*, 2006), and conversely, the partial inhibition of fatty acid synthesis by chemical inhibitors was shown to correlate with enhanced ACT biosynthesis in *S. coelicolor* (Craney *et al.*, 2012). Furthermore, the high TAG content of *S. lividans* indicates an excess of acetyl-CoA generation by highly active glycolysis that could be considered as an over-flow metabolism. In contrast, the low TAG content of *S. coelicolor* coupled with its high ATP/ADP ratio suggested that the metabolism of this strain was mainly oxidative (Esnault *et al.*, 2017); suggesting that antibiotic (ACT) production is triggered in a context of highly active oxidative metabolism. Altogether, these studies suggested that *S. coelicolor* and *S. lividans* have drastically different metabolic functioning and that they can serve as good models to study the regulation of secondary metabolites biosynthesis.

Genomic comparison between *S. coelicolor* M145, derivate from wild-type specie A3(2) lacking of plasmids SCP1 and SCP2, and *S. lividans* TK21 revealed that five genomic islands (> 25 kb) and 18 genomic islets (< 25 kb), representing a total of 625 genes, were found to be absents in *S. lividans* chromosome (Jayapal *et al.*, 2007). Among the 625 genes of *S. coelicolor* absent in *S. lividans*, it is noteworthy to mention three genes involved in the glyoxylate pathway (the regulator (*aceR*) SCO0981, isocitrate lyase (*aceA*) SCO0982 and malate synthase (*aceB2*) SCO0983), the sole agarase (*dagA*) SCO3471, two genes that encode an unknown type I PKS cluster SCO6826-SCO6827, two genes that encodes a methylmalonyl-CoA mutase SCO6832-SCO6833, two genes involved in lantibiotic biosynthesis SCO6929-SCO6930 and a

probable acyl-CoA dehydrogenase (SCO6938) involved in fatty acids degradation. In another comparative study, Lewis *et al.* (2010) suggested that the absence in *S. lividans* of three genes involved in methionine biosynthesis or S-adenosylmethionine (SAM)-dependent methyltransferases (SCO0985, SCO0995 and SCO3452) might be associated with the absence of ACT production in this specie. Indeed, high concentrations of SAM induce the expression of ACT by DNA-binding to *actII-ORF4* (Kim *et al.*, 2003).

Several studies have been conducted in order to understand the contrasting metabolic capacities of *S. coelicolor* and *S. lividans*. For instance, Butler *et al.* (2003) demonstrated the deletion of the *scbA* gene, involved in the synthesis of the signaling molecule γ-butyrolactone, was correlated with the activation of ACT or RED biosynthesis in *S. lividans*. Further studies in *S. lividans* showed that the inactivation of the *ppk* gene resulted in delayed degradation of polyP and activation of ACT production (Chouayekh and Virolle, 2002; Ghorbel *et al.*, 2006). Other attempt to activate ACT and RED biosynthesis in *S. lividans* was achieved by introducing mutations at different amino acids positions of the *rpoB* gene encoding a DNA-directed RNA polymerase beta chain subunit (Hu *et al.*, 2002). This work showed that *rpoB* activates directly or indirectly the key regulatory genes, *actII-ORF4* and *redD*, responsible for ACT and RED biosynthesis respectively. In other study, deletion mutants of the genes encoding the two initial steps of PPP (glucose 6 phosphate dehydrogenase (G6PDH, *zwf* genes) and 6-phosphogluconate dehydrogenase) in *S. coelicolor* resulted in reduced levels of ACT and RED production (Butler *et al.*, 2002). This suggested that part of the NADPH generated by the PPP is directly or indirectly utilized for antibiotic biosynthesis. Despite all these efforts, the metabolic features accompanying the synthesis of secondary metabolites and TAG as well as a global picture of the nature of the switch between primary and secondary metabolism in these species remains to emerge. The present project aims to contribute to the understanding of the metabolic links between primary and secondary metabolism in *S. coelicolor* and *S. lividans* using a label-free shotgun proteomic approach.

CHAPTER II. METHODS OF LABEL-FREE RELATIVE QUANTITATIVE PROTEOMICS

Proteins are important bio-functional molecules in living organisms. The entire proteins expressed by a genome and present in a cell, tissue, biofluid or organism at a particular time is known as the proteome. As a post-genomic discipline, proteomics refers to the study of the proteome concerning the abundance, structure, function, post-translational modifications (PTMs), interactions, and/or changes involved in different environments and conditions. The progress on the field of proteomics (Figure 2. 1) can be associated to the development of new technologies related to peptide/protein separation, mass spectrometry analysis, peptide/protein quantification and bioinformatic data analysis. These topics will be described in this chapter.

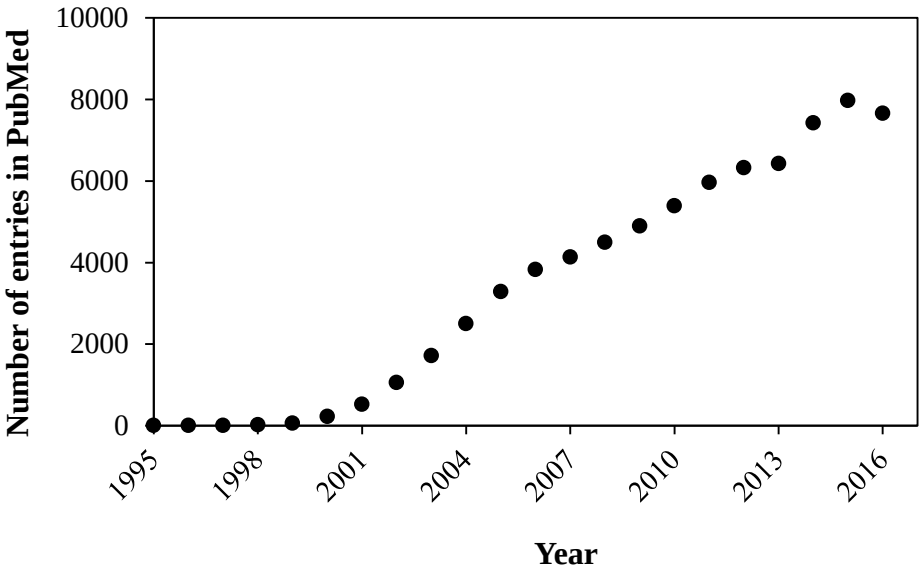

Figure 2. 1. Historical record of publications per year on the field of proteomics.

2.1. Shotgun proteomic preparation

There exist two MS-based proteomics approaches: top-down and bottom-up proteomics. Top-down proteomics is used to characterize intact proteins while bottom-up proteomics refers to the characterization of proteins by the reconstitution of the peptides obtained from previous protein proteolysis (Figure 2. 2). The bottom-up approach is the most popular method to cope with high-complexity samples as well as for large-scale analyses (Zhang *et al.*, 2013). When bottom-up analysis is performed on a mixture of proteins without pre-fractionation of sample before digestion it is called "shotgun proteomics", a term that makes reference to its analogy to shotgun genomic sequencing (Yates, 2004).

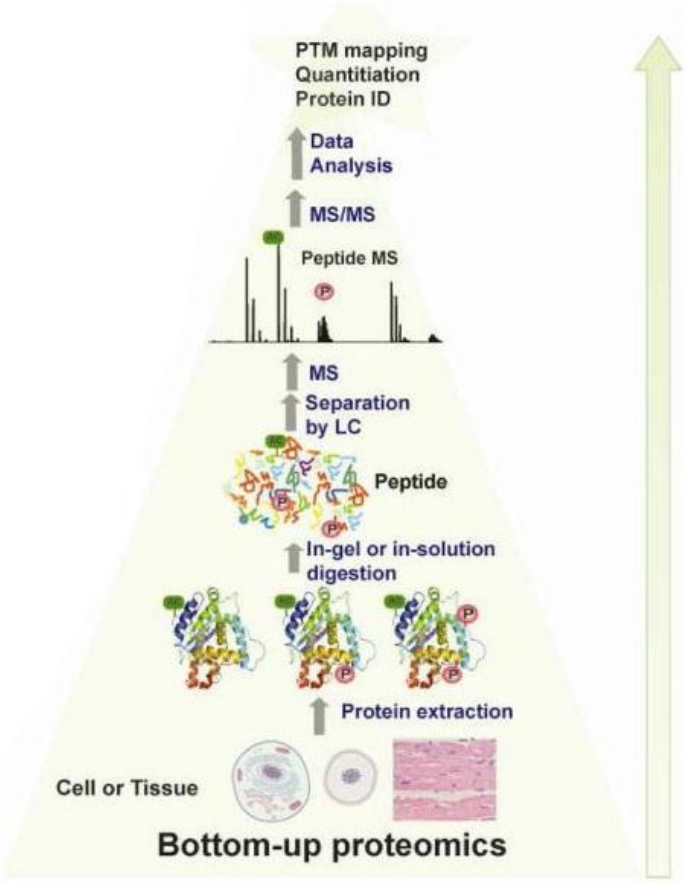

Figure 2. 2. Representation of bottom-up proteomics workflow. Adapted from (Gregorich *et al.*, 2014).

The selection of the suitable protocol for proteomics sample preparation should be considered by taking into account the complexity of samples, the experimental design and the MS analytical performance.

Protein extraction from cells, in general, include cells harvesting and washing, followed by lysis and subsequent centrifugation to collect the protein-enriched supernatant. Protein-enriched lysates are heterogeneous and complex mixtures, the aim of the proteolytic digestion step is to reduce this heterogeneity and complexity to analyze whole proteins within a sample (Zhang *et al.*, 2013). *In gel* or *in solution* digestion, depending if an optional clean-up step using sodium dodecyl sulfate-polyacrylamide gel electrophoresis (SDS-PAGE) was carried out or not, in shotgun proteomics is commonly conducted by using the protease trypsin which cleaves at the carboxyl side of arginine and lysine. This step can be optimized by using multiple enzymatic digestions. In this respect, the consecutive proteolytic digestion with trypsin and Lys-C have shown to increase the proteome coverage up to 40% more proteins in HeLa cells (Wisniewski and Mann, 2012).

Afterwards, peptide fractionation is also an optional step that can be implemented into the workflow in order to improve peptide detection and proteome coverage. The basis of fractionation is to reduce sample complexity prior to LC-MS/MS analysis; the most commonly used methods are SCX chromatography, high pH reversed-phase chromatography (C18) and hydrophilic interaction chromatography (HILIC) (Manadas *et al.*, 2010). At last, an additional desalting step could be carried out in the shotgun protocol in order to prevent salts accumulation in pre-column, column or in the ion transfer capillary of the mass spectrometer as well as to avoid analyte ion suppression due to impurities (Wither *et al.*, 2016).

2.2. Nano separation - Mass Spectrometry

Due to the complexity of the proteome, liquid chromatography (LC) coupled to Mass Spectrometry (MS) is the preferred technique to fractionate proteolytic peptides (Figure 2. 3) for further analysis of mixtures with lower complexity with the aim to increase the efficiency of proteins detection. LC uses a liquid mobile phase and a packed column as a stationary phase, where the mobile phase contains the peptides to be separated

according to their physicochemical properties that result in elution at different time points. In this respect, the most common LC method used is reverse phase chromatography that separate in function of hydrophobicity (Dakna *et al.*, 2009). The eluded peptide mixtures are then converted into ions by ElectroSpray Ionization (ESI) which is capable to ionize into multiple charged species per molecule without breaking the chemical bonds (Perkel, 2012). Then, peptides are passed through the mass spectrometer, the core of proteomics technology, as charged ions where their mass-to-charge ratio (m/z) will be measured by an analyzer and recorded by a detector. The mass spectrometric signal against the m/z ratio is known as the ion current (Mallick and Kuster, 2010). In order to determine the peptide sequence, the MS ion precursor is fragmented along its backbone to generate smaller ions which are referred as MS2 spectra or "tandem MS" (MS/MS) (Walther and Mann, 2010; Aebersold and Mann, 2016). The MS2 spectra generated are used to identify the peptide sequences considering also the exact mass of the peptide.

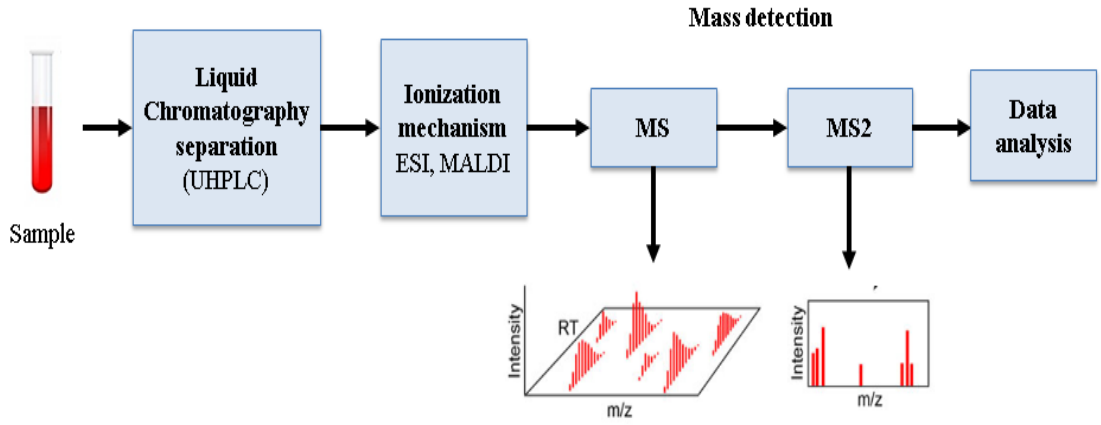

Figure 2. 3. MS-based pipeline representation.

The most widely used methods of ion fragmentation to produce MS2 spectra are collision-induced dissociation (CID) and the closely related higher-energy collisional dissociation (HCD, also known as higher-energy C-trap dissociation). In these methods, a selected ion is trapped and collided with inert gas atoms (N_2 or He), leading to increased vibrational energy and fragmentation of peptide amide bonds (Wither *et al.*, 2016). Two series of ions, termed "*b*" and "*y*" ions, are produced. The *b* ions contain the peptide amino terminus and the *y* ions contain the carboxy terminus (Figure 2. 4).

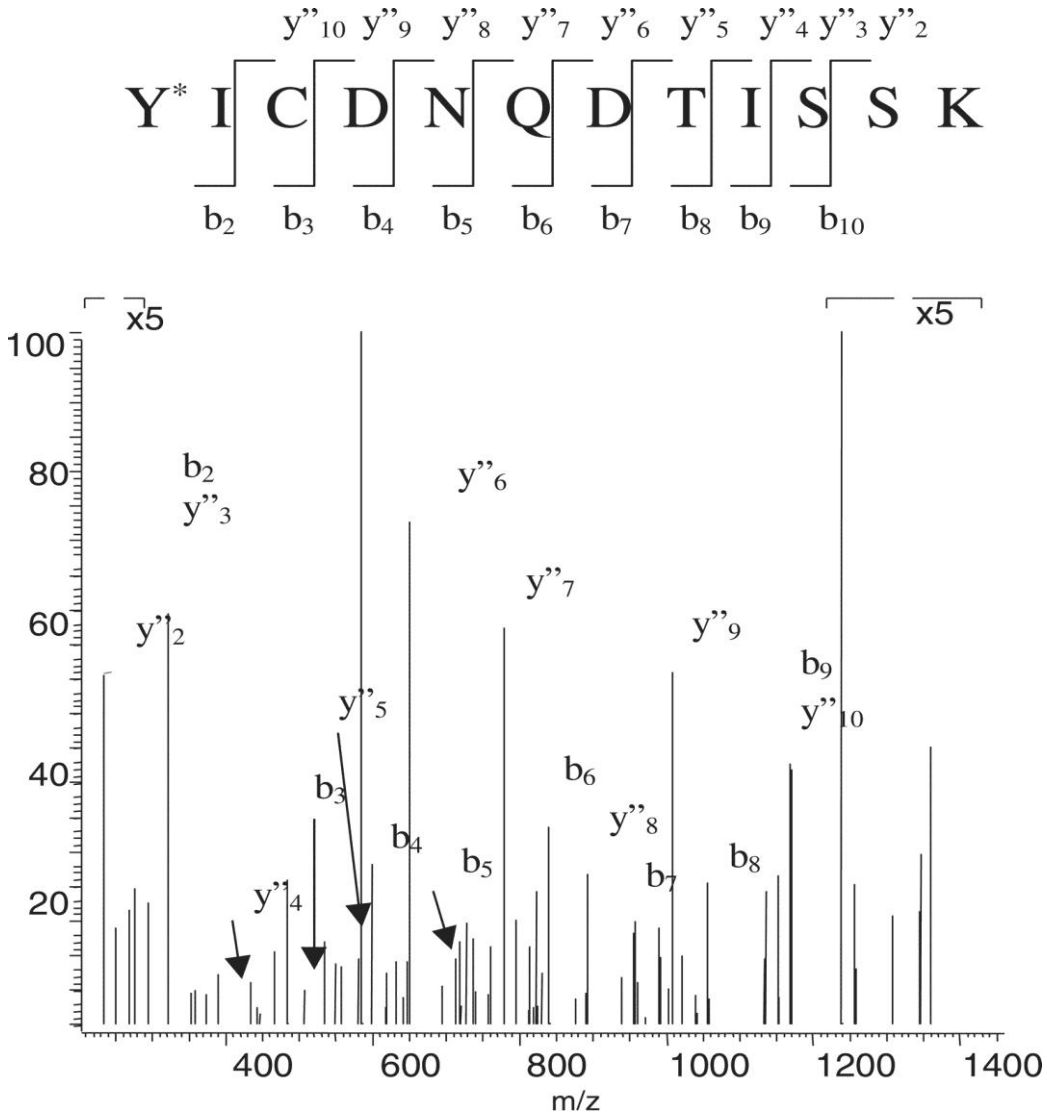

Figure 2. 4. MS2 spectra of the tryptic peptide $Y^{286}ICDNQDTISSK^{297}$ from bovine serum albumin (BSA). Respective b and y″ ions are indicated (Kanski *et al.*, 2005).

In early studies, proteomics research relied on mass spectrometers with ion trap and time-of-flight (TOF) mass analyzers (Mann and Kelleher, 2008). Currently there are five main mass analyzer technologies: quadrupole (Q) mass filters, TOF mass analyzers, linear ion traps (LIT), ion cyclotron resonance (ICR) mass analyzer and Orbitrap series analyzers. Their main analytical features related to peptide analysis are indicated below (Table 2. 1).

Table 2. 1. Analytical metrics of principal Mass analyzers used in the field of proteomics. Adapted from (Zhang *et al.*, 2013)

Analyzer	Instruments	Type	Resolution	Accuracy	Dynamic range (order of magnitude)
Quadrupole	QQQ	Beam	1-2 K	~1% parts per thousand	5-6
Linear ion trap	LIT	Trapping (electric field)	1-2 K	~1% parts per thousand	3-4
ToF	QToF	Beam	10-50 K	5-10 ppm	4
Orbitrap	FT	Trapping (electric field)	7.5-240 K	500-10 ppm	4
ICR	FT	Trapping (magnetic and axial fields)	~100-500 K	100 ppb	3

In recent years, proteomics analysis has driven technological advances due to the availability of new hybrid mass analyzers (i.e. quadrupole-TOF, LTQ-Orbitrap, TOF-TOF, etc.) with increasing mass accuracy that have facilitated better MS2 acquisition (Marshall and Hendrickson, 2008; Yates *et al.*, 2009).

2.2.1. LC-MS/MS

The MS instruments used for proteomics purposes along this project were the Q-Exactive and the Obitrap Fusion™ Lumos™ Tribrid™, both are high-resolution mass spectrometers produced by the company Thermo Fisher Scientific. LC was coupled to these instruments. The general features of these instruments are described thereafter.

2.2.1.1. Q-Exactive mass spectrometer

The Q-Exactive was introduced by Michalski *et al.* (2011) as an hybrid combination of a quadrupole mass filter, a C-trap and the Orbitrap analyzer (Figure 2. 5). The quadrupole is one of the most robust and mature mass filters which consists of four parallel rods arranged in the form of a square, ions are separated based on the stability of their trajectories in the oscillating electric fields applied to the rods (de Hoffman and Stroobant, 2007). The C-trap, named after its "C" shape, accumulates and stores the ions prior to analysis in the Orbitrap analyzer. The Orbitrap analyzer is a trap of ions that uses an electrostatic field which forces these ions to move them in spiral patterns. The axial component of these oscillations can be detected as an image current; afterwards, a Fourier transform (FT) is employed to obtain oscillation frequencies for ions with different masses, resulting in an accurate reading of their m/z (Scigelova and Makarov, 2006). The Q-Exactive became a powerful tool for proteomic-specialized laboratories and significantly boosted the number of proteins analyzable per hour (Nagaraj *et al.*, 2012; Eliuk and Makarov, 2015).

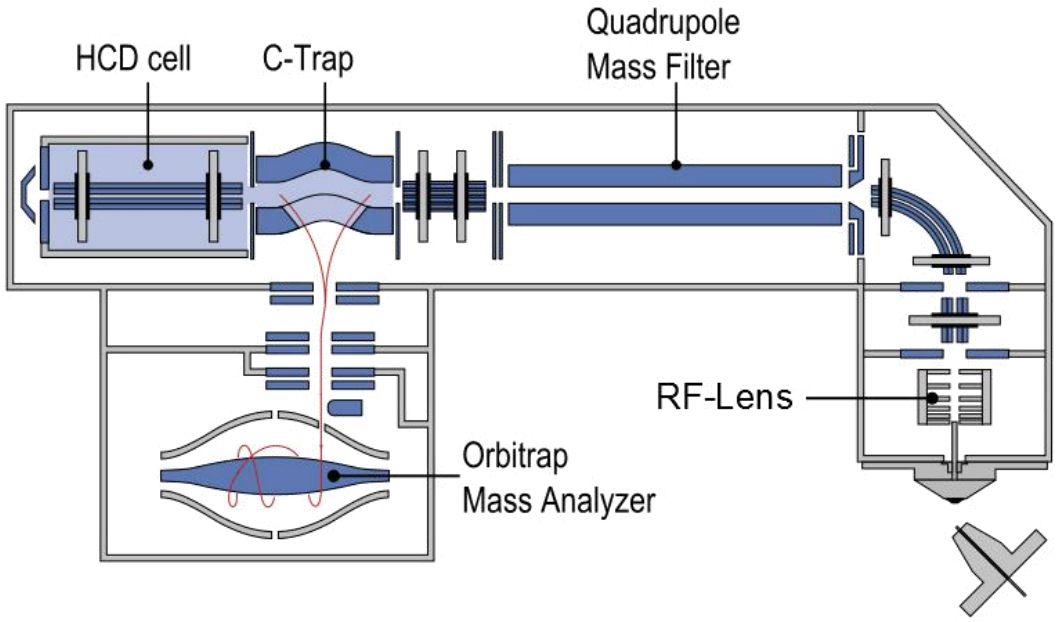

Figure 2. 5. Components of the Q-Exactive mass spectrometer. Image obtained from Thermo Fisher Scientific website https://www.thermofisher.com/order/catalog/product/IQLAAEGAAPFALGMAZR Accessed on May 8th, 2017.

2.2.1.2. Orbitrap Fusion™ Lumos™ Tribrid™ mass spectrometer

The Orbitrap Fusion™ Lumos™ Tribid™ was introduced in the 63rd ASMS Conference on Mass Spectrometry and Allied Topics in 2015 and is the last cutting-edge mass spectrometer produced by the Thermo Fisher Scientific Company. This tri-hybrid technology integrates a quadrupole mass filter, a high-field Orbitrap mass analyzer and a dual cell linear ion trap (Figure 2. 6).

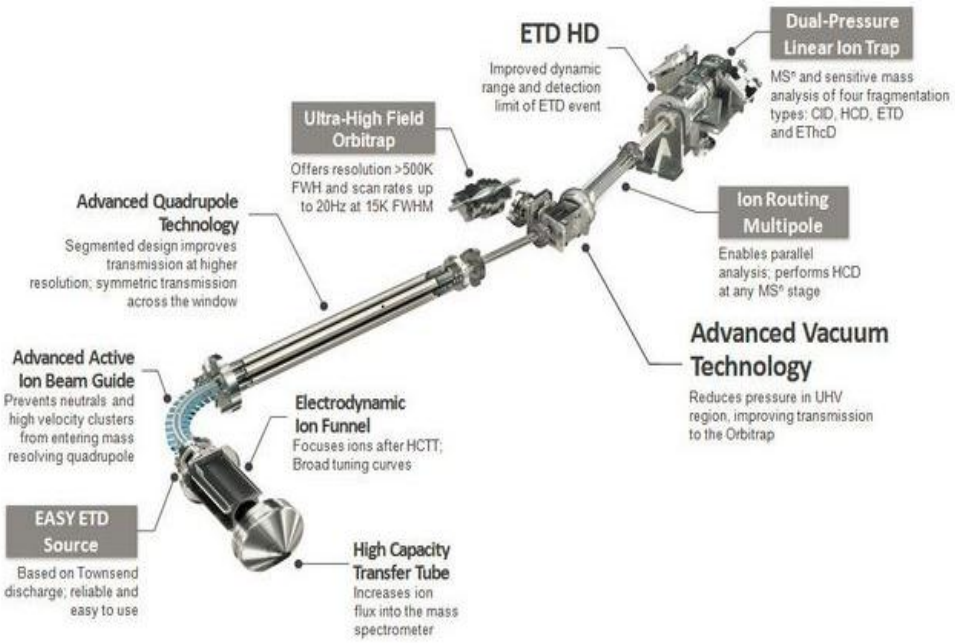

Figure 2. 6. Components of the Orbitrap Fusion™ Lumos™ Tribrid™ mass spectrometer.
Image obtained from http://proteomicsnews.blogspot.fr/2015/05/ Accessed on May 15th, 2017.

The architecture of tri-hybrid mass spectrometers has allowed significant improvements in proteomics due to the paralleled operation of its three analyzers (Senko *et al.*, 2013). This feature facilitates the analysis of complex samples, this on the basis that ions can be isolated within one analyzer and separately detecting ions in the two remaining analyzers. A recent study showed the performance of the new Orbitrap Fusion™ Lumos™ Tribid™ mass spectrometer to identify and quantify thousands of peptides and phosphopeptides in single-shot analyses of HeLa cell lysates with minimal sample fractionation and reduced chromatographic separation times (Espadas *et al.*, 2017).

2.3. Protein identification via mass-matching

The large amounts of data generated from tandem mass spectrometry (MS2) forced the field of proteomics to develop specialized software tools implementing different algorithms to identify the proteolytic peptides obtained from MS analysis. These tools are commonly known as MS search engines. These algorithms predict which peptides may be produced if a given protein is entirely or partially digested by an enzyme, commonly trypsin. Thus, a hypothetical mass spectrum is generated for each digested peptide produced (*in silico* digestion) which is therefore compared with the actual MS2 experimental spectrum. Then, a score function assigns the peptides containing a number of matched ion peaks belonging to a protein sequence (Wu *et al.*, 2006). The interpretation of the spectra MS2 by the "mass matching" approach consists in comparing the experimental spectra with theoretical spectra generated *in silico*. In this regard, the availability of genomic sequences of the organism of interest is fundamental to conduct a proteomic study.

Some of the most popular software packages to address the matching process of peptide fragmentation spectra to theoretical peptides sequences for protein identification are: Mascot (Perkins *et al.*, 1999), Sequest (Eng *et al.*, 1994), Andromeda (Cox *et al.*, 2011), OMSSA (Geer *et al.*, 2004), and X!Tandem (Craig and Beavis, 2004). Each one of them has different scoring algorithms to rank score matches between experimental and theoretical spectra.

During this thesis project, the identification of proteins from MS-identified peptides was conducted using the X!Tandem algorithm. This algorithm filters out sequence candidates in multiple searching steps; where the central assumption is that for each identifiable protein there is at least one detectable tryptic peptide (Craig and Beavis, 2004). The score function used by X!Tandem, also known as HyperScore (HS), is based on a hypergeometric distribution calculated as the dot product of the intensities of the matching ions, multiplied by the factorials of the number of matched b and y ions (Craig and Beavis, 2003). X!Tandem makes a histogram of all the HS for all the peptides in the database that might match the spectrum. It, then assumes that the peptide with the highest hyperscore is correct, and all others are incorrect. If the data on the right side of the histogram is taken and log-transformed on a straight line. A straight line is the

expected result from a statistical argument that assumes the incorrect results are random. Then, the expectation value (E-value), which relates to the likelihood of a peptide identification having being made by chance, is calculated based on how unlikely a greater hyperscore is to be found (Craig and Beavis, 2003).

After the generation of a list of proteins likely to be present in the MS samples, a refining process considering sequences redundancy (i.e. peptide sequences shared by members of protein families). This process, called protein inference, orders the proteins into groups and sub-groups taking into account that: a) proteins identified with the same pool of peptides are assembled (subgroups) while proteins identified without specific peptides compared to others are eliminated; and, b) the subgroups sharing at least one peptide are gathered to create groups and the subgroups identified only by peptides shared with other subgroups are discarded (Figure 2. 7).

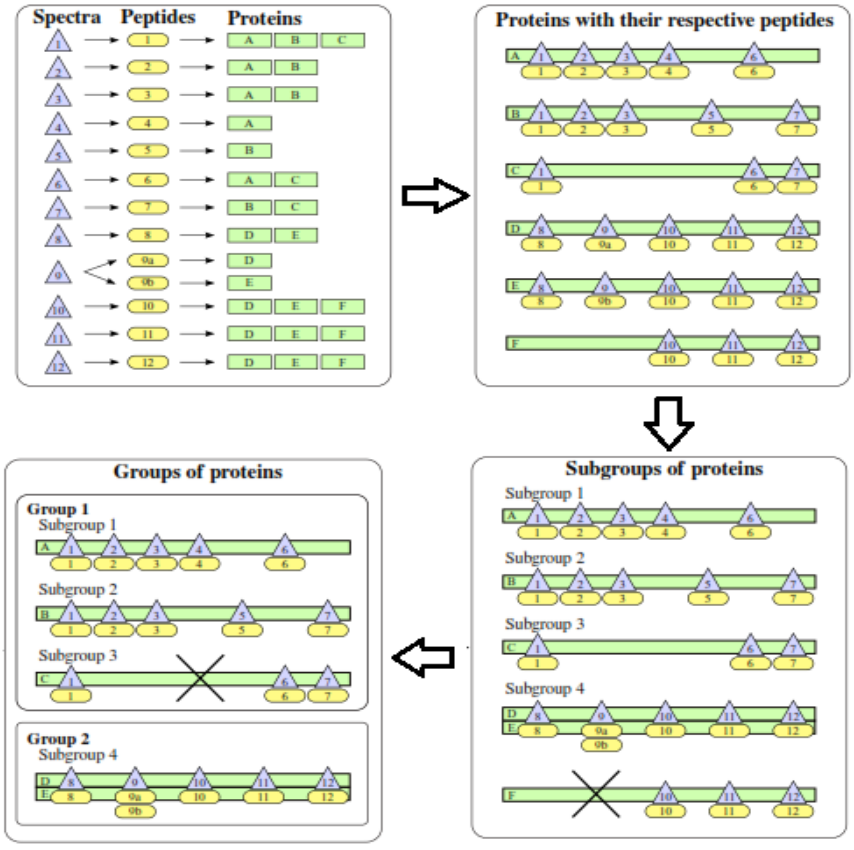

Figure 2. 7. Schematic representation of protein inference on X!TandemPipeline (Langella *et al.*, 2017).

2.4. Methods of label-free relative protein quantification

Relative quantitative proteomics can be classified into two major approaches: the use of isotope labeling and label-free methods. Accurate quantification of protein abundance can be achieved by using labeling techniques (Gygi *et al.*, 1999; Ong *et al.*, 2002; Thompson *et al.*, 2003; Ross *et al.*, 2004); however, the main drawbacks of these methods include the high cost of labeling reagents, time-consuming sample preparation, risk of inefficient labeling, incompatibility with all cell cultures and the limited number of samples that can be analyzed (Zhang *et al.*, 2013). An alternative to overcome most of these drawbacks is the use of label-free relative quantitative methods; the main advantages of label free-methods compared to labeling methods are their simpler implementation and their capacity to analyze larger amounts of samples in a single experiment (Wong *et al.*, 2008). Label-free methods can are classified into two main groups: spectral counting (SC)– and extracted ion current (XIC)– based approaches.

2.4.1. Spectral counting (SC)

SC is defined as the total number of spectra (MS2) attributed to a given protein and is proportional to the protein abundance (Liu *et al.*, 2004). SC-based quantification is a straightforward, simple and accurate approach to estimate protein abundances that present large abundance variations as well as the possibility to detect the presence and absence of a protein in different conditions of a dataset. However, SC is less accurate at measuring small differences between proteins (Liu *et al.*, 2004). In terms of implementation, SC-based methods are simpler than extracted ion current (XIC)-based methods (described below) since they do not require extensive computational processes to obtain peptide quantitative data (Lundgren *et al.*, 2010). This feature has allowed the diversification of SC-based strategies in order to improve accuracy of protein abundance quantification. These methods have been reviewed in detail elsewhere (Neilson *et al.*, 2011; Blein-Nicolas and Zivy, 2016). `

2.4.2. Extracted Ion Current (XIC)

Another label-free approach for relative quantification of proteins involves the measurement of the peak area of XIC for a given peptide at specific retention times. The

area under the curve is directly correlated with the concentration of peptides in the range of 10 fmol to 100 pmol (Bondarenko *et al.*, 2002). Several considerations must be taken into account to ensure an accurate quantification using XIC-based approaches. The latter involves computational "clean-up" of the MS data; including: retention time alignments, normalization of LC-MS runs and selection criteria of valid peptides (i.e. shared peptides, number of maximum missing values in the dataset, reproducibility of a peptide, etc., Figure 2. 8). For instance, these issues are related to a systematic bias inherent to MS-based data due to complex biological, experimental and technical processing. It is thus desirable to remove any excessive technical variability by utilizing peptide alignment and normalization techniques in order to perform proper MS data analysis (Callister *et al.*, 2006).

XIC-based methods are more complex to implement compared to SC-based approaches. However, these methods are finer and more accurate to quantitate protein abundance. Different strategies to conduct XIC quantification have been reviewer largely by Blein-Nicolas and Zivy (2016). In this concern the authors suggested the complementary use of XIC-based methods and SC-based methods to conduct a deeper analysis by combining the strengths of both approaches.

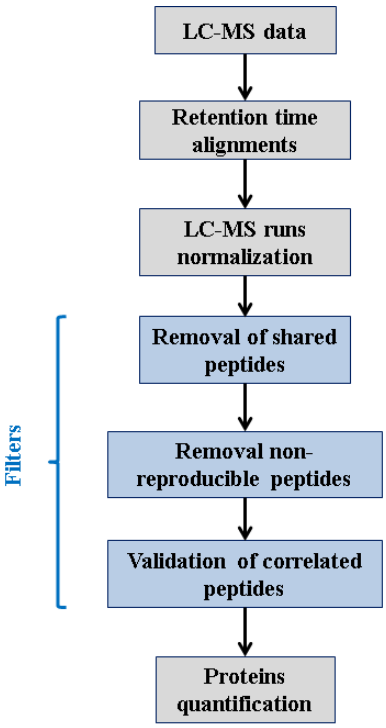

Figure 2. 8. Pipeline for XIC-based quantification approaches.

2.5. LC-MS/MS high-throughput proteomic studies in *Streptomyces*

The emerging technology of quantitative proteomics is a useful tool that has provided novel insights into the complex biology of the *Streptomyces* genus. A summary of the recent advancements related to *Streptomyces* by using high-throughput proteomics is presented below (Table 2. 2).

Table 2. 2. LC-MS/MS proteomic analysis of *Streptomyces*.

MS instrument	Quantification method	Observations	Reference
QSTAR-XL hybrid quadrupole-time of flight (Applied Biosystems)	Isobaric Tag for Relative and Absolute Quantitation (iTRAQ)	Comparative study of the transcriptome and proteome of growth and stationary phase adaptation in *S. coelicolor*. A total of 1100 proteins were identified.	(Jayapal *et al.*, 2008)
Q-TOF (Synapt, Waters)	iTRAQ	Study of the developmental cycle related to programmed cell death in liquid and solid cultures of *S. coelicolor*. *In gel* digestion was used. A total of 642 proteins were identified.	(Manteca *et al.*, 2010)
Q-TOF (Synapt, Waters)	iTRAQ	Proteomic characterization of the developmental stages of S. coelicolor grown in solid cultures. *In gel* digestion was used. A total of 345 proteins were identified.	(Manteca *et al.*, 2010)
HCT Ultra PTM Discovery System (Bruker Daltonics)	emPAI	Comparative study between S. coelicolor and *phoP* disrupted mutant. This study showed the metabolic changes related to phosphate availability and its impact on antibiotics production. *In gel* digestion was used. A total of 1535 proteins were identified.	(Thomas *et al.*, 2012)
LTQ-Orbitrap (Thermo Fisher)	Stable isotope dimethyl labeling	Proteomic study with focusing on carbon catabolite repression in *S. coelicolor* in liquid medium containing glucose, mannitol or	(Gubbens *et al.*, 2012)

		fructose as main carbon sources. A total of 2350 proteins were identified.	
LTQ-Orbitrap (Thermo Fisher)	emPAI	Label-free proteomic study to identify nucleoid-associated proteins in *S. coelicolor*; *in gel* digestion and sucrose gradient were used to detect a total of 1140 proteins.	(Bradshaw *et al.*, 2013)
LTQ linear ion trap (Thermo Fisher)	Protein Abundance Factor (PAF)	Study of extracellular proteins of *S. scabiei* grown in medium with casein and casein plus suberin. *In gel* digestion. A total of 907 proteins were identified.	(Komeil *et al.*, 2014)
Q-Exactive (Thermo Fisher)	Immunoaffinity-based acetyllysine peptide enrichment	Proteomic study that characterized the lysine acetylated proteins in *S. reseosporus*. A total of 667 proteins were identified.	(Liao *et al.*, 2014)
LTQ Orbitrap Velos (Thermo Fisher)	6-plex Tandem Mass Tagging	Proteomic analysis of the response of vancomycin resistant *S. coelicolor* to the exposure to sub-lethal levels of the antibiotic. A total of 804 proteins were identified.	(Hesketh *et al.*, 2015)
LTQ Orbitrap Velos (Thermo Fisher)	iTRAQ	Comparative study of between *S. clavuligerus* and deletion mutants of *bldA* and *bldg* that impacts on their ability to produce clavulanic acid. A total of 2496 proteins were identified.	(Ferguson *et al.*, 2016)

In the context of the post-genomic era, it is clear that MS-based proteomics is a discipline in expansion. The available datasets generated from proteomics analysis will complement the previously acquired knowledge from genetic tools concerning the functioning of diverse biological processes from *Streptomyces*.

As stated in the previous chapter, this thesis project aims to understand the contrasted abilities of the model species *S. coelicolor* and *S. lividans* to produce antibiotics and to accumulate lipids of the TAG family. In this regard, this work represents the first

attempt to study these model *Streptomyces* species using a high-throughput shotgun label-free proteomic approach.

CHAPTER III. ATTENUATED TOTAL REFLECTION FOURIER TRANSFORM INFRARED (ATR-FT-IR) FOR RAPID DETERMINATION OF MICROBIAL CELL LIPID CONTENT: CORRELATION WITH GAS CHROMATOGRAPHY-MASS SPECTROMETRY (GC-MS)

Article published on Applied Spectroscopy

DOI: 10.1177/0003702817709459

Aaron Millan-Oropeza [a]†, Rolando Rebois [b], Michelle David [a], Fathi Moussa [c], Alexandre Dazzi [b], Jean Bleton [c], Marie-Joelle Virolle [a]*, Ariane Deniset-Besseau [b]*

[a] Institute for Integrative Biology of the Cell (I2BC), CEA, CNRS, Univ. Paris-Sud, Université Paris-Saclay, 91198, Gif-sur-Yvette cedex, France.

[b] Laboratoire de Chimie Physique (LCP), CNRS, Univ. Paris-Sud, Université Paris-Saclay, 91405, Orsay cedex, France.

[c] Lip(Sys)², LETIAM§, Univ. Paris-Sud, Université Paris-Saclay. IUT d'Orsay, Plateau de Moulon, F-91400, Orsay, France. § (Formely included in EA4041 Groupe de Chimie Analytique de Paris-Sud)

* Contributed equally

Abstract

As there is a growing interest worldwide for the production of renewable oil without mobilizing agriculture lands, fast and reliable methods are needed to identify highly oleaginous micro-organisms of potential industrial interest. The aim of this study was to demonstrate the relevance of ATR spectroscopy to achieve this goal. To do so, the total lipid content of lyophilized samples of five *Streptomyces* strains with varying lipid content was assessed with two classical quantitative but time consuming methods, GC/MS and FT-IR spectroscopy in transmission mode with KBr pellets and the fast ATR method, often questioned for its lack of reliability. A linear correlation between these three methods was demonstrated allowing the establishment of equations to convert ATR values expressed as CO/amide I ratio, into µg of lipid per mg of biomass. The ATR method proved to be as reliable and quantitative as the classical GC/MS and FT-IR in transmission mode methods but faster and more reproducible than the latter since it involves far less manipulation for sample preparation than the two others. ATR could be regarded as an efficient fast screening method to identify natural or genetically modified oleaginous micro-organisms by the scientific community working in the field of bio-lipids.

3.1. Introduction

In the last decades the ability of various micro-organisms to accumulate oil has been actively assessed as they could constitute an alternative to fossil petroleum as well as to biodiesel originating from seeds of oleaginous plants. The latter is being criticized since it mobilizes arable land that could be used for human or animal feeding. Thereby, as an alternative, large-scale cultivation of oleaginous microbes could be envisaged to face the need of renewable biodiesel. Nowadays, the most extensively explored micro-organisms are yeasts (Zhu and Jackson, 2015), filamentous fungi and microalgae (Fischer *et al.*, 2008), as well as, to a lesser extent, Actinomycetes such as *Rhodococcus* (Kurosawa *et al.*, 2015; Shields-Menard *et al.*, 2015) and *Streptomyces* (Arabolaza *et al.*, 2008). A systematic research of the best triacylglycerol (TAG) accumulating micro-organisms is taking place worldwide. In order to accelerate this process, it is essential to

develop medium or high-throughput methods to quantify lipids content in micro-organisms.

Historically, lipid quantification was first carried out by gravimetric methods following solvent extraction (Bligh and Dyer, 1959). These methods require large amounts of biomass, are time-consuming and prone to human error since they involve a lot of manipulations. Other approaches involve neutral lipid staining techniques and fluorescence microscopy (Chen *et al.*, 2009; Govender *et al.*, 2012). However, these methods turned out to be poorly quantitative. The appropriate methods should be as reliable but more user-friendly and faster than the classical Gas Chromatography coupled to Mass Spectrometry (GC/MS) method extensively used by the biologists working in the field of bio-lipids or its alternative widely used by the chemists, the Fourier transform infrared (FT-IR) spectroscopy used in transmission configuration.

With the FT-IR in transmission mode, the band intensities of the absorption spectrum and the oscillation strength of the bonds can be used to quantify the amount of lipids within dehydrated samples. However, depending on the size of the analysed objects, some scattering effects may appear leading to errors in the determination of band intensity, band width and shifted maxima (Dazzi *et al.*, 2013) and to address these issues KBr pellets can be made. If they are well ground, the KBr pellets should provide a thin and homogenous layer of the samples. Consequently, the main drawback of the two methods mentioned above is the laborious and time consuming sample preparation protocol. To avoid these lengthy sample preparations, we propose to assess lipid content directly on dehydrated microbial samples (without KBr) also with FT-IR spectroscopy but using Attenuated Total Reflection (ATR) rather than transmission mode.

ATR provides a spectrum constituted of absorption bands, in the middle infrared (IR) range (400 – 4000 cm^{-1}), characteristic of chemical groups present in dehydrated microbial cells. However, whereas the ATR method proved to be quantitative to determine the fatty acids content in vegetable oils using multivariate partial least square (PLS) calibration models (Sherazi *et al.*, 2009; Mossoba *et al.*, 2013; Sherazi *et al.*, 2013), it is suspected to be semi-quantitative and poorly reliable for the analysis of lipids within micro-organisms that contain proteins and other carbohydrates besides fatty acids (Pistorius *et al.*, 2009).

In order to determine whether these criticism were justified or not, we assessed the total esterified fatty acid content of the same lyophilized bacterial samples with varying lipid content using ATR, FT-IR in transmission mode using KBr pellets as well as the classical GC/MS. FT-IR in transmission mode using KBr pellets is known to be as quantitative as GC/MS (Ramer and Lendl, 2006) and both techniques provide the amount of lipid per unit of biomass (usually µg mg^{-1}) whereas the ATR method provides measurements as CO/amide I ratio. So a calibration curve between ATR and the other two methods had to be established to fulfill biologists' needs.

To do so, the content of total esterified fatty acids (TEFA) present in the same bacterial samples was determined with the three methods. The bacteria chosen to carry out these studies belong to *Streptomyces* genus. *Streptomyces* are Gram positive soil born filamentous bacteria well known for their ability to produce antibiotics and other bioactive secondary metabolites useful for human health and agriculture (Berdy, 2005; Bibb, 2005). However, they are less well known for their ability to accumulate large reserve of storage lipids of the TAG family but some species are indeed oleaginous (Olukoshi and Packter, 1994). Considering that cultivation processes of *Streptomyces* have been mastered for decades by the pharmaceutical industry in large fermenters, the industrial production of lipids by these bacteria could be envisaged (Holmback *et al.*, 2014; Thevenieau *et al.*, 2014; Thevenieau *et al.*, 2014). The five *Streptomyces* species mentioned in this study were chosen on the basis of a previous screen achieved with the GC/MS method that determined that their TEFA content varied from 30 to 150 µg mg^{-1} (5-fold range). The two main goals of this study were, first to evaluate the reliability of the ATR method to quantify the esterified fatty acid content of *Streptomyces* samples in comparison with that of the two other quantitative methods mentioned above and second to establish calibration curves and corresponding equations between the ATR spectroscopy measurements and those achieved with the two other methods. Those curves will be used for the conversion of the ATR values, expressed as CO/amide I ratio, into µg of lipid per mg of biomass.

3.2. Materials and methods

3.3.1. Strains

The five *Streptomyces* strains analysed were: *S. coelicolor* M1144, *S. coelicolor* M1142, *S. ambofaciens* OS Maroc J5, *S. pristinaespiralis* ATCC 25486 and *S. acrimycini* JI2236. The strains *S. coelicolor* M1144 and *S. coelicolor* M1142 are derivative mutants of the model strain *S. coelicolor* M145 (Gomez-Escribano and Bibb, 2011). In *S. coelicolor* M1142, the biosynthetic pathways directing the synthesis of actinorhodin (ACT), undecylprodigiosin (RED) and a cryptic type I polyketide (CPK) were deleted whereas in *S. coelicolor* M1144 only the ACT and RED clusters were deleted. *S. ambofaciens* is known for the production of the macrolide spiramycin and the pyrrolamide congocidine (Aigle *et al.*, 2014). *S. pristinaespiralis* is an industrial strain known for synthesizing pristinamycin (Bamas-Jacques *et al.*, 1999) and *S. acrimycini* is known for the production of candicidin (Asturias *et al.*, 1994).

3.3.2. Cell culture and experimental design

Streptomyces strains were cultured on the surface of cellophane disks laid down on solid R2YE medium (Kieser *et al.*, 2000) with with glycerol 0.2 mol L^{-1} or glucose 0.1 mol L^{-1} as major carbon sources and limited in phosphate (no P added) to favour TAG accumulation. 10^6 spores were plated on the surface of plates that were incubated at 28 °C for 72 h. *S. coelicolor* M1144, *S. coelicolor* M1142, *S. pristinaespiralis* and *S. acrimycini* were cultivated on R2YE medium with glycerol 0.2 mol L^{-1} while *S. ambofaciens* and *S. coelicolor* M1144 were grown on R2YE medium with glucose 0.1 mol L^{-1}. These strains and conditions were chosen on the basis of a previous screen achieved with the GC/MS method that determined that their TEFA content varied from 30 to 150 µg mg^{-1} (5-fold range) approximately. Each condition was performed in 3 biological replicates.

3.3.3. FT-IR measurements

Samples of *Streptomyces* mycelium obtained from the cultures described above were lyophilized and hermetically stored in polypropylene tubes at room temperature (20° C)

in order to minimize the hydration of the samples. Indeed, water is characterized by important absorption bands centred at 3400 cm^{-1} and at 1645 cm^{-1} that could lead to misinterpretation of the spectra. The lyophilized mycelia samples were subjected to IR spectroscopy using a Bruker Vertex 70 FT-IR spectrometer with a liquid-nitrogen-cooled MCT detector. A reference without biological sample was performed before each sample analysis. The reference and the sample analysis were carried out using 100 averaged scans conducted from 4000 cm^{-1} to 400 cm^{-1} with a spectral resolution of 4 cm^{-1}. The absorbance is given with a precision of less than 1%.

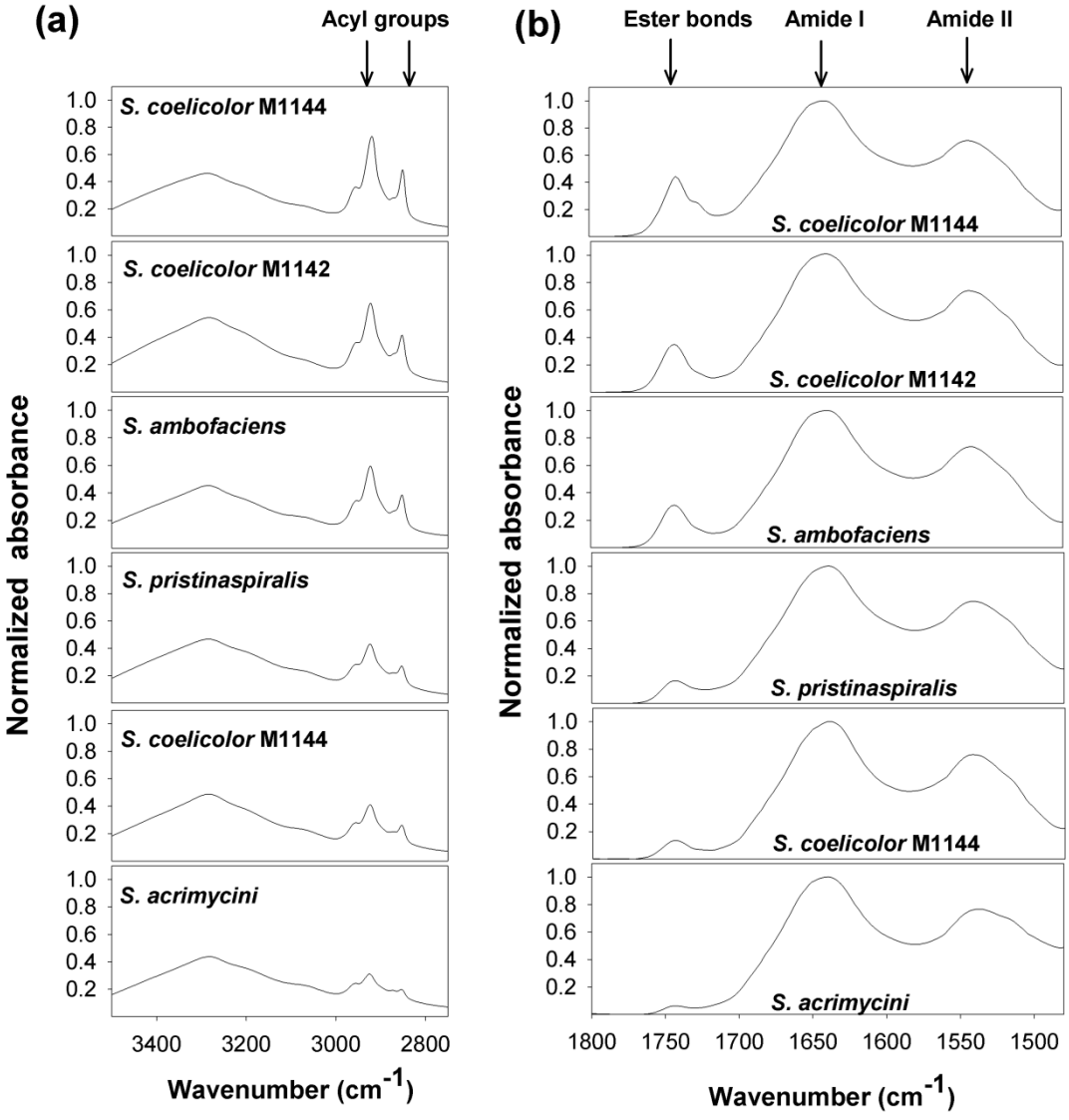

Figure 3. 1. Recorded ATR spectra of the analyzed *Streptomyces* strains.
To evaluate the total esterified fatty acids content of the different mycelial samples, the C=O absorption band at 1740 cm^{-1} (**a**) or the C-H absorption bands at 2953-2853 cm^{-1} can be used. (**b**)

The recorded spectra showed several important absorption bands (Figure 3. 1). Among them, the absorption band at 1740 cm^{-1} is characteristic of the stretching of C=O esters function from esterified fatty acids. The absorption band at 1650 cm^{-1} is characteristic of the stretching of C=O and C-N bonds from proteins (amide I), and the absorption band at 1550 cm^{-1} is characteristic of the stretching of C-N bonds and the bending of N-H bonds (amide II) respectively (Figure 3. 1a). The absorption bands at 2955 cm^{-1}, 2873 cm^{-1}, and 2923 cm^{-1}, 2853 cm^{-1} are characteristic of the antisymmetric and symmetric stretching modes of the C-H bond from the $-CH_3$ and $-CH_2$ bonds respectively (from the carbon chain of fatty acids for example, Figure 3. 1b). To evaluate the lipid content of the strains, the C-H absorption bands at 2953-2853 cm^{-1} or the absorption band at 1740 cm^{-1} can be used.

3.3.4. IR Transmission Measurements of KBr pellets

For measurements involving KBr pellets, 1 mg of the lyophilized biomass was mixed with 100 mg of ground KBr (Sigma-Aldrich, ref. 221864). After grinding the mixture, the powder was pressed in a die at 10 tons for two minutes. The resulting 12.5 mm pellets were stored in a stove at 50°C prior to analysis (to limit water absorption). The amount of esterified fatty acids is proportional to the intensity of the absorption band at 1740 cm^{-1}. Taking into account that the absorption band of amide I at 1650 cm^{-1} has a contribution to the intensity of the absorption band at 1740 cm^{-1}. The tail of the amide I absorption band can be fitted using an exponential decay using Origin 8.0 software and then subtracted from the spectrum. Then, in order to determine the amount of esterified fatty acids, the absorbance value was reported to a calibration curve obtained from commercial tripalmitin (Sigma-Aldrich, ref. T5888) with amounts ranging from 0 to 1.45 mg (Figure 3. 2).

Tripalmitin is a triglyceride derived from the palmitic acid (C16:0), we selected this compound as standard since C16-length lipids are the most abundant fatty acid species in the five *Streptomyces* strains used in this study (Table 3. 1). The calibration curve showed a statistically significant p value of the linear regression (p value = 2.4e-6, ANOVA test) and had the following equation:

$$y = 1.66\,x \qquad (1)$$

where, y is tripalmitin concentration in mg per mg of dry biomass and x is the intensity of the absorption band at 1740 cm^{-1} of each spectrum after mathematical treatment of the different spectra. With this calibration curve, it is possible to estimate the µg of esterified fatty acids per mg of biomass using the absorbance at 1740 cm^{-1}.

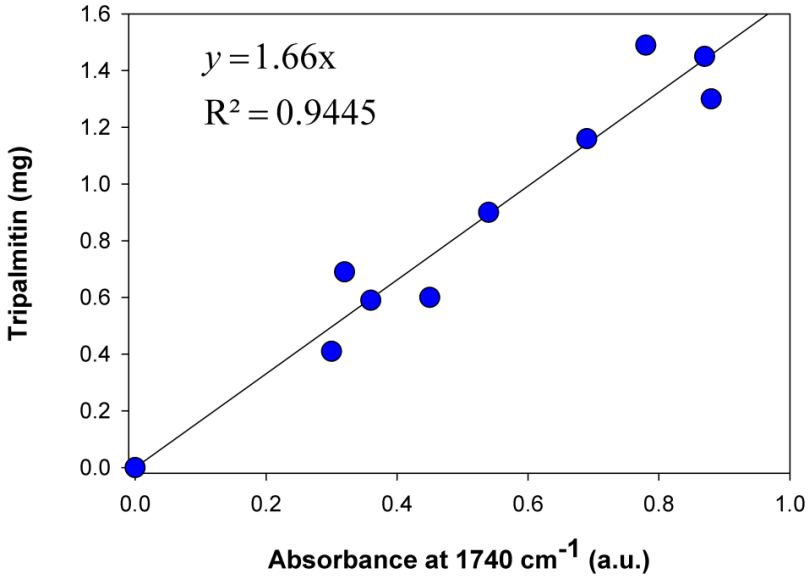

Figure 3. 2. Calibration curve of KBr pellets using different concentrations of tripalmitin.

3.3.5. ATR measurements

For the ATR measurements, lyophilized samples were carefully ground and deposited on the diamond/ZnSe internal reflection element (IRE) of a Pike Miracle single-reflection ATR accessory without any further treatment. To improve the contact, a mechanical High-Pressure clamp with a flat tip was used to press the solid samples onto the IRE (maximum pressure 689.18 bar). The applied pressure was the same as a ratchet-type clutch mechanism controls the maximum allowable pressure and the single-reflection sampling plate (1.8 mm round crystal surface) was fully covered. Even if all the experiments were carefully carried out, the contact between the IRE and the sample

can vary slightly from one measurement to another. Due to this contact variation the absorbance is given with an accuracy of 2% (technical variation). Still the deviation is better than the deviation observed due to biological variation in the 3 biological replicates (accuracy of 4%).

Table 3. 1. Relative abundance (%) of fatty acid methyl esters in the analyzed *Streptomyces* strains.

FAME species	***S. coelicolor* M1144 – glycerol**	***S. coelicolor* M1142 – glycerol**	***S. ambofaciens* – glucose**	***S. pristinaespiralis* – glycerol**	***S. coelicolor* M1144 – glucose**	***S. acrymicini* – glycerol**
iso C14:0	**7.4 ± 0.2**	**8.1 ± 0.2**	4.3 ± 0.2	5.1 ± 0.3	1.9 ± 0.1	4.6 ± 0.1
C14:0	1.4 ± 0.1	1.1 ± 0.1	-	-	-	-
iso C15:0	6.8 ± 0.1	7 ± 0	**9.8 ± 0.5**	5.4 ± 0.1	**7.7 ± 0.1**	5.5 ± 0.3
anteiso C15:0	**16.1 ± 0.1**	**18.4 ± 0.1**	**23.4 ± 0.7**	**21.7 ± 0.3**	**17.3 ± 0.2**	**15.9 ± 0.3**
C15:0	1.1 ± 0.1	-	0.9 ± 0.2	-	-	-
C16:1*	1.5 ± 0.1	2 ± 0.1	1.4 ± 0.2	-	5.1 ± 0.3	2.5 ± 0
iso C16:0	**32.5 ± 0.4**	**33.7 ± 0.4**	**25.9 ± 0.9**	**36.2 ± 0.5**	**31.4 ± 0.3**	**21.9 ± 0.3**
C16:1*	6.5 ± 0.2	5.9 ± 0.1	2.5 ± 0.2	1 ± 0	7.4 ± 0	8.5 ± 0.3
C16:0	**17.8 ± 0.6**	**13.5 ± 0.6**	**15.7 ± 2.7**	**6.2 ± 0.2**	6.4 ± 0.3	**16.5 ± 0.2**
C17:1*	0.8 ± 0.1	0.9 ± 0	1.8 ± 0.3	-	4.3 ± 0.1	1.7 ± 0
C17:1 cyclopropane	1 ± 0.1	1.3 ± 0.1	1.9 ± 0.3	-	5.7 ± 0.1	2.3 ± 0.1
iso C17:0	1.7 ± 0.1	1.8 ± 0.1	3.5 ± 0.3	5.5 ± 0.2	2.6 ± 0.1	3 ± 0.1
anteiso C17:0	5.5 ± 0.1	6.3 ± 0.2	8.8 ± 0.4	**16.4 ± 0.4**	**10.2 ± 0.1**	**10.4 ± 0.3**
C17:1 *	-	-	-	-	-	6.1 ± 0.1
C17:0	-	-	-	1 ± 0	-	-

In bold the most abundant FAMES per strain
± indicates the standard deviation (n = 3)
* Indicates different methyl branched unsaturated FAMES for C16 and C17

To evaluate the total esterified fatty acids content of the strains, the absorption band at 1740 cm^{-1} characteristic of the C=O stretching mode from the esterified fatty acids (Figure 3. 1) or the absorption band at 2923 cm^{-1} characteristic of the antisymmetric CH_2 stretching mode was used. Subsequently, a fast and most effective data processing was applied. At first glance, a simple polynomial first order baseline correction was applied using OPUS 6.5 software and both absorption bands (at 1740 cm^{-1} and 2923 cm^{-1}) were normalized using the absorption band of amide I at 1650 cm^{-1}. An assessment of the quantity of lipids within the samples was obtained expressed as CO/amide I (if considering 1740 cm^{-1}) or CH/amide I ratio (if considering 2923 cm^{-1}).

3.3.6. Esterified fatty acids quantification by GC/MS

The method used to trans-esterify the fatty acids was adapted from Lepage and Roy (1986). Samples of lyophilized *Streptomyces* mycelium (1 mg) were placed in 2 mL glass vials equipped with screw cap then 180 µL of methanol, 10 µL of acetyl chloride and 40 µL of first internal standard solution (0.3082 µg methyl tridecanoate μL^{-1}) were added to the samples. The mixture was homogenized by vortexing and incubated at 100°C for 1 hour in order to allow the acidic transesterification to take place. 200 µL of hexane and 100 µL of water were added to the resulting mixture. The mixture was homogenized by vortexing and centrifuged (5 minutes at 2990 g). The upper hexane phase was transferred to another vial and a second extraction was performed to obtain a final Fatty Acid Methyl Esters (FAME) extract of 400 µL. The FAME extract was dried under nitrogen flux and dissolved in 400 µL of hexane to which 40 µL of second internal standard solution (0.266 µg methyl eicosanoate μL^{-1}) was added. Aliquots of 1 µL were injected in a TRACE GC Ultra Gas Chromatograph coupled to a DSQ II quadrupole mass spectrometer (Thermo Scientific™). The separation was achieved using a 20 m x 0.18 mm HP-5MS capillary column (Agilent technologies) coated with 0.18 µm of 5%-diphenyl-95%-dimethylpolysiloxane. The carrier gas was helium at a constant pressure of 120 kPa. The injector temperature was set at 250 °C and the sample injected in splitless mode (0.5 min). The oven temperature was progressively increased from 100 °C to 310 °C at 20°C min^{-1} then kept 2 min at 310 °C. The mass spectrometer (MS) transfer line and ion source temperatures were 325 °C and 250 °C respectively. The MS was operated in the electron ionization (EI) positive mode (70 eV) with a scan

ranging from m/z 45 to 650 at 2 scans per second. The compounds were identified by comparing the obtained mass spectra to the mass spectra of the National Institute of Standards and Technology library (NIST, 2014).

For the quantification of FAME, the peak areas were normalized using the first internal standard (C13:0), and each FAME concentration was calculated according to the following equation:

$$L_i = A_i \; {A_{C20}}^{-1} \, C_{C20} \; V_{C20} \, B^{-1} \tag{2}$$

where, L_i is the FAME concentration in µg per mg of dry biomass, A_i is the normalized peak area of the FAME, A_{C20} is the peak area of the second internal standard (C20:0), C_{C20} represents the second internal standard concentration (0.266 µg of C20:0 μL^{-1}), V_{C20} is the added volume of second internal standard (40 µL) and B is the amount of biomass amount (mg) used for the extraction.

Total fatty acids production was obtained from the sum of all the FAME concentrations of the different FAME species present in each gas chromatogram (Figure 3. 3).

$$FA = \sum_{i}^{n} L_i \tag{3}$$

where, FA represents the total fatty acids production in µg per mg of dry biomass, i is the FAME specie, n the total FAME species, and L_i is the FAME concentration in µg per mg of dry biomass.

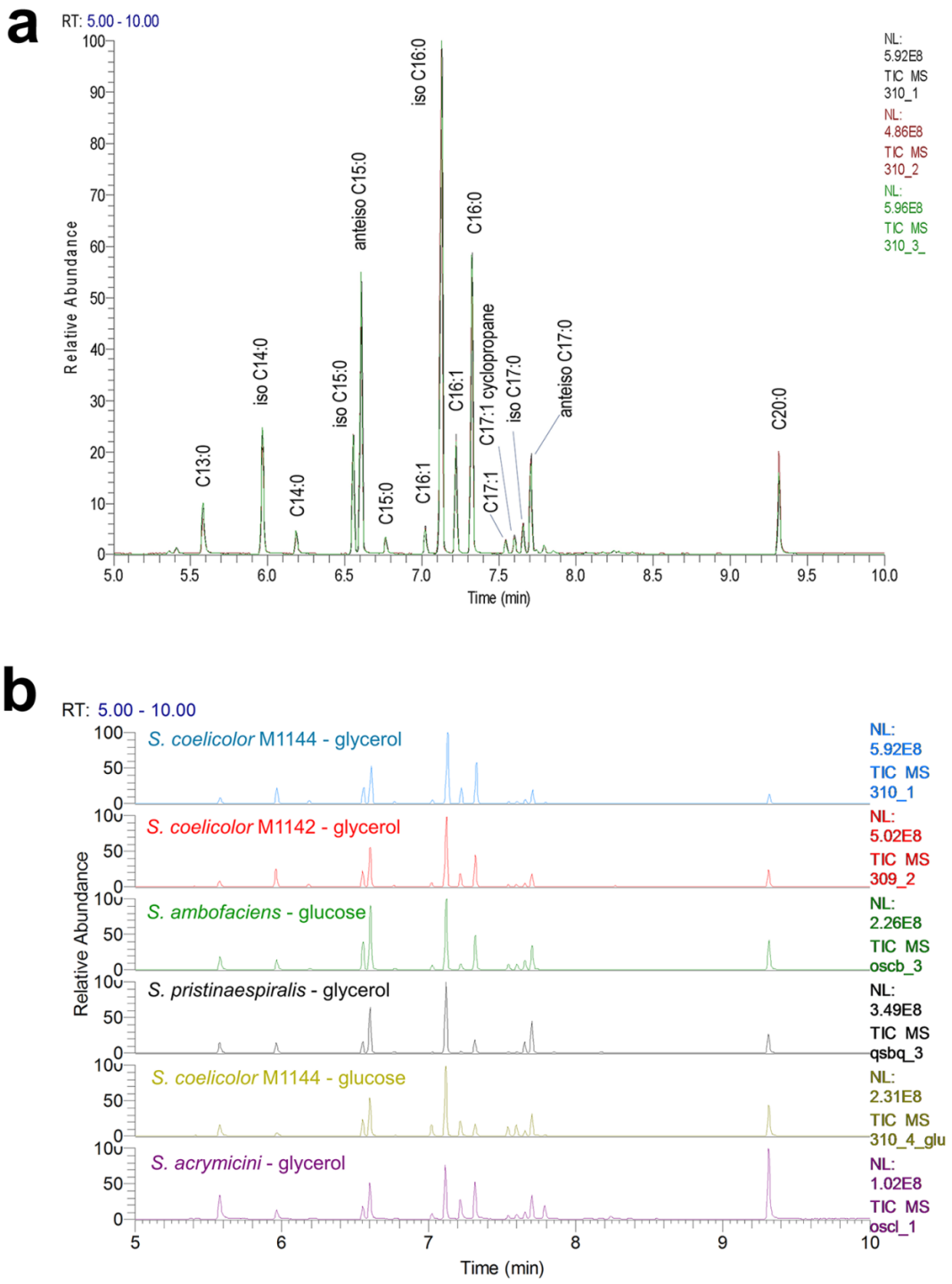

Figure 3. 3. Gas chromatograms illustrating the fatty acids methyl esters (FAMES) profile of *Streptomyces coelicolor* M1144 grown in R2YE medium supplemented with glycerol (**a**). Overlap of 3 biological replicates (chromatograms in black, red and green). C13:0 and C20:0 were two internal standards. Representative gas chromatograms of the analyzed *Streptomyces* strains grown in R2YE medium supplemented with glucose 0.1 M or glycerol 0.2 M (**b**).

3.3. Results and discussion

3.3.1. Correlation between the quantification of total esterified fatty acid content with FT-IR in transmission and ATR methods

IR spectroscopy in transmission mode is considered as a reliable and quantitative method (Ramer and Lendl, 2006) but it requires the laborious and time-consuming making of KBr pellets. In an attempt to overcome this constraint, the total fatty acids content of *Streptomyces* strains with varying levels of lipids was estimated by FT-IR spectrometry both by transmission and by ATR, which is faster and does not require any specific sample preparation besides lyophilization. The comparative analysis of the estimations provided by both techniques is shown in Figure 3. 4a. It represents the correlation between the µg of esterified fatty acids per mg of biomass given by the KBr pellets compared with the CO/amide I ratio obtained by ATR. Both techniques show a high correlation ($R^2 = 0.981$) resulting in the following equation:

$$y_a = 389.32\ x_a + 8.75 \quad (4)$$

where y_a represents the µg of esterified fatty acids per mg of biomass and x_a is the CO/amide I ratio from ATR. Furthermore, we observed a linear correlation ($R^2 = 0.951$, Figure 3. 4b) between the CO/amide I ratios of the FT-IR in transmission mode (using KBr pellets) and the CO/amide I ratios of the ATR configuration. Standard error of the mean (SEM) was calculated according to the following equation:

$$\mathrm{SEM} = \pm \mathrm{t}_\alpha\ \mathrm{CV}\ (N^{-0.5}) \quad (5)$$

with $t\alpha = 1.96$ being the student coefficient as function of α-error ≤ 5% for a confidence interval of 95%, *CV* is the coefficient of variation and *N* the number of samples. These calculations resulted in SEM ranging between 0.7-8.6% and 9.1-11.4% for FT-IR in transmission and ATR, respectively. FT-IR in transmission showed less variability than ATR. However, SEM of 10%, observed for ATR, is commonly accepted in biological studies. Our results interconnected both techniques and allowed us to propose a

calibration curve that can be used for quantitative and rapid measurements of total lipid content with ATR technique.

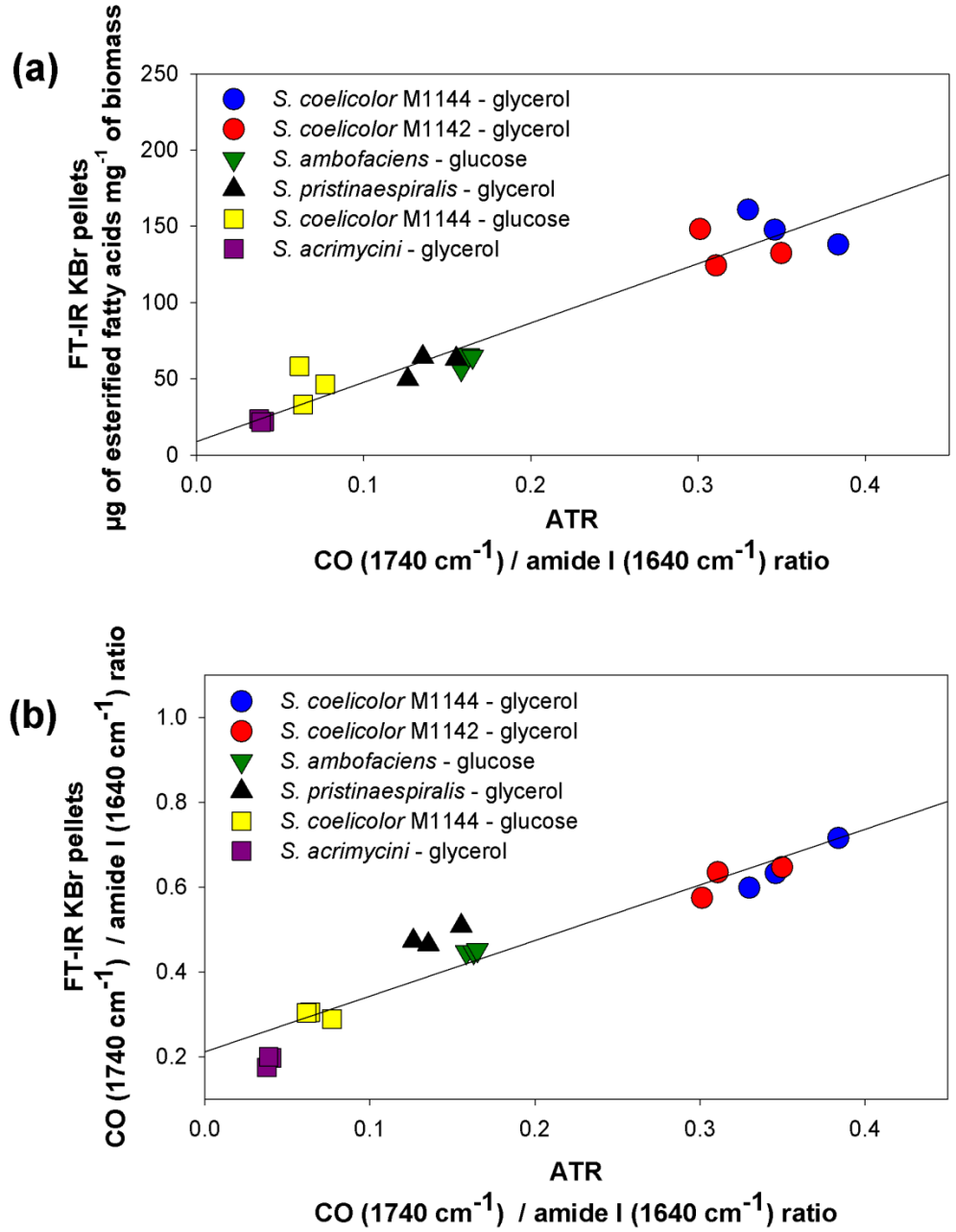

Figure 3. 4. Correlation between CO/amide I ratios determined by ATR with the esterified fatty acids content (**a**) and the CO/amide I ratios (**b**) determined by FT-IR in transmission using KBr pellets of the analyzed *Streptomyces* strains.

3.3.2. Correlation between the quantification of total esterified fatty acid content with GC/MS and ATR methods

GC/MS is the method the most extensively used by the biologists to assess lipid content of living organisms. The GC/MS method gives information regarding the chain length and degree of saturation/unsaturation of the fatty acids extracted from the bacteria whose summing up provides a good estimation of the total amount of esterified fatty acids. The estimations of the esterified fatty acids content obtained with the GC/MS and ATR (CO/amide I ratio) methods were compared for each strain (Figure 3. 5). Values obtained by ATR exhibited less SEM variation (9.1-11.4%) than those obtained with GC/MS (0.9-17.3%) likely because the latter involves more manipulations than the former. A good linear correlation was observed between CO/amide I ratios and total FAME content as assayed by GC/MS (R^2 = 0.992) and expressed in the following equation:

$$y_b = 352.06\ x_b + 22.72 \qquad (6)$$

where y_b represents the FAME in µg per mg of dry biomass and x_b is the CO/amide I ratio from ATR-FTIR.

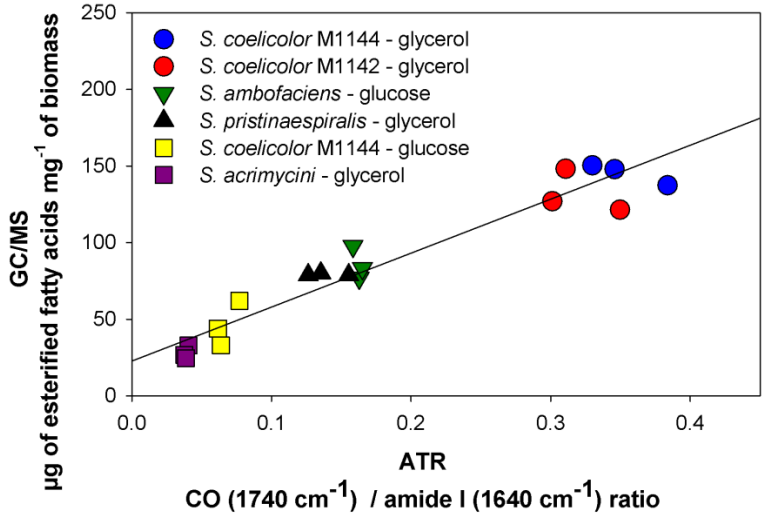

Figure 3. 5. Correlation between the CO/amide I ratios obtained with ATR and total FAME quantification as determined by GC/MS in the analysed *Streptomyces* samples.

Similarly, a good linear correlation was obtained between CH/amide I ratio (bands at 2923 cm^{-1} and 1650 cm^{-1}, respectively) and total FAME content assayed by GC/MS and expressed in the following equation:

$$y_c = 324.27 \ \ x_c - \ \ 59.52 \qquad (7)$$

where y_c represents the FAME in µg per mg of dry biomass and x_c is the CH/amide I ratio from ATR. The obtained correlation coefficient was $R^2 = 0.995$. The calculation of TEFA content using these two equations gave exactly the same values indicating that the other cellular components do not interfere in this assay. In another study where the lipid content of different microalgae strains was comparative assessed using FT-IR and gravimetric methods (Dean *et al.*, 2010), the authors were forced to use the characteristic band of acyl groups between 3000-2800 cm^{-1} to quantify the lipid content since the presence of pigments such as chlorophylls and carotenoids absorbing at 1740 cm^{-1} distorted the estimation of total lipid content using the CO/amide I ratio.

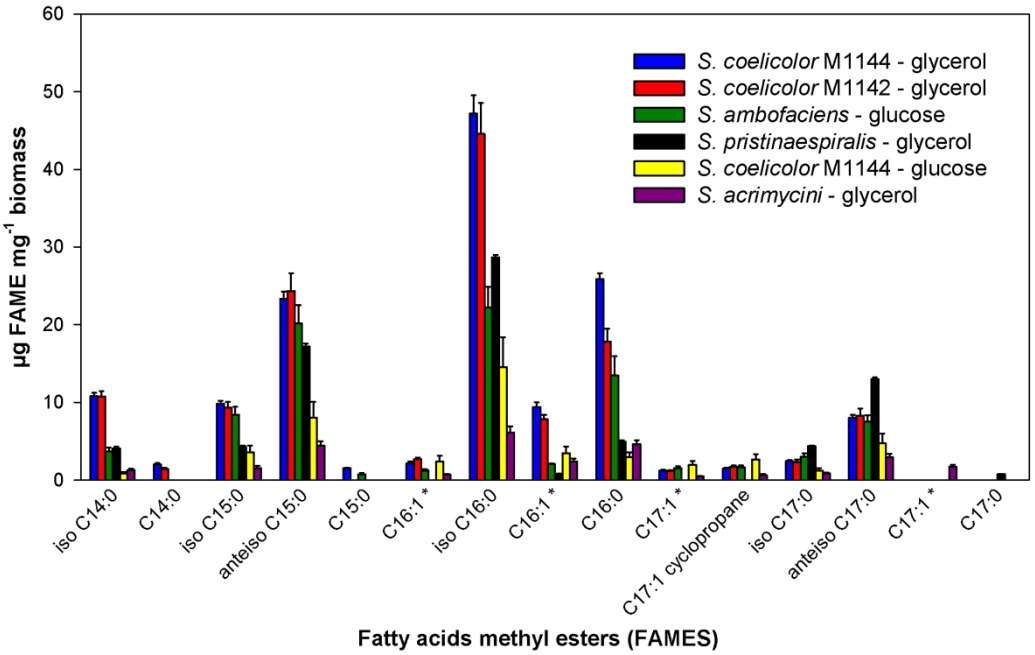

Figure 3. 6. FAME accumulation in the analysed *Streptomyces* strains, determined by GC/MS, showing mean and standard deviation (n = 3).
* Indicates different methyl branched unsaturated FAME for C16 and C17.

Interestingly, the GC/MS analysis revealed similar lipid profiles of the *Streptomyces* strains at quantitative (Figure 3. 6) and qualitative (Table 3. 1) levels. Using this method the ratio of lipid content between the least and most oleaginous strain was 5, ranging approximately from 30 to 150 µg of esterified fatty acids per mg of dry biomass. The most abundant FAME were anteiso C15:0, iso C16:0 and C16:0. These results are consistent with other studies carried out in *S. coelicolor* and *S. ambofaciens* (Schauner *et al.*, 1999; Li *et al.*, 2005). It is noteworthy that 90% of the FAME detected in the most oleaginous *Streptomyces* strains were saturated suggesting that these bacteria could be a promising renewable oil source fulfilling the biodiesel production specifications.

Our results interconnected both techniques and allowed us to propose a calibration curve that can be used for quantitative and rapid measurements of total lipid content with ATR technique.

3.4. Conclusions

In this study we assessed the suitability and reliability of the fast ATR method to quantify TEFA content of biological samples, in comparison with the two well recognized quantitative methods, GC/MS and FT-IR in transmission (Azizian *et al.*, 2012). Our study demonstrated a linear correlation between GC/MS, FT-IR in transmission (using KBr pellets) and ATR methods (Figure 3. 4 and Figure 3. 5) using the representative and well resolute absorption bands of esterified fatty acids either at 1740 cm^{-1} (CO absorption band) or 2923 cm^{-1} (CH absorption band). These were used to quantify the TEFA content of *Streptomyces* strains containing approximately 30 to 150 µg of esterified fatty acids per mg of dry biomass.

The ATR method thus allows the direct and rapid assessment of the total amount of esterified fatty acids that include indiscriminately polar membrane lipids and neutral storage lipids (TAG). To establish the repartition of TEFA between these two pools other preparative and analytical methods are required (Michael-Jubeli *et al.*, 2011; Abbott *et al.*, 2012; Heinzelmann *et al.*, 2014). The ATR method cannot provide the distribution of fatty acids chain length as do the standard methods GC/MS or GC/ flame ionization detector (FID). However, the ATR method bears many advantages in

comparison with the laborious and time-consuming quantitative GC/MS and FT-IR in transmission methods: (1) it results in as reliable measures of TEFA content in micro-organisms as the FT-IR in transmission or GC/MS approaches if proper experimental precautions described in materials and methods are used; (2) it is highly reproducible since it involves little manipulations and (3) it reduces substantially the processing time since signal treatment can be limited. For all these reasons, ATR is well suited for medium/high throughput screening of oleaginous micro-organisms or to follow evolution of lipid content throughout growth of microbial cells. At last, we wish to stress that the linear correlation curves obtained between the fast ATR method and the most widely accepted GC/MS or FT-IR in transmission methods are of great interest for the scientific community working in the field of bio-lipids.

3.5. Funding

This work was supported by the Université Paris-Sud, the CNRS and the ANR Bio-SoundIR project, grant ANR-15-CE09-0002-01 of the French National Research Agency. AMO and RR were respectively supported by the doctoral fellowships of the National Science and Technology Council (CONACYT, Mexico) number 314457 and the Université Paris-Sud, France.

CHAPTER IV. QUANTITATIVE PROTEOMIC ANALYSIS CONFIRMED OXIDATIVE METABOLISM PREDOMINATES IN *STREPTOMYCES COELICOLOR* VERSUS GLYCOLYTIC METABOLISM IN *STREPTOMYCES LIVIDANS*

"Reprinted with permission from Millan-Oropeza *et al.,* (2017) Quantitative proteomics analysis confirmed oxidative metabolism predominates in *Streptomyces coelicolor* versus glycolytic metabolism in *Streptomyces lividans*. Journal of Proteome Research 16(7), 2597-613. DOI: 10.1021/acs.jproteome.7b00163 Copyright 2017 American Chemical Society". http://pubs.acs.org/doi/abs/10.1021/acs.jproteome.7b00163

Aaron Millan-Oropeza [‡], Céline Henry [¶†], Mélisande Blein-Nicolas [#], Anne Aubert-Frambourg [¶], Fathi Moussa [⊥], Jean Bleton [⊥], Marie-Jöelle Virolle [‡†]*

‡ Institute for Integrative Biology of the Cell (I2BC), CEA, CNRS, Univ. Paris-Sud, Université Paris-Saclay, 91198, Gif-sur-Yvette cedex, France.

¶ Micalis Institute, INRA, PAPPSO, AgroParisTech, Université Paris-Saclay, 78350 Jouy-en-Josas, France.

Génétique Quantitative et Évolution (GQE) - Le Moulon, INRA, Univ Paris-Sud, CNRS, AgroParisTech, Université Paris-Saclay, F-91190, Gif-sur-Yvette, France.

⊥ Lip(Sys)², LETIAM[§], Univ. Paris-Sud, Université Paris-Saclay. IUT d'Orsay, Plateau de Moulon, F-91400, Orsay, France. [§](Formely included in EA4041 Groupe de Chimie Analytique de Paris-Sud).

† These authors contributed equally to this work

Abstract

Recent physiological studies indicated that *S. lividans* metabolism was mainly glycolytic whereas *S. coelicolor* metabolism was mainly oxidative. To determine whether such metabolic characteristics were correlated with consistent proteomic features, a comparative label-free, shotgun proteomic analysis of these strains was carried out. Among 2024 proteins identified, 360 showed significant differences in abundance between the strains. This study revealed that *S. coelicolor* catabolized glucose less actively than *S. lividans* whereas it catabolized more actively than *S. lividans* the amino acids present in the medium. The abundance of glycolytic proteins in *S. lividans* was consistent with its high glycolytic activity whereas the abundance of proteins involved in the catabolism of amino acids in *S. coelicolor* provided an explanatory basis for its predominantly oxidative metabolism. In this study, conducted in conditions of low O_2 availability, proteins involved in resistance to oxidative stress and those belonging to a DosR-like dormancy regulon were abundant in *S. coelicolor* whereas tellurium resistance proteins were abundant in *S. lividans*. This indicated that the strains reacted differently to O_2 limitation. Proteins belonging to the CDA, RED and ACT pathways, usually highly expressed in *S. coelicolor*, were not detected under these conditions, whereas proteins of siderophores, 5-hydroxyectoine and terpenoid biosynthetic pathways were present.

4.1. Introduction

Streptomycetes are filamentous, saprophytic Gram-positive bacteria, living in the superficial layers of terrestrial or marine soils. They are well known for their ability to synthesize antibiotics and other bio-active molecules useful in medicine or agriculture (Challis and Hopwood, 2003; Barka *et al.*, 2016). The biosynthesis of these so called "secondary metabolite" molecules usually occurs during the late growth phase and is elicited by some nutritional limitations (Lian *et al.*, 2008; Sanchez *et al.*, 2010; Liu *et al.*, 2013; He *et al.*, 2016; Xu *et al.*, 2016). Interestingly, upon growth on solid medium these biosynthetic processes are usually accompanied by a complex morphological differentiation process (Bibb, 2005; Manteca *et al.*, 2010). These intricate morphological and metabolic changes are regulated by an extremely complex network

of sensory and regulatory proteins as well as signaling molecules (like butyrolactone and c-di-GMP) (Takano, 2006; Kahrstrom, 2014; Tschowri *et al.*, 2014). Members of this network are thought to be involved in the sensing of carbon, nitrogen and/or phosphate availability as well as population cell density and in the appropriate adjustment of cellular metabolism (McCormick and Flardh, 2012; Urem *et al.*, 2016). These nutritional limitations, especially in phosphate, are correlated with energetic stress and thus slowdown of growth (Esnault *et al.*, 2017). In this context, a fraction of the metabolites generated by primary metabolism (amino acids and acetyl-CoA) is used for the biosynthesis of peptidic or polyketide antibiotics rather than contributing to biomass biosynthesis. Although numerous studies focusing on the regulation of antibiotic biosynthesis in *Streptomyces* have been published, the metabolic features accompanying these bio-productions, as well as the nature of the switch between primary and secondary metabolism remains to be fully elucidated (Alam *et al.*, 2010; van Wezel and McDowall, 2011).

S. coelicolor M145 (Bentley *et al.*, 2002) and its closely related *S. lividans* TK24 (Rückert *et al.*, 2015) are the model strains extensively used in the field to address these questions. These strains are phylogenetically closely related and over 90% of the proteins encoded by one species have orthologs in the other specie (Jayapal *et al.*, 2008; Lewis *et al.*, 2010). They possess identical pathways for lipid and secondary metabolite biosynthesis but they show drastically different abilities to accumulate storage lipid of the triacylglycerol (TAG) family and to produce antibiotics (Olukoshi and Packter, 1994; Le Marechal *et al.*, 2013; Esnault *et al.*, 2017). *S. coelicolor* is a well-known strong producer of three well-characterized peptidic (calcium dependent antibiotic, CDA), polyketide (actinorhodin, ACT) and hybrid peptidic-polyketide (undecylprodigiosin, RED) antibiotics and its TAG content is low, whereas *S. lividans* weakly produces these antibiotics and has a high TAG content (Le Marechal *et al.*, 2013). Since *S. coelicolor* was characterized by higher ATP/ADP ratio (>2-fold) than *S. lividans* the metabolism of *S. coelicolor* was proposed to be mainly oxidative whereas that of *S. lividans* was proposed to be mainly glycolytic. In *S. coelicolor*, antibiotic (ACT) production is thus triggered in a context of highly active oxidative metabolism. However as soon as ACT is produced, an abrupt drop in the ATP/ADP ratio was observed suggesting that ACT has a negative impact on oxidative phosphorylation

(Esnault *et al.*, 2017). In order to determine whether these apparent metabolic characteristics were correlated with consistent proteomic features, a comparative label-free, shotgun proteomic analysis of these two strains, grown in liquid R2YE medium, was carried out. Indeed, even if many proteomic studies exploring various aspects of *S. coelicolor* (Manteca *et al.*, 2010; Gubbens *et al.*, 2012; Thomas *et al.*, 2012) or *S. lividans* (Le Marechal *et al.*, 2013) biology have been published, comparative studies of these two strains under the same conditions have never been carried out.

Proteomic data of this study turned out to be consistent with predictions inferred from our previous physiological studies with cultures grown on solid R2YE medium as used here; in this medium, amino acids are the main nitrogen source but also constitute a carbon source, in addition to glucose. This study revealed higher abundance of glycolytic proteins in *S. lividans* than in *S. coelicolor* confirming the higher glycolytic activity of this strain consistent with its active glucose uptake. In contrast, proteomic data indicated that S. *coelicolor* catabolizes the amino acids present in the medium more efficiently than *S. lividans* providing an explanatory basis for its predominantly oxidative metabolism.

Furthermore, it should be stressed that under the conditions used, the liquid culture medium was poorly aerated. Therefore, our study also revealed that the two metabolically different strains reacted differently to O_2 limitation. Indeed, proteins associated with resistance to oxidative stress and those belonging to a DosR-like dormancy regulon were highly expressed in *S. coelicolor* whereas tellurium resistance proteins were highly expressed in *S. lividans*. In this context, proteins of the CDA, RED and ACT clusters, usually highly expressed in *S. coelicolor*, were not detected whereas proteins belonging to the siderophore, 5-hydroxyectoine and terpenoid biosynthetic pathways were present in this strain. The putative function of these secondary metabolites produced is discussed.

4.2. Experimental procedures

4.2.1. Bacterial growth

Spores of *S. coelicolor* M145, a derivative of the wild-type strain A3(2) (Bentley *et al.*, 2002) lacking the plasmids SCP1 and SCP2, and *S. lividans* TK24 (Rückert *et al.*, 2015) were prepared from solid SFM medium (Kieser *et al.*, 2000). 10^7 spores were used to inoculate 10 ml of R2YE medium with no phosphate and no sucrose added and supplemented with 0.1 M glucose in 50 ml tubes (Kieser *et al.*, 2000). The tubes, tightly screwed, were incubated at 28°C under constant agitation at 180 rpm on an INFORS Unitron orbital shaker. In order to estimate O_2 limitation, dissolved O_2 was monitored with an OxyFerm FDA 325 sensor connected to a Biostat B plus control station (Sartorius) in a tube inoculated with spores of *S. coelicolor*. Under these conditions, the culture was limited in O_2 16 h after inoculation (Figure S4. 1). Cell growth was assessed by dry cell weight every 12 h up to 72 h of cultivation (Figure S4. 2). To do so, the content of the tubes was homogenized by vigorous vortexing before sampling. Aliquots of 3 ml were centrifuged; mycelial pellets were washed twice with deionized water, lyophilized and weighted. Four biological replicates were carried out for each strain and for each time of cultivation.

4.2.2. Protein extraction and digestion

Proteomic analysis was carried out at three times of cultivation: 36, 48 and 72h. The total number of independent samples was 24 (2 strains x 3 culture times x 4 biological replicates). Mycelial samples of 3 ml were harvested by centrifugation (15 min at 5000 rpm, 4° C), pellets were washed twice with 50 mM Tris-HCl pH=7.8 and suspended on 3 ml of lysis buffer that contained 6 M urea (Sigma Aldrich, U5378), 2 M thiourea (Sigma Aldrich, T8656), 5 mM 1,4-dithiothreitol (Sigma Aldrich), 0.1 M Tris-HCl pH=8 and 150 µl of prepared proteases inhibitor cocktail (Sigma Aldrich, P8465). Cells were disrupted using a cell disruptor (Constant systems Ltd. One shot model) at 2.6 Kbars and cells debris were removed by centrifugation (15 min at 8000 rpm, 4° C). Soluble protein concentrations were measured according to the 2-D Quant kit protocol (GE Healthcare Life Sciences, 80-6483-56). Aliquots of 80 µg of total protein extract

were supplemented with RapiGest™ (Waters, 186001860) to obtain a final concentration of 0.1 % m/v. The total protein extracts (80 µg) were alkylated with iodoacetamide (10 mM final concentration) in the dark for 1 h. Samples were first digested in-solution for 3 h at room temperature by adding Lysyl-Endopeptidase (Wako, 125-05061) at a protein ratio of 1:50 (w/w). Following a 5-fold dilution with deionized water, samples were digested for 17 h with 80 µg of sequencing-grade modified trypsin (Promega) with 1:100 protein ratio at 37 °C (Wisniewski and Mann, 2012). To quench the digestion, the pH of the peptide mixtures was adjusted to 2 by adding trifluoroacetic acid (TFA). The resulting peptide mixtures were pre-cleaned with a Strata-X column (Phenomenex, ref. 8B-S100-TAK). Columns were washed with 1.5 ml of washing buffer (3% acetonitrile (ACN) and 0.06% glacial acetic acid). The peptide mixtures were charged into the columns, followed by three washing steps of 500 µl with washing buffer. Elution of peptides was performed using 600 µl of elution buffer (40% ACN and 0.06% glacial acetic acid). The resulting samples were concentrated under vacuum to dryness and resuspended in 160 µL of 0.1% TFA and 2% ACN for analysis in a high-resolution mass spectrometer (Figure 4. 1a).

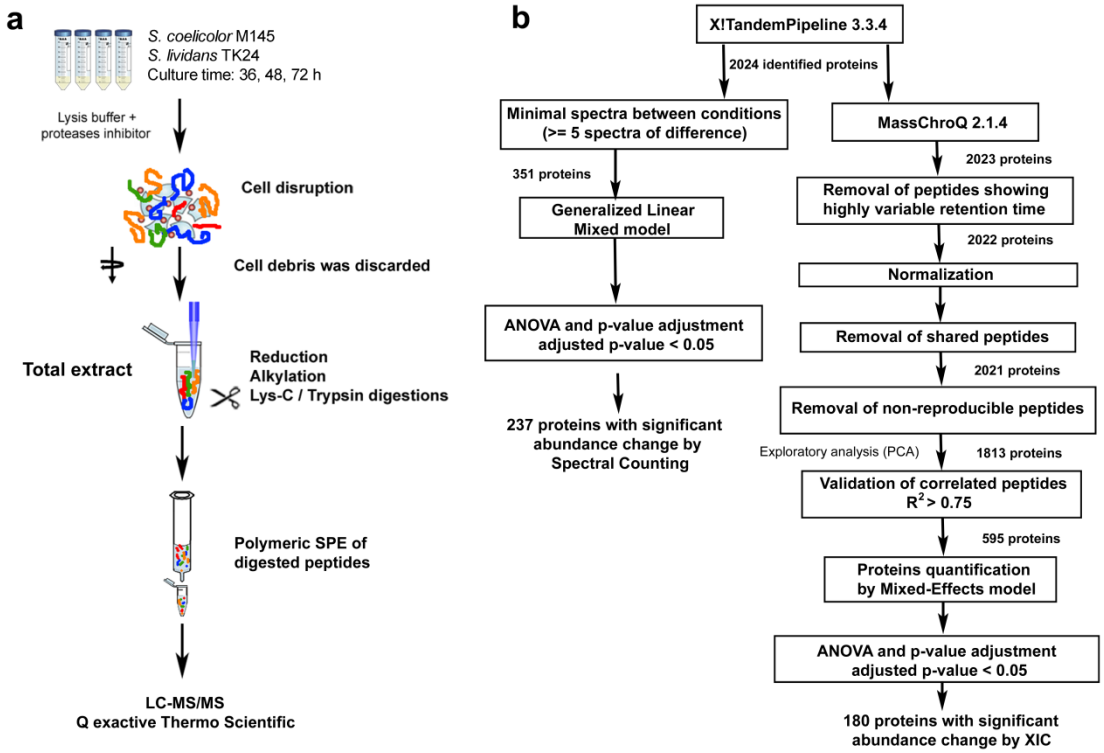

Figure 4. 1. General workflow of the samples preparation for shotgun proteomics (**a**) and the bioinformatic and statistical analysis of proteomic data (**b**).

4.2.3. LC-MS/MS analysis

Liquid chromatography was performed using a NanoLC Ultra system (Eksigent) coupled to a Q-Exactive mass spectrometer (Thermo Fisher Scientific). A 1 µg sample of protein digest was loaded at 7.5 µL/ min on a pre-column (stationary phase: C18, particles of 5 µm; column: 100 µm internal diameter, 2 cm length; NanoSeparations) and desalted with 0.1% (v/v) formic acid in 2% (v/v) ACN. After 3 min, the pre-column was connected to a separating C18 column (stationary phase BIOSPHERE C18, particles of 3 µm; column 75 µm internal diameter, 50 cm length; NanoSeparations). Buffers were 0.1% formic acid in water (solvent A) and 0.1% formic acid in ACN (solvent B). Peptide separation was achieved using a linear gradient from 5 to 35% of solvent B for 180 min at 300 nL/min. Including the regeneration step at 95% of solvent B and the equilibration step at 5% of solvent A, one run took 190 min. Ionization was performed with a 1.3-kV spray voltage applied to an uncoated capillary probe (10 µm internal diameter; New Objective). Xcalibur 2.2 SP1 interface was used to monitor data-dependent acquisition of peptide ions. This included a full MS scan covering the 400 to 1400 mass-to-charge ratio (m/z) with a resolution of 70 000 (AGC target 3e6; maximum IT: 250 ms, dynamic exclusion was set to 60 s) and the MS/MS step was reiterated for the eight major ions (charge state of 2 and 3) detected during the full MS scan (normalized collision energy: 26%; resolution: 17 500; AGC target 5e4; maximum IT: 150 ms). The number of MS1 and MS2 scans in *S. coelicolor* and in *S. lividans* is shown in Figure S4. 3.

4.2.4. Protein identification

A custom FASTA format database was constructed from the genomes of *S. coelicolor* M145 and *S. lividans* TK24 downloaded from The Universal Protein Resource (http://www.uniprot.org/, June 22th 2011, 7810 and 7551 entries respectively). Unique labels were attributed to proteins encoded by orthologous genes that fulfilled an E-value < 10E-10 as a top score after BLASTP (Camacho *et al.*, 2009) for both strains. This resulted in 6911 orthologous protein pairs and 1539 strain-specific proteins. The sub-cellular localization of each protein was predicted from the LocateP

database (Zhou *et al.*, 2008). The functional categories were assigned as described in several databases (StrepDB - The Streptomyces annotation server; Kanehisa and Goto, 2000; Karp *et al.*, 2005). A database of common contaminants and a reversed version of the custom FASTA database were also considered for the analysis.

Database searches were performed using the X!Tandem algorithm (version 2015.04.01; http://www.thegpm.org/TANDEM/, April 1st 2015) implemented in the open source search engine X!TandemPipeline (Langella *et al.*, 2016) (version 3.4.2; http://pappso.inra.fr/bioinfo/xtandempipeline/). Enzymatic cleavage was declared as a trypsin digestion with one possible miscleavage. Carboxyamidomethylation of cysteine residues and oxidation of methionine residues were set to static and possible modifications, respectively. Precursor mass tolerance was 10 ppm and fragment mass tolerance was 0.02 Th. Identified proteins were filtered and grouped using X!TandemPipeline. Data filtering was achieved according to a peptide E-value < 0.05, protein log(E-value) < –2 and to a minimum of two identified peptides per protein. Using such filtering criteria, the peptides false discovery rates (FDR) was estimated to 0.04 % (Supporting information File S-1). MS data were deposited online using PROTICdb database (Ferry-Dumazet *et al.*, 2005; Langella *et al.*, 2013) in the following URL: http://moulon.inra.fr/protic/soil_bacteria

4.2.5. Protein quantification based on extracted ion current

Proteins were quantified based on eXtracted Ion Current (XIC) of their peptides using MassChroQ 2.1.4 (Valot *et al.*, 2011). XIC extraction was performed using a peak detection threshold between 30000 – 50000 and a range of 10 ppm (Supporting information File S-2). The peptide intensities obtained were log10-transformed for further data analyses. Peptides showing a standard deviation of retention time higher than 40 s were removed.

Normalization was performed in order to remove systemic biases between samples as well as more complex variations resulting from transient stochastic events during LC-MS/MS run, such as ESI instability. For this, we used a local normalization method adapted from Lyutvinskiy *et al.* (2013). Briefly, intensity deviation between a given sample and a sample chosen as reference was computed for each peptide-charge

quantified in both samples. The values of intensity deviation thus obtained were ordered according to the peptides' retention time and smoothed using the smooth.spline function in R (R Core Team, 2015). The smoothed values of intensity deviation were used as correction factors to normalize the sample. The intensities of the peptides-charges that were present in the sample to be normalized and absent from the reference sample were corrected considering that intensity deviation was similar for temporally neighboring peptides.

Peptides that belonged to multiple proteins were removed. Reproducibility was set if the peptides have been quantified: 1) in at least 2 replicates per strain-culture time combination and 2) in 4 of the 6 possible strain-culture time combinations. In order to remove peptides whose intensity profiles deviated from the average profile of the peptides from the same protein, Pearson-correlation coefficients were computed for each pair of peptides belonging to a same protein. For each protein, a reference peptide was chosen as the peptide showing the highest number of significant correlations. Peptides correlated to the reference peptide with a coefficient of correlation > 0.75 were kept for further analysis (Figure 4. 1b).

4.2.6. Detection of protein abundance changes

As recommended by Blein-Nicolas and Zivy (2016), proteins were quantified by two complementary methods. The first, called spectral counting (SC), is a rough semi-quantitative method, which allows to detect large abundance variations, including presence/absence variations. The second, based on the peptide intensities obtained from XIC, provides more precise abundance measures allowing to detect smaller abundance changes. But is not suited for the analysis of presence/absence variations since in these cases, absences are considered as missing values. When both types of measurements were available for a protein, the intensity measurements were preferred over the spectral counts.

For SC, the proteins showing a maximal variation of 5 spectra between the different strain x culture time combinations were filtered out since their variation was considered as too low to be significant. For each remaining protein, the abundance in number of

spectra was modeled using the following generalized linear mixed model (GLM) with a Poisson distribution:

$$SC_{jkl} = \mu + S_j + T_k + (SxT)_{jk} + R_l + \varepsilon_{jkl}$$
$$where\ \epsilon_{jkl} \sim N(0, \sigma_\theta^2)$$

SC_{jkl} is the number of spectra measured in strain *j*, culture time *k* and replicate *l*. S_j represents the effect due to strain *j*. T_k represents the effect due to culture time *k*. $(SxT)_{jk}$ represents the effect due to strain *j* x culture time *k* interaction. R_l represents the effect due to biological replicate *l*. $\boldsymbol{\varepsilon}_{jkl}$ is the residual error. Protein abundance changes were detected by analysis of variance (ANOVA) using a Chi-square test.

For the XIC-based approach, the effects of the strain and of the culture time were tested for each protein by modeling the normalized peptide intensities using a mixed-effects model derived from Blein-Nicolas *et al.* (2012):

$$I_{ijkl} = \mu + S_j + T_k + (SxT)_{jk} + P_i + R_l + \theta_{jkl} + \varepsilon_{ijkl}$$
$$where\ \theta_{jkl} \sim N(0, \sigma_\theta^2),$$
$$\epsilon_{ijkl} \sim N(0, \sigma_\theta^2)$$

I_{ijkl} is the intensity measured for peptide *i* in strain *j*, culture time *k* and replicate *l*. S_j represents the effect due to strain *j*. T_k represents the effect due to culture time *k*. $(SxT)_{jk}$ represents the effect due to strain *j* x culture time *k* interaction. P_i represents the effect due to peptide *i*. R_l represents the effect due to biological replicate *l*. Θ_{jkl} represents the technical variation due to sample handling and injection in the mass spectrometer. $\boldsymbol{\varepsilon}_{ijkl}$ is the residual error. Parameters were estimated by maximizing the restricted log-likelihood (REML method). Protein abundance changes were detected by ANOVA.

For both methods (XIC and SC), the obtained p-values were adjusted for multiple testing by the Benjamini-Hochberg approach (Benjamini and Hochberg, 1995). The abundance of a given protein was considered as significantly variable when the adjusted p value was < 0.05 (Figure 4. 1b).

4.2.7. Data analysis

Descriptive analysis of the protein abundances was performed using Principal Component Analysis (PCA) and heatmap representations. Heatmaps were constructed using hierarchical clustering based on Euclidean distances. Volcano plots were made using the –log10 of the adjusted p value from a given protein and the log10-fold change between *S. lividans* / *S. coelicolor* at different culture times (36, 48 and 72h). Boxplots were constructed from the protein abundances obtained from the XIC and SC approaches, for the proteins showing significant abundance variation. Proteins quantification, statistical methods and data analysis were conducted in R (R Core Team, 2015).

4.2.8. Detection of organic acids by GC/MS

Triplicate samples of R2YE medium before inoculation of *S. coelicolor* or *S. lividans* and supernatant samples obtained after cultivation of these strains at 36 and 72 h were used to detect organic acids. 500 µl of NaCl 0.9 % (w/v) and 50 µl of internal standard (0.25 mg of phenyl-butyric acid per ml of methanol) were added to 500 µl of R2YE medium or supernatant samples into 6 ml glass vials. The mixture was acidified with 200 µl of 2.4 N HCl, then, solid NaCl was added until saturation of the samples. Extraction was achieved by the addition of 1.5 ml of ethyl acetate; samples were vigorously vortexed then centrifuged (5 min at 5000 rpm). The upper phase was collected, and a second extraction was performed. The extracts were dried under nitrogen flux. Samples were trimethylsilylated with 150 µl of BSTFA (SUPELCO, ref. 33027): Pyridine (2:1 v/v) for 1 hour at 80°C. After incubation, samples were centrifuged (5 min at 5000 rpm) and 1 µl of the resulting supernatant was injected in a TRACE GC Ultra Gas Chromatograph coupled to a DSQ II quadrupole mass spectrometer (Thermo Fisher Scientific). The separation was achieved using a 20 m x 0.18 mm HP-5MS capillary column (Agilent technologies) coated with 0.18 µm of 5%-diphenyl-95%-dimethylpolysiloxane. The carrier gas was helium at a constant pressure of 120 kPa. The injector temperature was set at 250 °C and the sample was injected in splitless mode (0.5 min). The oven temperature was kept 1 min at 80 °C, then programed from 80 °C to 320 °C at 8°C/ min. The MS transfer line and ion source

temperatures were 325 °C and 250 °C respectively. The mass spectrometer was operated in the electron ionization positive mode (70 eV) with a scan range from m/z 45 to 650 at 2 scans per second. The compounds were identified by comparing the obtained mass spectra to the mass spectra of the National Institute of Standards and Technology (NIST, USA) library. The quantified metabolites were compared according to their values obtained on each cultivation condition using a T-test. Statistically significant differences were set at a p value < 0.05. MS data source can be obtained from the following repository: http://moulon.inra.fr/protic/soil_bacteria

4.2.9. Glucose, proline, ammonia, nitrate/nitrite and external free phosphate quantification

These molecules were assayed in the R2YE medium before inoculation and in the supernatant of 36, 48 and 72 h grown cultures. To do so, were used; for glucose an enzymatic assay kit (Sigma-Aldrich, ref. GAHK-20); for proline a modified colorimetric method utilizing isatin as derivatizing agent (Long *et al.*, 2012); for ammonia an enzymatic assay kit (Sigma-Aldrich, ref. AA0100); for nitrates/nitrites photometric assay (Roche, ref. 11 746 081 001) and for phosphate, a colorimetric assay kit (Sigma-Aldrich, ref. MAK030). These assays were carried out in three independent biological samples.

4.2.10. Esterified fatty acids quantification by GC/MS

Esterified fatty acids methyl esters (FAMES) derived from total lipids of mycelial samples of 36, 48 and 72 h grown cultures were prepared with a method adapted from Lepage and Roy (Lepage and Roy, 1986) and quantified by GC/MS. Detailed information can be found in File S-3.

4.3. Results and discussion

4.3.1. Global proteome analysis

In the conditions used, both strains grew poorly but *S. coelicolor* started to grow earlier than *S. lividans* and yielded 20% more biomass than *S. lividans* after 24h of cultivation (Figure S4. 2). At that time no dissolved oxygen was detected (Figure S4. 1).

Beyond this point, the growth of *S. coelicolor* ceased abruptly whereas *S. lividans* pursued growth at a slow growth rate, reaching stationary phase after 36h of cultivation. After 72h of cultivation, the content of FAMES derived from total lipids reached 55.3 ± 8 µg and 76.4 ± 9 µg per mg of biomass for *S. coelicolor* and *S. lividans*, respectively (Figure S4. 4), being consistent with previous studies (Esnault *et al.*, 2017).

A total of 2024 proteins were identified, 1934 belonged to *S. coelicolor* M145 and, 1873 belonged to *S. lividans* TK24 (Figure 4. 2a, File S-4). These values represented approximately 24% of the theoretical proteome of the two strains, constituting one of the largest published proteome dataset for both strains. Sub-cellular localization of the identified proteins was obtained using the LocateP database (Zhou *et al.*, 2008). The intracellular proteins constituted as expected the largest part (83%) of the cellular proteome (Figure 4. 2b). Secreted proteins and proteins associated with the multi-transmembrane segments constituted 9.8% of the total proteome whereas the theoretical proteome predicted the double (19.6 – 19.8%, Figure S4. 5). Experimental and theoretical C-/N- terminally and lipid anchored protein ratios were similar.

Protein quantification was performed for 19 out of 24 samples. Five samples of *S. coelicolor* M145 (1 at 36h, 2 at 48h and 2 at 72h) were excluded from the analysis because they showed dubious LC-MS/MS results. First, the number of identified peptides was much lower in these 5 samples than in the other samples (<6000 versus >12000, respectively; Figure S4. 6). Second, the PCA based on the protein abundances estimated from peptide intensities showed that these 5 samples were clearly separated from the other samples on the second axis representing 9.5% of the total variability (Figure S4. 7). In contrast, the independent replicates of the remaining 19 samples (Figure 4. 2c and Figure S4. 8) were highly reproducible indicating that an experimental issue has probably affected the protein content of the excluded samples.

Among the 2024 identified proteins, 1429 were quantified by spectral counting and 595 by XIC. The PCA based on protein abundances, with both quantification methods, showed higher effect linked to strains on the first axis (60.2 % the total variability) than to time, on the second axis (11.5 % the total variability, Figure 4. 2c and Figure S4. 8). Detection of 360 proteins showing significant abundance variation in response to strain and time effects (adjusted p value < 0.05; File S-5) was obtained from statistical

analysis of SC-based (180 proteins) and XIC-based (180 proteins) methods (Figure 4. 2d).

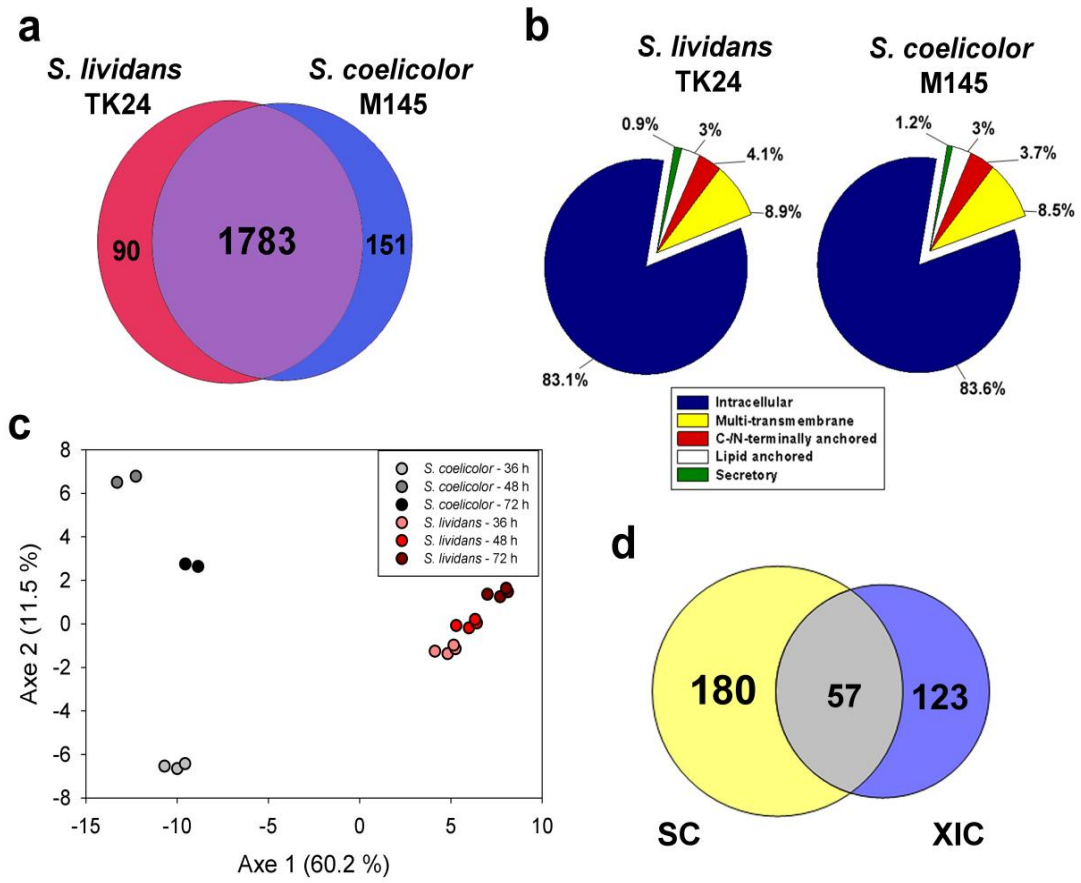

Figure 4. 2. Venn diagram of the 2024 identified proteins using X!TandemPipeline 3.3.4 **(a)**. Sub-cellular localization of the identified proteins in *S. coelicolor* and *S. lividans*. Results obtained from LocateP **(b)**. PCA based on the abundances of 595 proteins quantified by XIC in 19 LC-MS runs. **(c)**. Venn diagram of the 360 proteins showing significant abundance change between *S. coelicolor* and *S. lividans* (ANOVA, adjusted p value < 0.05, **d)**.

The 360 proteins that showed statistical abundance change were represented as a heatmap using Euclidean hierarchical clustering (Figure 4. 3). These 360 proteins belonged to 11 functional categories according to their annotation in the databases and data from the literature (File S-5). As expected, the 6 combinations of strains and culture times were clearly resolved in 2 main clusters corresponding to the strains (Figure 4. 3).

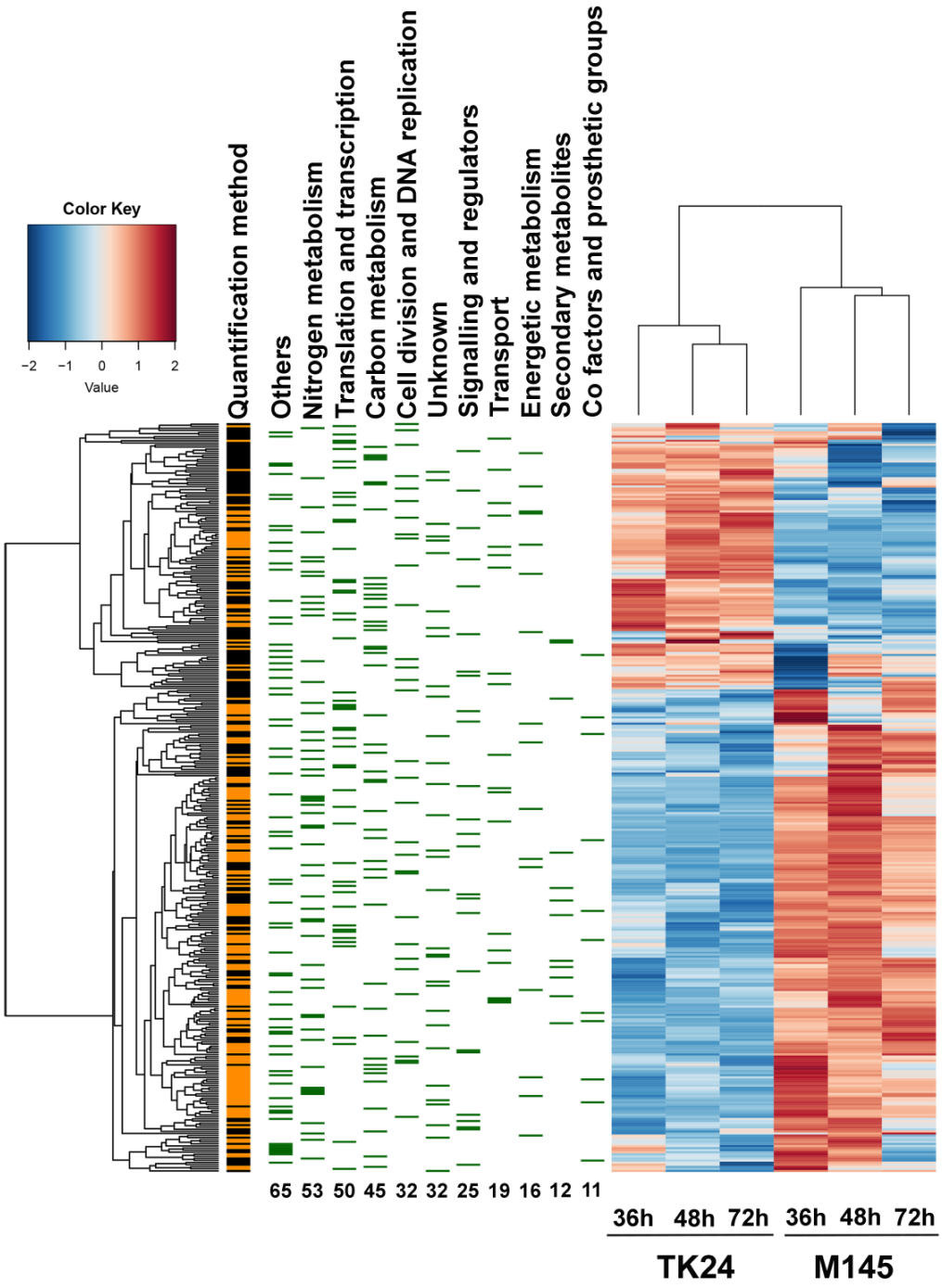

Figure 4. 3. Heatmap representation of the protein abundances estimated by the SC and XIC approaches in *S. coelicolor* (M145) and *S. lividans* (TK24) at 36, 48 and 72 h of culture.

Only proteins showing significant abundance change between the two strains (ANOVA, adjusted p value < 0.05) are displayed. The quantification methods are displayed in the vertical bar indicating those proteins quantified by SC (orange) and XIC (black). The annotated functional categories are shown above the green bars. Total numbers of proteins for each category are also indicated (bottom-left).

4.3.2. Central carbon metabolism

This study demonstrated the high coverage of the shotgun label-free approach since at least one protein was quantified for each step of the central carbon metabolism (Figure 4. 4a, supporting information File S-6 and S-7). A total of 27 proteins involved in the central carbon metabolism showed significant abundance variations (ANOVA, adjusted p value < 0.05) between the two strains.

Among them, 13 were more abundant in *S. lividans* than in *S. coelicolor* (Figure 4. 4b). These proteins included 4 from glycolysis, 2 from glycerol metabolism, 2 from pentose phosphate pathway (PPP), 3 from Krebs cycle, an anaplerotic enzyme and a protein from mannose metabolism. The enolase SCO7638 was the enzyme showing the highest variation between the two strains, being 12, 40 and 9-fold more abundant in *S. lividans* than *S. coelicolor* at 36, 48 and 72h, respectively (see File S-5 and Figure S4. 9). Interestingly, a strong induction of specific enolase isoforms was previously reported in other living organisms (*Zea mays*, *Echinochloa oryzoides* and *E. phyllopogon*) cultivated under anaerobic conditions (Fox *et al.*, 1995; Lal *et al.*, 1998).

Furthermore, the 2 proteins of the glycerol operon (*gyl*) (Seno and Chater, 1983; Hindle and Smith, 1994), glycerol kinase (SCO1660) and Gly3P dehydrogenase (SCO1661), were more abundant in *S. lividans* than in *S. coelicolor*. This indicated that Gly3P, the inducer of the *gyl* operon (Seno and Chater, 1983; Seno *et al.*, 1984; Smith and Chater, 1988), was more abundant in *S. lividans* than in *S. coelicolor*. In *S. lividans*, the high abundance of proteins of glycolysis, glycerol metabolism and PPP is consistent with the generation of sufficient acetyl-CoA, Gly3P and NADPH, the building-blocks and co-factors necessary for TAG accumulation (Le Marechal *et al.*, 2013; Esnault *et al.*, 2017).

The 14 remaining proteins were significantly more abundant in *S. coelicolor* than in *S. lividans* (Figure 4. 4c). These included 3 contributing to acetyl-CoA formation, one belonging to the PPP, 6 to the Krebs cycle, an anaplerotic enzyme and 3 likely to be involved in gluconeogenesis.

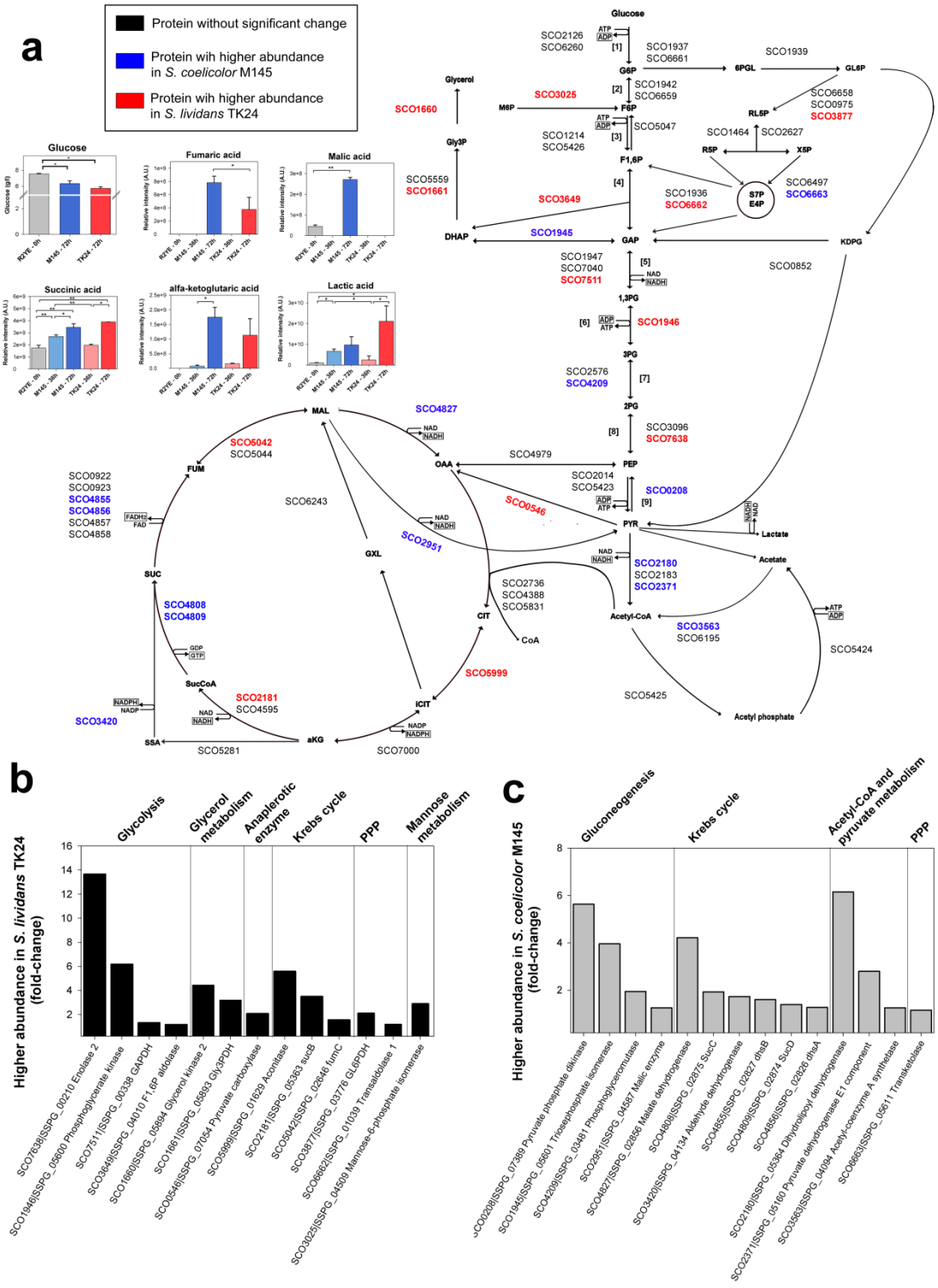

Figure 4. 4. Central carbon metabolism pathways indicating the proteins with higher abundance in *S. coelicolor* and in *S. lividans* **(a)**. Glycolytic steps are indicated in brackets. Histograms indicate the extracellular intermediate compounds of Krebs cycle detected by GC/MS and glucose consumption that showed significant difference (p value < 0.05 [*], p value < 0.01 [**]). Fold-change of proteins belonging to central carbon metabolism showing significantly higher abundance in *S. lividans* than in *S. coelicolor* **(b)** or in *S. coelicolor* than in *S. lividans* **(c)**.

Interestingly, the different reactions catalyzed by the 6 proteins of the Krebs cycle could potentially generate GTP or reduced co-factors that yield ATP from re-oxidation by the respiratory chain (Figure 4. 4a). This is consistent with a predominantly oxidative metabolism of this strain (Esnault *et al.*, 2017). Among the 3 proteins putatively involved in gluconeogenesis, 2 can also be involved in glycolysis (Figure 4. 4a): the phosphoglyceromutase (SCO4209) and the triose phosphate isomerase (TpiA, SCO1945). However, considering the concomitant high abundance of the malic enzyme (SCO2951, converting malate to pyruvate and yielding NADPH) and the gluconeogenic protein pyruvate phosphate dikinase (PPDK, SCO0208, converting pyruvate to phosphoenolpyruvate), SCO4209 and SCO1945 are proposed to be involved in gluconeogenesis. Therefore, *S. coelicolor* is characterized by a lower glycolytic activity, a higher oxidative metabolism and more active gluconeogenesis than *S. lividans*. The reduced glycolytic flux in *S. coelicolor* would result in a reduced flux through the PPP. This flux might be too weak to supply sufficient NADPH for membranous phospholipid as well as for TAG biosynthesis. In consequence, gluconeogenesis would be stimulated to enhance the flux through the malic enzyme and the PPP for NADPH generation.

In conditions of O_2 limitation, a reduction of Krebs cycle and respiratory chain activity is known to take place. In these conditions, pyruvate is converted into lactate by the lactate dehydrogenase that consumes a molecule of NADH generating NAD+ (Okino *et al.*, 2008). Consistently, lactate was present in the culture medium of both strains (Figure 4. 4a). However at 72h, lactate was 2-fold more abundant in the culture medium of *S. lividans* than in that of *S. coelicolor* (Figure 4. 4a), confirming the higher glycolytic activity of *S. lividans*. At last, intermediates of the Krebs cycle, fumaric and malic acids, were found to be more abundant in the growth medium of *S. coelicolor* than in that of *S. lividans* at 72h suggesting a blockage of conversion of malic acid into oxaloacetate in *S. coelicolor*. This blockage is proposed to be due to a lower NAD+ availability linked to the lower glycolytic activity of *S. coelicolor* compared to *S. lividans*.

4.3.3. Nitrogen and amino acids metabolism

In the R2YE medium used, it should be stressed that the amino acids constitute the main nitrogen source; they thus should be catabolized by both strains. However,

strikingly, a large number of proteins belonging to the catabolism of amino acids (18 among 21) were significantly (ANOVA, adjusted p value < 0.05) more abundant in *S. coelicolor* than in *S. lividans* (Figure 4. 5a).

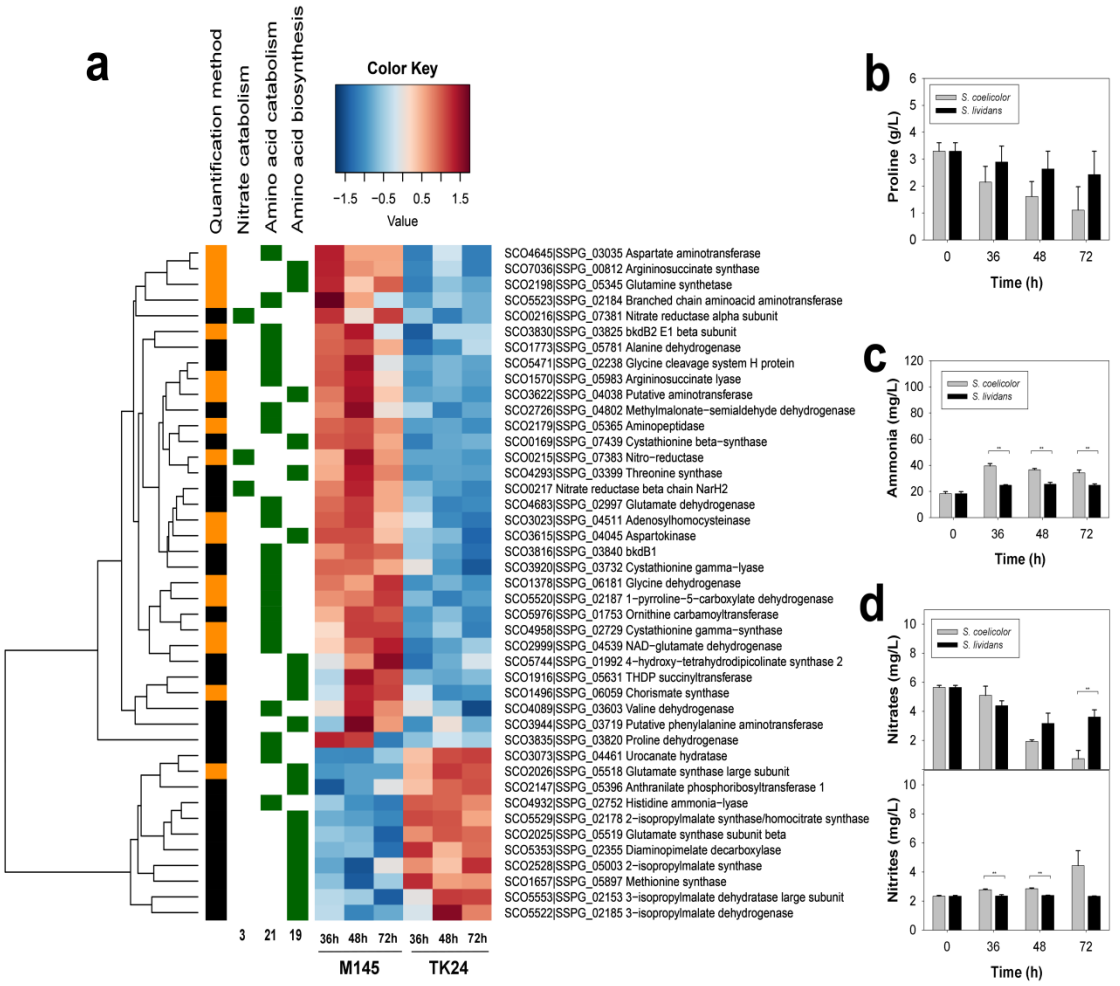

Figure 4. 5. Heatmap representation of proteins corresponding to amino acids and nitrate metabolism in *S. coelicolor* (M145) and *S. lividans* (TK24) at 36, 48 and 72 h **(a)**. The quantification methods are displayed in the vertical bar indicating those proteins quantified by SC (orange) and XIC (black). Total numbers of proteins for each sub-functional category are also indicated (bottom-left). All proteins showed a significant abundance change (ANOVA, adjusted p value < 0.05). Quantification of proline **(b)**, ammonia **(c)**, and nitrates/nitrites **(d)** concentration in growth medium (p value < 0.05 [*], p value < 0.01 [**]).

Since proline was the most abundant amino acid in the medium (3g/L), the decrease of its concentration throughout growth was assayed. This assay clearly indicated that *S. coelicolor* transported and thus likely catabolized far more actively proline than *S. lividans* (Figure 4. 5b). Furthermore, after 72 h of cultivation, 6 µmol and only 4 µmol

of glucose were consumed by *S. lividans* and *S. coelicolor* (Figure 4. 4a), respectively, to make one mg of biomass. This indicates that the "missing" carbon necessary to build one mg of biomass of *S. coelicolor* likely originates from the catabolism of amino acids. In this respect, 4 proteins involved in the catabolism of proline (SCO3835 and SCO5520) or arginine (SCO5976 and SCO1570, Supporting information File S-5) were more abundant in *S. coelicolor* than in *S. lividans*. The catabolism of these amino acids yields glutamate as well as $FADH_2$ and/or NADH. Glutamate will then be converted into α-ketoglutarate, an entry point of Krebs cycle, likely by the glutamate dehydrogenases (GDH, SCO2999 and SCO4683); yielding NH_4^+ and NADH/NADPH. These enzymes were found more abundant in *S. coelicolor* than in *S. lividans* (Supporting information File S-5). The alanine dehydrogenase (SCO1773), that catalyzes the deamination of alanine into pyruvate yielding NH_4^+ and NADH (Voelker and Altaba, 2001) was also more abundant in *S. coelicolor* than in *S. lividans*. In coherence with these deaminations, ammonia was found to be more abundant in the culture supernatants of *S. coelicolor* than in those of *S. lividans* (Figure 4. 5c). At last, 4 proteins known to be involved in the biosynthesis of cofactors or vitamins playing a role in nitrogen and amino acids metabolism (Table 4. 1, class 1) were more abundant in *S. coelicolor* than in *S. lividans* being consistent with the efficient catabolism of amino acids characterizing this strain.

Table 4. 1. Proteins involved in the biosynthesis of cofactors and prosthetic groups that showed significant variation (ANOVA, adjusted p value < 0.05).

SCO numbers	Protein	Observations	Higher abundance (fold-change)	
			S. coelicolor	*S. lividans*
Class 1. Cofactors involved in nitrogen and amino acids metabolism				
SCO1522	Glutamine amidotransferase subunit PdxT	Vitamin B6 biosynthesis, a cofactor of numerous enzymes linked to amino acids metabolism, including transamination, decarboxylation or β- and γ-substitutions (Mooney *et al.*, 2009).	3.6	-
SCO3180	MoaC	Molybdenum biosynthesis, an essential cofactor that forms the catalytic center of a large variety of enzymes such as	2.4	-

		nitrogenases, nitrate reductases, sulfite oxidases and xanthine oxidoreductases (Leimkühler, 2014).		
SCO2614	Folylpolyglutamate synthase	Folate and folate derivatives biosynthesis. FpgS catalyzes the ATP-dependent addition of glutamate moieties to folate and folate derivatives (Salcedo *et al.*, 2001).	1.4	-
SCO4824	FolD-like bifunctional protein	Vitamin B9 and tetrahydrofolate biosynthesis. These cofactors are involved in the biosynthesis of purine and pyrimidine as well as amino acids (met, his and ser).	1.3	-
Class 2. Cofactors involved in respiration				
SCO4506	Chorismate dehydratase	Vitamin K2 (menaquinone) biosynthesis. Important role in respiratoration.	3.3	-
SCO6041	Protoporphyrinogen oxidase	Heme biosynthesis. It catalyzes the last step of heme biosynthesis, the oxidation of protoporphyrinogen IX to protoporphyrin IX (Koch *et al.*, 2004).	3.0	-
SCO2917	Nicotinate phosphoribosyltransferase	NAD/NADP biosynthesis, the reduced forms of this cofactor (NADH/NADPH) donate electrons to the respiratory chain.	1.5	-
SCO1925	Cysteine desulfurase activator complex subunit SufB	Catalyzes the removal of sulfur from cysteine to produce alanine and deliver sulfur to a number of partners involved in Fe-S cluster assembly (Kiley and Beinert, 2003; Ayala-Castro *et al.*, 2008).	1.2	-
Class 3. Biosynthesis of biotin				
SCO5655	Putative aminotransferase	Biotin biosynthesis, a cofactor required for several carboxylation, decarboxylation, or transcarboxylation reactions. Some biotin-requiring enzymes include: acetyl-CoA carboxylase, pyruvate carboxylase, propionyl-CoA carboxylase and 3-methylcrotonyl-CoA carboxylase (Wakil *et al.*, 1983; Cronan Jr and Waldrop, 2002; Zhang *et al.*, 2010).	1.7	-
Class 4. Biosynthesis of cobalamin				
SCO1849	Cobaltochelatase CobN subunit	Cobalamin (vitamin B12) biosynthesis. Important for fatty acids biosynthesis.	-	2.0

The highly active amino acids catabolism that characterizes *S. coelicolor* is likely to be responsible for its highly active oxidative metabolism since it generates, directly or indirectly *via* the Krebs cycle, abundant reduced co-factors whose re-oxidation by the respiratory chain generates ATP (Esnault *et al.*, 2017). Similar observations related to the more efficient catabolism of glutamate over glucose by *S. coelicolor* were reported previously (van Wezel *et al.*, 2006; Wentzel *et al.*, 2012). The molecular basis responsible for the more efficient catabolism of amino acids of *S. coelicolor* compared to *S. lividans* is not known but it likely results in a higher nitrogen supply in *S. coelicolor* than in *S. lividans* and nitrogen proficiency is known to be anti-correlated with TAG accumulation in various micro-organisms (Boyle *et al.*, 2012; Jiang *et al.*, 2014).

Our data also indicate that *S.coelicolor* is characterized by reduced glucose uptake and glycolytic activity compared to *S. lividans*. However, it is unclear whether this reduced glucose uptake is the cause or the consequence of the efficient catabolism of amino acids. In *S. coelicolor*, glucose transport is achieved by the glucose permease *glcP* (SCO5578) (van Wezel *et al.*, 2005), a poor expression of glucose permease gene could lead to a reduced glucose uptake and thus a partial relief of repression by glucose of amino acids catabolism, as described in *S. clavuligerus* (Perez-Redondo *et al.*, 2010). Alternatively, efficient catabolism of amino acids might have a negative impact on glucose uptake and catabolism since abundant ATP generated by highly active oxidative metabolism is known to inhibit these processes in other micro-organisms (Berg JM, 2002).

Interestingly, two proteins involved in histidine catabolism (SCO4932 and SCO3073) and two subunits of the glutamate synthase (GOGAT, SCO2025 and SCO2026) were more abundant in *S. lividans* than in *S. coelicolor*. GOGAT is involved in the conversion of glutamine into glutamate and is mainly expressed in conditions of nitrogen limitation (Schreier, 1993; Reuther and Wohlleben, 2007). This suggests that the relative inefficiency of *S. lividans* to catabolize the amino acids present in the medium might lead to nitrogen limitation that is known to promote TAG accumulation.

4.3.4. Phosphate and energetic metabolism

Three proteins of the Pho regulon, MutT (SCO4144), polyphosphate kinase (Ppk, SCO4145) and the PhoH-like protein (SCO2532) (Kazakov *et al.*, 2003) were more abundant in *S. lividans* than in *S. coelicolor* (Figure 4. 6). The expression of genes from the Pho regulon is usually induced in conditions of inorganic phosphate (Pi) limitation that is correlated with low energetic charge (Santos-Beneit, 2015). The low expression of the genes of the Pho regulon in *S. coelicolor* might be linked to the high energetic charge that characterizes this strain (Esnault *et al.*, 2017). *In vivo* and under Pi limitation, Ppk acts as an adenosine diphosphate kinase, regenerating ATP from ADP and polyphosphate. Its low abundance in *S. coelicolor* is consistent with the fact that in this strain ATP is generated by active oxidative phosphorylation rendering the alternative Ppk-dependent ATP regeneration less necessary than in *S. lividans*. The low amount of phosphate present in the growth medium was readily taken up by both strains (Figure S4. 10). However, we note a slight but more pronounced increase in the concentration of Pi in *S. lividans* than in *S. coelicolor*, late in stationary phase (Figure S4. 10). This increase might be due to the excretion of short polyphosphate and their degradation into free Pi by extracellular phosphatases as reported previously (Smirnov *et al.*, 2015). Enzymes involved in these processes are known to belong to the Pho regulon that seems less strongly induced in *S. coelicolor* than in *S. lividans* as mentioned above.

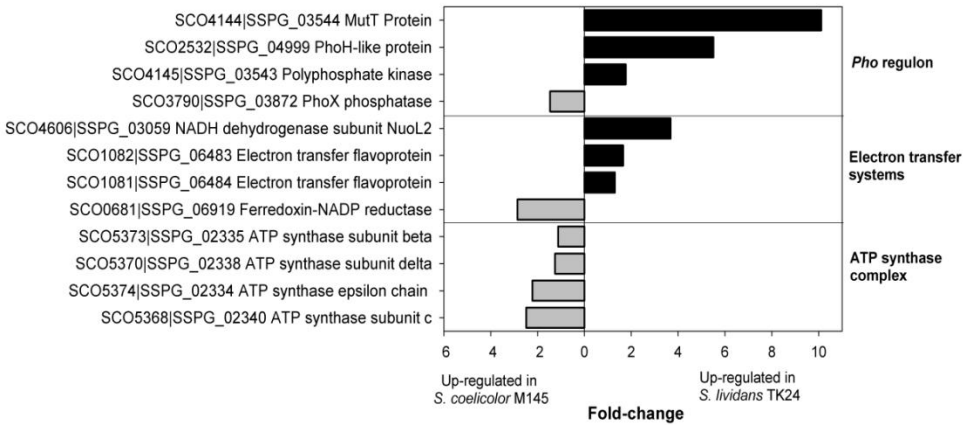

Figure 4. 6. Fold-change of proteins with significant abundance change (ANOVA, adjusted p value < 0.05) belonging to the functional category of energetic and phosphate metabolism. Protein identifiers are indicated as SCO numbers for *S. coelicolor* and their orthologous as SSPG numbers for *S. lividans*.

Furthermore, the subunits c (SCO5368), δ (SCO5370), β (SCO5373) and ε (SCO5374) of the ATP synthase complex were significantly more abundant in *S. coelicolor* than in *S. lividans* but no up-regulation of enzymes of the respiratory chain was seen in *S. coelicolor*. A ferredoxin-$NADP^+$ reductase (SCO0681) was 3-fold more abundant in *S. coelicolor* than in *S. lividans*. These enzymes are thought to catalyze the re-oxidation of reduced ferredoxin generating NADPH, an indispensable co-factor for fatty acid biosynthesis. The abundance of this enzyme in *S. coelicolor* might be a way to compensate the probably weak flux through the PPP that is the main NADPH generating route. Furthermore, 4 proteins known to be involved in the biosynthesis of cofactors or vitamins playing a role in respiration (Table 4. 1, class 2) were more abundant in *S. coelicolor* than in *S. lividans*. This is consistent with the active oxidative metabolism and thus respiration characterizing *S. coelicolor*.

In contrast, 3 proteins belonging to the respiratory chain were significantly more abundant in *S. lividans* than *S. coelicolor*. These included the electron transfer flavoproteins α and β (SCO1081 and SCO1082, respectively) as well as the NADH dehydrogenase subunit NuoL2 (SCO4606). The latter is encoded by a gene present in a large operon (SCO4599-SC04608) directing the synthesis of enzymes of the respiratory chain.

4.3.5. Stress responses

An oxidative metabolism is known to generate far more reduced co-factors than a glycolytic metabolism (Berg JM, 2002). The re-oxidation of reduced co-factors by the respiratory chain requires O_2, as final electron acceptor and results in the generation of H_2O. However, in conditions of limited O_2 availability, the re-oxidizing capacity of the respiratory chain is low, consequently electron leakage toward secondary acceptors is likely to occur, generating reactive oxygen/nitrogen species (Seaver and Imlay, 2004). Indeed, in *S. coelicolor*, several proteins known to be involved in the resistance to oxidative stress were more abundant than in *S. lividans* (Figure 4. 7a). These include DpsA (SCO0596, 12 fold over-expressed) that contributes to DNA protection during oxidative stress (Facey *et al.*, 2011). Therefore, in conditions of O_2 limitation, a glycolytic metabolism is advantageous since ATP is mainly generated *via* substrate level phosphorylation and not by oxidative phosphorylation.

The oxidative metabolism of *S. coelicolor* consumes more O_2 than the glycolytic metabolism of *S. lividans*, consequently *S. coelicolor* likely faces an earlier and more severe hypoxia than *S. lividans*. This situation obviously triggers an entry into a dormancy-like state. Indeed proteins orthologous to those belonging to the DosR dormancy regulon of *Mycobacterium tuberculosis* (Honaker *et al.*, 2010; Leistikow *et al.*, 2010) were more abundant in *S. coelicolor* than in *S. lividans* (Figure 4. 7a). These proteins are encoded by two large loci (SCO0161-SCO0181 and SCO0197-SCO0220) that are likely to be under the positive control of the LuxR response regulator (SCO0204), which is orthologous to the DosR regulator of *M. tuberculosis* (Boon and Dick, 2012). SCO0204 was found to be 3.5 fold more abundant in *S. coelicolor* than in *S. lividans* (Supporting information File S-6). These loci also include SCO0208 (PPDK); SCO0216 and SCO0217 (α and β subunits of the nitrate reductase) and in divergence SCO0215, encoding a nitro-reductase; as well as other genes orthologous to those belonging to the DosR regulon of *M. tuberculosis* (Figure 4. 7a) (Selvaraj *et al.*, 2012). The higher abundance of nitrate reductase sub-units in *S. coelicolor* strongly suggests that, in absence of O_2, nitrate (NO_3^-) might be used as an alternative electron acceptor, generating nitrite (NO_2^-) as reported previously (van Keulen *et al.*, 2005; Fischer *et al.*, 2010; Fischer *et al.*, 2014). The higher rate of nitrate consumption by *S. coelicolor* compared to *S. lividans* as well as the higher generation of nitrite by *S. coelicolor* (Figure 4. 5d) is consistent with this hypothesis.

In contrast in *S. lividans*, proteins of the DosR-like regulon were not induced but 5 proteins belonging to the tellurium resistance family were up-regulated versus only one (SCO5806) in *S. coelicolor* (Figure 4. 7a). It is noteworthy that the TerD-like protein SCO2368, a protein known to down-regulate the expression of genes of the DosR-like regulon (Daigle *et al.*, 2015), was more abundant in *S. lividans* than in *S. coelicolor*. The function of the other TerD proteins is not clearly known but some studies suggest that these proteins might play a role in growth slowdown in adverse conditions in order to improve cell survival (Sanssouci *et al.*, 2011; Sanssouci *et al.*, 2012). In addition, a proteomic study of *S. viridochromogenes* showed the up-regulation of tellurium resistance proteins in response to oxidative stress (Michta *et al.*, 2014). A protein of the universal stress protein (USP) family (SCO7299) was also found to be 5.7-fold more abundant in *S. lividans* than in *S. coelicolor*. Proteins of the UPS family are among the

most up-regulated proteins during growth arrest (Kvint *et al.*, 2003; Seifart Gomes *et al.*, 2011) but their role is not clearly understood.

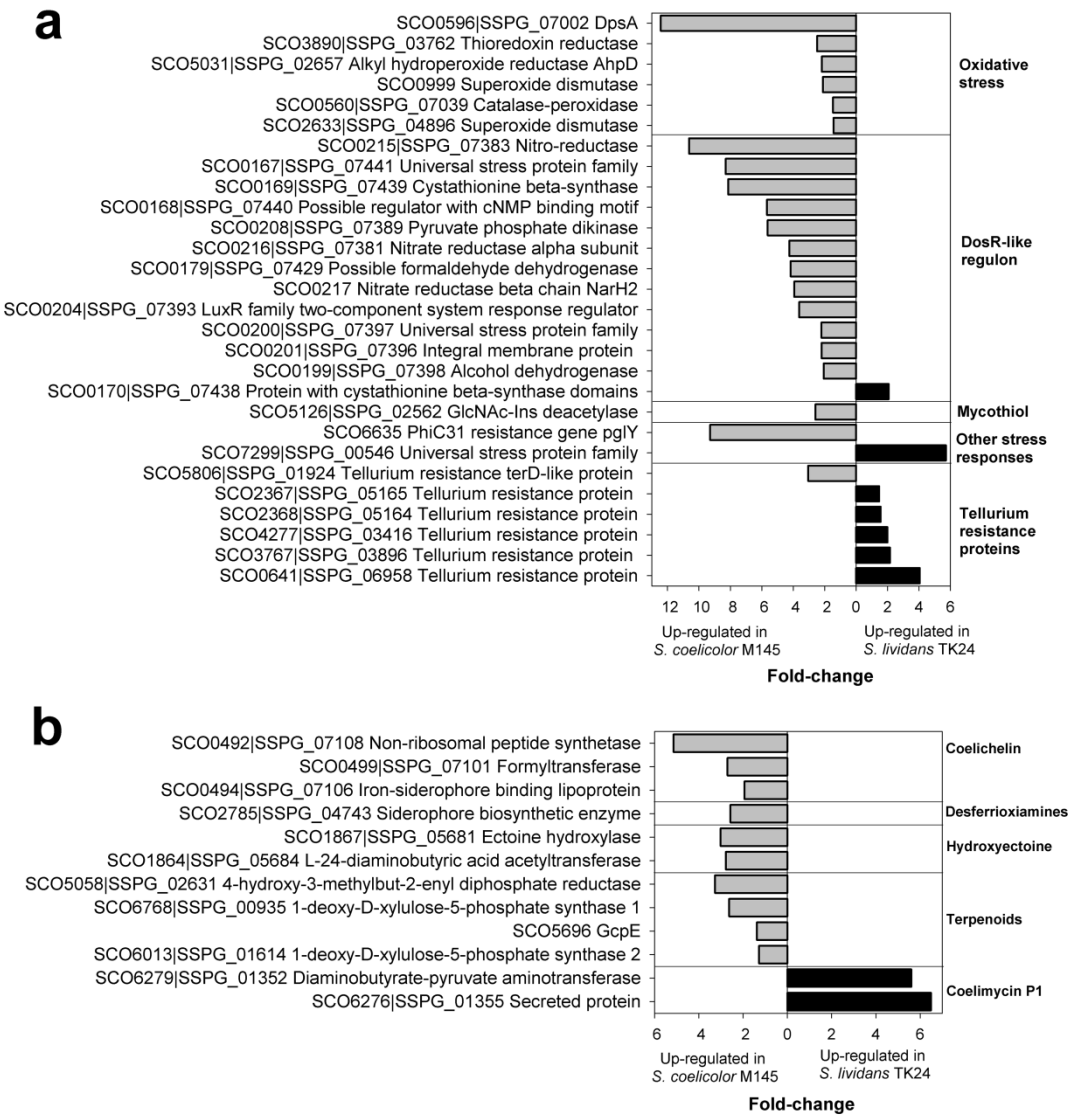

Figure 4. 7. Fold-change of proteins with significant abundance change (ANOVA, adjusted p value< 0.05) belonging to the functional categories of response to stress and defense (**a**) and secondary metabolites biosynthesis (**b**).
Protein identifiers are indicated as SCO numbers for *S. coelicolor* and their orthologous as SSPG numbers for *S. lividans*.

Finally, it should be mentioned that the specific metabolic features of *S. coelicolor* grown in O_2 limitation were strikingly similar to those described for the deletion mutant of SCO2127 (Tierrafría *et al.*, 2016), a gene located just upstream of the glucose kinase gene. This is thought to encode a transcriptional activator of the expression of the glucose transporter and glucose kinase genes and thus mediates indirectly glucose

catabolite repression (Forero *et al.*, 2012). In the ΔSCO2127 mutant, glycolysis was down-regulated whereas gluconeogenesis was up-regulated; the LuxR regulator SCO0204, as well as other proteins of the DosR-like dormancy regulon, including those of the nitrate reductase complex, were also up-regulated whereas ACT production was strongly reduced. Considering the similarities between our data and those obtained with this mutant we searched for SCO2127 peptides in our proteomic data. Very few were found suggesting that the expression of this gene was not expressed in O_2 limitation. We thus propose that SCO2127 might play a role in the adjustment of glucose uptake and catabolism in response to O_2 availability. Indeed it seems logical to slow down glucose entry and catabolism when O_2 is limiting.

4.3.6. Secondary metabolite pathways

Proteins belonging to four different secondary metabolite biosynthetic pathways showed a significantly higher abundance in *S. coelicolor* than in *S. lividans* (Figure 4. 7b). Four of these proteins correspond to two clusters directing the synthesis of the siderophores coelichelin (SCO0492, SCO0494 and SCO0499) and desferrioxamine (SCO2785). The higher abundance of proteins of these pathways in *S. coelicolor* is consistent with the oxidative metabolism of this strain. Indeed several enzymes of the Krebs cycle and of the respiratory chain require iron for their function (Oexle *et al.*, 1999). The low abundance of proteins of these pathways in *S. lividans* is also consistent with the higher abundance of the iron-repressor DmdR1 (SCO4394) in this strain (Supporting information File S-7). This protein is known to repress the synthesis of these siderophores (Flores and Martin, 2004; Flores *et al.*, 2005; Tunca *et al.*, 2007).

Two proteins related to 5-hydroxyectoine biosynthesis (SCO1864 and SCO1867) were also more abundant in *S. coelicolor* than in *S. lividans*. Molecules of the ectoine family are usually synthetized in conditions of hyper-osmotic shock (Kempf and Bremer, 1998; Bursy *et al.*, 2008; Tanne *et al.*, 2014). These water-trapping molecules might limit water loss in these conditions (Manzanera *et al.*, 2002; Smiatek *et al.*, 2012).

Proteins encoded by the terpenoid biosynthetic cluster (SCO5058, SCO5696, SCO6013, and SCO6768) were also more abundant in *S. coelicolor* than in *S. lividans* (Kuzuyama, 2017). The function of these molecules in bacteria is not known, although some reports suggest that they may function as electron acceptors contributing to the

alleviation of oxidative stress (Bosak *et al.*, 2008; Cane and Ikeda, 2012; Matsuura *et al.*, 2014).

Two proteins (SCO6276 and SCO6279) of the coelimycin P1 (CPK) biosynthetic pathway (Gomez-Escribano *et al.*, 2012), that directs the synthesis of a yellow pigmented alkaloid polyketide, were 5 to 6-fold more abundant in *S. lividans* than in *S. coelicolor* whereas 9 out of 16 proteins of this cluster did not present any significant abundance change (SCO6273-SCO6288, Supporting information File S-4). The biosynthesis of CPK relies on acetyl-CoA availability and was shown to be up-regulated in the presence of glucose (Romero-Rodríguez *et al.*, 2016). Since glucose uptake and glycolysis was shown to be more active in *S. lividans* than in *S. coelicolor*, this metabolite is likely to be more abundantly produced by *S. lividans* than by *S. coelicolor*. We thus propose that the function of this metabolite might be to remove excess of acetyl-CoA when its generation rate exceeds its assimilation rate by the Krebs cycle.

Our study thus suggested that the secondary metabolites produced fulfill specific roles in *S. coelicolor* and *S. lividans*. Interestingly, proteins belonging to the canonical CDA, RED and ACT clusters were not identified in *S. coelicolor* in this study. This indicated that their production might only be triggered in fully aerobic conditions as suggested previously (Esnault *et al.*, 2017).

4.3.7. Some speculation concerning the genetic basis possibly underpinning the different metabolic features of *S. coelicolor* and *S. lividans*

Two studies reporting whole-genome comparison of these two strains highlighted, despite over 90% conservation, some significant differences (Jayapal *et al.*, 2008; Lewis *et al.*, 2010). Indeed 46 regulatory proteins or two components systems were found to be absent or divergent between the two strains (Jayapal *et al.*, 2008). Furthermore genes involved in the biosynthesis of methionine (SCO0985) or encoding S-adenosyl methionine (SAM)-dependent methyltransferases (SCO0995 and SCO3452) were found to be absent in *S. lividans* (Lewis *et al.*, 2010) and SAM is known to play an important role in the regulation of antibiotic biosynthesis (Kim *et al.*, 2003; Huh *et al.*, 2004). The

presence/absence of these regulatory systems apparently compromises any rational thinking concerning the metabolic differences between the strains. However, Lewis *et al.*, (Lewis *et al.*, 2010) speculated that presence/absence of some specific genes might underlie the metabolic differences between the two strains.

For instance, the absence in *S. lividans* of genes thought to be involved in the degradation and assimilation of fatty acids, could suggest that these processes might be more active *in S. coelicolor* than in *S. lividans*. Among these genes, the acyl-CoA deshydrogenase (SCO6938), the enzymes of the glyoxylate cycle (isocitrate lyase SCO0982 and malate synthase SCO0983) and two methylmalonyl-CoA mutases (SCO6832/33) are present in *S. coelicolor* but not in *S. lividans*. The latter two systems are involved in the conversion of acetyl-CoA or methylmalonyl-CoA resulting from fatty acids or amino acids degradation, into succinate (Ensign, 2006). These differences might be consistent with the higher antibiotic production ability and lower TAG content of *S. coelicolor* compared to *S. lividans*. However, the proteins mentioned above were not found in *S. coelicolor* in this proteomic study and the small number of proteins involved in lipid metabolism detected (File S-5) do not seem to corroborate this hypothesis. Furthermore, on the basis of their physiological and transcriptomic analysis, Wentzel et al (Wentzel *et al.*, 2012) proposed the existence of a bottleneck in the conversion of pyruvate to acetyl-CoA in *S. coelicolor*. Our proteomic studies did not corroborate this hypothesis, either. However, one cannot exclude that these discrepancies could be linked to the conditions of O_2 limitation used in this study.

4.4. Conclusion

These studies indicated that *S. lividans* metabolism was mainly glycolytic. This strain thus generates its energy predominantly *via* glucose catabolism. In contrast, *S. coelicolor* generates its energy predominantly *via* oxidative phosphorylation, performing a metabolism predominantly oxidative. This specific feature of *S. coelicolor* is likely to be related to its higher efficiency to catabolize amino acids in comparison to *S. lividans*. This process generates directly and indirectly (*via* Krebs cycle feeding) abundant reduced co-factors whose re-oxidation by the respiratory chain yields ATP. This highly active oxidative metabolism induces a more active O_2 consumption than the mainly glycolytic metabolism of *S. lividans*. Therefore, in conditions of O_2 limitation, *S.*

coelicolor was exposed earlier than *S. lividans* to a more severe hypoxia. This was correlated with a marked oxidative stress and the induction of a dormancy-like state in *S. coelicolor*. However, the nature of the crucial genetic differences underpinning the different metabolic features characterizing these two model strains extensively studied by the *Streptomyces* scientific community remains to be elucidated.

4.5. Supplementary data

The following files are available online free of charge at
http://pubs.acs.org/doi/abs/10.1021/acs.jproteome.7b00163

File S1.xlsx X!Tandempipeline results of the identified proteins.
File S2.txt MassChroQ parameters for peptides quantification.
File S3.docx Protocol for Esterified fatty acids quantification by GCMS
File S4.xlsx Distribution of the proteins belonging to *S. coelicolor* and *S. lividans*.
File S5.xlsx Proteins with statistically significant change quantified by XIC-based and SC-based methods.
File S6.pdf Boxplots of each protein with significant variation quantified by SC-based method.
File S7.pdf Boxplots of each protein with significant variation quantified by XIC-based method.

4.6. Supplementary figures

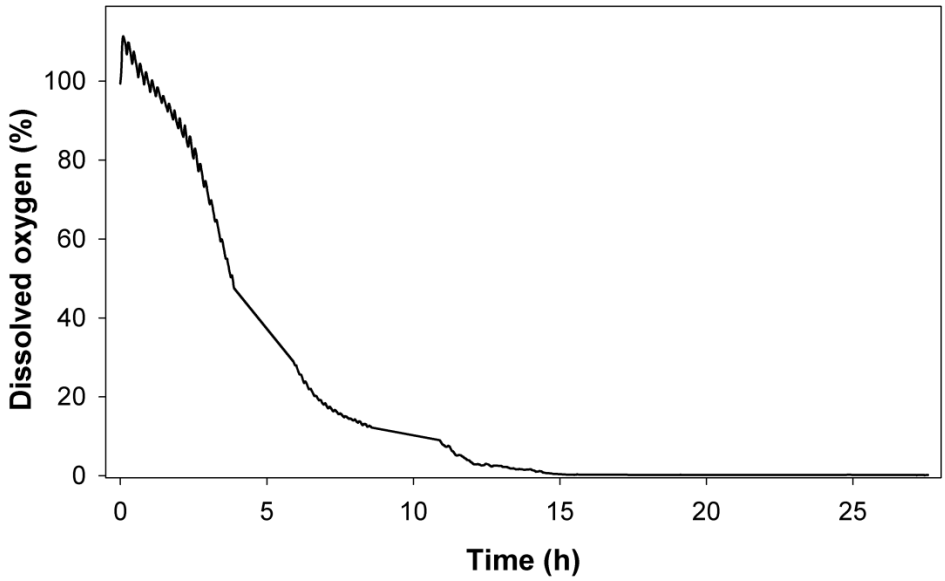

Figure S4. 1. Percentage of dissolved oxygen in *S. coelicolor* cultures. Continuous measurements were conducted using an oxygen sensor (OxyFerm FDA 325).

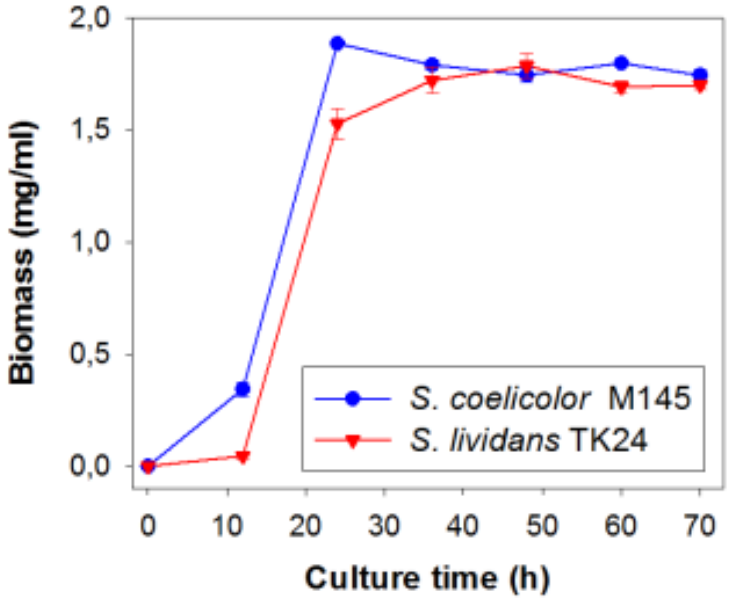

Figure S4. 2. Growth curves of *S. coelicolor* and *S. lividans*. Values represent the average of four independent experiments ± SD.

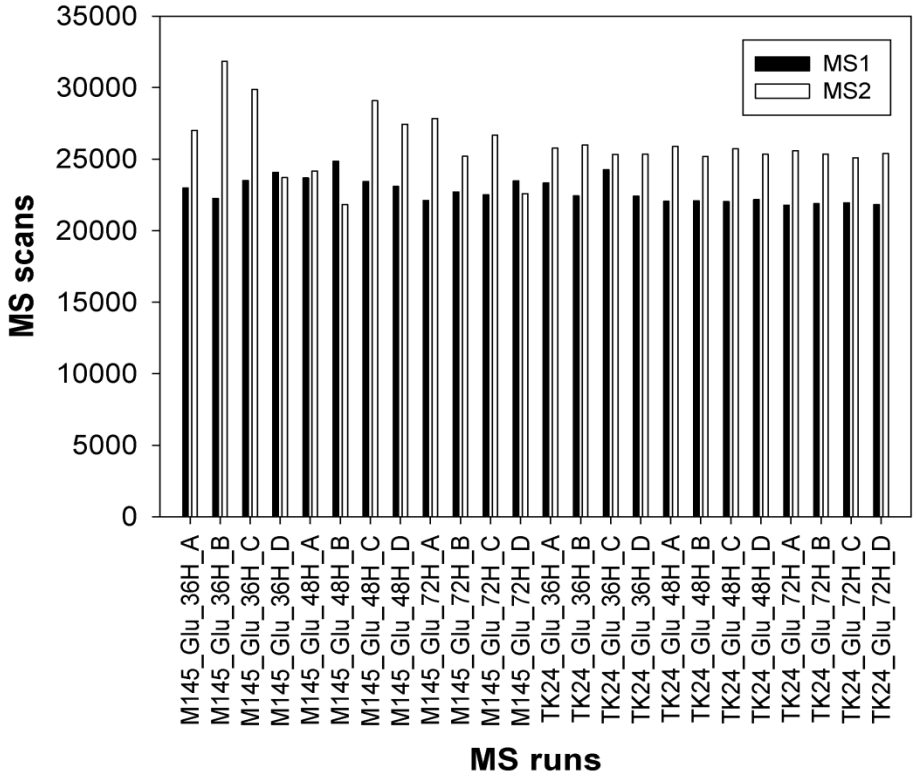

Figure S4. 3. Number of MS1 and MS2 scans from the LC-MS runs.

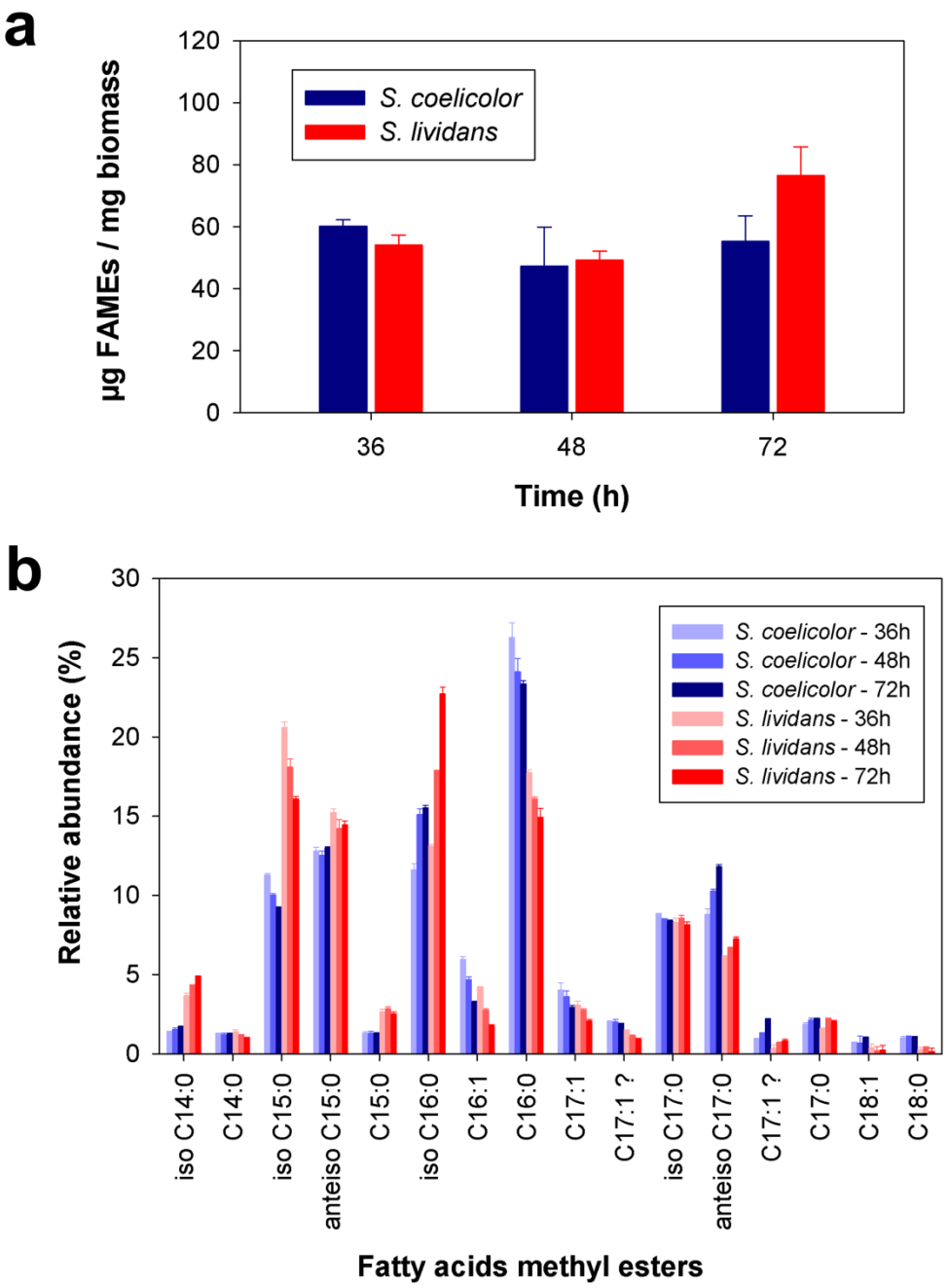

Figure S4. 4. Content of total lipid derived fatty acids methyl esters (FAMES) in *S. coelicolor* and *S. lividans* **(a).** Relative abundance of the various FAMES species determined by GC/MS **(b)**.
Values represent the mean and standard deviation (n = 3).

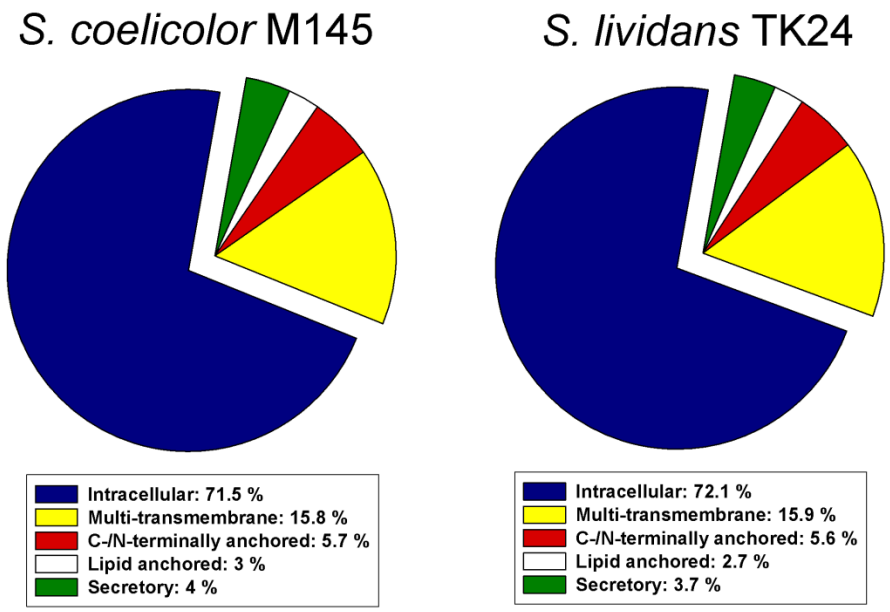

Figure S4. 5. Theoretical sub-cellular distribution of the proteomes of *S. coelicolor* and *S. lividans* using the LocateP database.

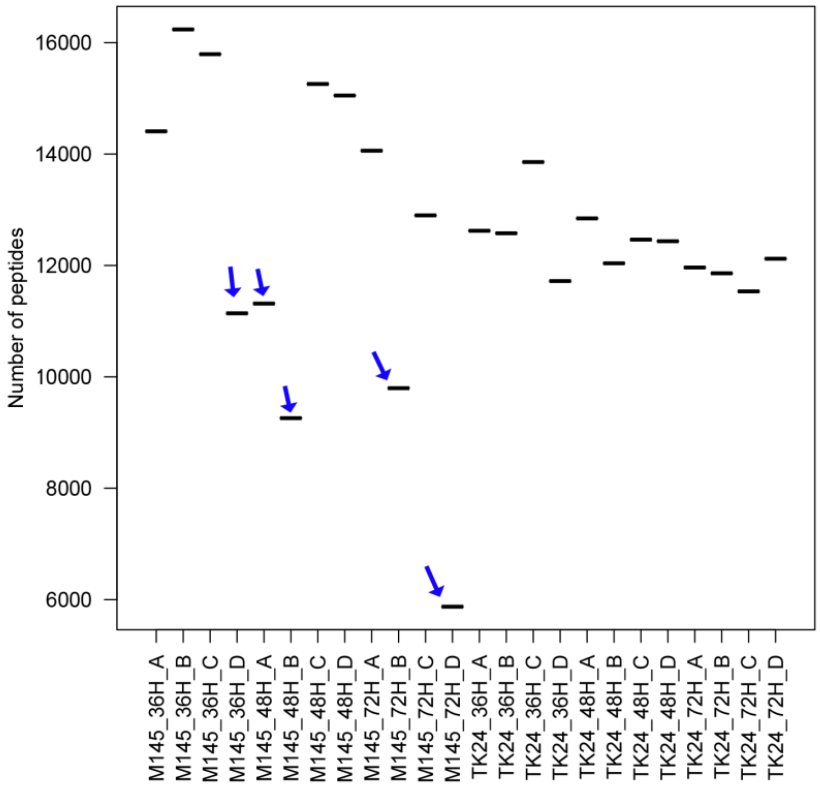

Figure S4. 6. Number of quantified peptides per LC-MS run of the dataset. Arrows indicate the dubious LC-MS runs for *Streptomyces coelicolor* M145.

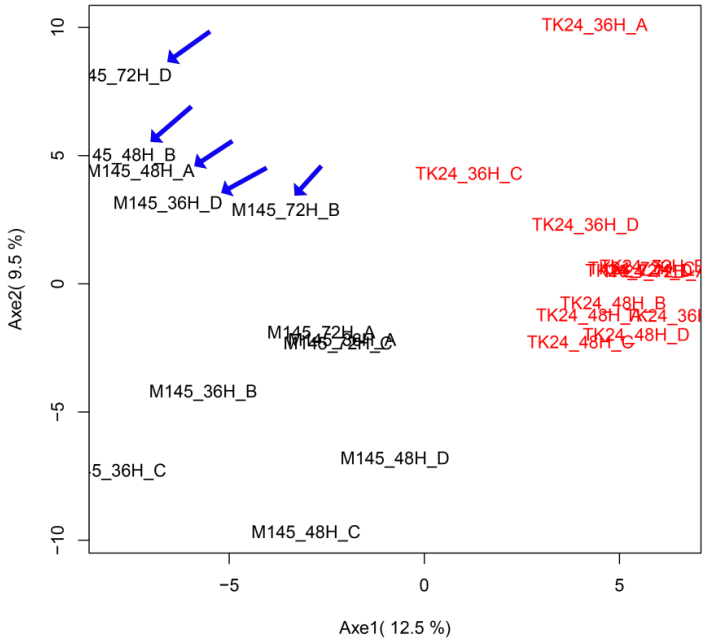

Figure S4. 7. PCA based on protein abundances estimated from normalized peptide intensities of all LC-MS runs of the dataset. LC-MS runs for *S. coelicolor* M145 and *S. lividans* TK24 are represented in black and red, respectively.
Arrows indicate the same LC-MS runs previously observed with low peptides per sample.

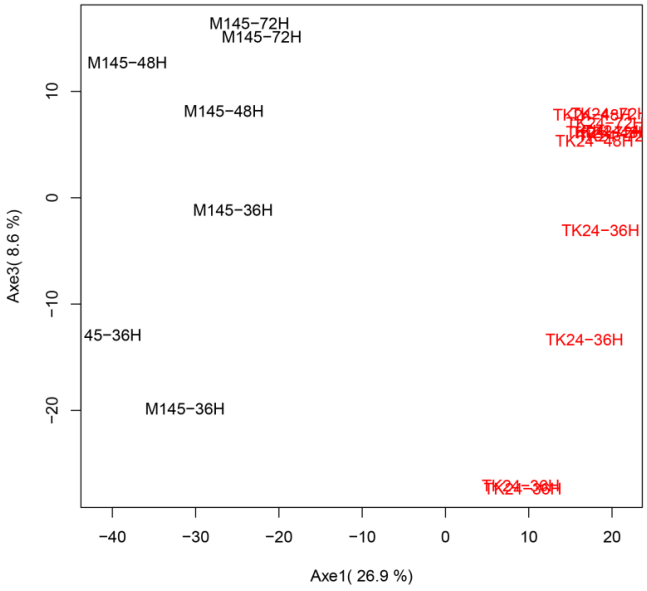

Figure S4. 8. PCA based on the abundances of 1429 protein estimated from spectral counts in the 19 selected LC-MS runs.
The LC-MS runs for *S. coelicolor* M145 and *S. lividans* TK24 are indicated in black and red, respectively.

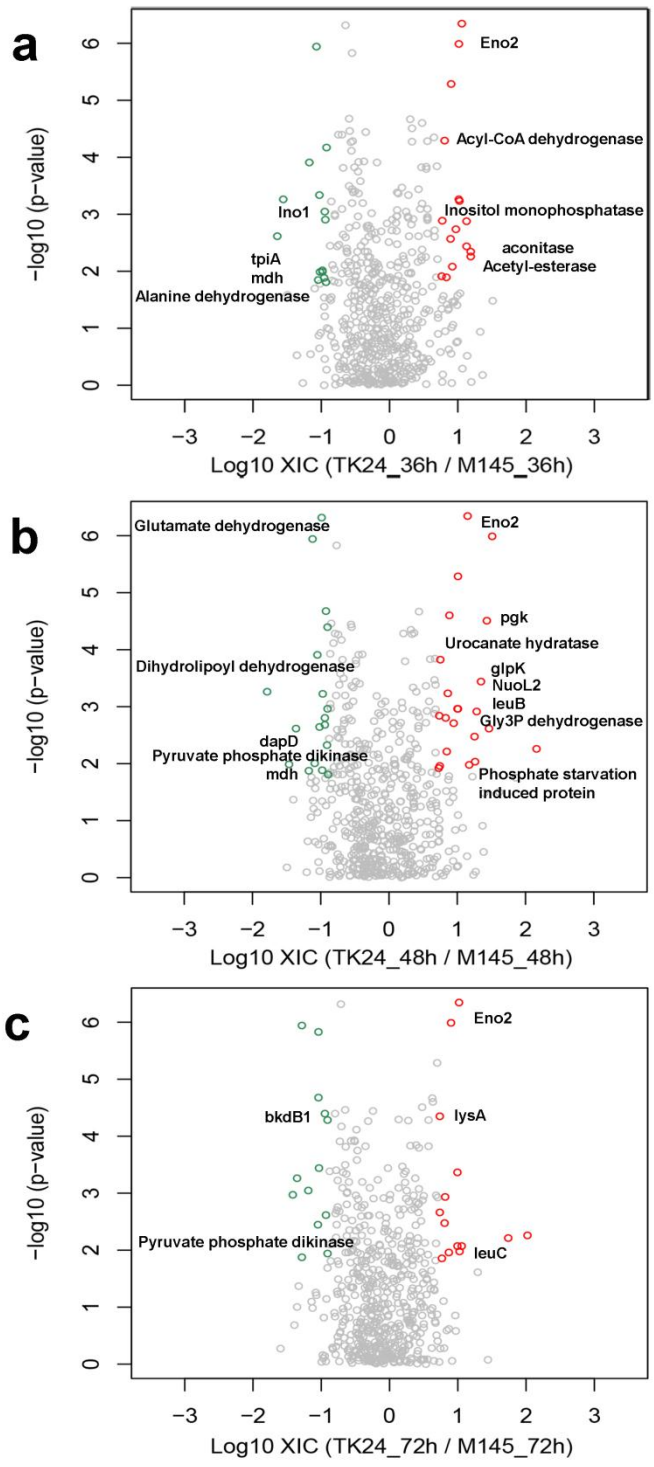

Figure S4. 9. Volcano plots of log10-fold change (*S. lividans* / *S. coelicolor*) of proteins abundance at 36 (**a**), 48 (**b**) and 72 h (**c**) of cultivation.
Representative proteins (adjusted p-value < 0.05, log10-fold change >0.8 and <-0.8) are highlighted in red (for *S. lividans*) and green (for *S. coelicolor*). Gene names are indicated for those corresponding to central carbon, nitrogen and energetic metabolism (detailed information in File S-5).

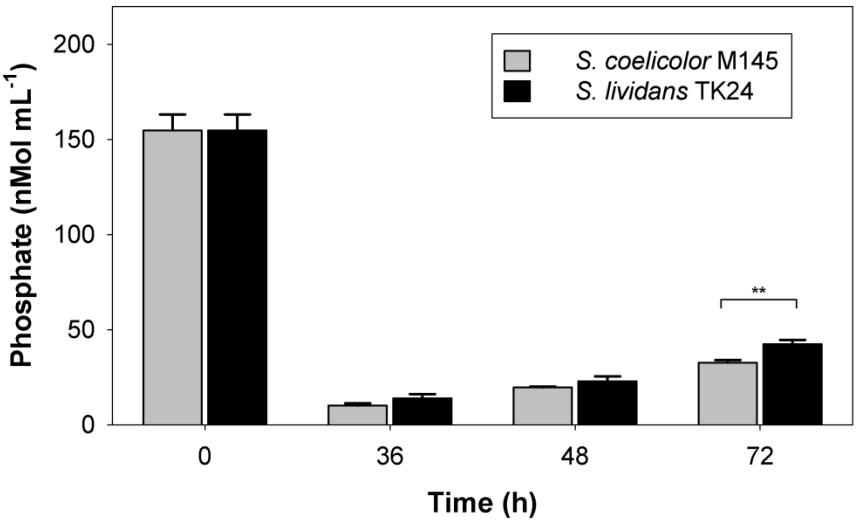

Figure S4. 10. Total free phosphate content in growth medium of *S. coelicolor* and *S. lividans*.
Values represent the average of three independent experiments ± SD. (p value < 0.01 [**]).

4.7. Acknowledgments

This work was supported by the CNRS, the Université Paris Sud and the ANR Bio-SoundIR (grant ANR-15-CE09-0002-01) of the French National Research Agency. The financial support for AMO thesis was provided by the National Science and Technology Council (CONACYT, Mexico) number 314457. Jos Boekhorst and Roland Siezen are kindly acknowledged for providing the subcellular distribution of *S. lividans* TK24 proteins. We are thankful to Ian-Barry Holland and David Hodgson for stimulating discussions.

CHAPTER V. COMPARATIVE PROTEOMIC ANALYSIS OF *STREPTOMYCES COELICOLOR* AND *STREPTOMYCES LIVIDANS* REVEALED DRASTIC DIFFERENCES IN THEIR METABOLIC FEATURES.

This article is still under interpretation process.

Aaron Millan-Oropeza[1*], Céline Henry [2¶], Mélisande Blein-Nicolas[3], Marie-Jöelle Virolle[1¶]

[1] Institute for Integrative Biology of the Cell (I2BC), CEA, CNRS, Univ. Paris-Sud, Université Paris-Saclay, F-91198, Gif-sur-Yvette cedex, France.

[2] Institut National de la Recherche Agronomique (INRA), Microbiologie de l'Alimentation au service de la Santé (MICALIS) UMR 1319, Plateforme d'Analyse Protéomique de Paris Sud-Ouest (PAPPSO), Université Paris-Saclay, Jouy-en-Josas, France.

[3] Génétique Quantitative et Évolution (GQE) - Le Moulon, INRA, Univ Paris-Sud, CNRS, AgroParisTech, Université Paris-Saclay, F-91190, Gif-sur-Yvette, France.

[¶] Contributed equally

5.1. Introduction

S. coelicolor A(3) and *S. lividans* TK24 are phylogenetically closely related species with drastically different abilities to produce four well characterized secondary metabolites. These include, from the earliest to the latest produced through cultivation, the cryptic type 1 polyketide synthase (CPK) (Pawlik *et al.*, 2006), the lipopeptide calcium-dependent antibiotic (CDA), the red-pigmented tripyrrole undecylprodigiosin (RED), and the blue pigmented polyketide actinorhodin (ACT) (Hopwood, 1999). CPK and ACT are polyketide antibiotics synthetized directly from acetyl- and malonyl-coenzyme A units by polyketide synthases (PKS) (Okamoto *et al.*, 2009; Challis, 2013) whereas CDA and RED are peptidic or hybrid peptidic/polyketide antibiotics respectively synthetized from proteinogenic and non-proteinogenic amino acids by non-ribosomal peptide synthases (NRPS) (Challis, 2013), RED bearing also an acyl moiety synthetized by PKS-like enzymes (Cerdeño *et al.*, 2001; Challis, 2013). The CDA, RED and ACT pathways are highly expressed in *S. coelicolor* but not in *S. lividans*. *In silico* analysis of the genomes of *S. coelicolor* M145 (Bentley *et al.*, 2002) and *S. lividans* TK24 (Rückert *et al.*, 2015) revealed that 91% of the genes present in one strain have orthologs in the other strain (Lewis *et al.*, 2010) and they both carry 25 clusters potentially directing the synthesis of different types of secondary metabolites including: 8 products from PKS, 3 products synthesized by NRPS, 3 terpenoid biosynthetic pathways (albaflavenone, isorenieratene and hopene), 4 ribosomally synthesized and post-translationally modified peptides (RiPPs, including sanglifehrin A, SapB, lactonamycin, and informatipeptin) (Mohimani *et al.*, 2014) and other products encoding the siderophores coelichelin and deferrioxiamine B or the osmolyte 5-hydroxyectoine (Challis and Hopwood, 2003; Weber *et al.*, 2015). These two species have been extensively studied by the *Streptomyces* scientific community over the last 40 years since they constitute models to decipher the regulation of antibiotics biosynthesis (Hopwood, 1999).

It was recently shown that on the rich R2YE solid medium containing glucose as main carbon source, the high antibiotic biosynthetic ability of *S. coelicolor* was shown to be correlated with a low lipid content whereas the poor ability of *S. lividans* to synthetize antibiotics was correlated with a 3 fold higher lipid content indicating the

ability of this strain to accumulate storage lipids of the triacylglycerol (TAG) family (Le Marechal *et al.,* 2013). This indicated a reverse correlation between the ability to accumulate TAG and that to synthetize antibiotics. In order to determine whether this anti-correlation was or not a general rule, a comparative label-free, shotgun proteomic analysis of these two strains, grown on solid R2YE medium, in presence of either glucose or glycerol as main carbon source was carried out. The comparison of these two carbon sources was judged interesting for this purpose since, whereas these two strains had very different TAG content and ACT producing abilities on R2YE with glucose, they had a similarly high TAG content on R2YE with glycerol.

Unexpectedly, this study revealed that *S. coelicolor* still produces ACT on R2YE glycerol at a similar level than on glucose "despite" its high TAG content but did not export it. This study also revealed drastic differences between the two strains in the abundance of some regulators as well as of elements of the transcriptional apparatus that probably underpin their different metabolic features. However the most unexpected feature revealed by this study was the extremely low abundance of most ribosomal proteins in *S. coelicolor* that was logically correlated with a lower protein abundance of most ontological classes with the noticeable and puzzling exception of proteins belonging to secondary metabolites pathways.

5.2. Materials and Methods

5.2.1. Bacterial growth

Spores of *S. coelicolor* M145, a derivative of the wild-type strain A3(2) lacking the plasmids SCP1 and SCP2 (Kieser *et al.*, 2000), and *S. lividans* TK24 were prepared from solid SFM medium (Kieser *et al.*, 2000). *Streptomyces* strains were cultured on solid R2YE medium (Kieser *et al.*, 2000) not supplemented with phosphate and sucrose but supplemented with glucose 0.1 M or glycerol 0.2 M as major carbon sources. 10^6 spores were plated on the surface of cellophane disks laid down on the top of agar plates and incubated at 28 °C in darkness. Cell growth was assessed by dry cell weight every 12 h until 72 h of culture. To do so, mycelial pellets were harvested using a spatula, washed twice with deionized water, lyophilized and weighted. Four independent biological replicates were carried out for each strain and for each culture time.

5.2.2. Total proteins extraction and digestion

Proteomic analysis was carried out at three culture times: 36, 48 and 72h. Four biological replicates were carried out for each strain cultivated in two different media and for the three culture times. The total number of samples was thus 48 (2 strains x 2 media x 3 culture times x 4 biological replicates, Figure 5. 1A). Half of the mycelial samples obtained from the cultures described above were harvested using a spatula, pellets were washed twice with 50 mM TRIS-HCl pH=7.8 and suspended on 3 mL of lysis buffer that contained 6 M urea (Sigma Aldrich, U5378), 2 M thiourea (Sigma Aldrich, T8656), 5 mM DTT (Sigma), 0.1 M TRIS-HCl pH=8 and 150 µL of prepared proteases inhibitor cocktail (Sigma Aldrich, P8465). Cells were disrupted using a cell disruptor (Constant systems Ltd. One shot model) at 2.6 Kbars and cells debris were removed by centrifugation (15 min at 8000 rpm, 4° C). Soluble protein concentrations were measured according to the 2-D Quant kit protocol (GE Healthcare Life Sciences, 80-6483-56). Aliquots of 80 µg of total protein extract were supplemented with RapiGest^{TM} (Waters, 186001860) to obtain a final concentration of 0.1 % m/v. This protein extract was used for the proteome analysis.

The total protein extracts (80 µg) were alkylated with iodoacetamide (10 mM final concentration) in the dark for 1 h. Samples were first digested in-solution for 3 h at room temperature by adding Lysyl-Endopeptidase (Wako, 125-05061) at a 1:50 (w/w) protein ratio. Then, following a 5-fold dilution with deionized water, they were digested for 17 h with 80 µg of sequencing-grade modified trypsin (Promega) with 1:100 protein ratio at 37 °C (Wisniewski and Mann, 2012). To quench the digestion, the pH of the peptide mixtures was adjusted to 2 by adding trifluoroacetic acid (TFA). The resulting peptide mixtures were pre-cleaned with a Strata-X column (Phenomenex, ref. 8B-S100-TAK). Columns were washed with 1.5 mL of washing buffer (containing 3% acetonitrile (ACN) and 0.06% glacial acetic acid). The peptide mixtures were charged into the columns, followed by three washing steps of 500 µL. Elution of peptides was achieved using 600 µL of elution buffer (40% ACN and 0.06% glacial acetic acid). The resulting samples were concentrated under vacuum to dryness and resuspended in 160 µL of 0.1% TFA and 2% ACN for analysis in a high-resolution mass spectrometer.

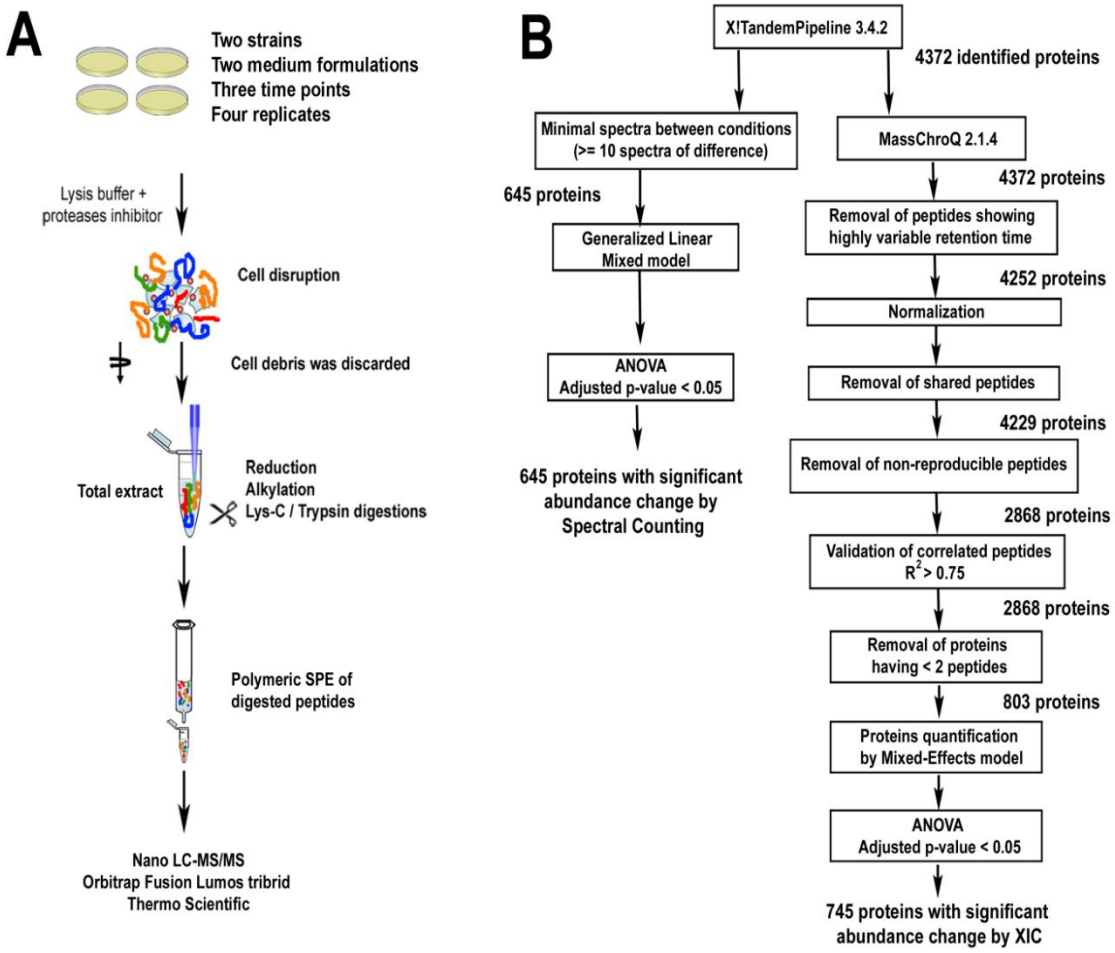

Figure 5. 1. Proteomic workflow. Samples preparation for quantitative proteomics (**A**). Bioinformatic and statistical analysis of proteomic data (**B**).

5.2.3. LC-MS/MS analysis

MS analyses were performed on a Dionex U3000 RSLC coupled to an Orbitrap Fusion™ Lumos™ Tribrid™ mass spectrometer (Thermo Fisher Scientific). Four µL containing 1 µg of sample were injected and separated using a 75-µm x 150-mm Acclaim PepMap RSLC column packed with 3-µm diameter superficially porous particles (Thermo Scientific). The gradient used was 0–45% of 80% ACN/0.1% formic acid over 180 min at a flow rate of 300 nL/min. LC-MS/MS analysis was performed utilizing a nanospray ionization source and the eluted peptides were ionized by applying 2.4 kV in positive mode. MS scans were performed at 120,000 resolution, m/z range 400–1,500. MS/MS analysis was performed in a data-dependent mode, with a top speed cycle of 3 s for the most intense doubly or multiple charged precursor ions. Ions in each

MS scan over threshold 10,000 were selected for fragmentation (MS2) by collision-induced dissociation (CID) for identification at 35% and detection in the ion trap followed by a top speed MS2 fragment ions. Precursors were isolated in the quadrupole with a 0.7 m/z window and dynamic exclusion within 10 ppm during 25 s was used for m/z-values already selected for fragmentation. The AGC targets are 4×10^{5} and 1×10^{4} and maximum ion filling times of 50 ms and 50 ms for MS and MS/MS respectively. Polysilaxolane ions m/z 445.12002, 519.13882 and 593.15761 were used for internal calibration.

5.2.4. Proteins identification

A custom FASTA format database was constructed from the genomes of *S. coelicolor* M145 and *S. lividans* TK24 downloaded from The Universal Protein Resource (http://www.uniprot.org/, June 22th 2011, 7810 and 7551 entries respectively). Unique labels were attributed to proteins encoded by orthologous genes that fulfilled an E-value < 10E-10 as a top score after BLASTP (Camacho *et al.*, 2009) for both strains. This resulted in 6911 orthologous protein pairs, and 1539 strain-specific proteins. The sub-cellular localization of each protein was predicted from the LocateP database (Zhou *et al.*, 2008). The functional categories were assigned as described in several databases (StrepDB - The Streptomyces annotation server; Kanehisa and Goto, 2000; Karp *et al.*, 2005). A database of common contaminants was also considered for the analysis.

A general bioinformatic workflow is shown on Figure 5. 1B. Database searches were performed using the X!Tandem algorithm (version 2015.12.15; http://www.thegpm.org/TANDEM/, December 15th 2015) implemented in the open source search engine X!TandemPipeline version 3.4.2 (Langella *et al.*, 2017). Enzymatic cleavage was declared as a trypsin digestion with one possible misscleavage. Carboxyamidomethylation of cysteine residues and oxidation of methionine residues were set to static and possible modifications, respectively. Precursor mass tolerance was 10 ppm and fragment mass tolerance was 0.02 Th. Identified proteins were filtered and grouped using X!TandemPipeline. Data filtering was achieved according to a peptide E-value < 0.05, protein log(E-value) < –2 and to a minimum of two identified peptides per protein. Using such filtering criteria, the peptides and proteins false discovery rates

(FDR) were estimated to 0.13 % and 0.05 % respectively (File S1). MS data were deposited online using PROTICdb database (Ferry-Dumazet *et al.*, 2005; Langella *et al.*, 2013).

5.2.5. Peptide quantification based on extracted ion current

Peptides were quantified based on XIC using MassChroQ 2.1.4 (Valot *et al.*, 2011). XIC extraction was performed using a peak detection threshold between 30000 – 50000 and a range of 10 ppm (File S2). The peptide intensities thus obtained were log10-transformed for further data analyses. Peptides showing a standard deviation of retention time higher than 20 s were removed.

Normalization was performed in order to remove systemic biases between samples as well as more complex variation resulting from transient stochastic events during LC-MS/MS run, such as ESI instability. For this, we used a local normalization method adapted from Lyutvinskiy *et al.* (2013). Briefly, intensity deviation between a given sample and a sample chosen as reference was computed for each peptide-charge quantified in both samples. The values of intensity deviation thus obtained were ordered according to the peptides' retention time and smoothed using the smooth.spline function in R (R Core Team, 2015). The smoothed values of intensity deviation were used as correction factors to normalize the sample. The intensities of the peptides-charges that were present in the sample to be normalized and absent from the reference sample were corrected considering that intensity deviation was similar for temporally neighboring peptides. The effect of normalization is shown in Figure 5. 2. Peptides that belonged to multiple proteins were removed. Reproducibility was set if the peptides have been quantified: 1) in at least 2 replicates per strain x media x culture time combination and 2) in 12 of the 12 possible strain x media x culture time combinations. In order to remove peptides whose intensity profiles deviated from the average profile of the peptides from the same protein, Pearson-correlation coefficients were computed for each pair of peptides belonging to a same protein. For each protein, a reference peptide was chosen as the peptide showing the highest number of significant correlations. Peptides correlated to the reference peptide with a coefficient of correlation > 0.75 were kept for further analysis.

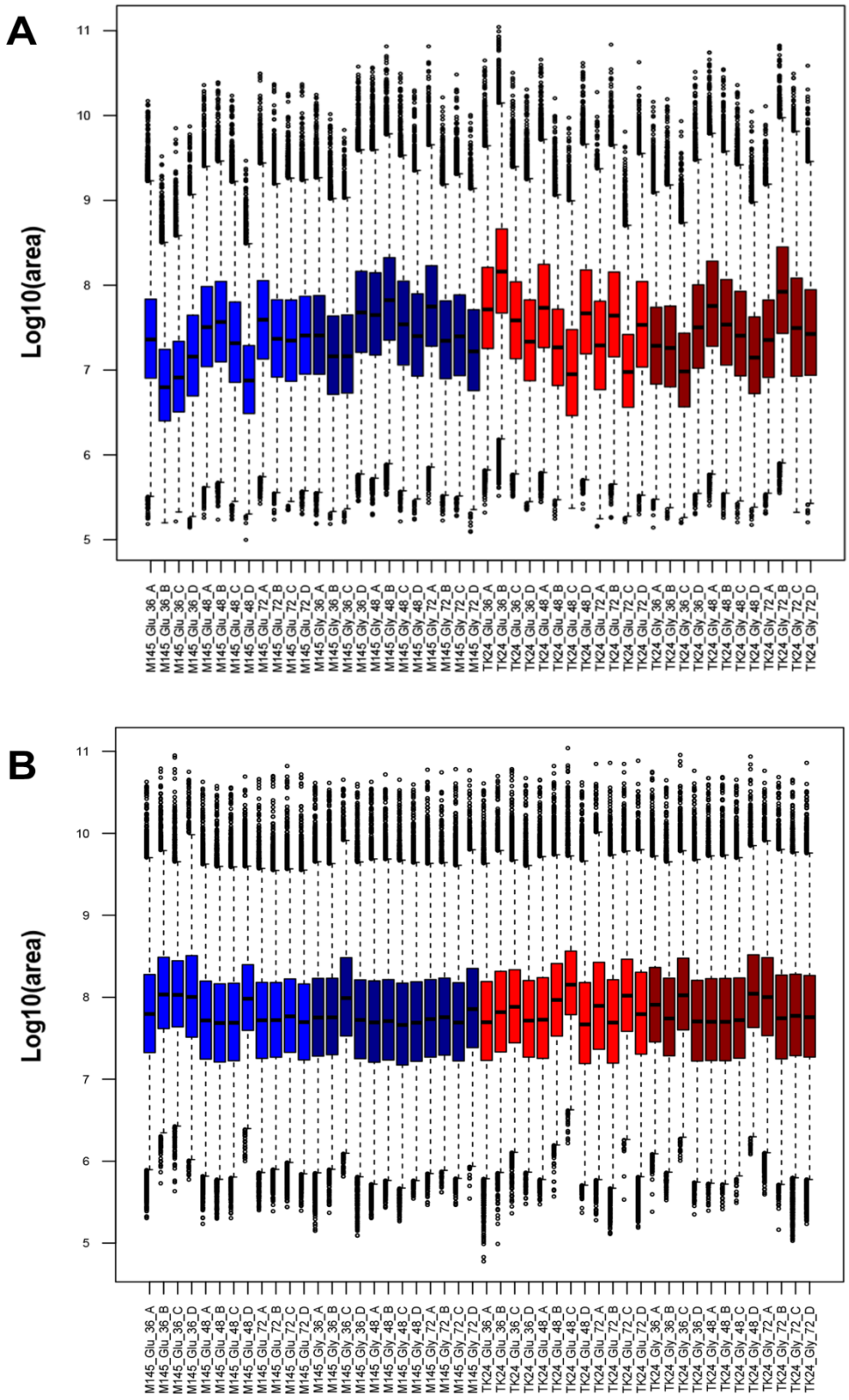

Figure 5. 2. LC-MS run samples before (**A**) and after (**B**) peptide intensities normalization.

5.2.6. Detection of protein abundance changes

To detect protein abundance changes, two protein quantification methods were used. As recommended by Blein-Nicolas and Zivy (2016), we first performed a rough protein quantification using spectral counting (SC) in order to detect semi-quantitative and presence/absence variations, then we performed a finer quantification using a extracted ion current (XIC)-based approach in order to detect smaller abundance changes.

For SC, proteins were filtered by selecting the ones that showed a minimal difference of 10 spectra when comparing the average of spectra for the different strain x medium x culture time combinations. For each protein, the abundance in number of spectra was modeled using the following generalized linear mixed model (GLM) with a Poisson distribution:

$$SC_{jklm} = \mu + S_j + M_k + T_l + (SxM)_{jk} + (SxT)_{jl} + (MxT)_{kl} + (SxMxT)_{jkl} + R_m + \varepsilon_{jklm}$$

$$where\ \epsilon_{jklm} \sim N\left(0, \sigma_\theta^2\right)$$

SC_{jklm} is the number of spectra measured in strain j, growth medium k, culture time l and replicate m. S_j represents the effect due to strain j. M_k represents the effect due to medium k. T_l represents the effect due to culture time l. $(SxM)_{jk}$ represents the effect due to strain j x growth medium k interaction. $(SxT)_{jl}$ represents the effect due to strain j x culture time l interaction. $(MxT)_{kl}$ represents the effect due to growth medium k x culture time l interaction. $(SxMxT)_{jkl}$ represents the effect due to strain j x growth medium k x culture time l interaction. R_m represents the effect due to biological replicate m. $\boldsymbol{\varepsilon}_{jklm}$ is the residual error. Protein abundance changes were detected by analysis of variance (ANOVA) using a Chi-square test.

For the XIC-based approach, the effects of the strain, growth medium and of the culture time were tested for each protein by modeling the normalized peptide intensities using a mixed-effects model derived from Blein-Nicolas *et al.* (2012):

$$I_{jklm} = \mu + S_j + M_k + T_l + (SxM)_{jk} + (SxT)_{jl} + (MxT)_{kl} + (SxMxT)_{jkl} + R_m + \theta_{jklm} + \varepsilon_{jklm}$$

$where\ \theta_{jklm} \sim N(0, \sigma_\theta^2)$,

$$\epsilon_{jklm} \sim N(0, \sigma_\theta^2)$$

I_{jklm} is the peptide intensity measured in strain *j*, growth medium *k*, culture time *l* and replicate *m*. S_j represents the effect due to strain *j*. M_k represents the effect due to medium *k*. T_l represents the effect due to culture time *l*. $(SxM)_{jk}$ represents the effect due to strain *j* x growth medium *k* interaction. $(SxT)_{jl}$ represents the effect due to strain *j* x culture time *l* interaction. $(MxT)_{kl}$ represents the effect due to growth medium *k* x culture time *l* interaction. $(SxMxT)_{jkl}$ represents the effect due to strain *j* x growth medium *k* x culture time *l* interaction. R_m represents the effect due to biological replicate *l*. Θ_{jklm} represents the technical variation due to sample handling and injection in the mass spectrometer. $\boldsymbol{\varepsilon}_{jklm}$ is the residual error. Parameters were estimated by maximizing the restricted log-likelihood (REML method). Protein abundance changes were detected by ANOVA.

For both methods (XIC and SC), the obtained p-values were adjusted for multiple testing by the Benjamini-Hochberg approach (Benjamini and Hochberg, 1995). The abundance of a given protein was considered significantly variable when the adjusted p-value was < 0.05.

5.2.7. Data analysis

Descriptive analysis of the protein abundances was performed using PCA and heatmap representations. Heatmaps were constructed using hierarchical clustering based on Euclidean distances. For proteins that were quantified with both methods (XIC and SC), only the values obtained by XIC-based approach were used in the heatmap constructions since the latter is a finer quantitative approach compared to the SC-based method. Boxplots were constructed from the protein abundances obtained from the XIC and SC approaches for the proteins showing significant abundance variation. Proteins quantification, statistical methods and data analysis were conducted in R (R Core Team, 2015).

5.2.8. Esterified fatty acids quantification by GC/MS

Total lipid derived fatty acids methyl esters (FAMES) were quantified from samples of lyophilized *Streptomyces* mycelium (1 mg). The method of trans-esterification was adapted from Lepage and Roy (1986) and previously described (Millan-Oropeza *et al.*, 2017). Four biological replicates were conducted for each condition.

5.2.9. Assay of ACT and RED production

Extracellular ACT as well as intracellular ACT and RED were quantified from four individual plates of each strain x growth medium x culture time condition. To quantify extracellular ACT, the volume of R2YE agar medium corresponding to an individual plate was cut into small pieces using a spatula and allowed to diffuse in 5 mL water for 2 h at 4°C. The first eluate was transferred into a new tube, and 5 mL of water was added again to the agar medium and allowed to diffuse for 2 h at 4°C. The two eluates (10 mL) were pooled filtered through a 0.2 µm polyethersulfone membrane (Pall Life Sciences) prior to analysis. 500 µL of HCl 4 M were added to 1.5 mL of the final eluate, the remaining eluate was immediately stored at -80 °C for further analyses. The mixture was incubated on ice for 10 min to allow ACT precipitation. Precipitated ACT was collected by centrifugation (17900 g for 10 min). Supernatants were discarded and the resulting pellets were suspended in 1 mL of KOH 1 N. Optical density of the solution was determined at 640 nm in a Shimadzu UV-1800 spectrophotometer using KOH 1 N as blank (Kieser *et al.*, 2000).

Approximately 10 mg of lyophilized mycelium were used to quantify intracellular RED and ACT by adding 1 mL of methanol or 1 mL of KOH 1 N in 2 mL tubes, respectively. Cells were disrupted using a MP Biomedicals Fast-Prep 24 System (2 cycles at 5 m/s during 30 seconds each cycle). Supernatants were collected after centrifugation (17900 g for 10 min). The methanolic extract of RED was acidified with the addition of 1 mL of HCl 1 N, and optical density was measured at 530 nm against a blank constituted of methanol: HCl 1 N (1:1 ratio in volume). Intracellular extracts of ACT were measured at a wavelength of 640 nm in a Shimadzu UV-1800 spectrophotometer using KOH 1 N as blank. (Kieser *et al.*, 2000).

5.2.10. Glucose, glycerol, proline and phosphate quantification assays

Samples were obtained from the diffusion of R2YE agar medium in water as described above. Different molecules were quantified from the medium extracts: for glucose and glycerol determination, enzymatic assay kits were used (GAHK-20 and MAK117, Sigma-Aldrich); for proline quantification, a modified colorimetric method was performed utilizing isatin as derivatizing agent (Long *et al.*, 2012); and for total free phosphate, a colorimetric assay kit (MAK030, Sigma-Aldrich) was used. These assays were carried out in four independent biological replicates.

5.3. Results

5.3.1. Bacterial growth

Spores of *S. coelicolor* M145 and *S. lividans* TK24 were spread on cellophane disks deposited on the surface of plates with solid R2YE medium supplemented with either glucose or glycerol. The two strains grew with a similar kinetic on R2YE glycerol but on R2YE glucose growth of *S. coelicolor* was slowed down after 36h of cultivation whereas *S. lividans* pursued active growth until 60h, time of entry into stationary phase (Figure 5. 3A). *S. lividans* and *S. coelicolor* yielded 43.4 and 50.9 mg of dry mycelium per plate on glycerol and 49.02 and 26.3 mg/plate on glucose, respectively, after 72h of cultivation.

The two species consumed glycerol at a similar rate (Figure 5. 3C) whereas the consumption of glucose by *S. coelicolor* was less efficient than that of *S. lividans*. This resulted in 4.2 and 2.2 g/L of glucose remaining in the growth medium of *S. coelicolor* and *S. lividans*, respectively, at 72h (Figure 5. 3C). On R2YE glucose, *S. coelicolor* consumed proline, the most abundant amino acid of the medium, more actively than *S. lividans* (Figure 5. 3C) whereas this difference was less pronounced on R2YE glycerol. These specific features characterizing each strain were previously observed in liquid R2YE glucose medium (Chapter IV). Furthermore, the two strains consumed the P of the growth medium at a similar rate (Figure 5. 3C).

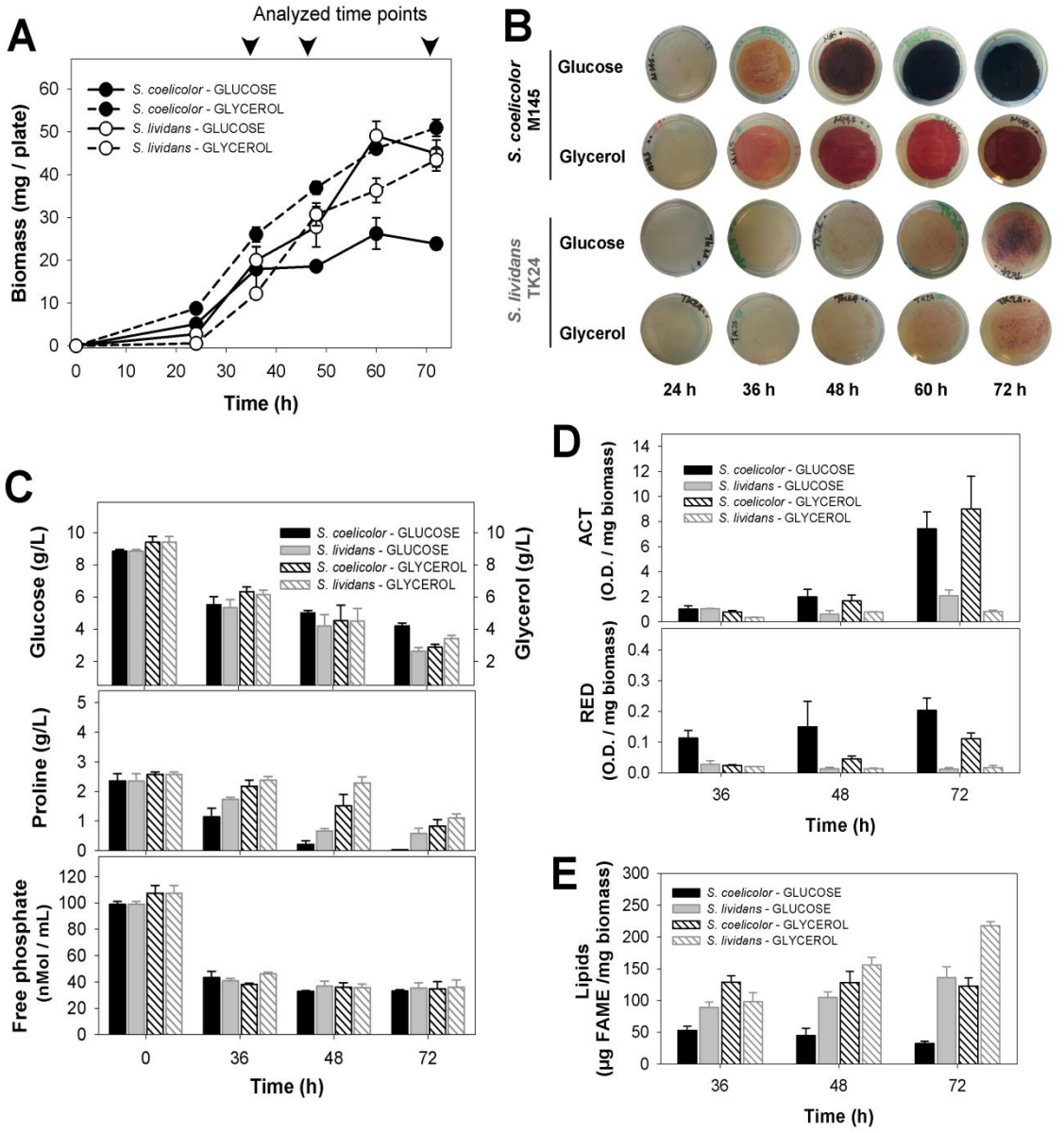

Figure 5. 3. Comparative features of *S. coelicolor* and *S. lividans*.
Growth curves on solid R2YE medium supplemented with glucose or glycerol (**A**). Continuous or dotted lines represent growth on R2YE with glucose and glycerol, respectively. Black and white circles represent *S. coelicolor* and *S. lividans*, respectively. Pictures of mycelial lawns of *S. coelicolor* and *S. lividans* cultivated for 24, 36, 48, 60 and 72 h (**B**). Concentration of glucose, glycerol, proline and free phosphate in R2YE medium (**C**). Mycelium-associated RED production and total (intra and extracellular) production of ACT after 36, 48 and 72h of cultivation (**D**). Accumulation of lipid derived total fatty acids methyl esters (FAMES) in *S. coelicolor* and *S. lividans* (**E**). Plain black and grey histograms represent *S. coelicolor* and *S. lividans* grown R2YE glucose, respectively whereas hatched black and grey histograms represent *S. coelicolor* and *S. lividans* grown R2YE glycerol, respectively. Data are presented as mean ± SD (n = 4 replicates per condition).

As repeatedly observed, lawns of *S. lividans* were rather colorless except at the latest time point (72h) where a slight reddish color was observed on both carbon sources (Figure 5. 3B). In contrast, on glucose, lawns of *S. coelicolor* showed reddish (36 – 48h) then blue (60 – 72h) pigmentation as indicators of the production of the secondary metabolites RED and ACT, respectively (Hopwood, 1999). On R2YE with glycerol, *S. coelicolor* mycelium showed a reddish pigmentation from 36h onward (Figure 5. 3B). RED and ACT assays confirmed that *S. coelicolor* produced RED at a lower level on glycerol than on glucose but produced ACT at a similar level on both carbon sources (Figure 5. 3D). However ACT was excreted on R2YE glucose while its remains intracellular on R2YE glycerol (Figure 5. 3B).

5.3.2. Global proteomes analysis

A total of 4372 different proteins were identified, 4088 originating from *S. coelicolor* and 3994 from *S. lividans* (Figure 5. 4A, File S3). These values represented 52.2% and 54.2% of the theoretical proteome of *S. coelicolor* M145 and *S. lividans* TK24, respectively. Compared to other proteomic studies of these model strains (Manteca *et al.*, 2010; Manteca *et al.*, 2010; Gubbens *et al.*, 2012; Thomas *et al.*, 2012; Le Marechal *et al.*, 2013) the present work represents the largest proteome dataset of *S. coelicolor* and *S. lividans*.

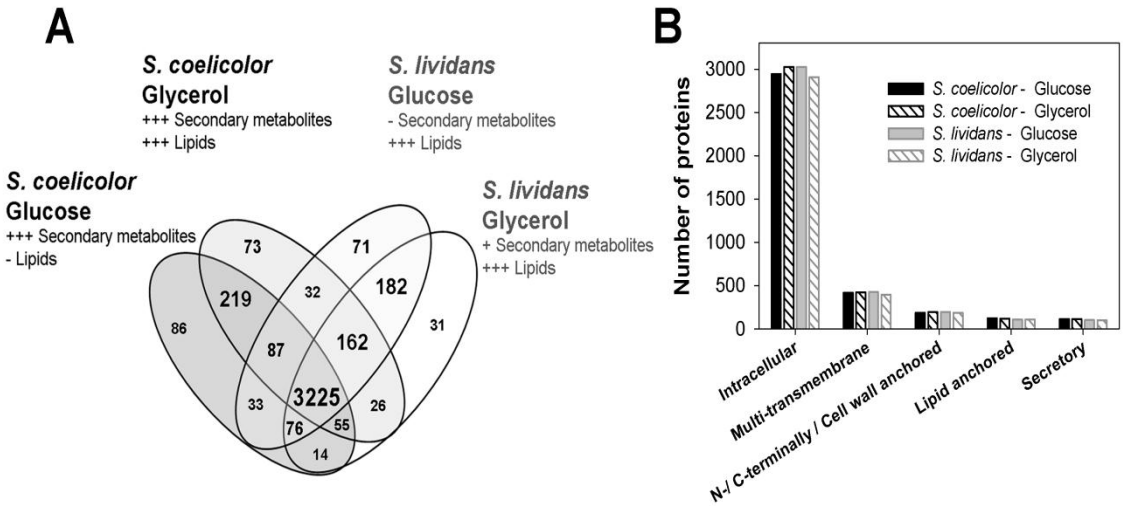

Figure 5. 4. Venn diagram of the 4372 identified proteins using X!TandemPipeline 3.4.2 (**A**). Sub-cellular localization of the identified proteins in *S. coelicolor* M145 and *S. lividans* TK24 inferred using the LocateP database (**B**).

Sub-cellular localization of the identified proteins was obtained using the LocateP database (Zhou *et al.*, 2008). In both strains, intracellular proteins constituted the largest part of the sub-cellular proteome, between 77.7 - 78.5% (Figure 5. 4B, File S3). The rest of the sub-cellular distribution included multi-transmembrane, C-/N- terminally/cell wall anchored, lipid anchored and secreted proteins that constituted 10.7 - 11%, 4.9 – 5.1%, 2.8 – 3.3% and 2.7 – 3.1%, respectively (Figure 5. 4B).

Protein quantification was performed for 42 samples out of 48. Among the dataset, five samples of *S. lividans*, two grown in glucose (one at 48h and one at 72h) and three grown in glycerol (one at 36h, one at 48h and one at 72h), as well as one sample of *S. coelicolor* grown in glucose at 48h were excluded from the analysis because they showed dubious LC-MS/MS results. This decision was motivated by the significantly lower number of peptides identified in these six samples compared to most of the other samples (mainly < 40,000 peptides, Figure 5. 5A) as well as by the principal component analysis (PCA, Figure 5. 5B-E).

Indeed, the PCA based on the protein abundances estimated from peptide intensities (Figure 5. 5B) and spectral counts (Figure 5. 5C) showed that these six samples were separated from the other groups. The fact that the independent replicates of the 42 remaining samples clustered together (Figure 5. 5D-E) strongly suggest that an experimental issue has affected the protein content of the excluded samples.

A total of 4372 proteins were quantified by Spectral Counts (SC) and eXtracted Ion Current (XIC). Statistical analysis of spectral counts and peptide intensities allowed to detect 1040 proteins with significant abundance variation according to strain, medium and/or time (adjusted p-value < 0.05, Figure 5. 6). Among them, 295 were detected by the SC-based method, 395 by the XIC-based method and 350 by both methods. As mentioned in materials and methods, when a given protein showed significant abundance change by both methods, only the values obtained by XIC-based approach were considered since this approach is more sensitive / accurate than the SC-based method.

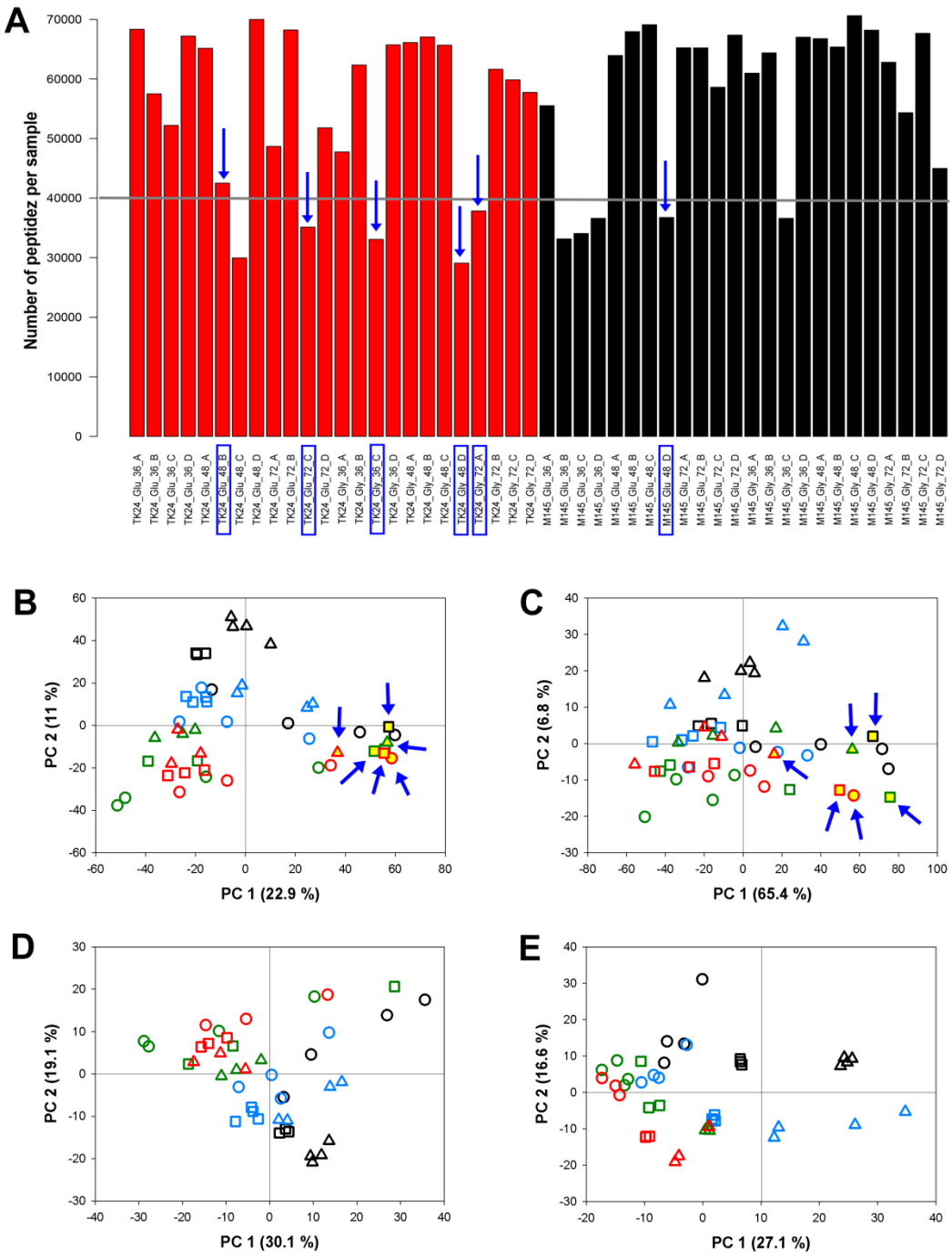

Figure 5. 5. Number of peptides per LC-MS/MS sample of the proteomic dataset (**A**). Principal Component Analysis (PCA) of proteins abundances from peptide intensities (**B** and **D**) and spectral counts (**C** and **E**) of the proteomic dataset.
PCA including dubious LC-MS/MS (**B** and **C**). PCA of the remaining 42 samples without dubious LC-MS/MS runs (**C** and **D**). Samples originated from glucose or glycerol grown cultures are indicated in black and blue for *S. coelicolor* and in green and red for *S. lividans*, respectively. Time points are represented by circles (36h), squares (48h) and triangles (72h). Arrows indicate dubious LC-MS/MS runs.

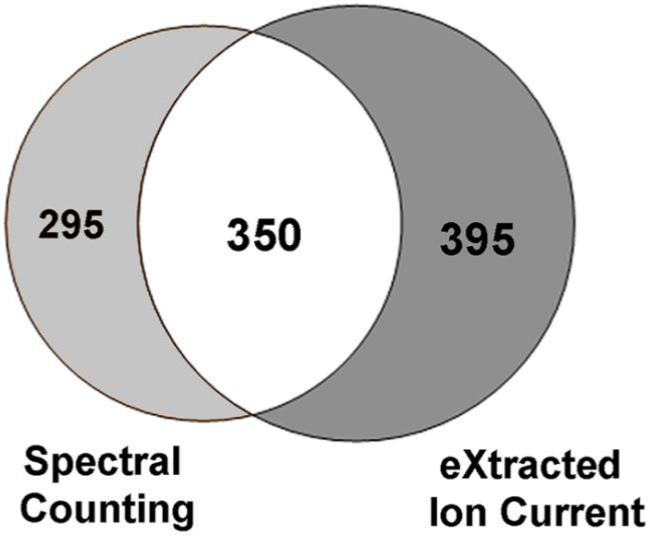

Figure 5. 6. Venn diagram of the 1040 proteins showing significant abundance change calculated using the XIC and SC approaches (ANOVA, adjusted p value < 0.05).

The 1040 proteins that showed statistical abundance changes were represented in a heatmap using hierarchical clustering with Euclidean distances (Figure 5. 7). These proteins belonged to 13 functional categories according to their annotation in the databases (File S4). The proteomes were clearly resolved in four main clusters. Cluster 1: proteins drastically down-regulated or absent in *S. coelicolor* at 72h of culture. Cluster 2: proteins down-regulated or absent in *S. lividans* at 72h of culture. Cluster 3: proteins constitutively more abundant in *S. coelicolor* than in *S. lividans*; and, Cluster 4: proteins with increasing abundance at late time points in both strains.

A progressive reduction of protein abundance resulting in clearly lower protein abundance for most clusters in *S. coelicolor* than in *S. lividans* was observed at 72h, with the noticeable exception of cluster 3 involved in secondary metabolism. This unexpected feature was seen on glucose as well as on glycerol although to a lesser extent. A careful analysis of the proteins differentially expressed between the two species was thus mainly carried out at 72h but extended to other times when meaningful.

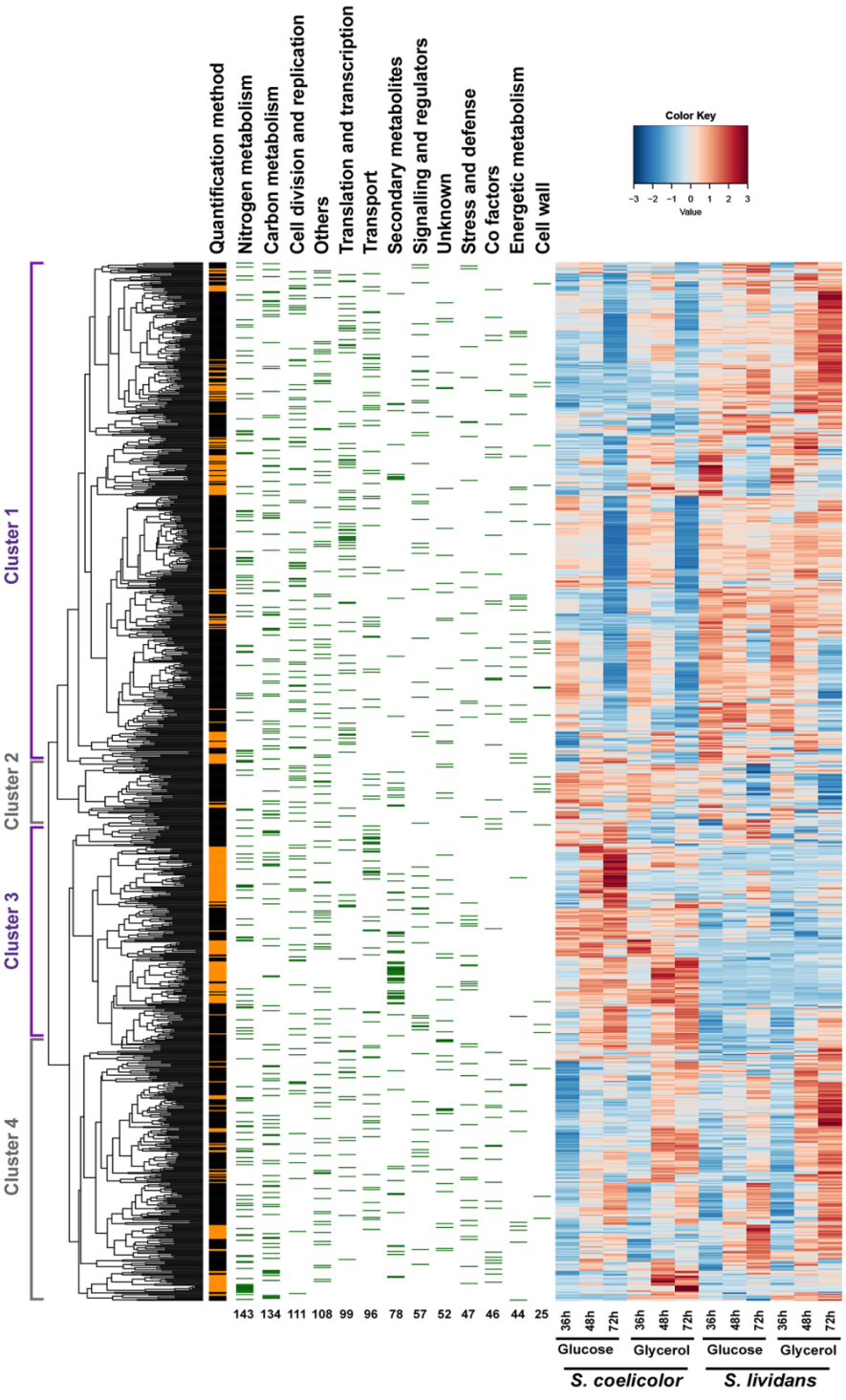

Figure 5. 7. Heatmap representation of the protein abundances estimated by XIC and SC.

The quantification methods are displayed in the vertical bar indicating those proteins quantified by SC (orange) and XIC (black). The green bars represent genes belonging to the functional categories mentioned above the diagram. The total numbers of proteins for each category are indicated below the heatmap.

5.3.3. Proteins of central carbon metabolism

A total of 67 proteins involved in the central carbon metabolism showed significant abundance variation (ANOVA, adjusted p value < 0.05) between the different conditions studied (Figure 5. 8).

The relative abundance of proteins belonging to glycolysis was analyzed in the two strains grown in the presence of glucose or glycerol. The three first reactions of the catabolism of glucose *via* glycolysis results in the production of two inter-convertible phosphorylated trioses, glyceraldehyde-3-phosphate (GAP) and dihydroxyacetone (DHAP). DHAP can also result from the catabolism of glycerol that is first phosphorylated by an ATP dependent glycerol kinase and oxidized into DHAP by glycerol-3-phosphate dehydrogenase. In *Streptomyces*, the genes encoding these proteins belong to the GylR operon that include the glycerol uptake facilitator protein *glpF* (SCO1659), the glycerol kinase (SCO1660) and the glycerol-3-phosphate dehydrogenase (SCO1661). These genes are under the negative control of the GylR regulator SCO1668 (Smith and Chater, 1988; Hindle and Smith, 1994).

Alternatively, in some micro-organisms, glycerol can be oxidized into DHA by a NAD(+) dependent glycerol dehydrogenase and then phosphorylated by a dihydroxyacetone kinase (DHAK) at the expense of phosphoenolpyruvate (PEP) by a phospho-transfer system (PTS). Genes encoding DHAK-like proteins are *SCO0580*, the second gene of a large operon of 6 genes and *SCO7073-72* located just upstream of a gene encoding a PTS EIIA-like protein. However, the expression of these genes was higher on glucose than on glycerol suggesting that they may not play a major role in glycerol metabolism.

The subsequent steps of glycolysis are common to glucose and glycerol. However a fraction of glycerol should be used for gluconeogenesis.

As expected proteins of the glycerol operon were more abundant in presence of glycerol than in presence of glucose in both strains at 48h whereas proteins catalyzing the first fourth steps of glycolysis specific to glucose did not show a great variation of abundance between the two carbon sources suggesting a constitutive expression (Figure 5. 8).

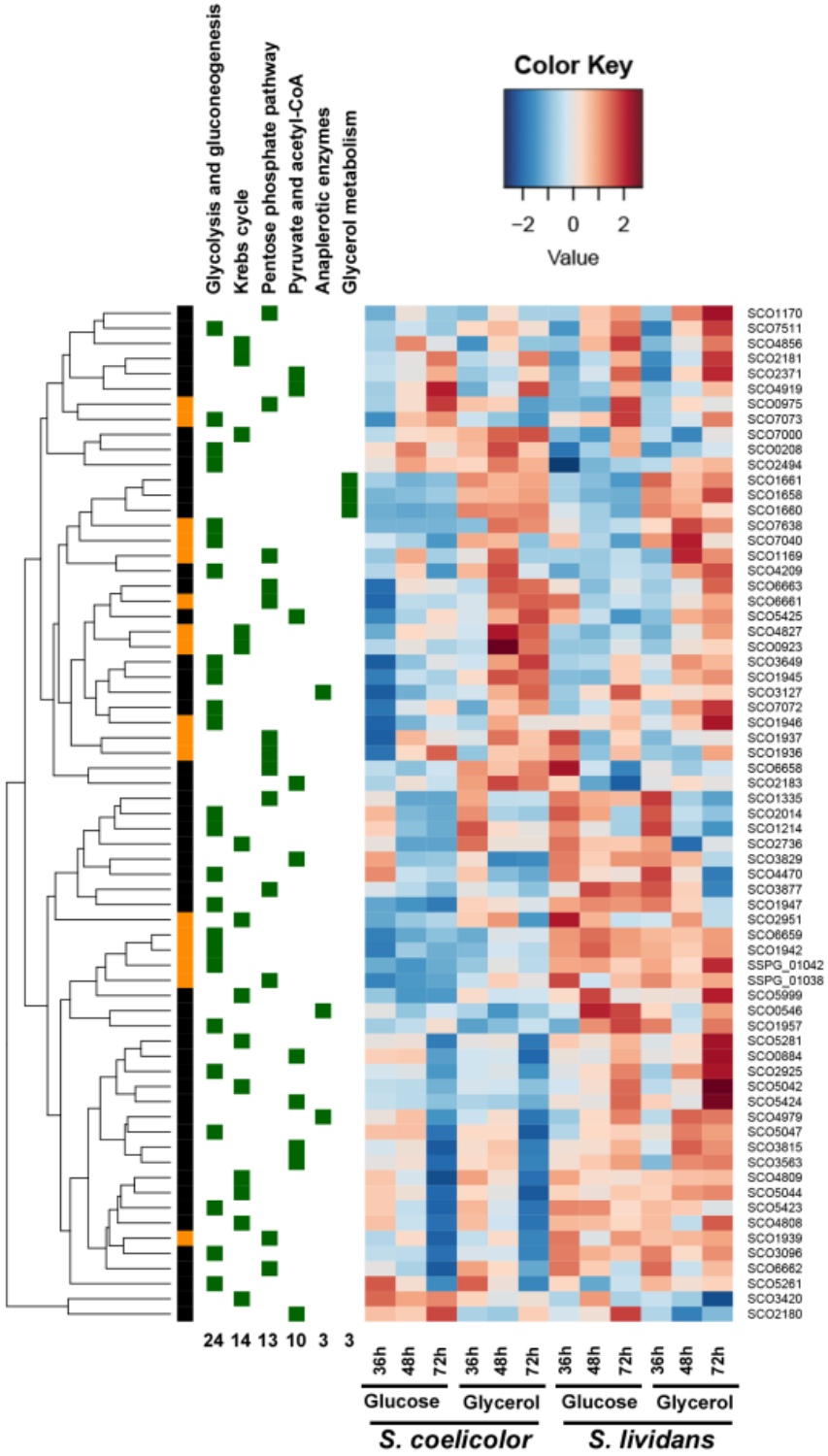

Figure 5. 8. Heatmap representation of proteins from central carbon metabolism with significant change (adjusted p value < 0.05).
Quantification methods are displayed in the vertical bar indicating those proteins quantified by SC (orange) and XIC (black). The annotated functional categories are shown above the green bars.

Upon growth on either glucose or glycerol, most proteins of glycolysis were clearly more abundant in *S. lividans* than in *S. coelicolor* at 72h (Figure 5. 9A-B). The most differentially expressed glycolytic enzymes between the two strains on glucose were GAP dehydrogenases (SCO1947, SCO7040 and SCO7511) and enolases (SCO3096 and SCO7638). These data as well as the more active glucose uptake of *S. lividans* compared to *S. coelicolor* (Figure 5. 3C) confirmed the more active glycolysis in *S. lividans* than in *S. coelicolor* as reported previously in liquid R2YE medium (Chapter IV). Consistently at 72h (but not at earlier time points), the protein lactate deshydrogenase (LDH) that converts pyruvate into lactate consuming a NADH molecule was more abundant in *S. lividans* than in *S. coelicolor* on both carbon sources. At the latest time point (72h), when anabolism is weak and glycolysis still active, this enzyme likely contributes to over-flow metabolism. In glycerol the enolase SCO7638 was expressed at a similar level between the two strains (Figure 5. 9B).

In *S. coelicolor*, most glycolytic proteins were more abundant on glycerol than on glucose (Figure 5. 9C) suggesting that the carbon flux through glycolysis was higher on glycerol than on glucose in that strain. This is consistent with the more active uptake of glycerol than glucose by that strain (Figure 5. 3C) as well as with the higher abundance of the anaplerotic enzyme PEP carboxylase SCO3127 on glycerol than on glucose in *S. coelicolor* at all time points (File 4).

In agreement with its high glycolytic activity, 6 out of 10 proteins involved in the pyruvate and acetyl-coA node were more abundant in *S. lividans* than in *S. coelicolor* on both carbon sources (Figure 5. 9). Interestingly, phosphate acetyltransferase (Pta) SCO5425 was more abundant on glycerol than on glucose in both strains but more so in *S. lividans* (Figure 5. 9) .The genes encoding Pta and the acetate kinase (AckA) constitute an operon and these enzymes can be considered as contributing to overflow metabolism (Halsey *et al.*, 2017).

Among the 13 proteins belonging to pentose phosphate pathway (PPP), 8 were more abundant in glycerol than in glucose-grown cultures of *S. coelicolor* and *S. lividans* (Figure 5. 9, File S4). This strongly suggested that gluconeogenesis that ought to take place on glycerol is going through the PPP which generates NADPH for phospholipids

and TAG biosynthesis as well to combat oxidative stress (Goldman *et al.*, 1963; Wasylenko *et al.*, 2015).

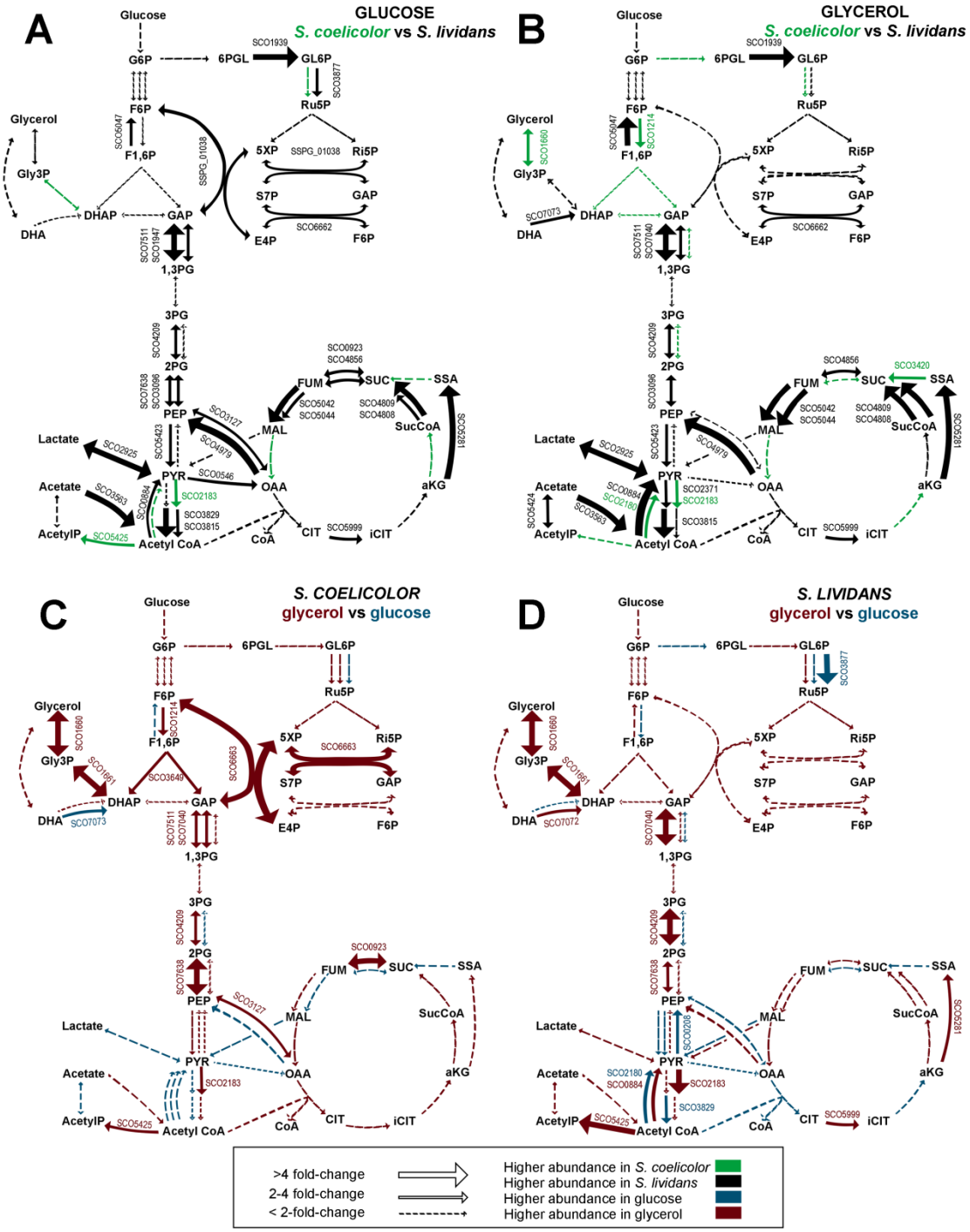

Figure 5. 9. Schematic representation of central carbon metabolism. Enzymatic reactions catalyzed by proteins with significant variation (ANOVA, adjusted p value > 0.05) are represented by arrows. The thickness of the arrows is proportional to proteins' abundance. Comparison of protein abundance in *S. coelicolor* and *S. lividans* on glucose (**A**) or glycerol (**B**) grown cultures at 72h. Comparison of protein abundance in glucose and glycerol grown cultures of *S coelicolor* (**C**) and *S. lividans* (**D**) at 72h.

At 72h, but not at earlier time points, 7 or 8 out of 12 putative proteins of the Krebs cycle were far more abundant in *S. lividans* than on *S. coelicolor* on both carbon sources (Figure 5. 9). This suggests an arrest of anabolism in *S. coelicolor*. It is noteworthy that at earlier time points three critical enzymes of the Krebs cycle generating reduced co-factors: the isocitrate dehydrogenase SCO7000, the succinate dehydrogenase SCO0923 and the malate dehydrogenase SCO4827 were more abundant in *S. coelicolor* than in *S. lividans* as reported previously in liquid R2YE cultures (Chapter IV).

5.3.4. Lipid metabolism

It was previously reported that *S. lividans* accumulated 3 to 4 fold more FAME than *S. coelicolor* on glucose (Le Marechal *et al.*, 2013). The results observed on Figure 5. 3E confirmed this statement and demonstrated that this feature was somehow conserved on glycerol and that glycerol was more lipogenic than glucose.

S. lividans FAMEs content was thus 1.6 fold higher on glycerol than on glucose whereas *S. coelicolor* FAMEs content was 3.6 fold higher on glycerol than on glucose. This was mainly linked to the very low FAMEs content of *S. coelicolor* on glucose. However, unexpectedly and despite its high FAMEs content, *S. coelicolor* produced the secondary metabolites RED and ACT on glycerol at a similar level as on glucose (Figure 5. 3D). However it is noteworthy that on glycerol at 72h the TAG content of *S. coelicolor* is 1.5 fold lower than that of *S. lividans* (Figure 5. 3D). So this observation does not totally challenge the proposed anti-correlation between TAG content and antibiotic production (Le Marechal *et al.*, 2013).

Comparative proteomic analysis of the two strains allowed the identification of a total of 40 proteins annotated as corresponding to lipid metabolism that showed statistically significant abundance difference between the two strains (ANOVA, adjusted p value < 0.05, File 4). Among them, 16 were annotated as involved in fatty acids biosynthesis (Figure 5. 10) and 24 involved in degradation (Figure 5. 11).

The 3.6 fold higher FAMEs content of *S. coelicolor* on glycerol than on glucose was correlated with higher abundance of proteins known to be involved in fatty acid biosynthesis, including the 4 proteins of the Fab operon (SCO2387 to SCO2390), known to be under the positive control of the regulator FasR (SCO2386) (Arabolaza *et*

al., 2010), the proteins of the FabI (NADPH-dependent enoyl reductase) /FabG (beta-ketoacyl-ACP reductase) operon (SCO1814-15) as well as the acetyl/propionylCoA carboxylase SCO4921 (Figure 5. 10).

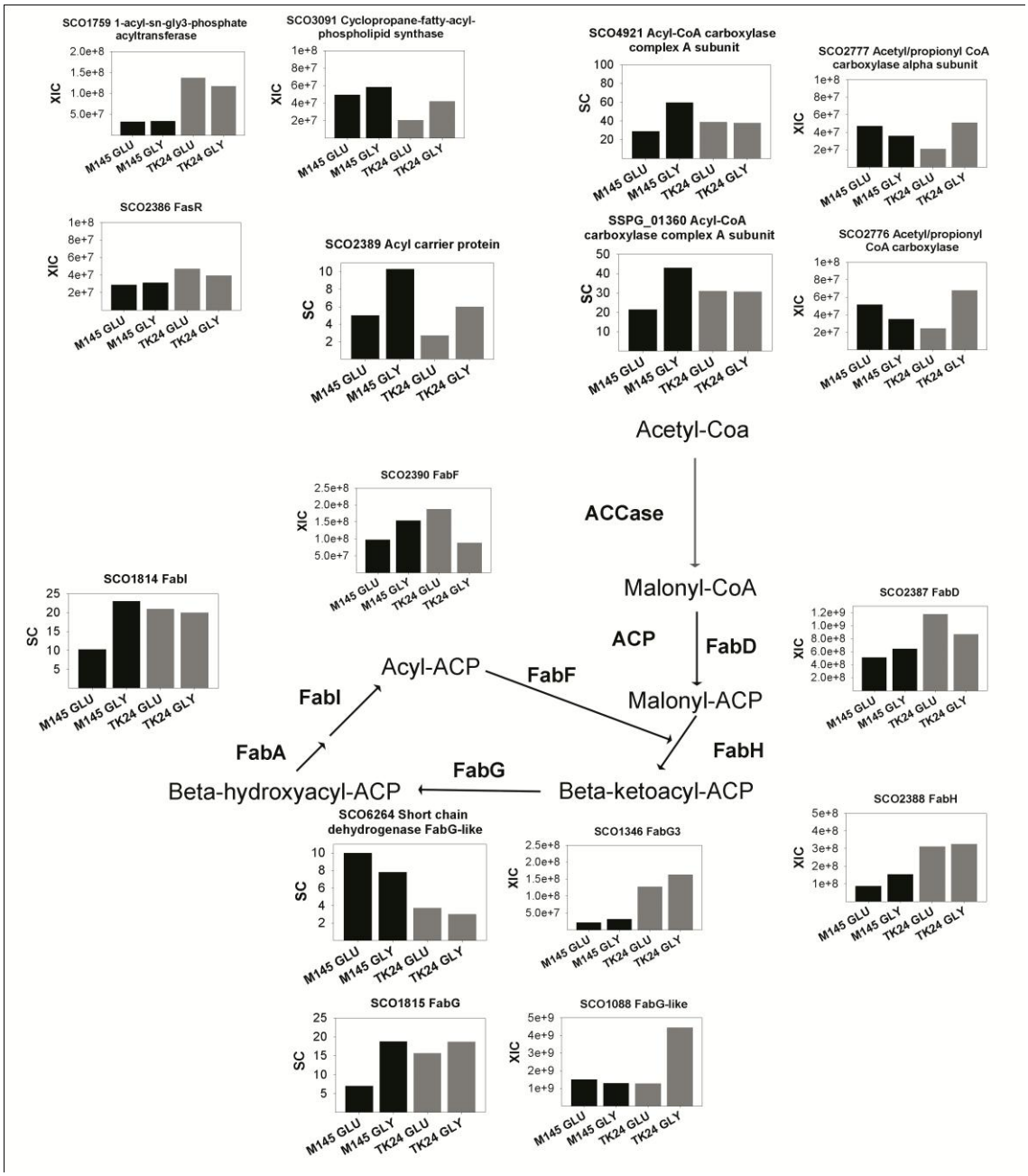

Figure 5. 10. Proteins of fatty acids biosynthesis that showed significant abundance variation between *S. coelicolor* and *S. lividans* (ANOVA, adjusted p value < 0.05). Protein abundances are represented by black and grey histograms for *S. coelicolor* (M145) and *S. lividans* (TK24) cultivated in R2YE glucose (GLU) or glycerol (GLY) after 72 h of cultivation. ACCase: Acyl-CoA carboxylase, ACP: Acyl carrier protein.

Paradoxically, despite its low lipid content on glucose, two other acetyl/propionyl CoA carboxylases (SCO2776 and SCO2777), the acyl carrier protein (ACP, SCO2389), the 3-ketoacyl-(acyl-carrier-protein) reductase FabG3-like (SCO6264) and the cyclopropane-fatty-acyl-phospholipid synthase (SCO3091) were 2 to 3 fold more abundant in *S. coelicolor* than in *S. lividans*. Acetyl/propionyl CoA carboxylases catalyze the carboxylation of acetyl-CoA or propionylCoA into malonyl or methylmalonyl CoA, both are indispensable starters for the biosynthesis of fatty acids with even or odd carbon number but also of the blue pigmented polyketide ACT and/or of the acyl moiety of RED (Rodríguez *et al.*, 2001). These molecules are generated from the degradation of fatty acids or amino acids (isoleucine and valine) so the high expression of these carboxylases in *S. coelicolor* is consistent with the known ability of this strain to degrade amino acids more actively than *S. lividans* (Chapter IV). Interestingly, the ACP SCO2389 was also more abundant in *S. coelicolor* than in *S. lividans* on both carbon sources. This can make sense since ACP are involved in both fatty acid and polyketide biosynthesis (Fischbach and Walsh, 2006). Interestingly the gene encoding the reductase FabG3-like (SCO6264) maps close to the *scbR/scbA* locus and might be involved in the biosynthesis of the γ–butyrolactone ScbA. that is known to have a positive impact on antibiotic production. At last, the cyclopropane fatty acyl phospholipid synthase SCO3091 that transfers a methylene group from S-adenosyl-L-methionine to the double bond of an unsaturated fatty acid, resulting in the replacement of the double bond with a methylene bridge, was shown to be 2.4 fold more abundant in *S. coelicolor* than in *S. lividans* on both carbon sources.

In *S. lividans* the acyl-sn-glycerol-3-phosphate acyltransferase (SCO1759), as well as two genes of the Fab operon SCO2387 (*fabD*) and SCO2388 (*fabH*) were more abundant than in *S. coelicolor* on both carbon sources. The two proteins of the FabI/FabG operon (SCO1814-15), catalyzing the first and last reductive steps of the chain elongation cycle of fatty acid as well as SCO2387 (FabD) were also 2 fold more abundant in *S. lividans* than in S. coelicolor but mainly on glucose.

Furthermore and most importantly, SCO1759 (putative 2-acylglycerophosphoethanolamine acyltransferase) whose encoding gene is likely to be co-transcribed with the upstream one encoding a cytidylate kinase (SCO1760) and the GTPase SCO1758 whose orthologs play a critical positive role in growth control in

other micro-organisms (Morimoto *et al.*, 2002; Kint *et al.*, 2014). These proteins were 3 to 4 fold more abundant in *S. lividans* than in *S. coelicolor* on glucose. Activation of DAG by cytidylate kinase to make CDP-DAG is known to be required for phospholipid biosynthesis (Dowhan, 2013). The very low expression of SCO1759 in *S. coelicolor* might be due to the reduced availability of DAG linked to the low biosynthesis of free fatty acids in this strain or to an altered genetic regulation of this gene (absence of an activator in *S. coelicolor*). In any case, the much lower expression of this operon on glucose in *S. coelicolor* than on *S. lividans* is likely to have an impact on membrane synthesis and thus on growth of *S. coelicolor*. On glycerol the difference of expression of these three genes between the strains is reduced and growth rate and biomass yields of *S. coelicolor* and *S. lividans* are similar. This suggests that on glycerol *S. coelicolor* generates sufficient fatty acids for membrane and storage lipid biosynthesis but not on glucose.

Overall these data are consistent with the observation that lipid content is lower in *S. coelicolo*r than in *S. lividans* on glucose as well as on glycerol, to a lesser extent.

A given lipid content results from an equilibrium between synthetic and degradative processes. Indeed 10 esterases and lipases, thought to catalyze the first step of the fatty acyl-CoA degradation *via* the hydrolysis of the bond between the acyl moiety and the glycerol backbone, showed statistically significant abundance changes between the two strains (Figure 5. 11). Most of them were more abundant in *S. lividans* than in *S. coelicolor* on both carbon sources at 72h. However, the secreted esterase SCO3053 was exclusively expressed on glucose whereas the thioesterase SCO2005 was mainly expressed on glycerol in *S. lividans*. The phospholipase C (SCO6691), that hydrolyzes the ester function between the glycerol and phosphate moieties yielding DAG and a phosphor-alcohol, and the lysophospholipase SCO6966, that cleaves off a fatty acid from a lysophospholipid, were expressed at an higher level in *S. lividans* than in *S. coelicolor*, in both medium.

Once fatty acid molecules are cleaved off the glycerol backbone, they can be degraded into acetyl-CoA *via* the process of beta-oxidation. Each β-oxidation cycle yields a new molecule of acetyl-CoA as well as NADH and $FADH_2$. The first step of β-oxidation involves the introduction of a double-bond in the acyl-CoA by acyl-CoA

dehydrogenases (Nouws *et al.*, 2010). Six of the 7 acyl-CoA dehydrogenases detected were more abundant in *S. lividans* than in *S. coelicolor*. Among these proteins, SCO3800, SCO1426, SCO2774 and SCO3051 had similar abundance on both carbon sources whereas SCO1209 (might belong to ethylmalonyl-CoA pathway, an alternative to the glyoxylate cycle absent in *S. lividans*) and SCO6469 (in an operon with ATP citrate lyase) were more abundant on glucose than on glycerol, in *S. lividans*.

SCO2779, likely to be co-transcribed with an upstream gene encoding a putative hydroxymethylglutaryl-CoA lyase (leucine catabolism) is encoding the only acyl-CoA dehydrogenase clearly more abundant in *S. coelicolor* than in *S. lividans* on both carbon sources (Figure 5. 11).

The second step of beta-oxidation is catalyzed by an enoyl-CoA hydratase that converts a trans-2-enoyl-CoA thioester into a beta-hydroxyacyl-CoA thioester. Only one enoyl-CoA hydratase (SCO5144) was detected and was highly abundant in *S. lividans* in glycerol. The next step is the conversion of beta-hydroxyacyl-CoA into beta-ketoacyl-CoA catalyzed by a hydroxyacyl-CoA dehydrogenase. Four hydroxyacyl-CoA dehydrogenases were identified. SCO5385 showed similar abundance in both strains on both carbon sources, SCO3834 showed higher abundance on glucose than on glycerol in both strains, SCO1591 and SCO4266 were more abundant in *S. coelicolor* than in *S. lividans* but on glycerol and glucose, respectively.

The last step of β-oxydation is catalyzed by a ketoacyl-CoA thiolase, likely encoded by SCO5399, an enzyme found to be 4.5 and 17.6-fold more abundant in *S. lividans* than in *S. coelicolor* cultivated in glucose and glycerol-grown culture, respectively (Figure 5. 11). In addition, the FadB fatty oxidation protein (SCO6789) was slightly more expressed in *S. lividans* than in *S. coelicolor*, especially on glycerol (Figure 13).

Altogether these data suggest that lipid degradation is more active in *S. lividans* than in *S. coelicolor*. However since the lipid content remains rather constant or even increases in *S. lividans*, this process should be balanced by even higher lipid biosynthesis. The apparent lower lipid degradation in *S. coelicolor* than in *S. lividans* might simply be related to its lower lipid content.

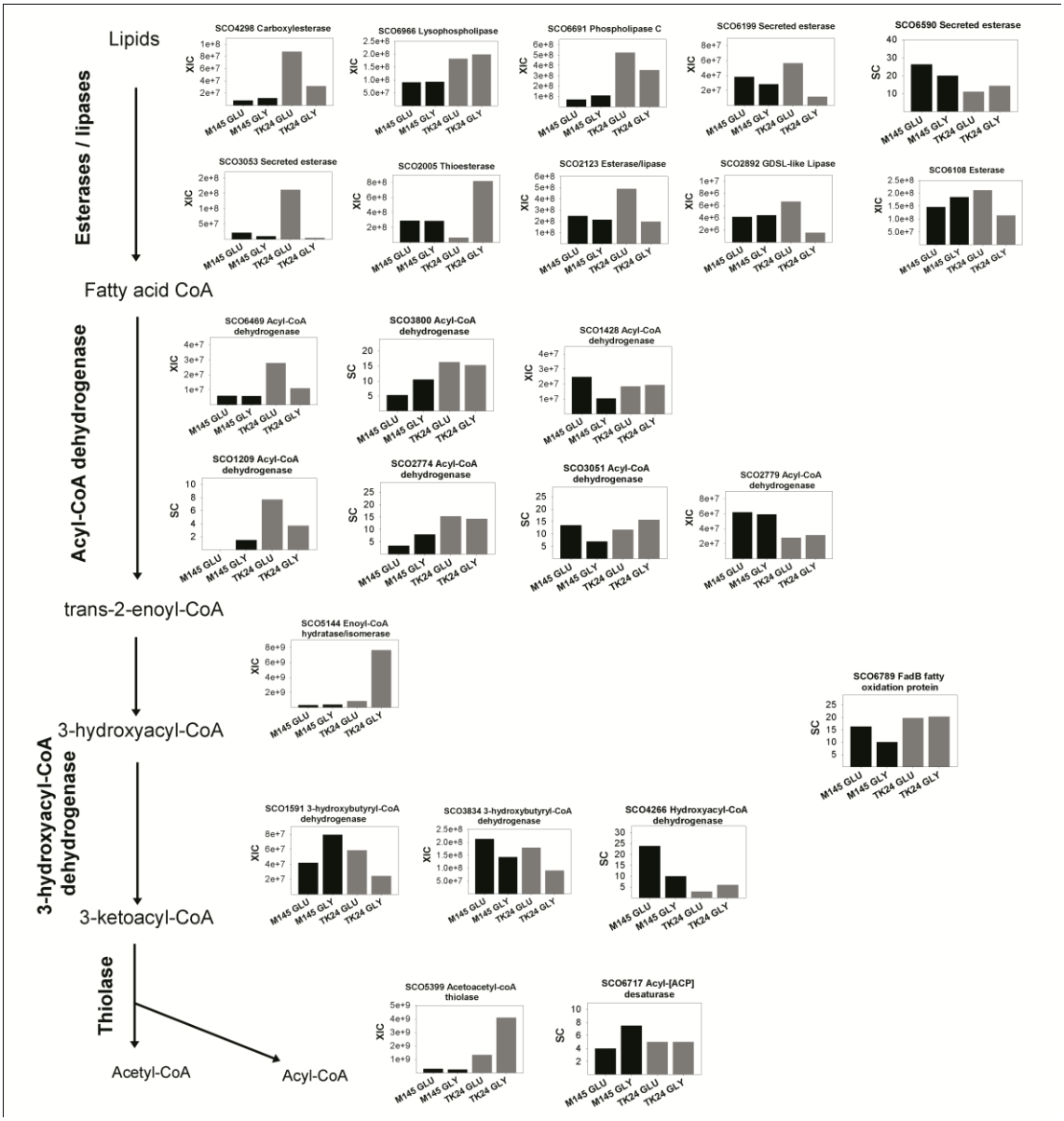

Figure 5. 11. Proteins annotated as involved in lipid and fatty acids degradation showing significant abundance variation between *S. coelicolor* and *S. lividans* (ANOVA, adjusted p value < 0.05). Protein abundances are represented by black and grey histograms for *S. coelicolor* (M145) and *S. lividans* (TK24) cultivated in R2YE glucose (GLU) or glycerol (GLY) after 72 h of cultivation.

5.3.5. Amino acids and nitrogen assimilation

A total of 11 proteins involved in proline, hydroxyproline and catabolism showed statistically significant abundant change (ANOVA, adjusted p value < 0.05, Figure 5. 12A). In the R2YE medium, proline is the most abundant amino acid (3 g/L), its consumption throughout growth was monitored (Figure 5. 3C). This clearly indicated

that *S. coelicolor* cultivated under glucose catabolized more actively proline than the other conditions (Figure 5. 3C). In this regard, 3 proteins involved in the catabolism of proline (SCO3835, SCO5519 and SCO5520) were up-regulated in *S. coelicolor* at early stages of growth (36h and 48h) whereas these proteins were up-regulated in *S. lividans* at late growth phases (48h and 72h). In addition, two proteins involved in the catabolism of hydroxyproline, a non-proteinogenic amino acid derived from proline, SCO1871 and SCO2298 were up-regulated in most of the conditions at 72h. Particularly, when *S. coelicolor* was cultivated in glucose, SCO2298 was 7.7 and 10.1-fold more abundant than in cultures of *S. coelicolor* in glycerol and *S. lividans* in glucose, respectively. The catabolism of hydroxyproline yields methylglyoxal and pyruvate while the catabolism of proline yields glutamate as well as FADH and/or NADH.

Glutamate can be also obtained from glutamine synthetases (SCO2198 and SCO2210). These two enzymes were highly abundant in cultures of *S. coelicolor* compared to *S. lividans* (Figure 5. 12A). Furthermore, the glutamate uptake system protein (GluA, SCO5777) was clearly up more abundant in glucose-grown cultures of both strains. This is in agreement with the fact that *Streptomyces* consume preferably glutamate rather than glucose (van Wezel *et al.*, 2006). However, that does not seem to be the case in glycerol-grown cultures. Glutamate is converted into a-ketoglutarate, an entry point of Krebs cycle, first by glutamate synthase (GOGAT, SCO2026) and then by glutamate dehydrogenase (GDH, SCO2999) yielding NH4+ and NADH/NADPH. GOGAT was up-regulated at the earliest stage of growth (36h) while GD was constitutively more abundant in cultures of *S. coelicolor* compared to *S. lividans* (Figure 5. 12A).

Concerning nitrogen assimilation, we detected 12 proteins with statistically significant change (ANOVA, adjusted p value < 0.05, File S4). These proteins were represented in a heatmap that showed a cluster of five proteins highly abundant in *S. coelicolor* cultivated in R2YE with glycerol at 72h of culture (Figure 5. 12B). This cluster contains: 4 nitrate reductases subunits (NirB, SCO2487; NasA, SCO2473; NarG3, SCO4947 and NarH3, SCO4948) and the GlnD regulator (SCO5585). GlnD encodes an uridylyltransferase that adenylates adenylylates, the nitrogen regulatory protein PII under low nitrogen availability (Hesketh *et al.*, 2002). Another protein involved in nitrogen assimilation, the regulatory enzyme GlnE, was found to be more

abundant at 72h of culture in both strains cultivated under the two medium (Figure 5. 12B). GlnE adenylylates/inactivates glutamine synthetase I (SCO2198) when ammonium is highly available (Hesketh *et al.*, 2002).

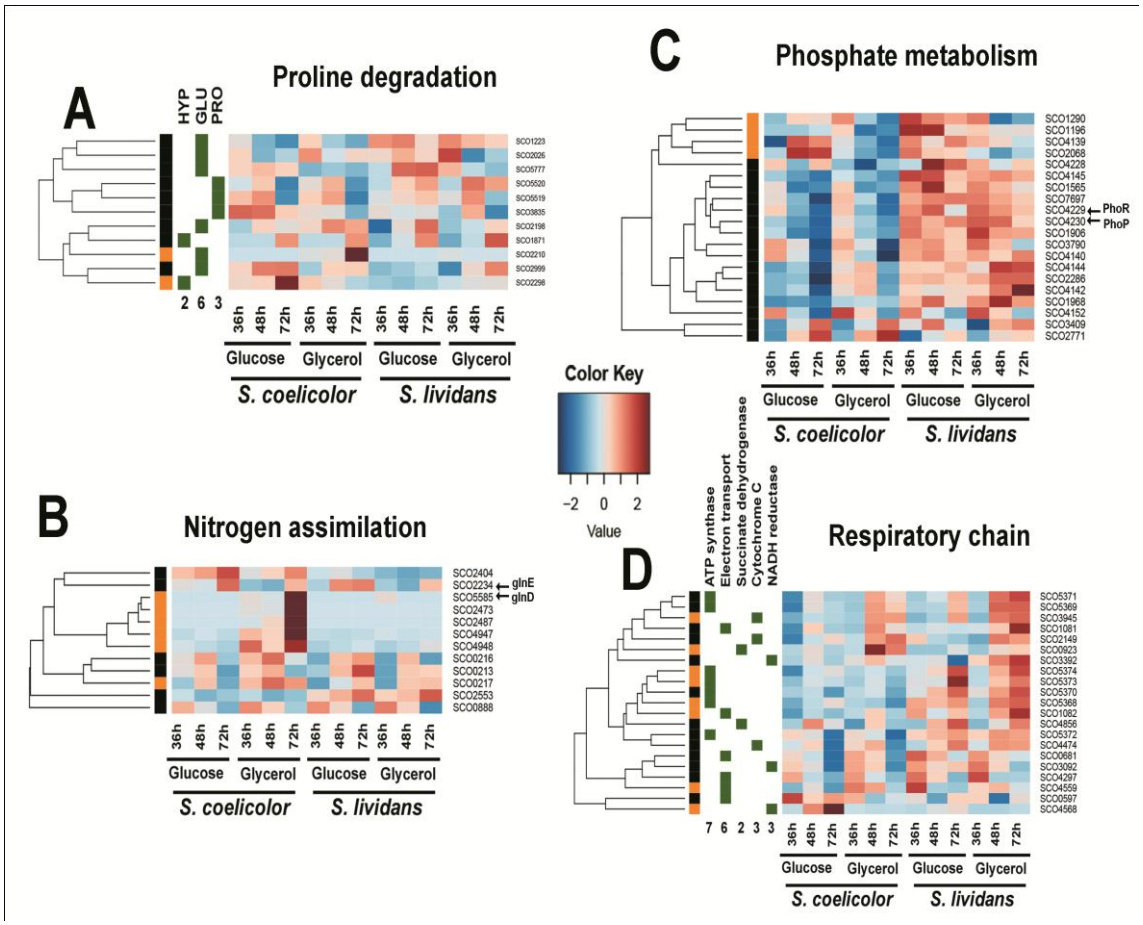

Figure 5. 12. Heatmap of proteins involved in: proline (PRO), hydroxyproline (HYP) and glutamate degradation (**A**), nitrogen assimilation (**B**), phosphate metabolism (**C**) and of respiratory chain (**D**) with significant abundance change (adjusted p value < 0.05).
Relevant proteins involved in nitrogen (**B**) and phosphate regulation (**C**) are indicated in arrows. The quantification methods are displayed in the vertical bar indicating those proteins quantified by SC (orange) and XIC (black). Annotated functional categories are shown above the green bars.

The regulatory protein GlnD is part of the amtB-glnK-glnD operon that is modulated by the major nitrogen regulator GlnR (SCO4159) (Fink *et al.*, 2002; Reuther and Wohlleben, 2007). *S. coelicolor* mutants lacking of GlnR showed glutamine auxotrophy (Wray *et al.*, 1991) for that reason this regulator is crucial for ammonia and glutamate assimilation. GlnR was detected in the present study but did not show statistically significant variation (Figure 5. 13). However, it exerted an incremental

tendency in *S. coelicolor* cultivated in glycerol-grown cultures which is in agreement with the proteomic profile of the nitrogen cluster observed in Figure 5. 12B as well as for glutamine synthetase (SCO2210, Figure 5. 12A).

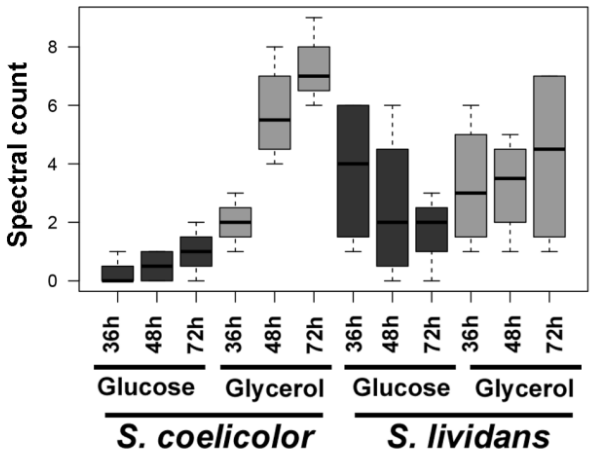

Figure 5. 13. Boxplots indicating the protein abundances of GlnR (SCO4159) in *S. coelicolor* and *S. lividans*. n = 4.

5.3.6. Phosphate and respiratory metabolism

Twenty proteins related to phosphate metabolism showed significant abundant change between the different conditions (ANOVA, adjusted p value < 0.05, Figure 5. 12C) and were resolved into two main and contrasted clusters with clearly higher abundance in *S. lividans* than in *S. coelicolor*.

It should be stressed that *Streptomyces* cultures were carried out in condition of P limitation (R2YE with no P added, Figure 5. 12C). In this condition, the expression of the two components system (TCS), PhoR (sensory kinase) and PhoP (response regulator) is induced. PhoP whose DNA binding ability is activated by phosphorylation by the kinase PhoR is known to regulate positively or negatively the expression of genes of the Pho regulon (Sola-Landa *et al.*, 2008; Allenby *et al.*, 2012). Consequently, in condition of Pi limitation, proteins under the positive control of PhoR/PhoP should be up-regulated whereas proteins under the negative control of this TCS shown be down-regulated (Sola-Landa *et al.*, 2003; Apel *et al.*, 2007).

Our data indicated a drastically different abundance of proteins known to belong to the Pho regulon in *S. lividans* and *S. coelicolor*. PhoR and PhoP were 2 to 5 fold more abundant in *S. lividans* than in *S. coelicolor* at all time points on both carbon sources. Consistently, most proteins known to be under the positive control of PhoR/PhoP were clearly more abundant in *S. lividans* than in *S. coelicolor* at 48h and 72h on both carbon sources (Figure 5. 12C). These included the polyphosphate kinase Ppk and MutT (SCO4145 and SCO4144). Ppk was up to 15 and 6.6 fold more abundant in *S. lividans* than in *S. coelicolor* at 48h on glucose and glycerol respectively whereas SCO4144 was 4 to 5 fold more abundant in *S. lividans* than in *S. coelicolor* at 72h on both carbon sources. Three proteins of the high affinity phosphate ABC transporter PstB (SCO4139), PstA (SCO4140) and PstS (SCO4142) (Diaz *et al.*, 2005) were also more abundant in *S. lividans* than in *S. coelicolor*. The protein PhoU (SCO4228), belonging to the Pho regulon thought to regulate P uptake was expressed at a similar level in both strains. Indeed, despite the lower abundance of transport proteins in *S. coelicolor* than in *S. lividans*, both strains transported P at a similar rate (Figure 5. 3C).

At last, several phosphatases, SCO1906 and SCO3790 (PhoX family), the alkaline phosphatase SCO2286, the phytase (SCO7697) as well as 3 glycerophosphoryl diester phosphodiesterases (SCO1196, SCO1968 and SCO1565) were also more abundant in *S. lividans* than in *S. lividans*. The letter enzymes hydrolyze the phosphodiester bond of glycerophospholipid resulting from the action of lipases, yielding glycerol 3P and an alcohol. These enzymes are known to be involved in the scavenging and recycling of phosphate present in the phospholipids. The weaker abundance of proteins of the Pho regulon in *S. coelicolor* was also noticed in our previous study carried out in liquid R2YE (Chapter IV).

Fifteen of the 21 proteins annotated as involved in respiration showed statistically significant higher abundance in *S. lividans* than in *S. coelicolor* on both carbon sources at 72h (Figure 5. 3D). These included: the NADH dehydrogenase subunit NuoD2 (SCO3392), the ATP synthase (subunits SCO5368, SCO5369, SCO5370, SCO5371, SCO5372, SCO5373, SCO5374); the ubiquinol-cytochrome c reductase (SCO2149), the cytochrome C biogenesis protein (SCO4474), cytochrome oxidase subunit (SCO3945), two succinate dehydrogenases (SCO0923, SCO4856) and two electron transfer flavoproteins (SCO1081 and SCO1082).

The exception to this general law is the 5.5 and 2.7fold higher abundance of the NADH dehydrogenase subunit NuoG (SCO4568) in *S. coelicolor* than in *S. lividans* in the presence of glucose at 72h. It is noteworthy that SCO4568 is encoded by a gene belonging to a 14 genes operon encoding proteins of the NADH dehydrogenase complex. It is surprising to see that only one protein of this large cluster was differentially expressed between the two strains. Similar comments could be made for SCO2149 (Ubiquinol-cytochrome c reductase iron-sulfur subunit/qcrA, Rieske iron-sulfur protein) encoded by a gene belonging to a 4 genes operon encoding cytochrome C and B oxidase complexes.

Since previous physiological studies carried out in the same conditions as the present study (Esnault *et al.*, 2017) revealed a highly active metabolism of *S. coelicolor* resulting in 2 to 3 fold higher ATP content in *S. coelicolor* than in *S. lividans.* We proposed that these high ATP levels might have a down regulatory effect on the expression of enzymes of the respiratory chain as well as on the expression of genes of the Pho regulon, the latter being rather expressed in condition of energetic deficit.

5.3.7. Stress and defense

A total amount of 47 proteins belonging to response to stress and defense showed a statistically significant variation according to strains, conditions and/or time (ANOVA, adjusted p value < 0.05, File S4, Figure 5. 14). It is noticeable that *S. coelicolor* stress response took place at all times whereas that of *S. lividans* occurred mainly at 72h.

Three Universal stress proteins (USP, SCO0167, SCO0198 and SCO0200) and two tellurium resistance proteins (SCO1965 and SCO0641) were more abundant in *S. coelicolor* than in *S. lividans* at 36h and throughout growth, respectively. These USP are encoded by the two large loci of the DosR regulon (SCO0161-SCO0181 and SCO0197-SCO0220) that are likely to be under the positive control of the LuxR response regulator (SCO0204), orthologous to the DosR regulator of *M. tuberculosis*. Proteins of this regulon as well as Tellurium resistance proteins are usually expressed in condition of growth slow-down.

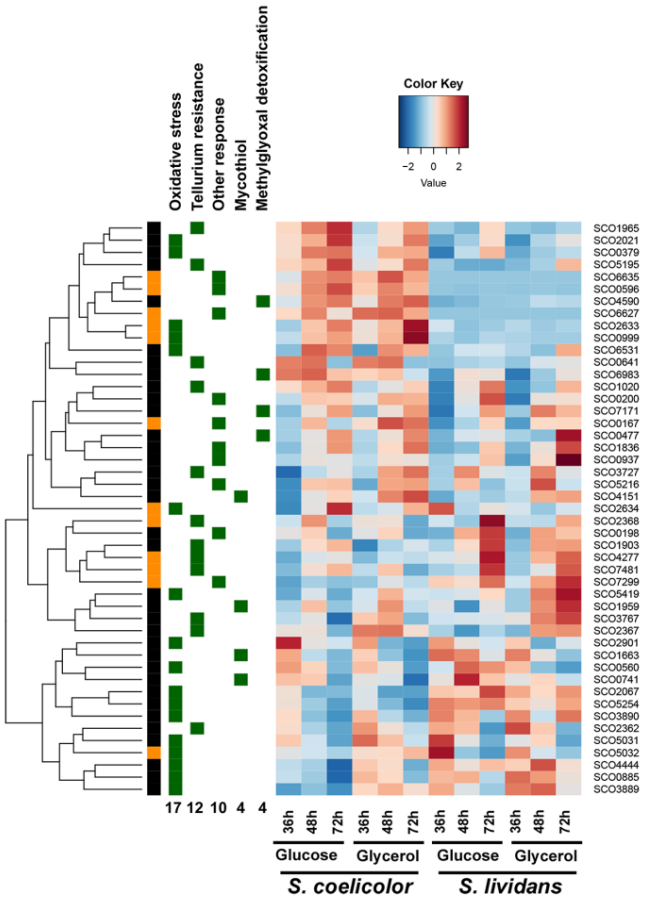

Figure 5. 14. Heatmap of proteins related to response to stress and defense with significant abundance change (adjusted p value < 0.05).
The quantification methods are displayed in the vertical bar indicating those proteins quantified by SC (orange) and XIC (black). Annotated functional categories are shown above the green bars.

Other proteins known to be directly involved in the resistance to oxidative stress, the superoxide dismutases (SOD, SCO2633 and SCO0999) and the hydroperoxide reductases (SCO5032 and SCO653), were more abundant in *S. coelicolor* than in *S. lividans* at 36/48h and at 48/72h, respectively. Furthermore, the protein DpsA (SCO0596) that contributes to DNA protection during oxidative stress, the catalase (SCO0379), the oxidative stress defense protein (SCO2021), SCO6635 (PhiC31 resistance gene pglY) and SCO6627 (PglX) were also more abundant in *S. coelicolor* than in *S. lividans* at all time points. Similar features previously observed in liquid R2YE medium (Chapter IV), are thought to be linked to the highly active oxidative metabolism of the *S. coelicolor*. Furthermore, studies related to the White B- like

proteins (Wbl) in *Streptomyces*, suggest a link between the sensing of oxidative stress and the triggering of antibiotic production (Kim *et al.*, 2012; Yan *et al.*, 2017).

At last, two proteins annotated as glyoxylases (SCO4590 and SCO6983) were more abundant in *S. coelicolor* than in *S. lividans* at the three time points. Glyoxylases are thought to be involved in the degradation of methylglyoxal, a toxic product synthetized from DHAP or GAP. Since GAPDH are expressed at a much lower level in *S. coelicolor* than in *S. lividans*, DHAP/GAP and thus methylglyoxal might accumulate. The toxicity of this molecule that is known to be associated with ROS production (Lee and Park, 2017) might contribute to the growth delay of *S. coelicolor* on glucose (Figure 5. 14).

Moreover, four tellurium resistance proteins (SCO4277, SCO2368, SCO3767 and SCO1903), the USP of the DosR regulon SCO0198, the thioredoxin SCO5419 and the hydroxymethyl) mycothiol dehydrogenase (SCO0741) were more abundant in *S. lividans* than in *S. coelicolor* mainly at 72h. And, the USP SCO7299, the SOD SCO5254 and the thioredoxins (SCO0885 and SCO2067) were more abundant in *S. lividans* than in *S. coelicolor* throughout growth (Figure 5. 14).

Altogether these results indicated that proteins indicative of growth slowdown at stationary phase in *S. lividans* on glucose are consistently expressed earlier in *S. coelicolor*.

5.3.8. Secondary metabolites pathways

A total of 74 proteins were quantified and showed a statistically significant abundance change (ANOVA, adjusted p value < 0.05). These proteins were resolved in three main clusters belonging to 17 secondary metabolite biosynthetic pathways (File S4, Figure 5. 15).

Cluster 1 included the secondary metabolites biosynthetic pathways expressed early in growth (36h): 9 proteins from the cryptic polyketide CPK (SCO6273, SCO6274, SCO6275, SCO6276, SCO6278, SCO6279, SCO6282, SCO6283 and SCO6284) (Pawlik *et al.*, 2007; Pawlik *et al.*, 2010), 2 proteins involved in terpenoids biosynthesis

(SCO2509 and SCO5058), 3 involved in desfierroxiamine biosynthesis (SCO2782, SCO2783 and SCO2785) and 1 of coelichelin biosynthesis (SCO0493).

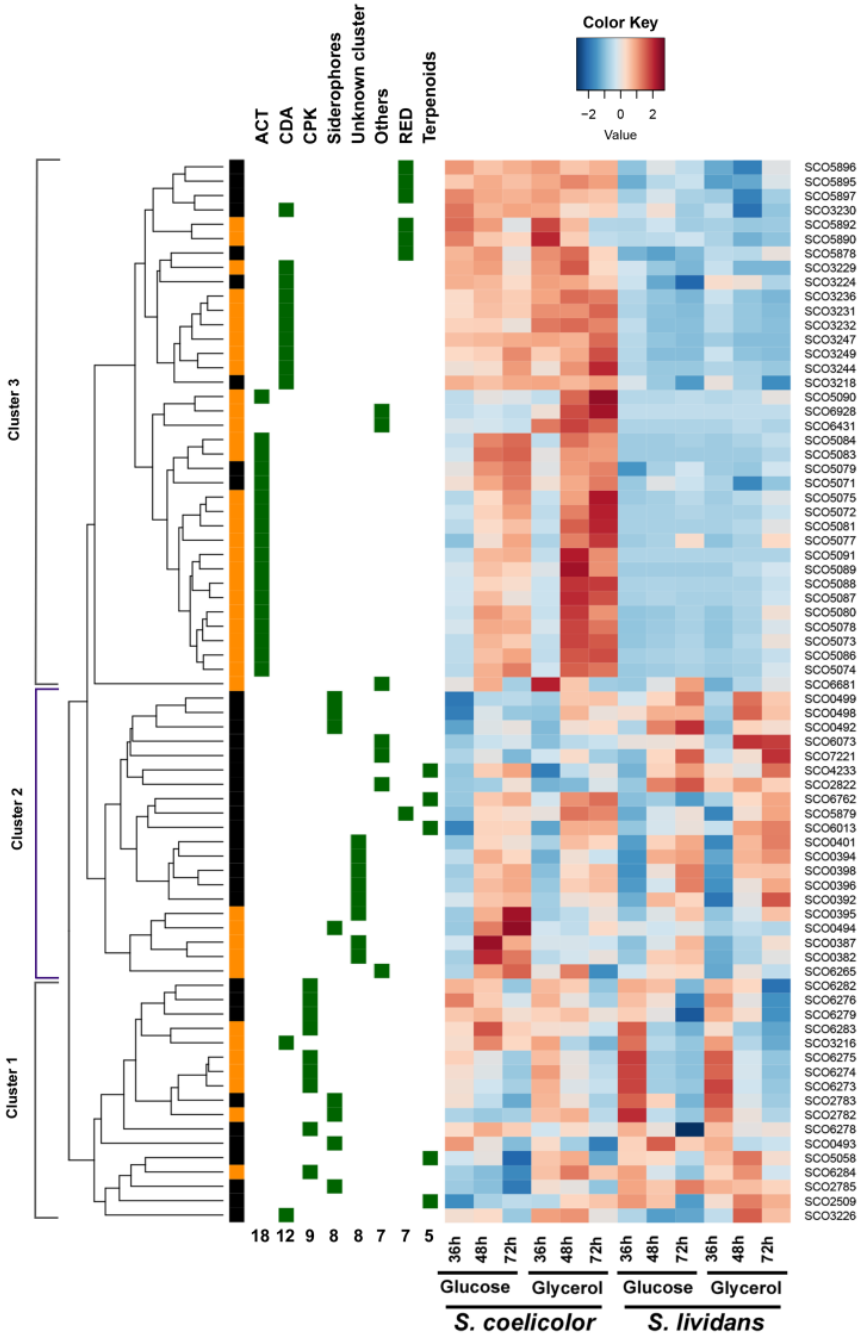

Figure 5. 15. Heatmap of proteins from secondary metabolites biosynthetic pathways with significant abundance change (adjusted p value < 0.05).
Quantification methods are displayed in the vertical bar indicating those proteins quantified by SC (orange) and XIC (black). Annotated functional categories are shown above the green bars.

Cluster 2 included the secondary metabolites biosynthetic pathways expressed later in growth (48 and 72h): 3 proteins involved in terpenoids biosynthesis (SCO4233, SCO6013 and SCO6762), 5 of coelichelin biosynthesis (SCO0492, , SCO0494, SCO0498 and SCO0499) and 8 corresponding to an unknown metabolite (SCO0382, SCO0387, SCO0392, SCO0394, SCO0395, SCO0396, SCO0398 and SCO0401) thought to be a deoxysugar (Challis and Hopwood, 2003).

Cluster 3 included those proteins belonging to the canonical CDA (12 proteins), RED (7 proteins) and ACT (18 proteins) antibiotic biosynthetic pathways that were produced mainly by *S. coelicolor* cultivated in either glucose or glycerol-grown cultures. This proteomic profile was validated with assays of ACT and RED antibiotics (Figure 5. 3D).

5.4. Discussion

Previous physiological studies from our group carried out in the same conditions as the present study (cultures grown on solid R2YE medium with glucose as main carbon source) contributed to define the metabolic features in correlation with high/low TAG content and weak/strong antibiotic production (Esnault *et al.*, 2017). Indeed, the high TAG content of *S. lividans* indicates the generation of excess of acetyl-CoA by a highly active glycolysis that could be considered as an over-flow metabolism. In this respect, this study revealed that numerous uptake systems involved in iron acquisition were up-regulated in *S. lividans*. This suggests that iron might be limiting in *S. lividans*. Since iron is necessary to numerous enzymes of the Krebs cycle and the functioning of respiratory chain, a limitation of the oxidative metabolism of the strain due to iron scarcity might be responsible for overflow metabolism and thus TAG biosynthesis characterizing this strain. Storage lipid accumulation occurs usually in the late growth stages in most microorganisms (Alvarez and Steinbuchel, 2002), in this study lipid accumulation clearly accompanies growth in *S. lividans* (Figure 5. 3C).

In *S. coelicolor*, the low TAG content coupled with the high rate of consumption of its polyphosphates stores and its high ATP/ADP ratio suggested that this strain was characterized by a highly active oxidative metabolism (Esnault *et al.*, 2017).. The latter was proposed to be due to its preferential consumption of amino acids present in the

growth medium rather than glucose (Chapter IV). The more active consumption of proline by *S. coelicolor* than by S. *lividans* was confirmed in solid R2YE supplemented with glucose (Figure 5. 3C). Such metabolism was correlated with the trigger of CDA, RED and ACT antibiotics biosynthesis and with a low TAG content (Figure 5. 3D-E). This suggested the existence of a reverse correlation between the ability to accumulate TAG and that to synthesize antibiotics.

In order to determine whether this constituted a general rule and whether TAG accumulation and antibiotic biosynthesis were mutually exclusive, a comparative proteomic study of *S. lividans* and *S. coelicolor* was conducted on solid R2YE medium in presence of either glucose or glycerol as main carbon source. The comparison of these two carbon sources was judged interesting since preliminary studies indicated these two strains had similar high TAG content when grown on R2YE with glycerol whereas on R2YE with glucose *S. coelicolor* had lower TAG content than *S. lividans*. This study unexpectedly showed that *S. coelicolor* produces ACT on R2YE supplemented with glycerol at similar levels than on R2YE supplemented with glucose despite its high lipid content. This indicated that on glycerol, but not on glucose, *S. coelicolor* produces sufficient acetyl-CoA to support the concomitant biosynthesis of these two types of molecules.

Furthermore, this study revealed that the overall abundance of proteins of different ontological classes were not so different between the two species at 36 and 48h of incubation (Figure 5. 7). But at 72h, a drastic down regulation of proteins of most ontological classes was observed in *S. coelicolor* with the noticeable exception of proteins belonging to secondary metabolite biosynthetic pathways. The proteins of the CDA, RED and ACT clusters were already detected at 36h and were still present at 48 and 72h. Interestingly, at 72h, on glucose as well as on glycerol, the abundance of proteins involved in the biosynthesis of fatty acids and lipids was greatly reduced in *S. coelicolor* compared to *S. lividans* (Figure 5. 10). This likely reduced lipogenic feature was correlated with a high biosynthesis of ACT.

In this study, we established for the first time the metabolic features involved in fatty acids accumulation and secondary metabolites production in glycerol grown cultures of *S. coelicolor* and *S. lividans*. Furthermore, this study represents the largest proteomic

dataset of *S. coelicolor* and *S. lividans* and could be a useful resource for the scientific community working on the field of Streptomycetes to better understand the links between primary and secondary metabolism of these fascinating bacteria.

5.5. Supplementary material

Supplementary material will be publicly available on the online version.

File S1. Lumos_gly_glu_sco_livi.xlsx

File S2. MassChroQ_parameters.docx

File S3. Venn_LocateP.xlsx

File S4. Proteomics_SC_XIC.xlsx

5.6. Acknowledgments

The financial support for AMO thesis was provided by the National Science and Technology Council (CONACYT, Mexico) number 314457. The authors acknowledge the region Ile-de-France for contributing to the acquisition of the Orbitrap Fusion™ Lumos™ Tribrid™ mass spectrometer (Thermo Fisher Scientific).

DISCUSSION AND PERSPECTIVES

The first part of the present work (Chapter III) was aimed to the validation the use of FT-IR spectroscopy in Attenuated Total Reflection (ATR) mode to determine total fatty acids content in *Streptomyces* cells. The ATR method was previously proven to be suitable to determine quantitatively the fatty acids content of pure vegetable oils (Sherazi *et al.*, 2009; Mossoba *et al.*, 2013; Sherazi *et al.*, 2013). However, it was suspected to be semi-quantitative and poorly reliable for the analysis of lipids within micro-organisms since the latter that contain proteins and other carbohydrates besides fatty acids that could interfere with the quantification process (Pistorius *et al.*, 2009). In a multidisciplinary context that involved the collaboration of research groups from the Laboratoire de Chimie Physique (LCP, http://www.lcp.u-psud.fr/spip.php?article358&lang=fr) and the Laboratoire d'Études des Techniques et Instruments d'Analyse Moléculaire (LETIAM, http://www.iut-orsay.u-psud.fr/fr/laboratoires/letiam.html), both belonging to the Université Paris-Saclay, we demonstrated the reliability of the ATR-FT-IR approach that showed a linear correlation with the GC/MS and FT-IR in transmission (using KBr pellets) methods. This led to the establishment of a calibration curve allowing the conversion of the ATR-FTIR measures expressed in CO/amide I ratio into µg of FAME per mg of biomass for FAMES content ranging from 30 to 150 µg of esterified fatty acids per mg of dry biomass.

The second and third parts of this thesis were carried out in close collaboration with the proteomic platform PAPPSO (Plateforme d'Analyse Protéomique de Paris Sud Ouest, http://pappso.inra.fr/). Comparative proteomic analysis of the model strains *S. lividans* and *S. coelicolor* grown either in liquid or solid R2YE medium with glucose or glycerol as main carbon sources were carried out. These two strains are phylogenetically closely related and bear similar functional biosynthetic pathways for the biosynthesis of specific secondary metabolites. Nonetheless, they have contrasted abilities to produce these metabolites as well as to accumulate storage lipid of the triacylglycerol (TAG) family (Le Marechal *et al.*, 2013). Indeed on solid R2YE glucose,

S. coelicolor produces antibiotics and its lipid content is low whereas *S. lividans* has a 3 to 4 fold higher lipid content than *S. coelicolor* and does not produce antibiotics.

This indicated that *S. lividans* metabolism was mainly glycolytic and that this strain generated its energy predominantly *via* active glucose catabolism generating excess of acetyl-CoA stored as TAG. Our proteomic studies carried out in liquid or solid R2YE with glucose corroborated this view since glycolytic enzymes were far more abundant in *S. lividans* than in *S. coelicolor* in both conditions.

This observation also suggested the existence of a reverse correlation between the ability to accumulate TAG and that to synthetize antibiotics suggesting that the biosynthesis of these two molecules might be mutually exclusive. However, our last studies showed that it was not the case since *S. coelicolor* was able to accumulate TAG as well as to produce antibiotics on R2YE with glycerol. In contrast, this strain did not accumulate TAG but did produce antibiotics on R2YE with glucose and its growth rate was delayed on this medium for unknown reasons. We can hypothesize that the high ATP content characteristic of this strain has a negative impact on glucose uptake and catabolism. Indeed it is known that high levels of ATP inhibits allosterically an important glycolytic enzyme, the phosphofructose kinase (Berg *et al.*, 2002). In consequence, on R2YE with glucose, the strain would generate insufficient amount of acetyl-CoA to even synthetized its membrane lipids explaining its drastic growth retardation as well as its low TAG content. The effect is not seen on R2YE glycerol since the entry point of this carbon source in glycolysis is the DHAP/GAP node that is located below the reaction catalyzed by the phosphofructose kinase.

As mentioned above, a recent finding of our group showed that on solid R2YE glucose, *S. coelicolor* was characterized by a faster consumption of its polyphosphate stores and a higher ATP/ADP ratio than *S. lividans*, suggesting that the metabolism of this strain was mainly oxidative (Esnault *et al.*, 2017). Further uptake studies revealed that *S. coelicolor* transports and catabolizes preferentially the amino acids (mainly proline) present in the growth medium rather than glucose. Our proteomic studies confirmed that enzymes involved in the catabolism of amino acids, specific enzymes of the Krebs cycle generating energy and enzymes of the respiratory chain were more abundant in *S. coelicolor* than in *S. lividans*. This suggests that *S. coelicolor* generates

its energy predominantly *via* amino acid (rather than glucose) catabolism, Krebs cycle activation and oxidative phosphorylation. This process generates directly and indirectly (*via* Krebs cycle feeding) abundant reduced co-factors whose re-oxidation by the respiratory chain yields ATP. The higher abundance of proteins related to siderophores biosynthetic pathways, coelichelin and desferrioxamine, was consistent with the oxidative metabolism of *S. coelicolor* since several enzymes of the Krebs cycle and of the respiratory chain require iron for their functioning. The high abundance of proteins involved in the response to oxidative stress in both liquid and solid cultures, is also consistent with a highly active oxidative metabolism that is known to generate reactive oxygen species.

An unexpected outcome of this study was the striking lack of induction of genes of the Pho regulon in *S. coelicolor*. Proteins of the Pho regulon are usually induced in condition of phosphate limitation that correlates with an ATP deficit. The high ATP content of *S. coelicolor* linked to its highly active oxidative metabolism might thus have a negative impact on the expression of genes of the Pho regulon as well as on its glycolytic activity. The expression of the genes of the Pho regulon are under the positive or negative control of the two components system PhoR (sensory kinase) and PhoP (response regulator) (Sola-Landa *et al.*, 2008; Allenby *et al.*, 2012). In *S. coelicolor*, this important master regulator of phosphate metabolism was shown to negatively control the expression of the master regulator protein of nitrogen metabolism GlnR. The lack of PhoP induction in *S. coelicolor* is expected to correlate with an enhancement of GlnR expression that could explain the enhanced ability of *S. coelicolor* to catabolize the amino acids (proline) present in the growth medium preferentially to glucose.

The very low TAG content of *S. coelicolor* was due to a lack of synthesis rather than to an enhanced degradation of these molecules. Again this feature might be indirectly linked to the lack of induction of PhoP thought to lead to an enhanced catabolism of amino acids generating ATP, an inhibitory molecule of glycolysis as well as nitrogen also known to have a negative impact on TAG biosynthesis. This study also identified proteins of this specific metabolism highly expressed in our tested conditions among the hundreds of proteins annotated as involved in lipid metabolism.

This work constitutes a courageous attempt to decipher the crucial genetic differences that underpin the different metabolic features of *S. coelicolor* and *S. lividans*. Our studies point to the crucial default of induction of the master regulator of phosphate metabolism, PhoP that also controls nitrogen metabolism and the cascade of events resulting from this default that is summarized below (Figure C).

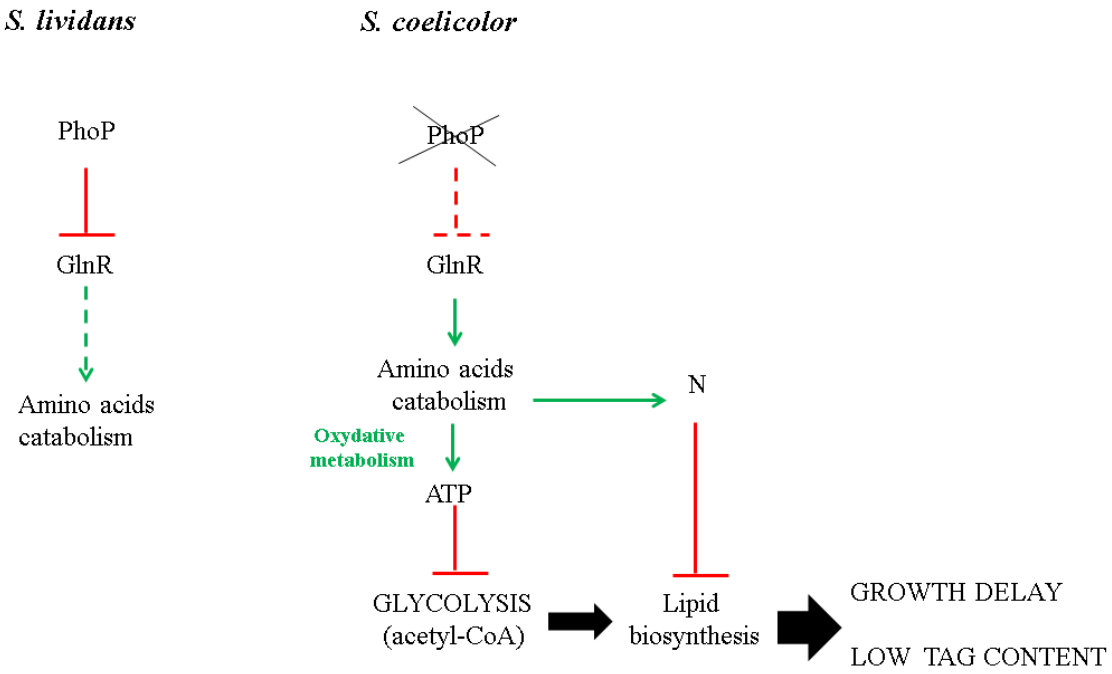

Figure C. Schematic representation of regulatory cascades of PhoP likely involved in *S. coelicolor* and *S. lividans* metabolism.

However the genetic cause of the lack of induction of the expression of genes of the Pho regulon remains to be determined. We hope that the large proteomic datasets generated in the course of this thesis, that will be made publicly available, will stimulate further research to better understand the metabolic functioning of strong antibiotic-producing strains such as *S. coelicolor*. This knowledge is of crucial importance to construct strains with enhanced antibiotic producing abilities in order to discover most needed novel antibiotics.

ANNEXE A. RÉSUMÉ DES TRAVAUX DE RECHERCHE

Les *Streptomyces* sont des bactéries filamenteuses du sol à Gram +. Elles sont connues pour leur capacité à produire des métabolites secondaires utiles en médecine et en agriculture. *S. coelicolor* et *S. lividans* sont des souches phylogénétiquement proches souvent utilisées comme modèles pour l'étude de la régulation de la biosynthèse d'antibiotiques. Un étude comparative *in silico* des génomes de *S. coelicolor* (Bentley *et al.*, 2002) et de *S. lividans* (Rückert *et al.*, 2015) a révélé que 91% des gènes présents chez *S. lividans* sont des gènes orthologues chez *S. coelicolor* (Lewis *et al.*, 2010) et possèdent notamment les même voies de biosynthèse pour la production de trois antibiotiques bien caractérisés CDA (Calcium Dependent Antibiotic), RED (Undecylprodigiosin) et ACT (Actinorhodin). Cependant, ces deux espèces ont des capacités très contrastées à produire ces métabolites secondaires et à accumuler des lipides de réserve de la famille des triacylglycérol (TAG). Sur le milieu solide riche R2YE contenant du glucose comme source principale de carbone, *S. coelicolor* produit CDA, RED et ACT à des niveaux élevés et son contenu en TAG est faible alors que *S. lividans* ne produit pas ces métabolites secondaires et a un contenu en TAG 3 à 4 fois supérieur à celui de *S. coelicolor* (Le Marechal *et al.*, 2013). Le but de la présente thèse était de déterminer les caractéristiques métaboliques différentielles qui sous-tendent les différentes capacités biosynthétiques de ces deux souches modèles. Pour ce faire, des analyses protéomique comparatives sans marquage des souches cultivées en milieu R2YE liquide ou solide en présence de glucose ou de glycérol comme principales sources de carbone ont été réalisée en utilisant la technique de chromatographie liquide couplée à de la Spectrométrie de Masse en tandem (LC-MS / MS).

Une première partie de ce projet a été consacré à la validation de la méthode de spectroscopie infrarouge à transformée de Fourier (FTIR) en mode de réflectance totale atténuée (ATR) pour doser le contenu lipidique des souches de *Streptomyces* qui est constitué des phospholipides membranaires polaires et des lipides neutres de la famille des TAG. Ces derniers sont stockés dans des corps lipides qui se constituent au niveau de la membrane plasmique et sont visibles dans le cytoplasme. La spectroscopie

infrarouge est une méthode qui permet l'identification de molécules organiques et inorganiques du fait que chaque groupe fonctionnel possède des fréquences vibrationnelles spécifiques (Figure A. 1). Pour le dosage des lipides les deux bandes d'absorption représentatives de ces derniers sont utilisées: la bande C=O à 1740 cm^{-1} et la bande C-H à 2953-2853 cm^{-1}. Ces valeurs sont standardisées par l'intensité vibrationnelle de la bande amide I à 1650 cm^{-1} qui représente les protéines. Les valeurs obtenues sont donc exprimées comme un rapport de l'intensité vibrationnelle de la bande C=O (ou CH) sur celle de la bande amide I.

Cette étude a démontré l'existence une corrélation linéaire entre la méthode ATR-FT-IR et deux méthodes quantitatives classiques: la chromatographie gazeuse couplée à la spectrométrie de masses (GC/MS, Figure A. 2) et la spectroscopie FT-IR en Transmission. Ces deux méthodes bien que couramment utilisées requièrent une préparation longue des échantillons et donc sont sujettes à erreur expérimentale d'origine humaine.

Par contre, la méthode ATR permet une évaluation directe et rapide de la quantité totale d'acides gras estérifiés et présente de nombreux avantages par rapport à la GC/MS et la méthode FT-IR en transmission: i) elle est rapide et hautement reproductible car elle requière peu de manipulations, ii) le temps de traitement des données est substantiellement réduit par rapport à celui des deux autres méthodes iii) elle permet des mesures fiables comparables à celles obtenues avec les méthodes quantitatives classiques. En effet, des droites de corrélation ont été établies entre les valeurs obtenues pour les mêmes échantillons biologiques par la méthode ATR-FT-IR et les méthodes GC/MS ou FT-IR en transmission permettant la conversion des valeurs des rapports C=O/ Amide I en μg de lipides par mg de biomasse. Pour toutes ces raisons, l'ATR-FT-IR est très bien adaptée pour le repérage à moyen/haut débit de microorganismes oléagineux ou pour suivre l'évolution du contenu en lipides tout au long de la croissance des cellules microbiennes.

Dans la deuxième partie de ce projet, une étude protéomique de type «shotgun» sans marquage a été menée avec les souches *S. coelicolor* et *S. lividans* cultivées en milieu R2YE liquide avec glucose comme principale, mais non exclusive, source de carbone. Les acides aminés du milieu, et notamment la proline, constituent la principale source

d'azote du milieu mais peuvent également constituer une source de carbone. Ce milieu est largement utilisé par la communauté scientifique car qu'il permet, du moins sous sa forme solide, une bonne production d'antibiotique.

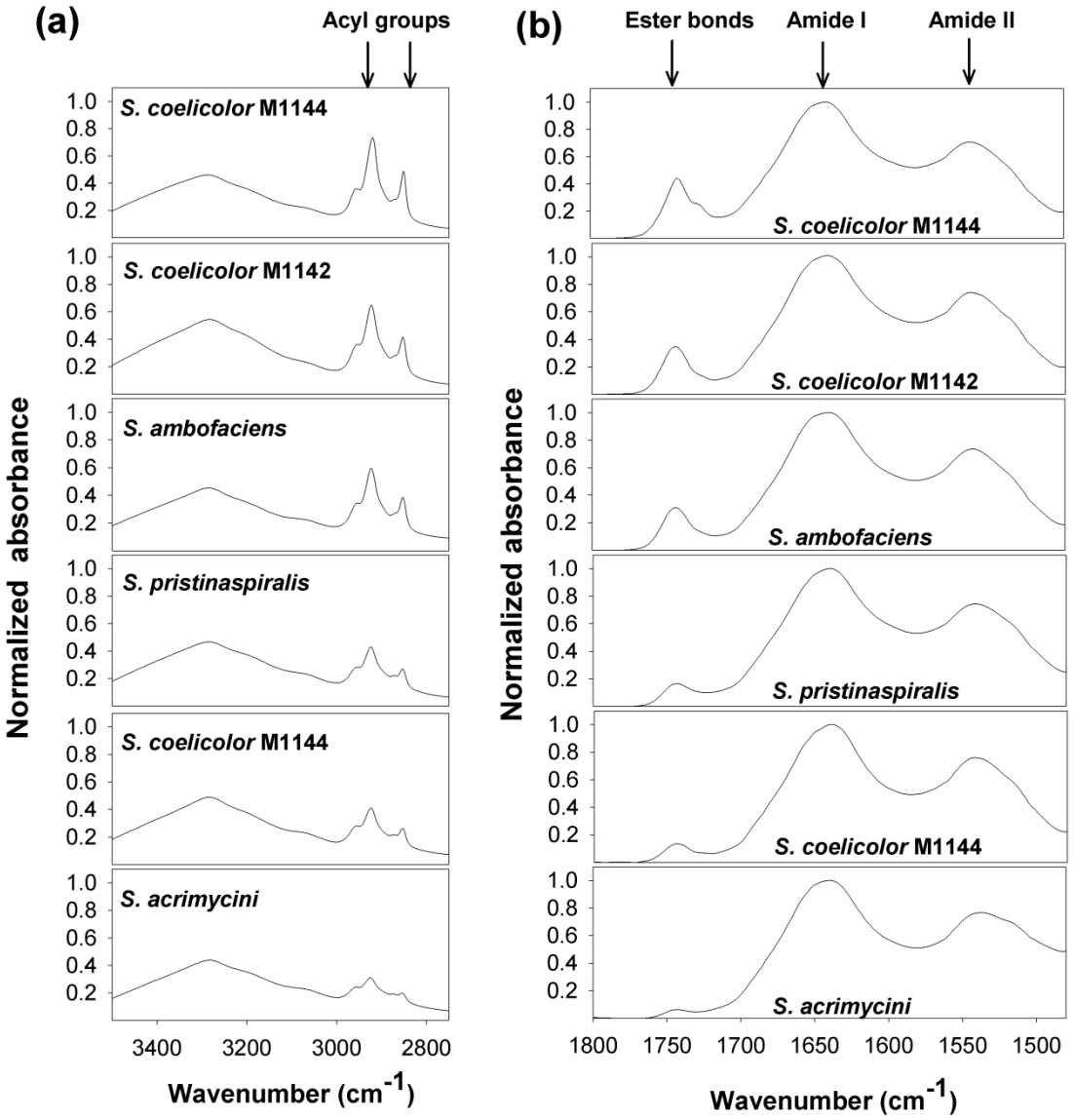

Figure A. 1. Spectres d'absorption ATR-FT-IR normalisés des bactéries *Streptomyces*. Le contenu total des acides lipidiques estérifiés peut être mesuré en utilisant les bandes d'absorption à 1740 cm^{-1} (bande C=O, **a**) où celle de 2953-2853 cm^{-1} (bande C-H, **b**).

L'analyse par LC-MS / MS a été conduit avec un spectromètre de masse à haute résolution (Q-exactive, Thermo Fisher Scientific). Au total, 2024 protéines ont été identifiées à partir des cultures liquides, représentant 24% du protéome théorique (Figure A. 3a). La fraction des protéines intracellulaires était la plus abondante dans les

protéomes des deux souches étudiées (83% du protéome totale, Figure A. 3b). Deux méthodes de quantification relative «label free» ont été menées: l'un à base du comptage des spectres (Spectral Counting /SC) et l'autre à partir d'extraits du courant d'ion (eXtracted Ion Current: XIC) et trois cent soixante protéines présentant une variation significative d'abondance relative en fonction de la souche et du temps («p-value» ajustée <0.05, Figure A. 3c) ont été obtenues à partir de l'analyse statistique (SC : 180 protéines, XIC : 123 protéines, et 57 protéines présentes dans le deux méthodes de quantification).

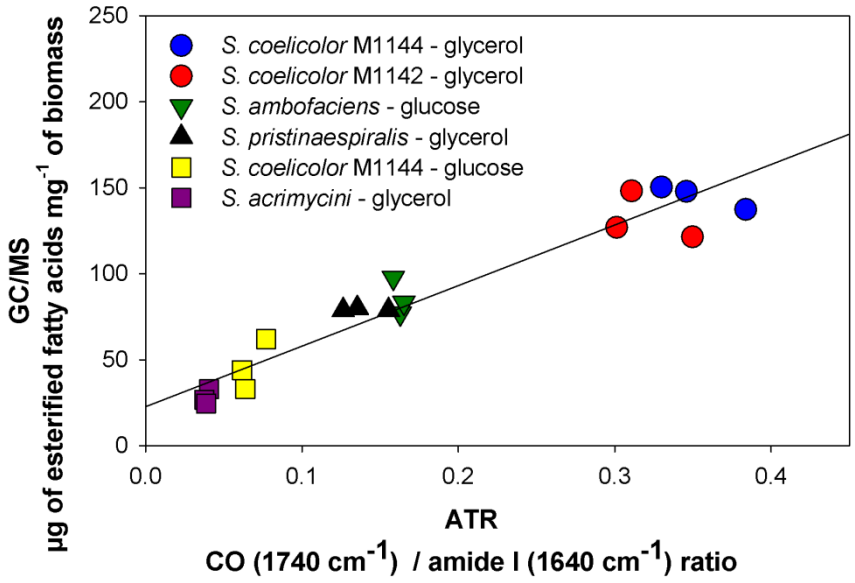

Figure A. 2. Corrélation entre les rapports CO/amide I obtenus avec l'ATR-FT-IR et la quantification totale des acides gras estérifiés déterminée par GC/MS dans les échantillons des *Streptomyces*.

Les 360 protéines qui ont montré un changement d'abondance statistiquement représentatif ont été représentées sous la forme d'une carte de chaleur (Heat Map) en utilisant un regroupement hiérarchique Euclidien (Figure A. 4). Les 6 combinaisons de souches et temps de culture ont été résolues clairement dans 2 groupes principaux correspondant principalement à la réponse liée à l'effet souches.

Les principaux résultats issus de cette étude protéomique «préparation en milieu liquide» ont confirmé que le métabolisme de *S. lividans* est principalement glycolytique alors que le métabolisme de *S. coelicolor* est principalement oxydatif. La plus grande

abondance de protéines glycolytiques chez *S. lividans* que chez *S. coelicolor* est en accord avec l'assimilation plus active du glucose par cette dernière que *S. coelicolor* (Figure A. 5). En revanche, les données protéomiques indiquent que, contrairement à *S. lividans*, *S. coelicolor* cataboliserait les acides aminés présents dans le milieu de manière plus efficace que le glucose (Figure A. 6 a-b). L'entrée directe des molécules issues de cette dégradation dans le cycle de Krebs expliquerait le métabolisme principalement oxydatif de cette souche.

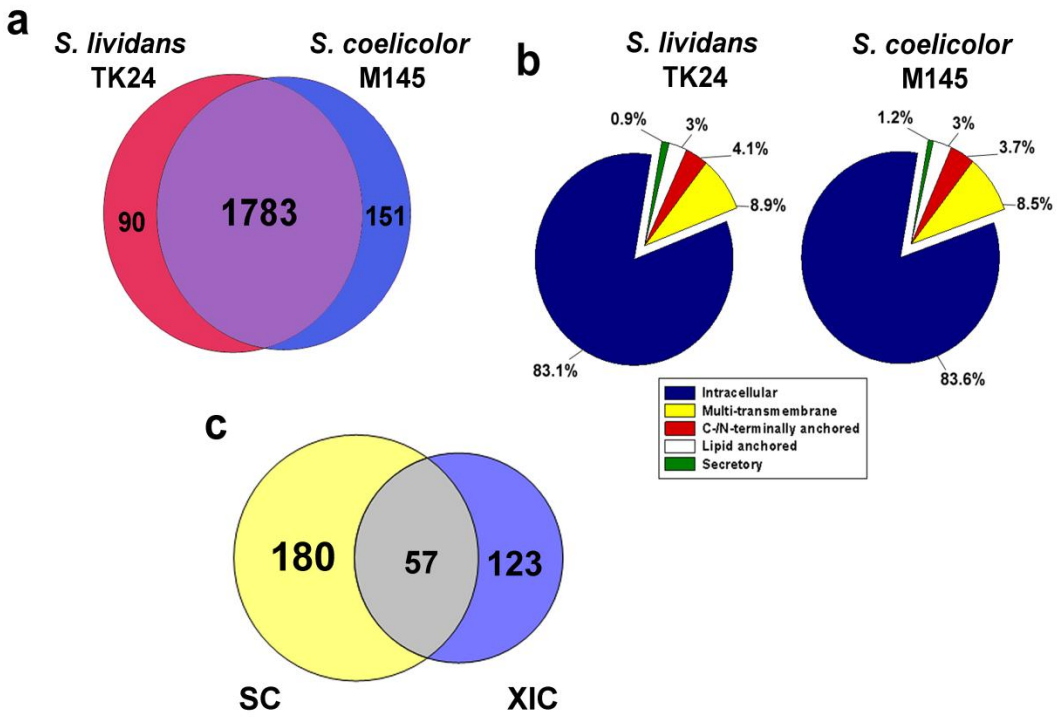

Figure A. 3. Diagramme de Venn des 2024 protéines identifiées en utilisant X! TandemPipeline 3.3.4 (**a**). Localisation sous-cellulaire des protéines identifiées chez *S. coelicolor* et chez *S. lividans*. Résultats obtenus à partir de la base de données LocateP (**b**). Diagramme de Venn des 360 protéines qui ont montré un changement d'abondance significatif entre *S. coelicolor* et *S. lividans* (ANOVA, «p-value» ajustée <0.05, **c**).

Le catabolisme de la proline, l'acide aminé le plus abondant du milieu R2YE, génère du glutamate ainsi que des cofacteurs réduits ($FADH_2$ et NADH). Le glutamate serait ensuite converti en α-kétoglutarate, un point d'entrée dans le cycle de Krebs qui induit la génération des cofacteurs réduits dont la ré-oxydation par la chaîne respiratoire génère de l'ATP. Ces résultats sont cohérents avec une étude physiologique précédemment réalisée en milieu R2YE solide (Esnault *et al.*, 2017). Cette étude a révélé que *S.*

coelicolor était caractérisé par une consommation très active de ses réserves de polyphosphates et par un rapport ATP/ADP très supérieur à celui de *S. lividans* indiquant une activation de son métabolisme oxydatif (Esnault *et al.*, 2017). C'est dans ce contexte d'un métabolisme oxydatif hautement actif qu'est déclenchée la production d'ACT. Cependant, dès qu'ACT est produit, une chute abrupte du contenu en ATP de *S. coelicolor* a été observée. Ceci suggère qu'ACT aurait un impact négatif sur la phosphorylation oxydative et donc régulerait l'excès d'ATP (Esnault *et al.*, 2017). Un excès d'ATP peut survenir lors des phases de ralentissement ou d'arrêt de croissance quand l'énergie générée par le catabolisme excède les besoins énergétiques d'un l'anabolisme ralenti. C'est en effet dans ces phases de ralentissement/arrêt de croissance qu'est généralement déclenchée la production d'antibiotiques dont la fonction serait de contribuer à mettre en cohérence génération et besoin en ATP. Cependant dans notre étude, les cultures ont été réalisées en milieu R2YE liquide et se sont révélées insuffisamment oxygénées. De ce fait, la croissance des deux souches a été faible et la production d'antibiotiques n'a pas été observée (CDA, RED et ACT). En effet une oxygénation suffisante du milieu est nécessaire pour soutenir un métabolisme oxydatif et générer de l'ATP en abondance.

Dans ce contexte, *S. coelicolor* et *S. lividans* ont réagi différemment à la limitation d'oxygène. *S. coelicolor*, du fait de son métabolisme oxydatif, a consommé plus activement que *S. lividans* la faible quantité d'O_2 dissout dans le milieu de culture et se trouve donc plus rapidement en anoxie que cette dernière. La consommation plus active de nitrate par *S. coelicolor* et la plus forte abondance des sous-unités de nitrate-réductase chez cette dernière que chez *S. lividans* indique que, pour faire face à cette situation, *S. coellicolor* utilise le nitrate (NO_3^-) comme accepteur final d'électrons alternatif à l'O2 et ce faisant génère du nitrite (NO_2^-) (Figure A. 6c-d). Par ailleurs l'abondance des protéines impliquées dans la résistance au stress oxydant est plus grande chez *S. coelicolor* que chez *S. lividans* ce qui est cohérent avec le métabolisme oxydatif de *S. coelicolor* plus générateur des espèces réactives d'oxygène que le métabolisme glycolytique de *S. lividans* (Figure A. 7a). Les protéines appartenant au régulon de dormance DosR-like se sont révélées également plus abondantes chez *S. coelicolor* que chez *S. lividans* (Figure A. 7a). Ceci indique un ralentissement du

métabolisme de *S. coelicolor* qui intervient plus tôt que chez *S. lividans* du fait de son état d'anoxie plus précoce et donc plus sévère que celui de *S. lividans*.

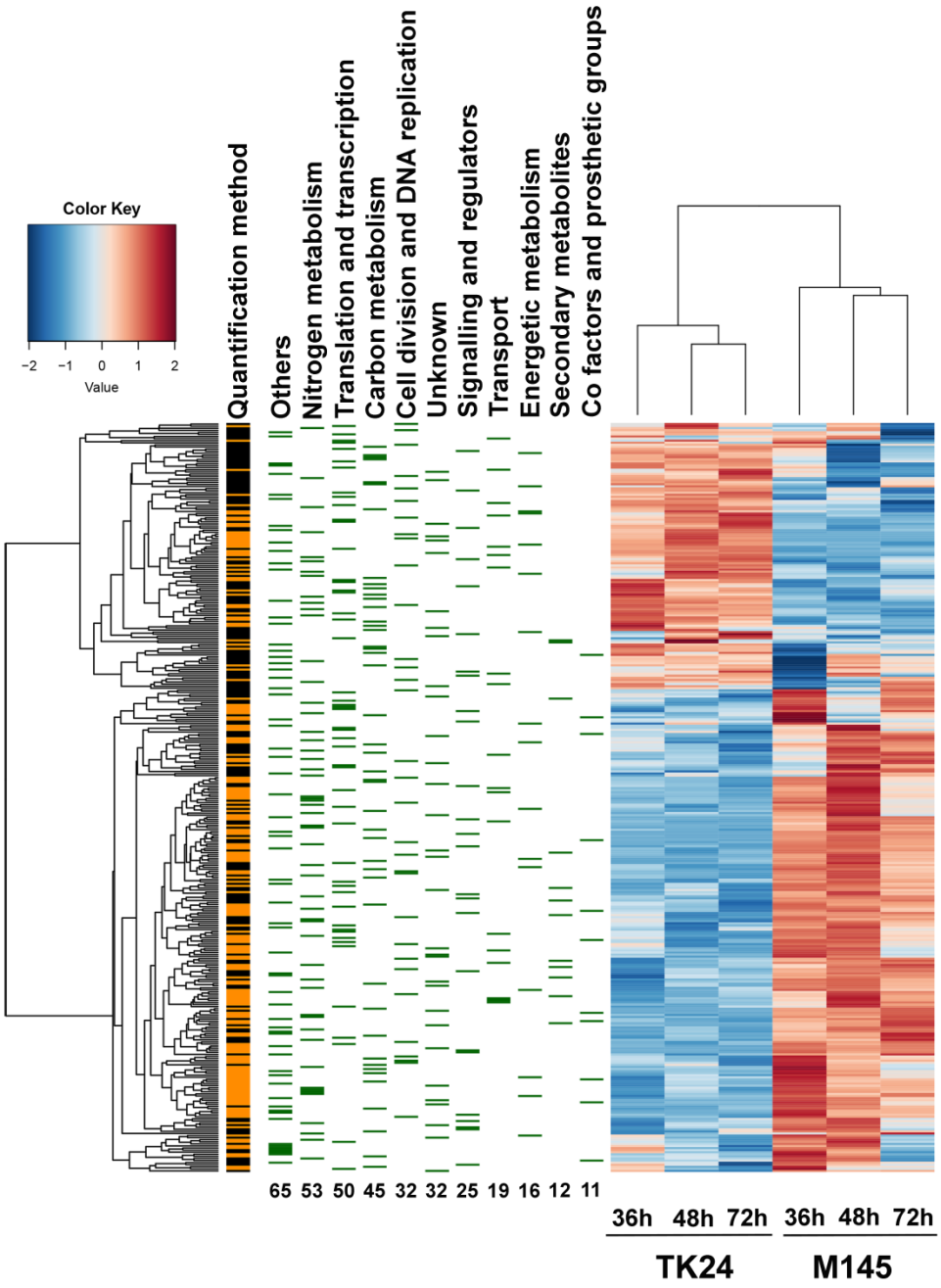

Figure A. 4. Représentation en carte de chaleur (Heat Map) des abondances relatives des 360 protéines dont la différence l'abondance est jugée significativement statistiquement différente entre *S. coelicolor* (M145) et chez *S. lividans* (TK24) à 36, 48 et 72 h de culture. Chaque barre verte dans partie gauche du schéma représente une protéine. La méthode utilisée pour quantifier chaque protéine est affichée en orange (SC) ou noir (XIC) sur la barre verticale à gauche du schéma. Les catégories fonctionnelles et le nombre total de protéines pour chaque catégorie sont affichées, respectivement, au-dessus et en dessous des barres vertes.

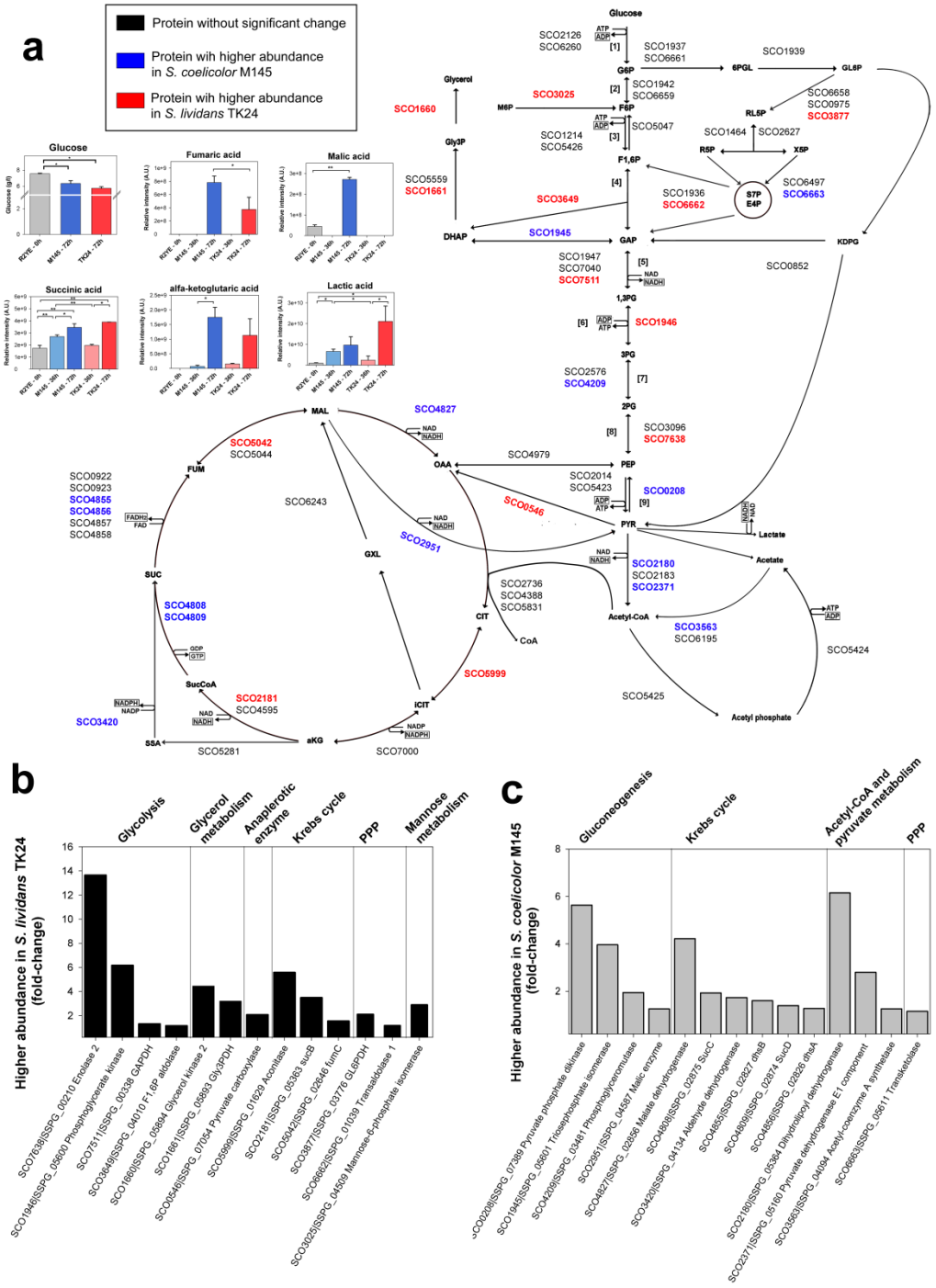

Figure A. 5. Schéma des voies du métabolisme carboné central et histogrammes représentant les dosages, au cours du temps, de différents composés présents dans le milieu de culture (glucose et intermédiaires du cycle Krebs détectés par GC/MS, **a**). Les protéines plus abondantes chez *S. lividans* que chez *S. coelicolor* sont en rouge et celles plus abondantes chez *S. coelicolor* que chez *S. lividans* sont en bleu. Histogrammes représentant certaines enzymes du métabolisme carboné central présentant une abondance significativement plus élevée chez *S. lividans* que chez *S. coelicolor* (histogrammes noirs, **b**) ou plus élevée chez S. *coelicolor* que chez *S. lividans* (histogrammes gris, **c**).

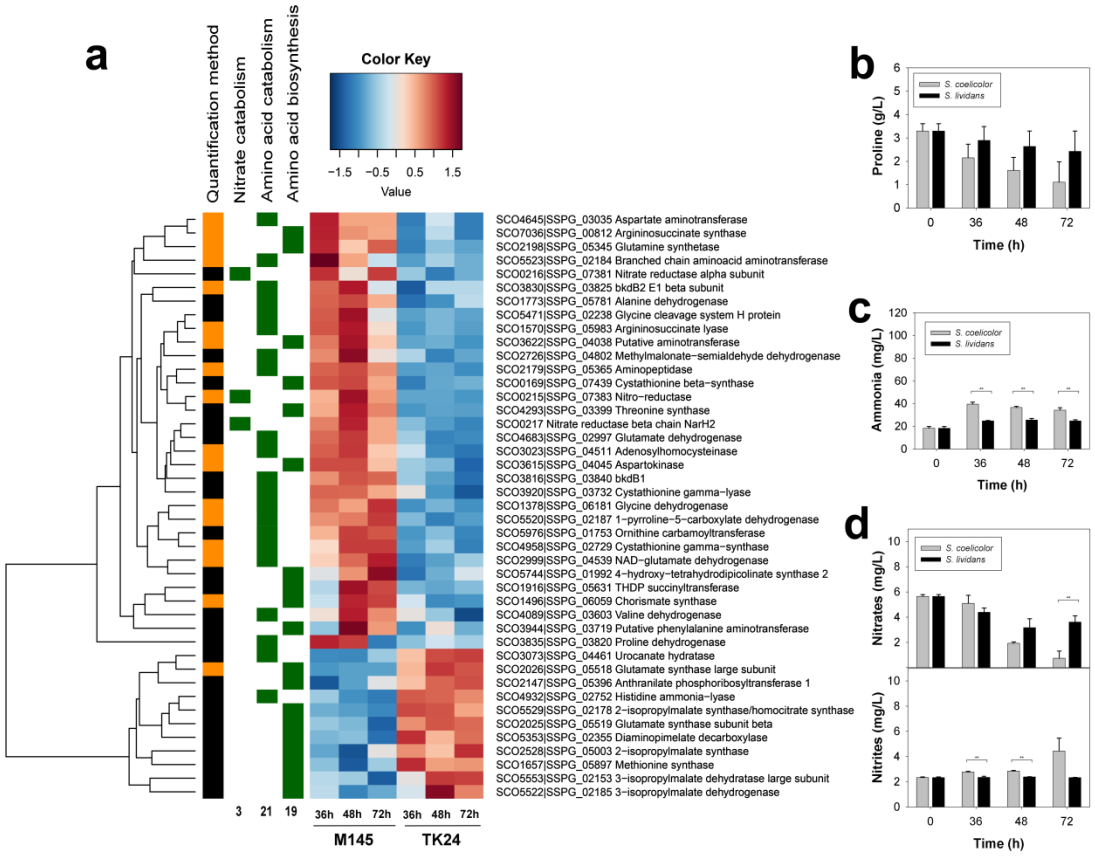

Figure A. 6. «Heat Map» des protéines correspondant au métabolisme des acides aminés et au métabolisme du nitrate dont la différence d'abondance est jugée significativement statistiquement différente entre *S. coelicolor* (M145) et chez *S. lividans* (TK24) à 36, 48 et 72 h de culture (**a**). Chaque carré vert dans partie gauche du schéma représente une protéine. La méthode utilisée pour quantifier chaque protéine est affichée en orange (SC) ou noir (XIC) sur la barre verticale à gauche. Les catégories fonctionnelles et le nombre total de protéines pour chaque catégorie sont affichées, respectivement, au-dessus et en dessous des barres vertes. Histogrammes représentant les concentrations en proline (**b**), ammoniac (**c**) et nitrates / nitrites (**d**) présentes dans le milieu de culture (p-value <0.05 [*], p-value <0.01 [**]) de *S coelicolor* (histogrammes gris) et *S lividans* (histogrammes noirs).

Chez *S. lividans*, ce sont les protéines appartenant à la famille de résistance au tellurium (protéines avec un domaine du type TerD) qui se sont révélées plus abondantes que chez *S. coelicolor* (Figure A. 7a). La fonction de ces protéines n'est pas clairement connue, certaines études suggèrent que ces protéines pourraient jouer un rôle dans le ralentissement de la croissance dans des conditions défavorables afin d'améliorer la survie cellulaire (Sanssouci *et al.*, 2011; Sanssouci *et al.*, 2012). Le fait qu'une de ces protéines SCO2368 réprime l'expression de gènes du régulon DosR suggère que *S.*

lividans fait face à un stress moins sévère que *S. coelicolor* qui ne justifie pas l'entrée dans un état de dormance cellulaire.

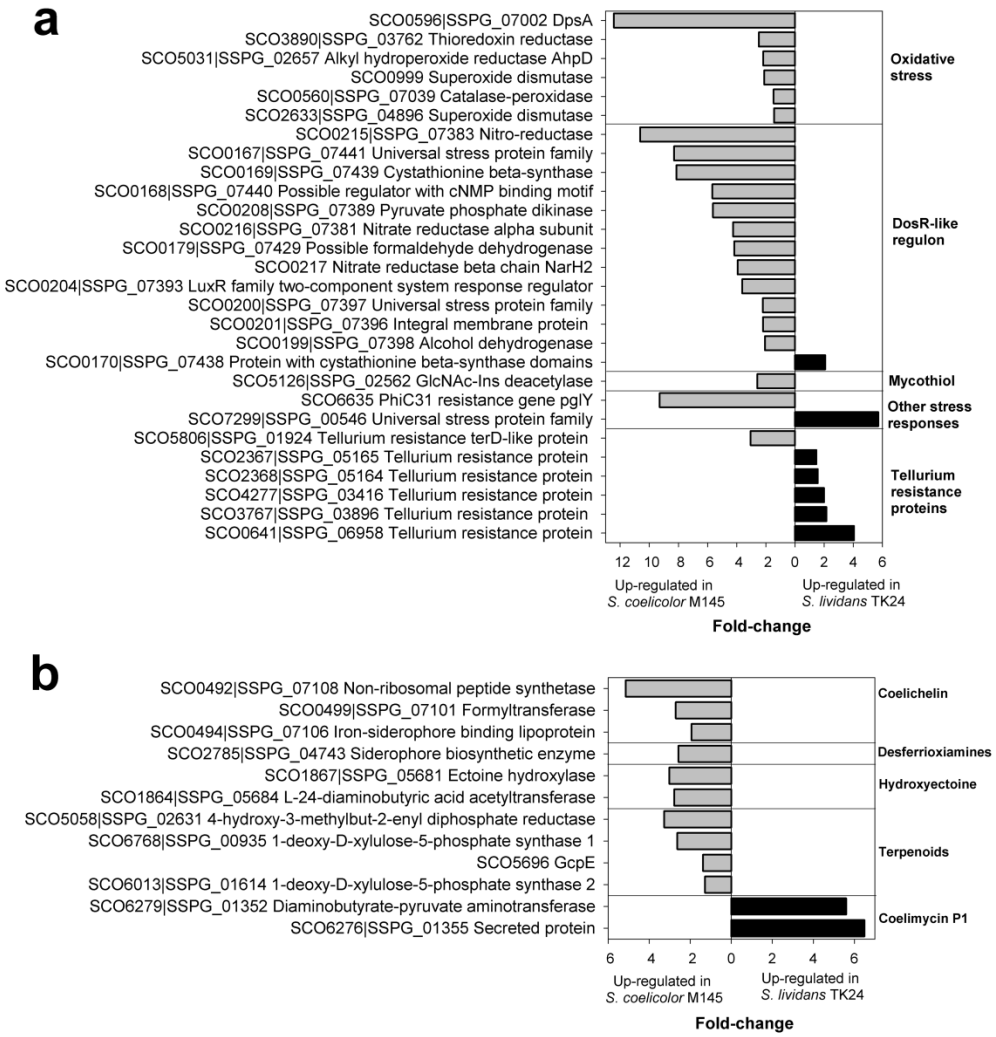

Figure A. 7. Histogrammes représentant certaines protéines appartenant aux catégories fonctionnelles de réponse au stress (**a**) et biosynthèse de métabolites secondaires (**b**) présentant une abondance significativement plus élevée chez *S. coelicolor* que chez *S. lividans* (histogrammes gris) ou chez *S. lividans* que chez *S. coelicolor* (histogrammes noirs). Les identifiants de protéines sont indiqués comme «SCO» pour *S. coelicolor* et leurs orthologues chez *S. lividans* comme «SSPG».

Les protéines appartenant à quatre voies différentes de biosynthèse de métabolites secondaires ont montré une abondance significativement plus élevée chez *S. coelicolor* que chez *S. lividans* (Figure A. 7b). Parmi ces protéines, quatre correspondent à des protéines dirigeant la synthèse des siderophores: coelicheline et desferrioxamine. La plus grande abondance de protéines de ces voies chez *S. coelicolor* est en accord avec le

métabolisme oxydatif de cette souche. En effet, plusieurs enzymes du cycle de Krebs et de la chaîne respiratoire nécessitent du fer pour leur fonctionnement. Il est important de mentionner que les protéines appartenant aux voies de biosynthèse des antibiotiques «canoniques» CDA, RED et ACT n'ont pas été identifiées chez *S. coelicolor* dans cette étude en milieu liquide faiblement oxygéné. Cela indique que leur production ne pouvait être déclenchée que dans les conditions d'anoxie utilisées au cours de cette étude comme mentionné précédemment.

Une troisième partie de ce projet de thèse a porté sur l'analyse protéomique comparative de type «shotgun» sans marquage de *S. coelicolor* et *S. lividans*, cultivées sur le milieu R2YE solide en présence de glucose ou de glycérol comme source de carbone majeures. Il est à noter que les résultats obtenus n'ont été mis en forme que récemment et leur analyse complète n'a pu être réalisée, faute de temps.

Cette analyse protéomique comparative en présence de ces deux sources de carbone différentes a été jugée intéressante car nos études précédentes ayant démontré l'existence d'une corrélation inverse entre contenu en TAG et capacité à produire des antibiotiques (Le Marechal *et al.*, 2013; Esnault *et al.*, 2017) nous souhaitions déterminer si constituait une loi générale et donc si l'accumulation de TAG et la biosynthèse des antibiotiques étaient en quelque sorte mutuellement exclusive. En effet, ces deux souches ont une teneur comparable et élevée en TAG en présence de glycérol alors qu'en présence de glucose la teneur en TAG de *S. coelicolor* est environ 3 à 4 fois plus faible que celle de *S. lividans*. Cette étude a révélé de manière inattendue que *S. coelicolor* produisait ACT sur le glycérol R2YE à un niveau similaire à celui produit sur glucose R2YE et ceci tout en ayant un contenu en TAG élevé.

La cinétique de croissance et de consommation du glycérol des deux souches était similaire sur R2YE glycérol (Figure A. 8A). Par contre en R2YE glucose, la croissance de *S. coelicolor* était considérablement ralentie par rapport à celle de *S. lividans*. Cette faible croissance corrélait avec une consommation moins active du glucose de *S. coelicolor* par rapport à *S. lividans*. Par contre sur R2YE glucose *S. coelicolor* semblait consommer la proline, acide aminé le plus abondant du milieu, plus activement que *S. lividans* (Figure A. 8C), alors que cette différence était moins prononcée sur le milieu R2YE contenant du glycérol. Cette caractéristique de *S. coelicolor* à métaboliser les

acides aminés du milieu préférentiellement au glucose avait été précédemment établie par nos études en R2YE liquide ainsi que par d'autres groupes (van Wezel *et al.*, 2006).

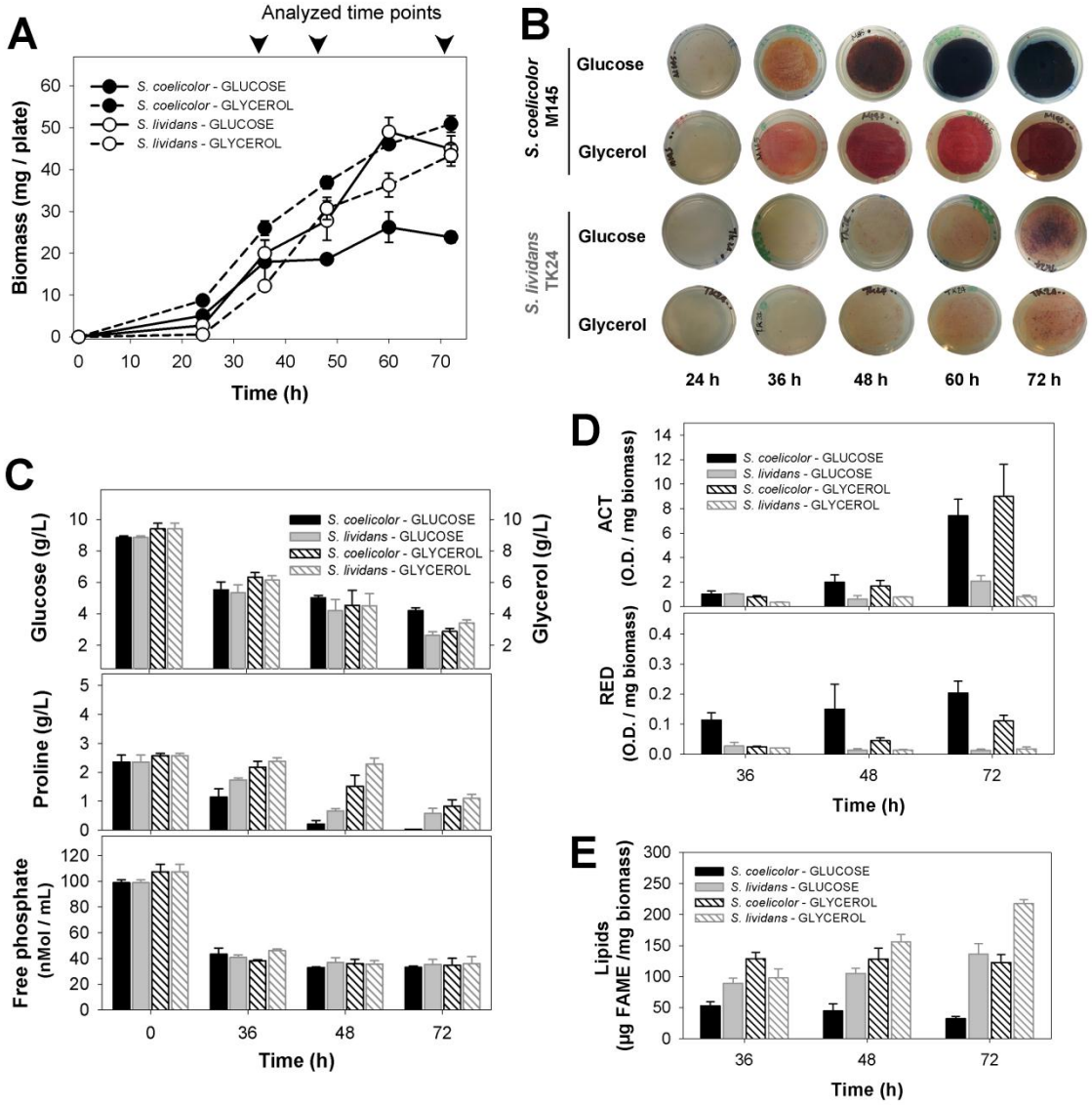

Figure A. 8. Caractéristiques comparatives de *S. coelicolor* et de *S. lividans*. Courbes de croissance sur milieu R2YE solide supplémenté avec glucose ou avec glycérol (**A**). Les lignes continues ou pointillées représentent la croissance de R2YE avec du glucose et du glycérol, respectivement. Les cercles noirs et blancs représentent *S. coelicolor* et *S. lividans*, respectivement. Images des mycéliums de *S. coelicolor et S. lividans* cultivées pendant 24, 36, 48, 60 et 72 h (**B**). Concentration de glucose, de glycérol, de proline et de phosphate dans le milieu R2YE (**C**). Production des antibiotiques RED (intracellulaire) et ACT (intra et extracellulaire) après 36, 48 et 72h de culture (**D**). Accumulation d'esters méthyliques d'acides gras totaux dérivés de lipides (FAMES) chez *S. coelicolor* et chez *S. lividans* (**E**). Les données sont présentées comme moyen ± écar type (n = 4 répliques par condition).

Sur R2YE glucose, le mycélium chez *S. coelicolor* présentait une pigmentation rougeâtre (36 - 48h) puis bleue (60 - 72h) indiquant la production des métabolites secondaires RED et ACT, respectivement (Figure A. 8B et D). Sur R2YE glycérol, le mycélium de *S. coelicolor* présentait une pigmentation rougeâtre dés 36h (Figure A. 8B). Les dosages de RED et ACT ont confirmé que *S. coelicolor* produisait RED sur R2YE glycérol mais à un niveau inférieur que celui produit sur R2YE glucose. Par contre *S. coelicolor* produisait ACT à un niveau similaire sur les deux sources de carbone (Figure A. 8D). Curieusement ACT était excrété en R2YE glucose alors qu'il restait dans la fraction intracellulaire en R2YE glycérol (Figure A. 8D).

Au total, 4372 protéines différentes ont été identifiées par LC-MS/MS avec un spectromètre de masses à haute résolution (Orbitrap Fusion™ Lumos™ Tribrid™, Thermo Fisher Scientific). Parmi ces 4372 protéines, 4088 ont été identifiées chez *S. coelicolor* et 3994 chez *S. lividans* (Figure A. 9A). Ces valeurs représentent 52.2% et 54.2% du protéome théorique de *S. coelicolor* et de *S. lividans*, respectivement. Par rapport à d'autres études protéomiques de ces souches modèles (Manteca *et al.*, 2010; Manteca *et al.*, 2010; Gubbens *et al.*, 2012; Thomas *et al.*, 2012; Le Marechal *et al.*, 2013), le présent travail représente le plus grand ensemble de données protéiques de *S. coelicolor* et *S. lividans*.

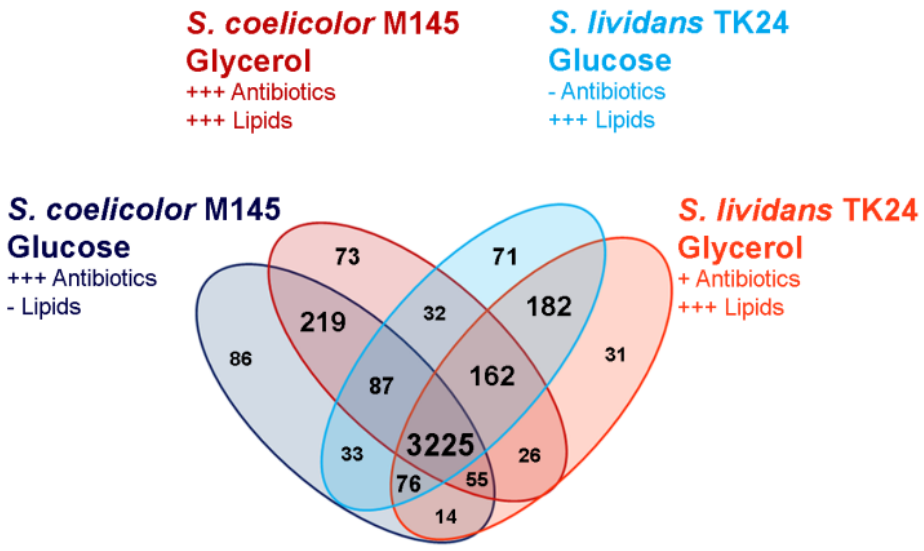

Figure A. 9. Diagramme de Venn des 4372 protéines identifiées en utilisant le logiciel X!TandemPipeline 3.4.2.

Les 4372 protéines ont été quantifiées par SC ou par XIC. Après les analyses statistique des SC et des XIC, 1040 protéines ont montré une variation d'abondance significative en fonction de la souche, de la nature de la source de carbone et/ou du temps (p-value ajustée <0.05, Figure A. 10). Parmi eux, 295 ont été détectés par la méthode SC, 395 par la méthode XIC et 350 par les deux méthodes (Figure A. 10).

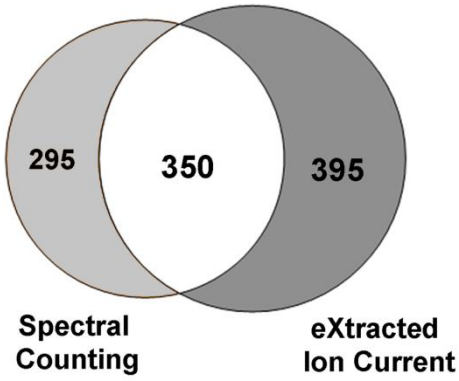

Figure A. 10. Diagramme de Venn des 1040 protéines ayant une variation d'abondance significative calculée en utilisant les approches XIC et SC (ANOVA, p-value ajustée <0.05).

Les 1040 protéines ayant eu des variations d'abondance statistiquement représentatives entre les deux souches ont été représentées dans une carte de chaleur (Heat map) en utilisant un regroupement hiérarchique avec des distances Euclidiennes (Figure A. 11). Les protéomes ont été clairement résolus dans quatre groupes principaux:

- Groupe 1: protéines de faible abondance ou absentes chez *S. coelicolor* à 72h.
- Cluster 2: protéines de faible abondance ou absentes chez *S. lividans* à 72h.
- Groupe 3: protéines constitutivement plus abondantes chez *S. coelicolor* que chez *S. lividans*.
- Cluster 4: protéines ayant une abondance croissante avec le temps.

Ces 1040 protéines appartenaient à 13 catégories fonctionnelles en fonction de leurs annotations sur les bases de données (StrepDB - The Streptomyces annotation server; Kanehisa and Goto, 2000; Karp *et al.*, 2005).

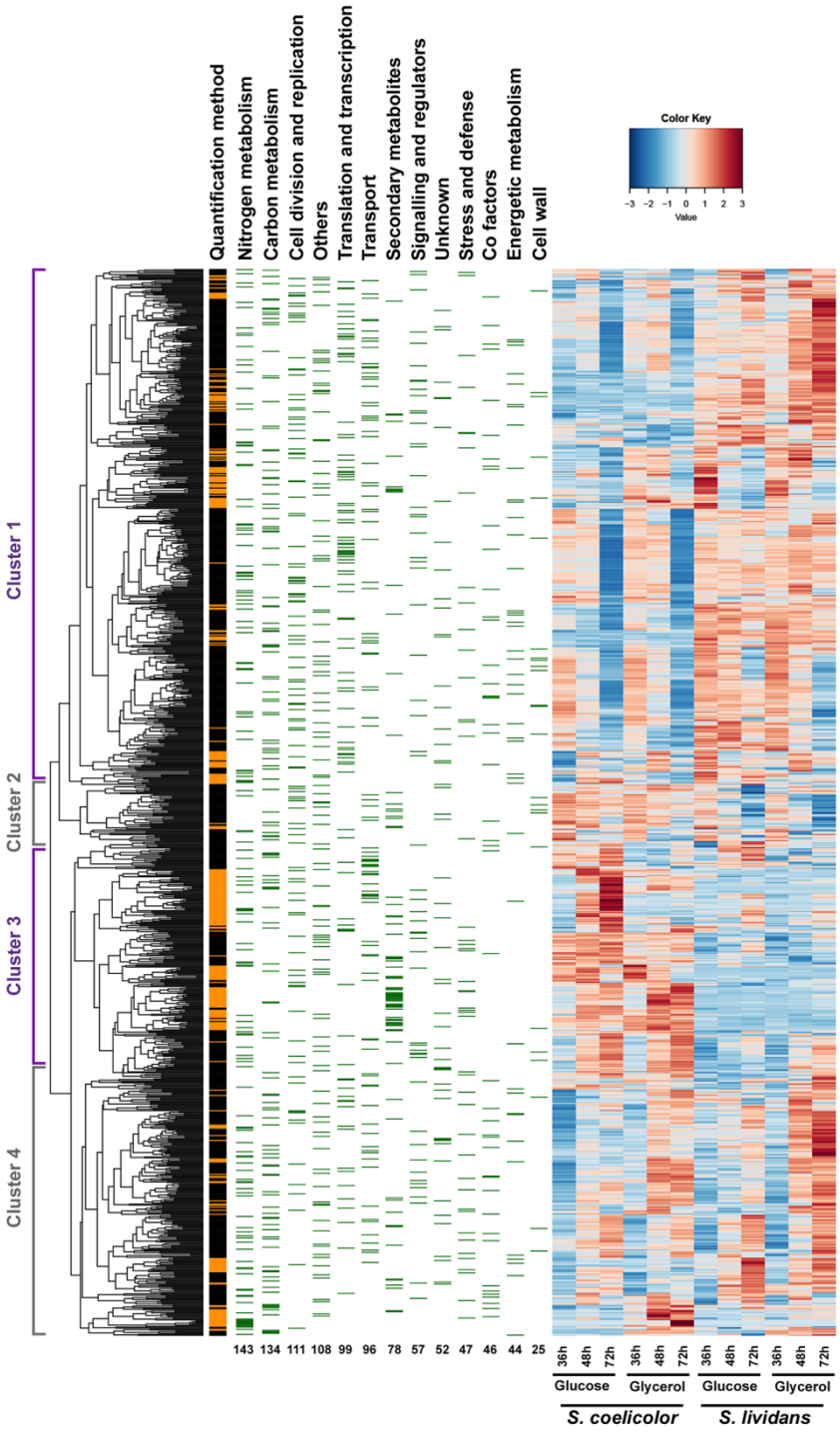

Figure A. 11. «Heat Map» des abondances relatives de 1040 protéines dont la différence l'abondance est jugée significativement statistiquement différente entre *S. coelicolor* (M145) et chez *S. lividans* (TK24) à 36, 48 et 72 h de culture. Chaque barre verte dans la partie gauche du schéma représente une protéine. La méthode utilisée pour quantifier chaque protéine est affichée en orange (SC) ou noir (XIC) sur la barre verticale à gauche. Les catégories fonctionnelles et le nombre total de protéines pour chaque catégorie sont affichées, respectivement, au-dessus et en dessous des barres vertes.

Cette analyse globale a révélé de manière inattendue que l'abondance globale de protéines de différentes classes ontologiques n'était pas si différente entre les deux espèces jusqu'à 48h d'incubation mais à 72h, une réduction drastique de l'abondance des protéines de la plupart des classes ontologiques a été observée chez *S. coelicolor* avec l'exception notable des protéines des voies de biosynthèse de métabolites secondaires. Les protéines des clusters CDA, RED et ACT étaient détectées dès 36h et étaient encore présentes à 48 et 72h, ce qui suggère qu'elles sont extrêmement stables. Malgré la présence précoce de protéines du cluster ACT, une production significative d'ACT n'a été détectée qu'à 72 heures. L'analyse de ces données de protéomique a été conduite en priorité à 72h car c'est pour ce temps que les caractéristiques de chaque souche étaient les plus contrastées.

A 72h, dans les deux milieux testés (glucose ou glycérol), la plupart des protéines de la glycolyse étaient largement plus abondantes chez *S. lividans* que chez *S. coelicolor* (Figure A. 12A-B). Dans les cultures avec glucose, les enzymes glycolytiques les plus différentiellement exprimées entre les deux souches étaient: glycéraldéhyde-3-phosphate déshydrogénase (SCO1947, SCO7040 and SCO7511) et enolase (SCO3096 and SCO7638). Ces résultats couplés avec une assimilation du glucose plus active chez *S. lividans* que chez *S. coelicolor* ont confirmé une glycolyse plus active chez *S. lividans* que chez *S. coelicolor* (Figure A. 8C), corroborant ainsi nos résultats précédents obtenus en solide (Esnault *et al.*, 2017) ou en liquide (Chapitre IV).

Sur R2YE glucose, 3 protéines impliquées dans le catabolisme de la proline (SCO3835, SCO5519 et SCO5520) étaient plus abondantes chez *S. coelicolor* que chez *S. lividans* à 36h et 48h alors que chez *S. lividans* ces protéines étaient abondantes à des temps plus tardifs de la croissance (48h et 72h, Figure A. 13A). Ceci indique que *S. coelicolor* catabolise préférentiellement la proline plutôt que le glucose (Figure A. 8C).

Par ailleurs 20 protéines liées au métabolisme du phosphate étaient nettement plus abondantes chez *S. lividans* que chez *S. coelicolor* (Figure A. 13B). Il est important de souligner que les cultures ont été conduites en limitation en phosphate (Figure A. 8C). Dans cette condition, l'expression du système à deux composants, PhoR (kinase sensorielle) et PhoP (régulateur de réponse) est normalement induite.

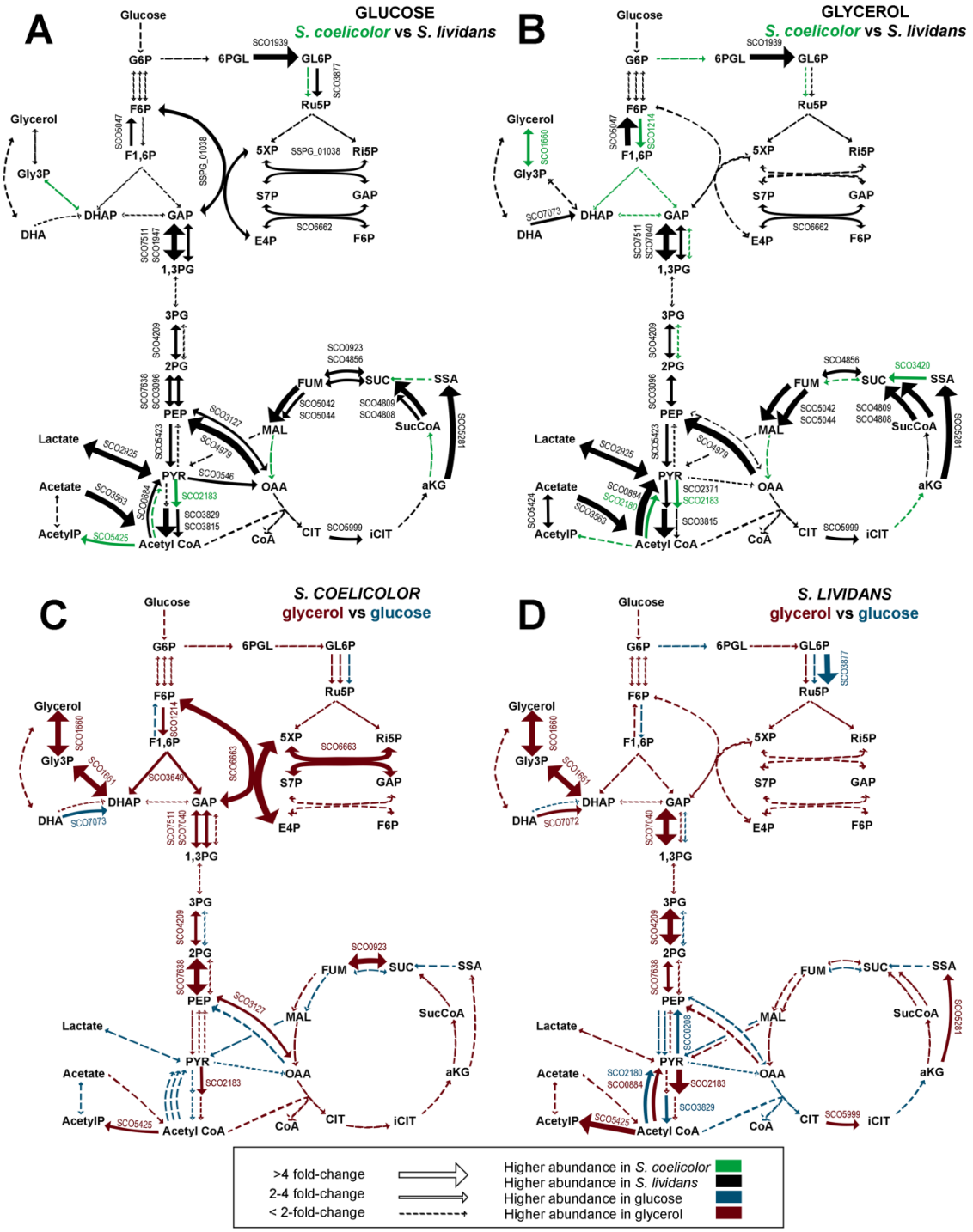

Figure A. 12. Représentation du métabolisme central du carbone. Les réactions enzymatiques catalysées par des protéines avec une variation significative (ANOVA, p-value ajustée> 0.05) sont représentées par des flèches. L'épaisseur des flèches est proportionnelle à l'abondance des protéines. Comparaison de l'abondance des protéines chez *S. coelicolor* et *S. lividans* sur les cultures cultivées en glucose (**A**) ou en glycérol (**B**) à 72h. Comparaison de l'abondance des protéines entre les cultures en glucose et en glycérol chez *S coelicolor* (**C**) et chez *S. lividans* (**D**) à 72h.

PhoP est activé par phosphorylation par la kinase PhoR et il est connu pour réguler positivement ou négativement l'expression des gènes du regulon Pho (Sola-Landa *et al.*, 2008; Allenby *et al.*, 2012). Cette faible abondance des protéines du régulon Pho chez *S. coelicolor* suggère un défaut d'induction du régulon Pho. Si tel est le cas on peut s'attendre à ce que *S. coelicolor* soit sévèrement carencé en Pi. A cet égard il est important de rappeler que la délétion du régulateur PhoP chez *S. lividans* corrèle en effet avec une forte augmentation de la production d'antibiotique (Ghorbel *et al.*, 2006).

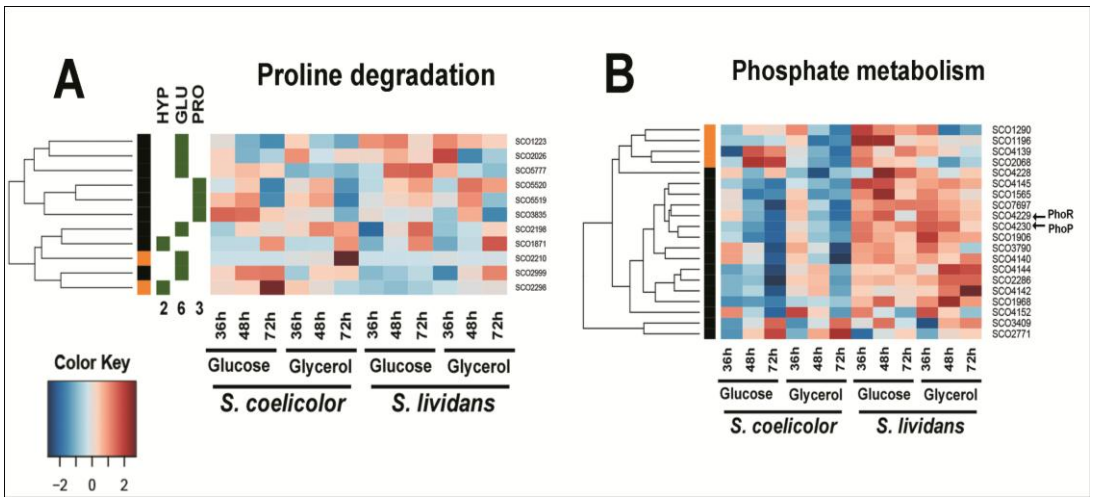

Figure A. 13. Représentation de carte chaleur d'abondance de protéines appartenant à la dégradation de proline (PRO), hydroxyproline (HYP) et glutamate (GLU) (**A**) et du métabolisme du phosphate (**B**) avec un changement d'abondance significatif (p-value < 0.05). Les méthodes de quantification sont affichées dans la barre verticale indiquant les protéines quantifiées par SC (orange) et XIC (noir).

Une étude précédente avait signalée qu'en milieu R2YE glucose solide le contenu en lipide (phospholipides + TAG) de *S. lividans* était 3 à 4 fois élevé que celui de *S. coelicolor* (Le Marechal *et al.*, 2013). Nous avons confirmé cette observation en dosant les FAMEs en utilisant la GC/MS (Figure A. 8E). L'analyse protéomique comparative des deux souches a permis de quantifier un total de 40 protéines appartenant au métabolisme lipidique dont 16 annotées comme étant impliquées dans la biosynthèse (Figure A. 14) et 24 impliquées dans la dégradation des acides gras (Figure A. 15). L'abondance de ces protéines a été jugé statistiquement significative entre les deux souches (ANOVA, p-value ajustée <0.05) à 72h. Le contenu en FAMEs de *S. coelicolor*, 3.6 fois plus élevé en glycérol qu'en glucose, a été corrélé avec une plus grande abondance des protéines connues pour être impliquées dans la biosynthèse des acides gras (Figure A. 14).

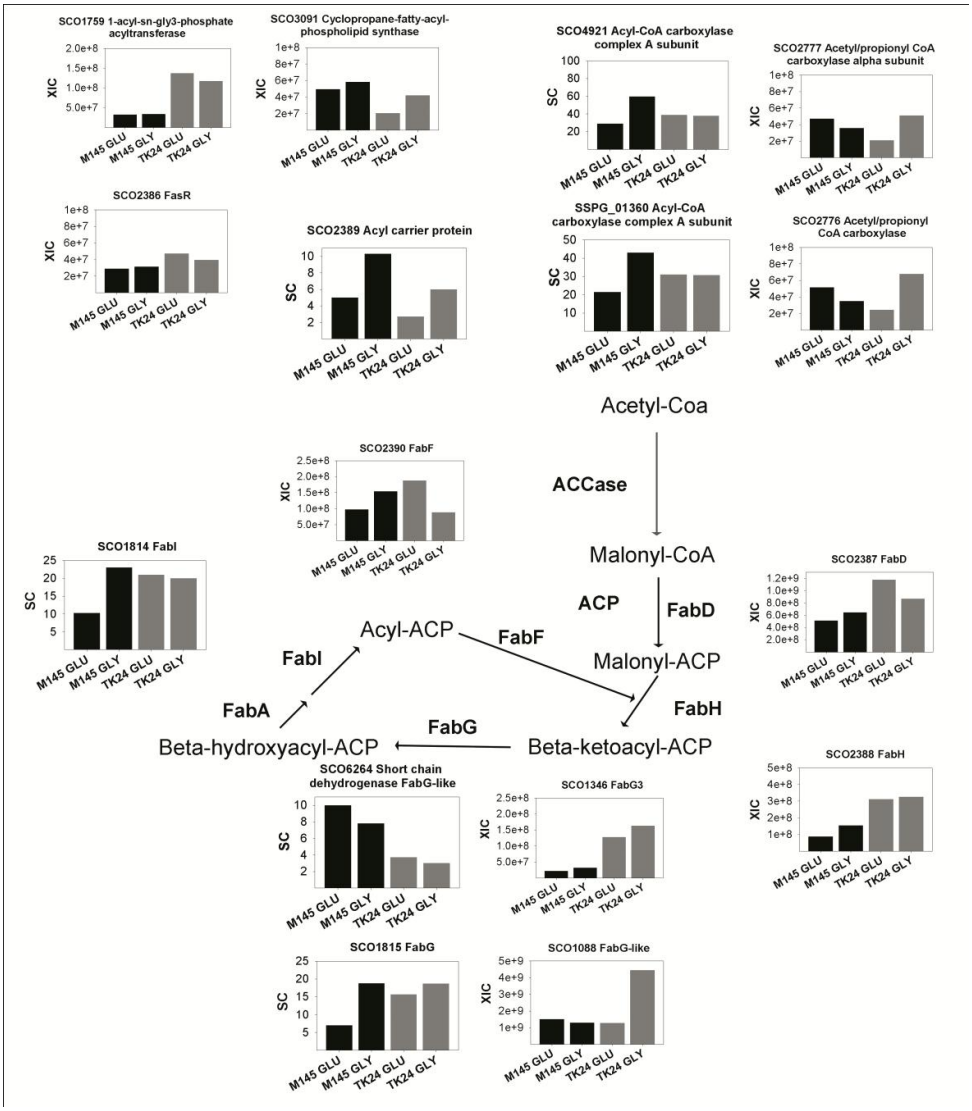

Figure A. 14. Protéines de la biosynthèse des acides gras qui ont montré une variation d'abondance significative entre *S. coelicolor* et *S. lividans* (ANOVA, p-value ajustée <0.05). Les abondances de protéines sont représentées par des histogrammes en noir et gris pour *S. coelicolor* (M145) et *S. lividans* (TK24) cultivés dans milieu R2YE contenant glucose (GLU) ou glycérol (GLY) après 72h de culture.

Des enzymes connues pour être impliquées dans la biosynthèse des acides gras ont également été trouvées plus abondantes chez *S. lividans* que chez *S. coelicolor*. Cependant, de façon étonnante les protéines annotées comme contribuant à la dégradation des acides gras se sont révélées plus abondantes chez *S. lividans* que chez *S. coelicolor* (Figure A. 15). Ceci suggère que la dégradation des lipides est plus active chez *S. lividans* que chez *S. coelicolor*. Cependant, puisque le contenu en lipide reste plutôt constant ou même augmente chez *S. lividans*, ce processus est sans doute équilibré par une biosynthèse de lipides encore plus active. Le fait que la dégradation

des lipides apparaisse moins active chez *S. coelicolor* que chez *S. lividans* pourrait simplement être liée à son faible contenu en lipides de réserve.

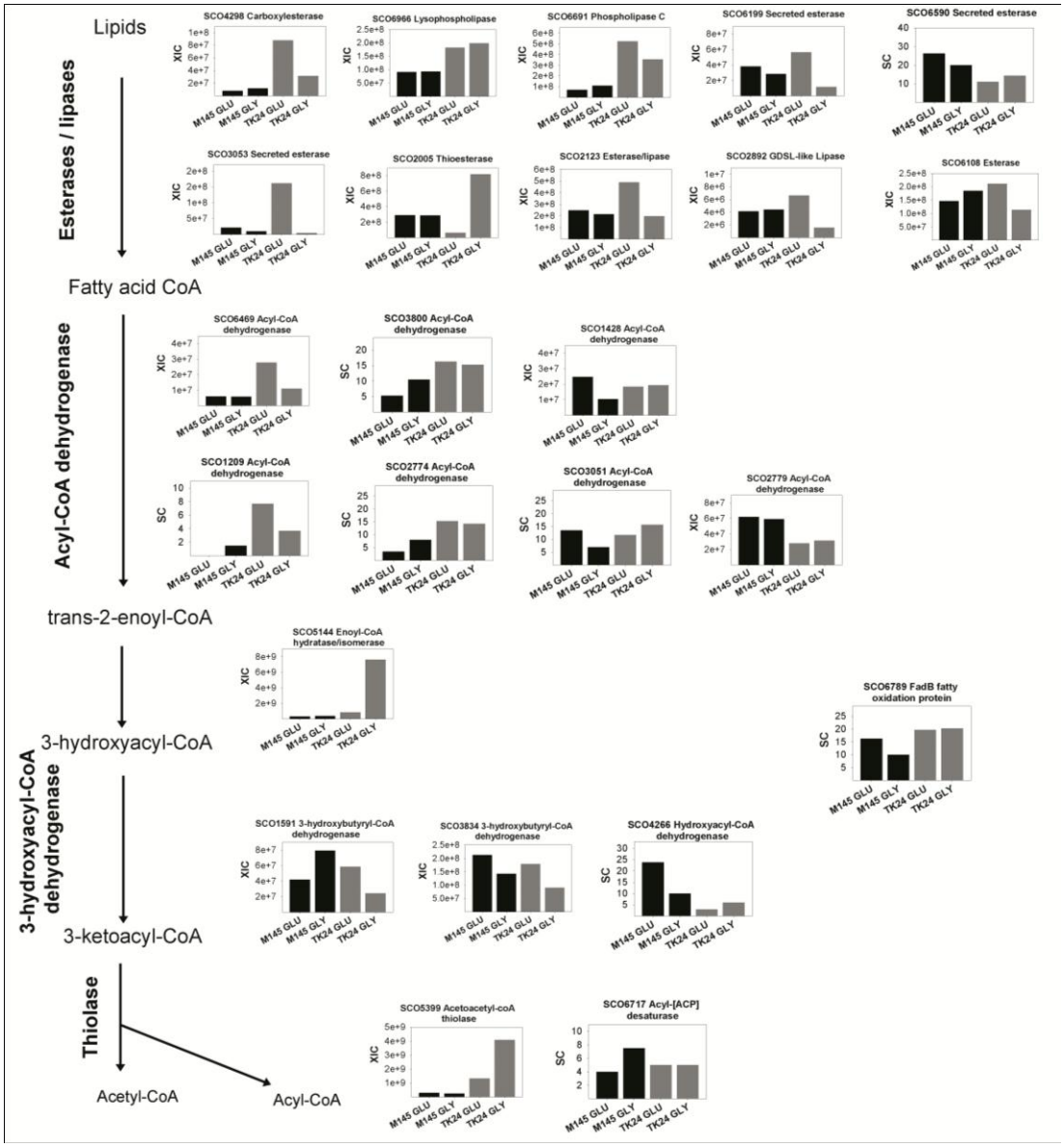

Figure A. 15. Protéines annotées comme impliquées dans la dégradation des lipides et des acides gras qui montrent une variation d'abondance significative entre *S. coelicolor* et *S. lividans* (ANOVA, valeur p ajustée <0.05). Les abondances de protéines sont représentées par des histogrammes noirs et gris pour *S. coelicolor* (M145) et *S. lividans* (TK24) cultivés dans le glucose R2YE (GLU) ou le glycérol (GLY) après 72 h de culture.

Enfin, un total de 74 protéines appartenant à 17 voies différentes de biosynthèse des métabolites secondaires ont été groupées dans trois groupes principaux (Figure A. 16). Le groupe 1 comprend les voies de biosynthèse des métabolites secondaires exprimées

en début de la croissance (36h): 9 protéines impliquées dans la biosynthèse de CPK, 2 protéines impliquées dans la biosynthèse des terpenoids, 3 impliquées dans la biosynthèse de desfierroxiamine et 1 dans la biosynthèse de coelicheline. Le groupe 2 contient des protéines impliquées dans les voies de biosynthèse des métabolites secondaires exprimées plus tard dans la croissance (48 et 72h): 3 protéines sont impliquées dans la biosynthèse des terpenoids, 5 dans la biosynthèse de coelicheline et 8 correspondant à la synthèse d'un métabolite inconnu (SCO0382, SCO0387, SCO0392, SCO0394, SCO0395, SCO0396, SCO0398 et SCO0401) considéré comme un sucre-deoxy (Challis and Hopwood, 2003). Le groupe 3 comprend les protéines appartenant aux voies de biosynthèse des antibiotiques CDA (12 protéines), RED (7 protéines) et ACT (18 protéines) qui ont été produites principalement par *S. coelicolor* cultivé en glucose ou glycérol. Ces différences métaboliques sont vraisemblablement sous-tendues par des différences dans les appareils transcriptionnels et traductionnels des souches

Au cours de ce travail, nous avons pour la première fois caractérisé les différences métaboliques des souches modèles *S. coelicolor* et *S. lividans* en utilisant une approche protéomique à haute débit du type « shotgun » avec des instruments de très à haute résolution. Ce travail pourrait conduire à une meilleure compréhension de la régulation de la biosynthèse d'antibiotiques et de son lien avec le métabolisme basal. Il convient de souligner que cette étude est la première ayant permis d'identifier les déterminants génétiques susceptibles d'être impliqués dans la biosynthèse de lipides dans des cultures de *S. coelicolor* et de *S. lividans* cultivées en glycérol ou en glucose. Cette étude qui constitue le plus grand protéome de *S. coelicolor* et *S. lividans* jamais obtenu et représente une ressource utile pour la communauté scientifique travaillant dans le domaine des Streptomycètes afin de mieux comprendre les liens entre le métabolisme primaire et secondaire de ces bactéries.

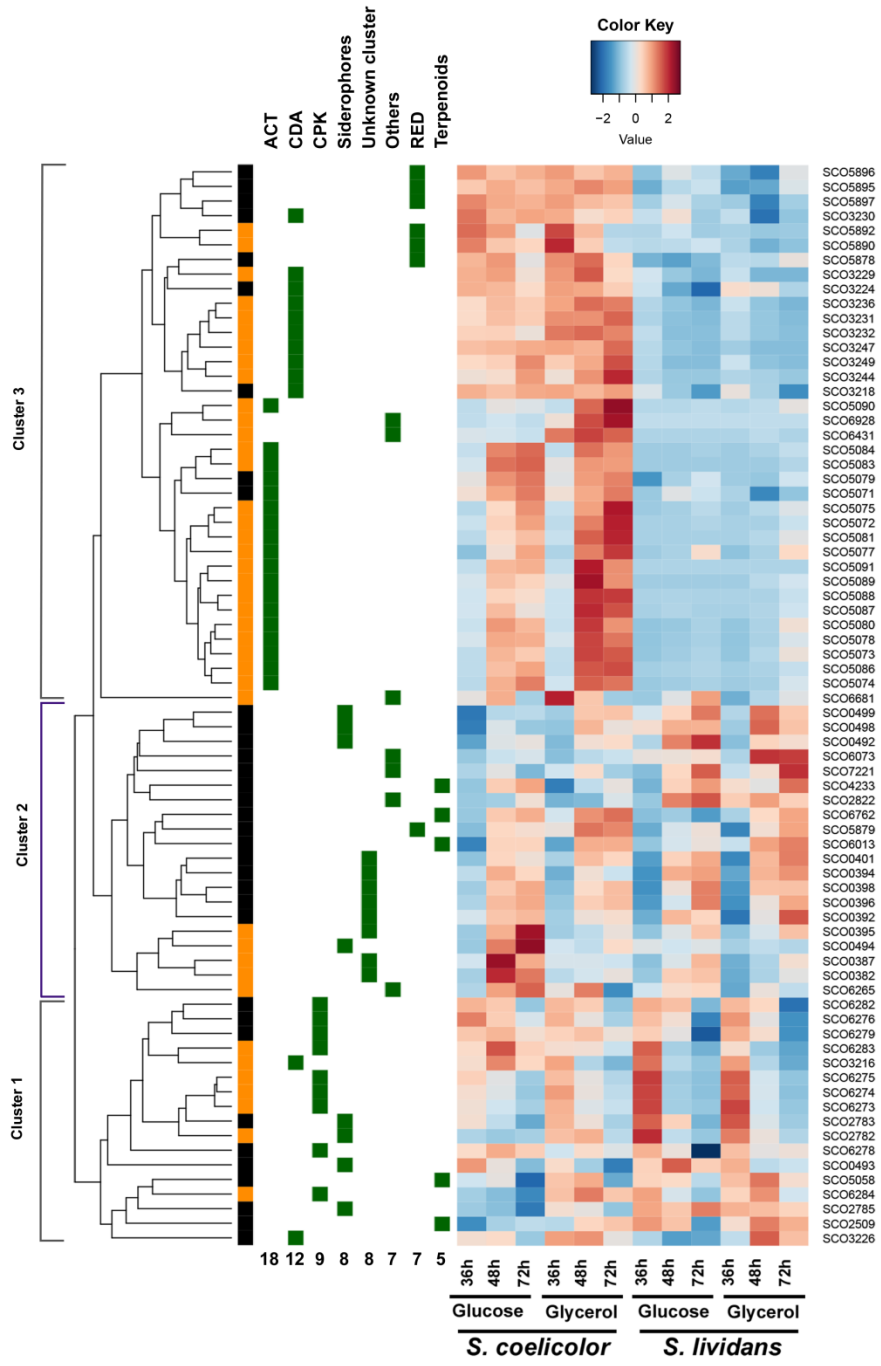

Figure A. 16. «Heat Map» des abondances relatives de protéines appartenant aux voies de biosynthèse de métabolites secondaires dont la différence d'abondance entre *S. coelicolor* (M145) et chez *S. lividans* (TK24) à 36, 48 et 72 h de culture a été jugée statistiquement significative. Chaque barre verte dans partie gauche du schéma représente une protéine. La méthode utilisée pour quantifier chaque protéine est affichée en orange (SC) ou noir (XIC) sur la barre verticale à gauche. Les catégories fonctionnelles et le nombre total de protéines pour chaque catégorie sont affichées, respectivement, au-dessus et en dessous des barres vertes.

REFERENCES

Abbott, S.K., Else, P.L., Atkins, T.A. and Hulbert, A. J. **2012**. Fatty acid composition of membrane bilayers: Importance of diet polyunsaturated fat balance. BBA - Biomembranes, 1818(5): 1309-17.

ACS, National Historic Chemical Landmarks, **2005**. Selman Waksman and antibiotics. American Chemical Society. Accessed on April 7th, 2017. Available from: https://www.acs.org/content/acs/en/education/whatischemistry/landmarks/selmanwaksman.html

Aebersold, R. and Mann, M. **2016**. Mass-spectrometric exploration of proteome structure and function. Nature, 537(7620): 347-55.

Aigle, B., Lautru S., Spiteller, D., Dickschat, J.S., Challis, G.L., Leblond, P. and Pernodet, J.L. **2014**. Genome mining of *Streptomyces ambofaciens*. J Ind Microbiol Biotechnol, 41(2): 251-63.

Alam, M.T., Merlo, M.E., Hodgson, D.A., Wellington, E.M., Takano, E. and Breitling, R. **2010**. Metabolic modeling and analysis of the metabolic switch in *Streptomyces coelicolor*. BMC Genomics, 11: 202.

Alvarez, H.M. and Steinbuchel, A. **2002**. Triacylglycerols in prokaryotic microorganisms. Appl Microbiol Biotechnol, 60(4): 367-76.

Allenby, N.E.E., Laing, E., Bucca, G., Kierzek, A.M. and Smith, C.P. **2012**. Diverse control of metabolism and other cellular processes in *Streptomyces coelicolor* by the PhoP transcription factor: genome-wide identification of *in vivo* targets. Nucleic Acids Res, 40(19): 9543-56.

Angell, S., Lewis, C.G., Buttner, M.J. and Bibb M.J. **1994**. Glucose repression in *Streptomyces coelicolor* A3(2): a likely regulatory role for glucose kinase. Mol Gen Genet, 244(2): 135-43.

Apel, A.K., Sola-Landa, A., Rodriguez-Garcia, A. and Martin, J.F. **2007**. Phosphate control of *phoA*, *phoC* and *phoD* gene expression in *Streptomyces coelicolor* reveals significant differences in binding of PhoP to their promoter regions. Microbiol, 153(Pt 10): 3527-37.

Arabolaza, A., Banchio, C. and Gramajo, H. **2006**. Transcriptional regulation of the *macs1-fadD1* operon encoding two acyl-CoA synthases involved in the physiological differentiation of *Streptomyces coelicolor*. Microbiol, 152(Pt 5): 1427-39.

Arabolaza, A., D'Angelo, M., Comba, S. and Gramajo, H. **2010**. FasR, a novel class of transcriptional regulator, governs the activation of fatty acid biosynthesis genes in *Streptomyces coelicolor*. Mol Microbiol, 78(1): 47-63.

Arabolaza, A., Rodriguez, E., Altabe, S., Alvarez, H. and Gramajo, H. **2008**. Multiple pathways for triacylglycerol biosynthesis in *Streptomyces coelicolor*. Appl Environ Microbiol, 74(9): 2573-82.

Argüelles-Arias, A., Craig, M. and Fickers, P. **2011**. Gram-positive antibiotic biosynthetic clusters: a review In: Science against microbial pathogens: communicating current research and technological advances A. Méndez-Vilas (Ed.) Formatex Research Center: Badajoz.

Arias, P., Fernandez-Moreno, M.A. and Malpartida, F. **1999**. Characterization of the pathway-specific positive transcriptional regulator for actinorhodin biosynthesis in *Streptomyces coelicolor* A3(2) as a DNA-binding protein. J Bacteriol, 181(22): 6958-68.

Asturias, J.A., Martín, J.F. and Liras, P. **1994**. Biosynthesis and phosphate control of candicidin by *Streptomyces acrimycini* JI2236: effect of amplification of the *pabAB* gene. J Ind Microbiol, 13(3): 183-9.

Austin, M.B. and Noel, J.P. **2003**. The chalcone synthase superfamily of type III polyketide synthases. Nat Prod Rep, 20(1): 79-110.

Ayala-Castro, C., Saini, A. and Outten, F.W. **2008**. Fe-S cluster assembly pathways in bacteria. Microbiol Mol Biol Rev, 72(1): 110-25.

Azizian, H., Kramer, J.K.G. and Mossoba, M.M. **2012**. Evaluating the transferability of FT-NIR calibration models for fatty acid determination of edible fats and oils among five same-make spectrometers using transmission or transflection Modes with different pathlengths. J Am Oil Chem Soc, 89(12): 2143-54.

Bamas-Jacques, N., Lorenzon, S., Lacroix, P., De Swetschin, C. and Crouzet, J. **1999**. Cluster organization of the genes of *Streptomyces pristinaespiralis* involved in pristinamycin biosynthesis and resistance elucidated by pulsed-field gel electrophoresis. J Appl Microbiol, 87(6): 939-48.

Banchio, C. and H. Gramajo 2002. A stationary-phase acyl-coenzyme A synthetase of Streptomyces coelicolor A3(2) is necessary for the normal onset of antibiotic production. Appl Environ Microbiol, 68(9): 4240-4246.

Barka, E.A., Vatsa, P., Sanchez, L., Gaveau-Vaillant, N., Jacquard, C., Klenk, H.-P., Clément, C., Ouhdouch, Y. and van Wezel, G.P. **2016**. Taxonomy, physiology, and natural products of Actinobacteria. Microbiol Mol Biol Rev, 80(1): 1-43.

Benjamini, Y. and Hochberg, Y. **1995**. Controlling the false discovery rate: A practical and powerful approach to multiple testing. J R Stat Soc Series B, 57(1): 289-300.

Bentley, S.D., Chater, K.F., Cerdeno-Tarraga, A.M., Challis, G.L., Thomson, N.R., James, K. D., Harris, D.E., Quail, M.A., Kieser, H., Harper, D., Bateman, A., Brown, S., Chandra, G., Chen, C.W., Collins, M., Cronin, A., Fraser, A., Goble, A., Hidalgo, J., Hornsby, T., Howarth, S., Huang, C.H., Kieser, T., Larke, L., Murphy, L., Oliver, K., O'Neil, S., Rabbinowitsch, E., Rajandream, M.A.,

Rutherford, K., Rutter, S., Seeger, K., Saunders, D., Sharp, S., Squares, R., Squares, S., Taylor, K., Warren, T., Wietzorrek, A., Woodward, J., Barrell, B.G., Parkhill, J. and Hopwood, D.A. **2002**. Complete genome sequence of the model actinomycete *Streptomyces coelicolor* A3(2). Nature, 417(6885): 141-7.

Berdy, J. **2005**. Bioactive microbial metabolites. J Antibiot, 58(1): 1-26.

Berdy, J. **2012**. Thoughts and facts about antibiotics: Where we are now and where we are heading. J Antibiot, 65(8): 385-95.

Berg, J., Tymoczko, J. and Stryer, L. **2002**. Biochemistry. 5th Edition, W.H. Freeman and Company: New York, 2002. https://www.ncbi.nlm.nih.gov/books/NBK21154/

Bhukya, H., Bhujbalrao, R., Bitra, A. and Anand, R. **2014**. Structural and functional basis of transcriptional regulation by TetR family protein CprB from *S. coelicolor* A3(2). Nucleic Acids Res, 42(15): 10122-33.

Bibb, M.J. **2005**. Regulation of secondary metabolism in Streptomycetes. Curr Opin Microbiol, 8(2): 208-15.

Blein-Nicolas, M., Xu, H., de Vienne, D., Giraud, C., Huet, S. and Zivy, M. **2012**. Including shared peptides for estimating protein abundances: A significant improvement for quantitative proteomics. Proteomics, 12(18): 2797-01.

Blein-Nicolas, M. and Zivy, M. **2016**. Thousand and one ways to quantify and compare protein abundances in label-free bottom-up proteomics. BBA - Proteins and Proteomics, 1864(8): 883-95.

Bligh, E.G. and Dyer, W.J. **1959**. A rapid method of total lipid extraction and purification. Can J Biochem Phys, 37(8): 911-7.

Bobek, J., Strakova, E., Zikova, A. and Vohradsky, J. **2014**. Changes in activity of metabolic and regulatory pathways during germination of *S. coelicolor*. BMC Genomics, 15(1): 1173.

Bondarenko, P.V., Chelius, D. and Shaler, T.A. **2002**. Identification and relative quantitation of protein mixtures by enzymatic digestion followed by capillary reversed-phase liquid chromatography-tandem mass spectrometry. Anal Chem, 74(18): 4741-9.

Boon, C. and Dick, T. **2012**. How *Mycobacterium tuberculosis* goes to sleep: the dormancy survival regulator DosR a decade later. Future Microbiol, 7(4): 513-8.

Borodina, I., Krabben, P. and Nielsen, J. **2005**. Genome-scale analysis of *Streptomyces coelicolor* A3(2) metabolism. Genome Res, 15(6): 820-9.

Borodina, I., Siebring, J., Zhang, J., Smith, C.P., van Keulen, G., Dijkhuizen, L. and Nielsen, J. **2008**. Antibiotic overproduction in *Streptomyces coelicolor* A3(2) mediated by phosphofructokinase deletion. J Biol Chem, 283(37): 25186-99.

Bosak, T., Losick, R.M. and Pearson, A. **2008**. A polycyclic terpenoid that alleviates oxidative stress. Proc Nat Acad Sci, 105(18): 6725-9.

Boyle, N.R., Page, M.D., Liu, B., Blaby, I.K., Casero, D., Kropat, J., Cokus, S.J., Hong-Hermesdorf, A., Shaw, J., Karpowicz, S.J., Gallaher, S.D., Johnson, S., Benning, C., Pellegrini, M., Grossman, A. and Merchant, S.S. **2012**. Three acyltransferases and nitrogen-responsive regulator are implicated in nitrogen starvation-induced triacylglycerol accumulation in *Chlamydomonas*. J Biol Chem, 287(19): 15811-25.

Bradshaw, E., Saalbach, G. and McArthur, M. **2013**. Proteomic survey of the *Streptomyces coelicolor* nucleoid. J Proteomics, 83: 37-46.

Braña, A.F., Eandez, C.M., Diiaz, L.A., Manzanal, M.B. and Hardisson, C. **1986**. Glycogen and trehalose accumulation during colony development in *Streptomyces antibioticus*. Microbiol, 132(5): 1319-26.

Bruckner, R. and Titgemeyer, F. **2002**. Carbon catabolite repression in bacteria: choice of the carbon source and autoregulatory limitation of sugar utilization. FEMS Microbiol Lett, 209(2): 141-8.

Bursy, J., Kuhlmann, A.U., Pittelkow, M., Hartmann, H., Jebbar, M., Pierik, A.J. and Bremer, E. **2008**. Synthesis and uptake of the compatible solutes ectoine and 5-hydroxyectoine by *Streptomyces coelicolor* A3(2) in response to salt and heat stresses. Appl Environ Microbiol, 74(23): 7286-96.

Butler, M.J., Bruheim, P., Jovetic, S., Marinelli, F., Postma, P.W. and Bibb, M.J. **2002**. Engineering of primary carbon metabolism for improved antibiotic production in *Streptomyces lividans*. Appl Environ Microbiol, 68(10): 4731-9.

Butler, M.J., Takano, E., Bruheim, P., Jovetic, S., Marinelli F. and Bibb, M.J. **2003**. Deletion of *scbA* enhances antibiotic production in *Streptomyces lividans*. Appl Microbiol Biotechnol, 61(5-6): 512-6.

Callister, S.J., Barry, R.C., Adkins, J.N., Johnson, E.T., Qian, W.J., Webb-Robertson, B.J., Smith, R.D. and Lipton, M.S. **2006**. Normalization approaches for removing systematic biases associated with mass spectrometry and label-free proteomics. J Proteome Res, 5(2): 277-86.

Camacho, C., Coulouris, G., Avagyan, V., Ma, N., Papadopoulos, J., Bealer, K. and Madden, T.L. **2009**. BLAST+: architecture and applications. BMC Bioinformatics, 10: 421.

Cane, D.E. and Ikeda, H. **2012**. Exploration and mining of the bacterial terpenome. Acc Chem Res, 45(3): 463-72.

Center for Disease Control and Prevention, 2017. Antibiotic - Antimicrobial Resistance. Accessed on April 7th, **2017**. Available from: https://www.cdc.gov/drugresistance/index.html

Cerdeño, A.M., Bibb, M.J. and Challis, G.L. **2001**. Analysis of the prodiginine biosynthesis gene cluster of *Streptomyces coelicolor* A3(2): new mechanisms for chain initiation and termination in modular multienzymes. Chem Biol, 8(8): 817-29.

Claessen, D., de Jong, W., Dijkhuizen, L. and Wosten, H.A. **2006**. Regulation of *Streptomyces* development: reach for the sky! Trends Microbiol, 14(7): 313-9.

Clardy, J., Fischbach, M.A. and Walsh, C.T. **2006**. New antibiotics from bacterial natural products. Nat Biotech, 24(12): 1541-50.

Collins, M.D. and Jones, D. **1981**. Distribution of isoprenoid quinone structural types in bacteria and their taxonomic implication. Microbiol Rev, 45(2): 316-4.

Cox, J., Neuhauser, N., Michalski, A., Scheltema, R.A., Olsen, J.V. and Mann, M. **2011**. Andromeda: a peptide search engine integrated into the MaxQuant environment. J Proteome Res, 10(4): 1794-05.

Coze, F., Gilard, F., Tcherkez, G., Virolle, M.J. and Guyonvarch, A. **2013**. Carbon-flux distribution within *Streptomyces coelicolor* metabolism: a comparison between the actinorhodin-producing strain M145 and its non-producing derivative M1146. PloS one, 8(12): e84151.

Craig, R. and Beavis, R.C. **2003**. A method for reducing the time required to match protein sequences with tandem mass spectra. Rapid Commun Mass Spectrom, 17(20): 2310-6.

Craig, R. and Beavis, R.C. **2004**. TANDEM: matching proteins with tandem mass spectra. Bioinformatics, 20(9): 1466-7.

Craney, A., Ozimok, C., Pimentel-Elardo, S.M., Capretta, A. and Nodwell, J.R. **2012**. Chemical perturbation of secondary metabolism demonstrates important links to primary metabolism. Chem Biol, 19(8): 1020-7.

Cronan, J.E. and Thomas, J. **2009**. Bacterial fatty acid synthesis and its relationships with polyketide synthetic pathways. Methods Enzymol, 459: 395-433.

Cronan Jr, J.E. and Waldrop, G.L. **2002**. Multi-subunit acetyl-CoA carboxylases. Prog Lip Res, 41(5): 407-35.

Challis, G.L. **2014**. Exploitation of the *Streptomyces coelicolor* A3(2) genome sequence for discovery of new natural products and biosynthetic pathways. J Ind Microbiol Biotechnol, 41(2): 219-32.

Challis, G.L. and Hopwood, D.A. **2003**. Synergy and contingency as driving forces for the evolution of multiple secondary metabolite production by *Streptomyces* species. Proc Nat Acad Sci, 100(suppl 2): 14555-61.

Chandra, G., Chater, K.F. and Bornemann, S. **2011**. Unexpected and widespread connections between bacterial glycogen and trehalose metabolism. Microbiol, 157(6): 1565-72.

Chang, H.M., Chen, M.Y., Shieh, Y.T., Bibb, M.J. and Chen, C.W. **1996**. The cutRS signal transduction system of *Streptomyces lividans* represses the biosynthesis of the polyketide antibiotic actinorhodin. Mol Microbiol, 21(5): 1075-85.

Chater, K.F. **2001**. Regulation of sporulation in *Streptomyces coelicolor* A3(2): a checkpoint multiplex? Curr Opin Microbiol, 4(6): 667-73.

Chater, K.F., Biro, S., Lee, K.J., Palmer, T. and Schrempf, H. **2010**. The complex extracellular biology of *Streptomyces*. FEMS Microbiol Rev, 34(2): 171-98.

Chavez, A., Forero, A., Sanchez, M., Rodriguez-Sanoja, R., Mendoza-Hernandez, G., Servin-Gonzalez, L., Sanchez, B., Garcia-Huante, Y., Rocha, D., Langley, E., Ruiz, B. and Sanchez, S. **2011**. Interaction of SCO2127 with BldKB and its possible connection to carbon catabolite regulation of morphological differentiation in *Streptomyces coelicolor*. Appl Microbiol Biotechnol, 89(3): 799-806.

Chen, W., Zhang, C., Song, L., Sommerfeld, M. and Hu, Q. **2009**. A high throughput Nile red method for quantitative measurement of neutral lipids in microalgae. J Microbiol Methods, 77(1): 41-7.

Chouayekh, H. and Virolle, M.J. **2002**. The polyphosphate kinase plays a negative role in the control of antibiotic production in *Streptomyces lividans*. Mol Microbiol, 43(4): 919-30.

Daigle, F., Lerat, S., Bucca, G., Sanssouci, E., Smith, C.P., Malouin, F. and Beaulieu, C. **2015**. A terD domain-encoding gene (*SCO2368*) is involved in calcium homeostasis and participates in calcium regulation of a DosR-like regulon in *Streptomyces coelicolor*. J Bacteriol, 197(5): 913-23.

Dakna, M., He, Z., Yu, W.C., Mischak, H. and Kolch, W. **2009**. Technical, bioinformatical and statistical aspects of liquid chromatography-mass spectrometry (LC-MS) and capillary electrophoresis-mass spectrometry (CE-MS) based clinical proteomics: a critical assessment. J Chromatog B Analyt Technol Biomed Life Sci, 877(13): 1250-8.

Darbon, E., Ito, K., Huang, H.S., Yoshimoto, T., Poncet, S. and Deutscher, J. **1999**. Glycerol transport and phosphoenolpyruvate-dependent enzyme I- and HPr-catalysed phosphorylation of glycerol kinase in *Thermus flavus*. Microbiol, 145 (Pt 11): 3205-12.

Dazzi, A., Deniset-Besseau, A. and Lasch, P. **2013**. Minimising contributions from scattering in infrared spectra by means of an integrating sphere. Analyst, 138(14): 4191-201.

de Hoffman, E. and Stroobant, V. **2007**. Mass spectrometry: principles and applications. 3rd Ed., John Wiley & Sons Ltd: West Sussex.

de Jong, W., Manteca, A., Sanchez, J., Bucca, G., Smith, C.P., Dijkhuizen, L., Claessen, D. and Wosten, H.A. **2009**. NepA is a structural cell wall protein involved in

maintenance of spore dormancy in *Streptomyces coelicolor*. Mol Microbiol, 71(6): 1591-03.

Dean, A.P., Sigee, D.C., Estrada, B. and Pittman, J.K. **2010**. Using FTIR spectroscopy for rapid determination of lipid accumulation in response to nitrogen limitation in freshwater microalgae. Bioresour Technol, 101(12): 4499-507.

Demain, A.L. and Sanchez, S. **2009**. Microbial drug discovery: 80 years of progress. J Antibiot, 62(1): 5-16.

Derouaux, A., Halici, S., Nothaft, H., Neutelings, T., Moutzourelis, G., Dusart, J., Titgemeyer, F. and Rigali, S. **2004**. Deletion of a cyclic AMP receptor protein homologue diminishes germination and affects morphological development of *Streptomyces coelicolor*. J Bacteriol, 186(6): 1893-7.

Diaz, M., Esteban, A., Fernandez-Abalos, J.M. and Santamaria, R.I. **2005**. The high-affinity phosphate-binding protein PstS is accumulated under high fructose concentrations and mutation of the corresponding gene affects differentiation in *Streptomyces lividans*. Microbiol, 151(Pt 8): 2583-92.

Diaz, M., Sevillano, L., Rico, S., Lombo, F., Brana, A.F., Salas, J.A., Mendez, C. and Santamaria, R.I. **2013**. High level of antibiotic production in a double polyphosphate kinase and phosphate-binding protein mutant of *Streptomyces lividans*. FEMS Microbiology Lett, 342(2): 123-9.

Doull, J.L. and Vining, L.C. **1990**. Nutritional control of actinorhodin production by *Streptomyces coelicolor* A3(2): suppressive effects of nitrogen and phosphate. Appl Microbiol Biotechnol, 32(4): 449-54.

Dowhan, W. **2013**. A retrospective: use of *Escherichia coli* as a vehicle to study phospholipid synthesis and function. BBA-Mol Cell Biol Lip, 1831(3): 471-94.

Eliuk, S. and Makarov, A. **2015**. Evolution of Orbitrap Mass Spectrometry Instrumentation. Annu Rev Anal Chem, 8: 61-80.

Eng, J.K., McCormack, A.L. and Yates, J.R. **1994**. An approach to correlate tandem mass spectral data of peptides with amino acid sequences in a protein database. J Am Soc Mass Spectrom, 5(11): 976-89.

Ensign, S.A. **2006**. Revisiting the glyoxylate cycle: alternate pathways for microbial acetate assimilation. Mol Microbiol, 61(2): 274-6.

Esnault, C., Dulermo, T., Smirnov, A., Askora, A., David, M., Deniset-Besseau, A., Holland, I.B. and Virolle, M.J. **2017**. Strong antibiotic production is correlated with highly active oxidative metabolism in *Streptomyces coelicolor* M145. Sci Rep, 7(1): 200.

Espadas, G., Borras, E., Chiva, C. and Sabido, E. **2017**. Evaluation of different peptide fragmentation types and mass analyzers in data-dependent methods using an Orbitrap Fusion Lumos Tribrid mass spectrometer. Proteomics, 17(9).

Facey, P.D., Sevcikova, B., Novakova, R., Hitchings, M.D., Crack, J.C., Kormanec, J., Dyson, P.J. and Del Sol, R. **2011**. The *dpsA* gene of *Streptomyces coelicolor*: induction of expression from a single promoter in response to environmental stress or during development. PloS one, 6(9): e25593.

Fair, R.J. and Tor, Y. **2014**. Antibiotics and bacterial resistance in the 21st Century. Perspect Medicin Chem, 6: 25-64.

Ferguson, N.L., Pena-Castillo, L., Moore, M.A., Bignell, D.R. and Tahlan, K. **2016**. Proteomics analysis of global regulatory cascades involved in clavulanic acid production and morphological development in *Streptomyces clavuligerus*. J Ind Microbiol Biotechnol, 43(4): 537-55.

Ferry-Dumazet, H., Houel, G., Montalent, P., Moreau, L., Langella, O., Negroni, L., Vincent, D., Lalanne, C., de Daruvar, A., Plomion, C., Zivy, M. and Joets, J. **2005**. PROTICdb: a web-based application to store, track, query, and compare plant proteome data. Proteomics, 5(8): 2069-81.

Fink, D., Falke, D., Wohlleben, W. and Engels, A. **1999**. Nitrogen metabolism in *Streptomyces coelicolor* A3(2): modification of glutamine synthetase I by an adenylyltransferase. Microbiol, 145(Pt 9): 2313-22.

Fink, D., Weissschuh, N., Reuther, J., Wohlleben, W. and Engels, A. **2002**. Two transcriptional regulators GlnR and GlnRII are involved in regulation of nitrogen metabolism in *Streptomyces coelicolor* A3(2). Mol Microbiol, 46(2): 331-47.

Finking, R. and Marahiel, M.A. **2004**. Biosynthesis of nonribosomal peptides. Annu Rev Microbiol, 58: 453-88.

Fischbach, M.A. and Walsh, C.T. **2006**. Assembly-line enzymology for polyketide and nonribosomal peptide antibiotics: logic, machinery, and mechanisms. Chem Rev, 106(8): 3468-96.

Fischer, C.R., Klein-Marcuschamer, D. and Stephanopoulos, G. **2008**. Selection and optimization of microbial hosts for biofuels production. Met Eng, 10(6): 295-304.

Fischer, M., Alderson, J., van Keulen, G., White, J. and Sawers, R.G. **2010**. The obligate aerobe *Streptomyces coelicolor* A3(2) synthesizes three active respiratory nitrate reductases. Microbiol, 156(Pt 10): 3166-79.

Fischer, M., Falke, D., Pawlik, T. and Sawers, R.G. **2014**. Oxygen-dependent control of respiratory nitrate reduction in mycelium of *Streptomyces coelicolor* A3(2). J Bacteriol, 196(23): 4152-62.

Flores, F.J., Barreiro, C., Coque, J.J. and Martin, J.F. **2005**. Functional analysis of two divalent metal-dependent regulatory genes *dmdR1* and *dmdR2* in *Streptomyces coelicolor* and proteome changes in deletion mutants. FEBS J, 272(3): 725-35.

Flores, F.J. and Martin, J.F. **2004**. Iron-regulatory proteins DmdR1 and DmdR2 of *Streptomyces coelicolor* form two different DNA-protein complexes with iron boxes. Biochem J, 380(Pt 2): 497-503.

Forero, A., Sanchez, M., Chavez, A., Ruiz, B., Rodriguez-Sanoja, R., Servin-Gonzalez, L. and Sanchez, S. **2012**. Possible involvement of the *sco2127* gene product in glucose repression of actinorhodin production in *Streptomyces coelicolor*. Can J Microbiol, 58(10): 1195-201.

Fowler-Goldsworthy, K., Gust, B., Mouz, S., Chandra, G., Findlay, K.C. and Chater, K.F. **2011**. The actinobacteria-specific gene *wblA* controls major developmental transitions in *Streptomyces coelicolor* A3(2). Microbiol, 157(Pt 5): 1312-28.

Fox, T.C., Mujer, C.V., Andrews, D.L., Williams, A.S., Cobb, B.G., Kennedy, R.A. and Rumpho, M.E. **1995**. Identification and gene expression of anaerobically induced enolase in *Echinochloa phyllopogon* and *Echinochloa crus-pavonis*. Plant Phys, 109(2): 433-43..

Fujii, T., Gramajo, H.C., Takano, E. and Bibb, M.J. **1996**. *redD* and *actII-ORF4*, pathway-specific regulatory genes for antibiotic production in *Streptomyces coelicolor* A3(2), are transcribed *in vitro* by an RNA polymerase holoenzyme containing sigma *hrdD*. J Bacteriol, 178(11): 3402-5.

Gago, G., Diacovich, L., Arabolaza, A., Tsai, S.C. and Gramajo, H. **2011**. Fatty acid biosynthesis in Actinomycetes. FEMS Microbiol Rev, 35(3): 475-97.

Geer, L.Y., Markey, S.P., Kowalak, J.A., Wagner, L., Xu, M., Maynard, D.M., Yang, X., Shi, W. and Bryant, S.H. **2004**. Open mass spectrometry search algorithm. J Proteome Res, 3(5): 958-64.

Ghorbel, S., Kormanec, J., Artus, A. and Virolle, M.J. **2006**. Transcriptional studies and regulatory interactions between the phoR-phoP operon and the *phoU*, *mtpA*, and *ppk* genes of *Streptomyces lividans* TK24. J Bacteriol, 188(2): 677-86.

Goldman, P., Alberts, A.W. and Vagelos, P.R. **1963**. The condensation reaction of fatty acid biosynthesis. II. Requirement of the enzymes of the condensation reaction for fatty acid synthesis. Journal Biol Chem, 238: 1255-61.

Gomez-Escribano, J.P., Alt, S. and Bibb, M.J. **2016**. Next generation sequencing of Actinobacteria for the discovery of novel natural products. Marine Drugs, 14(4).

Gomez-Escribano, J.P. and Bibb, M.J. **2011**. Engineering *Streptomyces coelicolor* for heterologous expression of secondary metabolite gene clusters. Microbial Biotechnol, 4(2): 207-15.

Gomez-Escribano, J.P., Song, L., Fox, D.J., Yeo, V., Bibb, M.J. and Challis, G.L. **2012**. Structure and biosynthesis of the unusual polyketide alkaloid coelimycin P1, a metabolic product of the *cpk* gene cluster of *Streptomyces coelicolor* M145. Chem Sci, 3(9): 2716-20.

Gorke, B. and Stulke, J. **2008**. Carbon catabolite repression in bacteria: many ways to make the most out of nutrients. Nat Rev Micro, 6(8): 613-24.

Govender, T., Ramanna, L., Rawat, I. and Bux, F. **2012**. BODIPY staining, an alternative to the Nile Red fluorescence method for the evaluation of intracellular lipids in microalgae. Bioresour Technol, 114: 507-11.

Gregorich, Z.R., Chang, Y.H. and Ge, Y. **2014**. Proteomics in heart failure: top-down or bottom-up? Eur J Phys, 466(6): 1199-209.

Gubbens, J., Janus, M., Florea, B.I., Overkleeft, H.S. and van Wezel, G.P. **2012**. Identification of glucose kinase-dependent and -independent pathways for carbon control of primary metabolism, development and antibiotic production in *Streptomyces coelicolor* by quantitative proteomics. Mol Microbiol, 86(6): 1490-507.

Guerra, S.M., Rodriguez-Garcia, A., Santos-Aberturas, J., Vicente, C.M., Payero, T.D., Martin, J.F. and Aparicio, J.F. **2012**. LAL regulators SCO0877 and SCO7173 as pleiotropic modulators of phosphate starvation response and actinorhodin biosynthesis in *Streptomyces coelicolor*. PloS one, 7(2): e31475.

Guzman, S., Carmona, A., Escalante, L., Imriskova, I., Lopez, R., Rodriguez-Sanoja, R., Ruiz, B., Servin-Gonzalez, L., Sanchez, S. and Langley, E. **2005**. Pleiotropic effect of the *sco127* gene on the glucose uptake, glucose kinase activity and carbon catabolite repression in *Streptomyces peucetius var. caesius*. Microbiol, 151(Pt 5): 1717-23.

Gygi, S.P., Rist, B., Gerber, S.A., Turecek, F., Gelb, M.H. and Aebersold, R. **1999**. Quantitative analysis of complex protein mixtures using isotope-coded affinity tags. Nature Biotechnol, 17(10): 994-9.

Halsey, C.R., Lei, S., Wax, J.K., Lehman, M.K., Nuxoll, A.S., Steinke, L., Sadykov, M., Powers, R. and Fey, P.D. **2017**. Amino acid catabolism in *Staphylococcus aureus* and the function of carbon catabolite repression. mBio, 8(1).

Hardwood, J.L. **2010**. Plant fatty acid synthesis. Accessed on April 10th, 2017. Available from: http://lipidlibrary.aocs.org/Biochemistry/content.cfm?ItemNumber=40304

Harrison, J. and Studholme, D.J. **2014**. Recently published *Streptomyces* genome sequences. Microbial Biotechnol, 7(5): 373-80.

Hayes, A., Hobbs, G., Smith, C.P., Oliver, S.G. and Butler, P.R. **1997**. Environmental signals triggering methylenomycin production by *Streptomyces coelicolor* A3(2). J Bacteriol, 179(17): 5511-5.

He, J.M., Zhu, H., Zheng, G.S., Liu, P.P., Wang, J., Zhao, G.P., Zhu, G.Q., Jiang, W.H. and Lu, Y.H. **2016**. Direct involvement of the master nitrogen metabolism regulator GlnR in antibiotic biosynthesis in *Streptomyces*. J Biol Chem, 291(51): 26443-54.

Heath, R.J., Jackowski, S. and Rock, C.O. **2002**. Fatty acid and phospholipid metabolism in prokaryotes. New Comp Biochem, 36: 55-92.

Heinzelmann, S.M., Bale, N.J., Hopmans, E.C., Damsté, J.S.S., Schouten, S. and van der Meer, M.T. **2014**. Critical assessment of glyco-and phospholipid separation by using silica chromatography. Appl Environ Microbiol, 80(1): 360-5.

Hesketh, A., Chen, W.J., Ryding, J., Chang, S. and Bibb, M. **2007**. The global role of ppGpp synthesis in morphological differentiation and antibiotic production in *Streptomyces coelicolor* A3(2). Genome Biol, 8(8).

Hesketh, A., Deery, M.J. and Hong, H.J. **2015**. High-resolution mass spectrometry based proteomic analysis of the response to vancomycin-induced cell wall stress in *Streptomyces coelicolor* A3(2). J Proteome Res, 14(7): 2915-28.

Hesketh, A., Fink, D., Gust, B., Rexer, H.U., Scheel, B., Chater, K., Wohlleben, W. and Engels, A. **2002**. The GlnD and GlnK homologues of *Streptomyces coelicolor* A3(2) are functionally dissimilar to their nitrogen regulatory system counterparts from enteric bacteria. Mol Microbiol, 46(2): 319-30.

Hindle, Z. and Smith, C.P. **1994**. Substrate induction and catabolite repression of the *Streptomyces coelicolor* glycerol operon are mediated through the GyIR protein. Mol Microbiol, 12(5): 737-45.

Holmback, M., Lehesto, M., Koskinen, P. and Selin, J.F. **2014**. Process and microorganisms for production of lipids., Neste Oil Oyj. European patent: 148056.

Honaker, R.W., Dhiman, R.K., Narayanasamy, P., Crick, D.C. and Voskuil, M.I. **2010**. DosS responds to a reduced electron transport system to induce the *Mycobacterium tuberculosis* DosR regulon. J Bacteriol, 192(24): 6447-55.

Hopwood, D.A. **1999**. Forty years of genetics with *Streptomyces*: from *in vivo* through *in vitro* to *in silico*. Microbiol, 145(Pt 9): 2183-202.

Hopwood, D.A., **2007**. *Streptomyces* in nature and medicine: the antibiotic makers. Oxford University Press: New York.

Horinouchi, S. **2003**. AfsR as an integrator of signals that are sensed by multiple serine/threonine kinases in *Streptomyces coelicolor* A3(2). J Ind Microbiol Biotechnol, 30(8): 462-7.

Hu, H., Zhang, Q. and Ochi, K. **2002**. Activation of antibiotic biosynthesis by specified mutations in the *rpoB* gene (encoding the RNA polymerase beta subunit) of *Streptomyces lividans*. J Bacteriol, 184(14): 3984-91.

Huang, J., Lih, C.J., Pan, K.H. and Cohen, S.N. **2001**. Global analysis of growth phase responsive gene expression and regulation of antibiotic biosynthetic pathways in *Streptomyces coelicolor* using DNA microarrays. Genes Dev, 15(23): 3183-92.

Huang, J., Shi, J., Molle, V., Sohlberg, B., Weaver, D., Bibb, M.J., Karoonuthaisiri, N., Lih, C.J., Kao, C.M., Buttner, M.J. and Cohen, S.N. **2005**. Cross-regulation among disparate antibiotic biosynthetic pathways of *Streptomyces coelicolor*. Mol Microbiol, 58(5): 1276-87.

Huh, J.H., Kim, D.J., Zhao, X.Q., Li, M., Jo, Y.Y., Yoon, T.M., Shin, S.K., Yong, J.H., Ryu, Y.W., Yang, Y.Y. and Suh, J.W. **2004**. Widespread activation of antibiotic biosynthesis by S-adenosylmethionine in Streptomycetes. FEMS Microbiol Lett, 238(2): 439-47.

Jayapal, K.P., Lian, W., Glod, F., Sherman, D.H. and Hu, W.S. **2007**. Comparative genomic hybridizations reveal absence of large *Streptomyces coelicolor* genomic islands in *Streptomyces lividans*. BMC Genomics, 8(1): 229.

Jayapal, K.P., Philp, R.J., Kok, Y.J., Yap, M.G.S., Sherman, D.H., Griffin, T.J. and Hu, W.S. **2008**. Uncovering genes with divergent mRNA-protein dynamics in *Streptomyces coelicolor*. PloS one, 3(5): e2097.

Jiang, P.L., Pasaribu, B. and Chen, C.S. **2014**. Nitrogen-deprivation elevates lipid levels in *Symbiodinium* spp. by lipid droplet accumulation: morphological and compositional analyses. PloS one, 9(1): e87416.

Kahrstrom, C.T. **2014**. Bacterial physiology: *Streptomyces* teams up with c-di-GMP. Nat Rev Microbiol, 12(11): 724-5.

Kalscheuer, R., Syson, K., Veeraraghavan, U., Weinrick, B., Biermann, K.E., Liu, Z., Sacchettini, J.C., Besra, G., Bornemann, S. and Jacobs, W.R. **2010**. Self-poisoning of *Mycobacterium tuberculosis* by targeting GlgE in an alpha-glucan pathway. Nature Chem Biol, 6(5): 376-84.

Kanehisa, M. and Goto, S. **2000**. KEGG: Kyoto encyclopedia of genes and genomes. Nucleic Acids Res, 28(1): 27-30.

Kang, S.H., Huang, J., Lee, H.N., Hur, Y.A., Cohen, S.N. and Kim, E.S. **2007**. Interspecies DNA microarray analysis identifies WblA as a pleiotropic down-regulator of antibiotic biosynthesis in *Streptomyces*. J Bacteriol, 189(11): 4315-9.

Kanski, J., Behring, A., Pelling, J. and Schoneich, C. **2005**. Proteomic identification of 3-nitrotyrosine-containing rat cardiac proteins: effects of biological aging. Am J Physiol Heart Circ Physiol, 288(1): H371-81.

Karp, P.D., Ouzounis, C.A., Moore-Kochlacs, C., Goldovsky, L., Kaipa, P., Ahrén, D., Tsoka, S., Darzentas, N., Kunin, V. and López-Bigas, N. **2005**. Expansion of the BioCyc collection of pathway/genome databases to 160 genomes. Nucleic Acids Res, 33(19): 6083-9.

Kazakov, A.E., Vassieva, O., Gelfand, M.S., Osterman, A. and Overbeek, R. **2003**. Bioinformatics classification and functional analysis of PhoH homologs. In Silico Biol, 3(1-2): 3-15.

Keatinge-Clay, A.T. **2012**. The structures of type I polyketide synthases. Nat Prod Rep, 29(10): 1050-73.

Kelemen, G.H., Brian, P., Flärdh, K., Chamberlin, L., Chater, K.F. and Buttner, M.J. **1998**. Developmental regulation of transcription of *whiE*, a locus specifying the polyketide spore pigment in *Streptomyces coelicolor* A3(2). J Bacteriol, 180(9): 2515-21.

Kempf, B. and Bremer, E. **1998**. Uptake and synthesis of compatible solutes as microbial stress responses to high-osmolality environments. Arch Microbiol, 170(5): 319-30.

Kieser, T., Bibb, M.J., Buttner, M.J., Chater, K.F. and Hopwood, D.A. **2000**. Practical *Streptomyces* Genetics. John Innes Foundation: Norwich.

Kiley, P.J. and Beinert, H. **2003**. The role of Fe–S proteins in sensing and regulation in bacteria. Curr Opin Microbiol, 6(2): 181-5.

Kim, D.J., Huh, J.H., Yang, Y.Y., Kang, C.M., Lee, I.H., Hyun, C.G., Hong, S.K. and Suh, J.W. **2003**. Accumulation of S-adenosyl-l-methionine enhances production of actinorhodin but inhibits sporulation in *Streptomyces lividans* TK23. J Bacteriol, 185(2): 592-600.

Kim, J.S., Lee, H.N., Kim, P., Lee, H.S. and Kim, E.S. **2012**. Negative role of *wblA* in response to oxidative stress in *Streptomyces coelicolor*. J Microbiol Biotechnol, 22(6): 736-41.

Kim, S.H., Traag, B.A., Hasan, A.H., McDowall, K.J., Kim, B.G. and van Wezel, G.P. **2015**. Transcriptional analysis of the cell division-related *ssg* genes in *Streptomyces coelicolor* reveals direct control of *ssgR* by *atrA*. Antonie van Leeuwenhoek, 108(1): 201-13.

Kint, C., Verstraeten, N., Hofkens, J., Fauvart, M. and Michiels, J. **2014**. Bacterial Obg proteins: GTPases at the nexus of protein and DNA synthesis. Crit Rev Microbiol, 40(3): 207-24.

Kirby, R. **2011**. Chromosome diversity and similarity within the Actinomycetales. FEMS Microbiol Lett, 319(1): 1-10.

Koch, M., Breithaupt, C., Kiefersauer, R., Freigang, J., Huber, R. and Messerschmidt, A. **2004**. Crystal structure of protoporphyrinogen IX oxidase: a key enzyme in haem and chlorophyll biosynthesis. EMBO J, 23(8): 1720-8.

Komeil, D., Padilla-Reynaud, R., Lerat, S., Simao-Beaunoir, A.M. and Beaulieu, C. **2014**. Comparative secretome analysis of *Streptomyces scabiei* during growth in the presence or absence of potato suberin. Proteome Sci, 12:35.

Kulaev, I.S., Vagabov, V.M. and Kulakovskaya, T.V. **2005**. The chemical structures and properties of condensed inorganic phosphates. In: The biochemistry of inorganic polyphosphates, John Wiley & Sons Ltd, pp: 3-13.

Kurosawa, K., Radek, A., Plassmeier, J.K. and Sinskey, A.J. **2015**. Improved glycerol utilization by a triacylglycerol-producing *Rhodococcus opacus* strain for renewable fuels. Biotechnol Biofuels, 8(1): 1-11.

Kuzuyama, T. **2017**. Biosynthetic studies on terpenoids produced by *Streptomyces*. J Antibiot. 70(7):811-8.

Kvint, K., Nachin, L., Diez, A. and Nystrom, T. **2003**. The bacterial universal stress protein: function and regulation. Curr Opin Microbiol, 6(2): 140-5.

Kwakman, J.H. and Postma, P.W. **1994**. Glucose kinase has a regulatory role in carbon catabolite repression in *Streptomyces coelicolor*. J Bacteriol, 176(9): 2694-8.

Lal, S.K., Lee, C. and Sachs, M.M. **1998**. Differential regulation of enolase during anaerobiosis in maize. Plant Physiol, 118(4): 1285-93.

Langella, O., Valot, B., Balliau, T., Blein-Nicolas, M., Bonhomme, L. and Zivy, M. **2017**. X!TandemPipeline: a tool to manage sequence redundancy for protein inference and phosphosite identification. J Proteome Res. 16(2), 494–503.

Langella, O., Valot, B., Jacob, D., Balliau, T., Flores, R., Hoogland, C., Joets, J. and Zivy, M. **2013**. Management and dissemination of MS proteomic data with PROTICdb: example of a quantitative comparison between methods of protein extraction. Proteomics, 13(9): 1457-66.

Le Marechal, P., Decottignies, P., Marchand, C.H., Degrouard, J., Jaillard, D., Dulermo, T., Froissard, M., Smirnov, A., Chapuis, V. and Virolle, M.J. **2013**. Comparative proteomic analysis of *Streptomyces lividans* wild-type and *ppk* mutant strains reveals the importance of storage lipids for antibiotic biosynthesis. Appl Environ Microbiol, 79(19): 5907-17.

Leblond, P. and Decaris, B. **1994**. New insights into the genetic instability of *Streptomyces*. FEMS Microbiol Lett, 123(3): 225-32.

Lee, C. and Park, C. **2017**. Bacterial responses to glyoxal and methylglyoxal: reactive electrophilic species. Int J Mol Sci, 18(1): 169.

Lee, H.N., Kim, J.S., Kim, P., Lee, H.S. and Kim, E.S. **2013**. Repression of antibiotic downregulator WblA by AdpA in *Streptomyces coelicolor*. Appl Environ Microbiol, 79(13): 4159-63.

Lee, H.N., Huang, J., Im, J.H., Kim, S.H., Noh, J.H., Cohen, S.N. and Kim, E.S. **2010**. Putative TetR family transcriptional regulator SCO1712 encodes an antibiotic downregulator in *Streptomyces coelicolor*. Appl Environ Microbiol, 76(9): 3039-43.

Lee, P.C., Umeyama, T. and Horinouchi, S. **2002**. AfsS is a target of AfsR, a transcriptional factor with ATPase activity that globally controls secondary metabolism in *Streptomyces coelicolor* A3(2). Mol Microbiol, 43(6): 1413-30.

Leimkühler, S. **2014**. The biosynthesis of the molybdenum cofactor in *Escherichia coli* and its connection to FeS cluster assembly and the thiolation of tRNA. Adv Biol, 2014: 21.

Leistikow, R.L., Morton, R.A., Bartek, I.L., Frimpong, I., Wagner, K. and Voskuil, M.I. **2010**. The *Mycobacterium tuberculosis* DosR regulon assists in metabolic homeostasis and enables rapid recovery from nonrespiring dormancy. J Bacteriol, 192(6): 1662-70.

Lepage, G. and Roy, C.C. **1986**. Direct transesterification of all classes of lipids in a one-step reaction. J Lip Res, 27(1): 114-20.

Lewis, R.A., Laing, E., Allenby, N., Bucca, G., Brenner, V., Harrison, M., Kierzek, A.M. and Smith, C.P. **2010**. Metabolic and evolutionary insights into the closely-related species *Streptomyces coelicolor* and *Streptomyces lividans* deduced from high-resolution comparative genomic hybridization. BMC Genomics, 11(1): 682.

Li, L., Jiang, W. and Lu, Y. **2017**. A novel two-component system, GluR-K, involved in glutamate sensing and uptake in *Streptomyces coelicolor*. J Bacteriol. DOI: 10.1128/JB.00097-17.

Li, W., Ying, X., Guo, Y., Yu, Z., Zhou, X., Deng, Z., Kieser, H., Chater, K.F. and Tao, M. **2006**. Identification of a gene negatively affecting antibiotic production and morphological differentiation in *Streptomyces coelicolor* A3(2). J Bacteriol, 188(24): 8368-75.

Li, X., Wang, J., Li, S., Ji, J., Wang, W. and Yang, K. **2015**. ScbR- and ScbR2-mediated signal transduction networks coordinate complex physiological responses in *Streptomyces coelicolor*. Sci Rep, 5: 14831.

Li, Y., Florova, G. and Reynolds, K.A. **2005**. Alteration of the fatty acid profile of *Streptomyces coelicolor* by replacement of the initiation enzyme 3-ketoacyl acyl carrier protein synthase III (FabH). J Bacteriol, 187(11): 3795-9.

Lian, W., Jayapal, K.P., Charaniya, S., Mehra, S., Glod, F., Kyung, Y.S., Sherman, D.H. and Hu, W.S. **2008**. Genome-wide transcriptome analysis reveals that a pleiotropic antibiotic regulator, AfsS, modulates nutritional stress response in *Streptomyces coelicolor* A3(2). BMC Genomics, 9: 56.

Liao, G., Xie, L., Li, X., Cheng, Z. and Xie, J. **2014**. Unexpected extensive lysine acetylation in the trump-card antibiotic producer *Streptomyces roseosporus* revealed by proteome-wide profiling. J Proteomics, 106: 260-9.

Lin, Y.S. and Chen, C.W. **1997**. Instability of artificially circularized chromosomes of *Streptomyces lividans*. Mol Microbiol, 26(4): 709-19.

Liu, G., Chater, K.F., Chandra, G., Niu, G. and Tan, H. **2013**. Molecular regulation of antibiotic biosynthesis in *Streptomyces*. Microbiol Mol Biol Rev, 77(1): 112-43.

Liu, H., Sadygov, R.G. and Yates, J.R. **2004**. A model for random sampling and estimation of relative protein abundance in shotgun proteomics. Analyt Chem, 76(14): 4193-201.

Long, D., Wilkinson, K.L., Poole, K., Taylor, D.K., Warren, T., Astorga, A.M. and Jiranek, V. **2012**. Rapid method for proline determination in grape juice and wine. J Agric Food Chem, 60(17): 4259-64.

Lounes, A., Lebrihi, A., Benslimane, C., Lefebvre, G. and Germain, P. **1996**. Regulation of spiramycin synthesis in *Streptomyces ambofaciens*: effects of glucose and inorganic phosphate. Appl Microbiol Biotechnol, 45(1-2): 204-11.

Lu, Y., Wang, W., Shu, D., Zhang, W., Chen, L., Qin, Z., Yang, S. and Jiang, W. **2007**. Characterization of a novel two-component regulatory system involved in the regulation of both actinorhodin and a type I polyketide in Streptomyces coelicolor. Appl Microbiol Biotechnol, 77(3): 625-35.

Ludwig, W., Euzéby, J., Schumann, P., Busse, H.J., Trujillo, M.E., Kämpfer, P. and Whitman, W.B. **2012**. Road map of the phylum Actinobacteria. In: Bergey's manual of systematic bacteriology: volume five The Actinobacteria, part A and B, Goodfellow, M., Kämpfer, P., Busse, H.J., Trujillo, M.E., Suzuki, K., Ludwig, W. and Whitman, W.B. (Eds). Springer : New York, pp: 1-28.

Lundgren, D.H., Hwang, S.I., Wu, L. and Han, D.K. **2010**. Role of spectral counting in quantitative proteomics. Exp Rev Proteomics, 7(1): 39-53.

Lyutvinskiy, Y., Yang, H., Rutishauser, D. and Zubarev, R.A. **2013**. *In silico* instrumental response correction improves precision of label-free proteomics and accuracy of proteomics-based predictive models. Mol Cell Proteomics, 12(8): 2324-31.

Mallick, P. and Kuster, B. **2010**. Proteomics: a pragmatic perspective. Nature Biotechnol, 28(7): 695-709.

Manadas, B., Mendes, V.M., English, J. and Dunn, M.J. **2010**. Peptide fractionation in proteomics approaches. Exp Rev Proteomics, 7(5): 655-63.

Mann, M. and Kelleher, N.L. **2008**. Precision proteomics: the case for high resolution and high mass accuracy. Proc Nat Acad Sci USA, 105(47): 18132-8.

Manteca, A., Alvarez, R., Salazar, N., Yagüe, P. and Sanchez, J. **2008**. Mycelium differentiation and antibiotic production in submerged cultures of *Streptomyces coelicolor*. Appl Environ Microbiol, 74(12): 3877-86.

Manteca, A., Jung, H.R., Schwammle, V., Jensen, O.N. and Sanchez, J. **2010**. Quantitative proteome analysis of *Streptomyces coelicolor* nonsporulating liquid cultures demonstrates a complex differentiation process comparable to that occurring in sporulating solid cultures. J Proteome Res, 9(9): 4801-11.

Manteca, A., Mader, U., Connolly, B.A. and Sanchez, J. **2006**. A proteomic analysis of *Streptomyces coelicolor* programmed cell death. Proteomics, 6(22): 6008-22.

Manteca, A., Sanchez, J., Jung, H.R., Schwammle, V. and Jensen, O.N. **2010**. Quantitative proteomics analysis of *Streptomyces coelicolor* development demonstrates that onset of secondary metabolism coincides with hypha differentiation. Mol Cell Proteomics, 9(7): 1423-36.

Manzanera, M., Garcia de Castro, A., Tondervik, A., Rayner-Brandes, M., Strom, A.R. and Tunnacliffe, A. **2002**. Hydroxyectoine is superior to trehalose for anhydrobiotic engineering of *Pseudomonas putida* KT2440. Appl Environ Microbiol, 68(9): 4328-33.

Marshall, A.G. and Hendrickson, C.L. **2008**. High-resolution mass spectrometers. Annu Rev Anal Chem, 1: 579-99.

Martin, J.F., Rodriguez-Garcia, A. and Liras, P. **2017**. The master regulator PhoP coordinates phosphate and nitrogen metabolism, respiration, cell differentiation and antibiotic biosynthesis: comparison in *Streptomyces coelicolor* and *Streptomyces avermitilis*. J Antibiot, 70(5): 534-41.

Martín, M.C., Díaz, L.A.. Manzanal, M.B. and Hardisson, C. **1986**. Role of trehalose in the spores of *Streptomyces*. FEMS Microbiol Lett, 35(1): 49-54.

Matsuura, H.N., Rau, M.R. and Fett-Neto, A.G. **2014**. Oxidative stress and production of bioactive monoterpene indole alkaloids: biotechnological implications. Biotechnol Lett, 36(2): 191-200.

McCormick, J.R. and Flardh, K. **2012**. Signals and regulators that govern *Streptomyces* development. FEMS Microbiol Rev, 36(1): 206-31.

McKenzie, N.L. and Nodwell, J.R. **2007**. Phosphorylated AbsA2 negatively regulates antibiotic production in *Streptomyces coelicolor* through interactions with pathway-specific regulatory gene promoters. J Bacteriol, 189(14): 5284-92.

Medema, M.H., Blin, K., Cimermancic, P., de Jager, V., Zakrzewski, P., Fischbach, M.A., Weber, T., Takano, E. and Breitling, R. **2011**. AntiSMASH: rapid identification, annotation and analysis of secondary metabolite biosynthesis gene clusters in bacterial and fungal genome sequences. Nucleic Acids Res, 39: W339-46.

Medema, M.H., Kottmann, R., Yilmaz, P., Cummings, M., Biggins, J.B., Blin, K., de Bruijn, I., Chooi, Y.H., Claesen, J., Coates, R.C., Cruz-Morales, P., Duddela, S., Dusterhus, S., Edwards, D.J., Fewer, D.P., Garg, N., Geiger, C., Gomez-Escribano, J.P., Greule, A., Hadjithomas, M., Haines, A.S., Helfrich, E.J.N., Hillwig, M.L., Ishida, K., Jones, A.C., Jones, C.S., Jungmann, K., Kegler, C., Kim, H.U., Kotter, P., Krug, D., Masschelein, J., Melnik, A.V., Mantovani, S.M., Monroe, E.A., Moore, M., Moss, N., Nutzmann, H.W., Pan, G., Pati, A., Petras, D., Reen, F.J., Rosconi, F., Rui, Z., Tian, Z., Tobias, N.J., Tsunematsu, Y., Wiemann, P., Wyckoff, E., Yan, X., Yim, G., Yu, F., Xie, Y., Aigle, B., Apel, A.K., Balibar, C.J., Balskus, E.P., Barona-Gomez, F., Bechthold, A., Bode, H.B., Borriss, R., Brady, S.F., Brakhage, A.A., Caffrey, P., Cheng, Y.Q., Clardy, J., Cox, R.J., De Mot, R., Donadio, S., Donia, M.S., van der Donk,

W.A., Dorrestein, P.C., Doyle, S., Driessen, A.J.M., Ehling-Schulz, M., Entian, K.D., Fischbach, M.A., Gerwick, L., Gerwick, W.H., Gross, H., Gust, B., Hertweck, C., Hofte, M., Jensen, S.E., Ju, J., Katz, L., Kaysser, L., Klassen, J.L., Keller, N.P., Kormanec, J., Kuipers, O.P., Kuzuyama, T., Kyrpides, N.C., Kwon, H.J., Lautru, S., Lavigne, R., Lee, C.Y., Linquan, B., Liu, X., Liu, W., Luzhetskyy, A., Mahmud, T., Mast, Y., Mendez, C., Metsa-Ketela, M., Micklefield, J., Mitchell, D.A., Moore, B.S., Moreira, L.M., Muller, R., Neilan, B.A., Nett, M., Nielsen, J., O'Gara, F., Oikawa, H., Osbourn, A., Osburne, M.S., Ostash, B., Payne, S.M., Pernodet, J.L., Petricek, M., Piel, J., Ploux, O., Raaijmakers, J.M., Salas, J.A., Schmitt, E.K., Scott, B., Seipke, R.F., Shen, B., Sherman, D.H., Sivonen, K., Smanski, M.J., Sosio, M., Stegmann, E., Sussmuth, R.D., Tahlan, K., Thomas, C.M., Tang, Y., Truman, A.W., Viaud, M., Walton, J.D. Walsh, C.T., Weber, T., van Wezel, G.P., Wilkinson, B., Willey, J.M., Wohlleben, W., Wright, G.D., Ziemert, N., Zhang, C., Zotchev, S.B., Breitling, R. Takano, E. and Glockner, F.O. **2015**. Minimum information about a biosynthetic gene cluster. Nat Chem Biol, 11(9): 625-31.

Melo, A.M., Bandeiras, T.M. and Teixeira, M. **2004**. New insights into type II NAD(P)H:quinone oxidoreductases. Microbiol Mol Biol Rev, 68(4): 603-16.

Michael-Jubeli, R., Bleton, J. and Baillet-Guffroy, A. **2011**. High-temperature gas chromatography-mass spectrometry for skin surface lipids profiling. J Lip Res, 52(1): 143-51.

Michalski, A., Damoc, E., Hauschild, J.P., Lange, O., Wieghaus, A., Makarov, A., Nagaraj, N., Cox, J., Mann, M. and Horning, S. **2011**. Mass Spectrometry-based proteomics using Q-Exactive, a high-performance benchtop quadrupole Orbitrap mass spectrometer. Mol Cell Proteomics, 10(9): M111.011015.

Michta, E., Ding, W., Zhu, S., Blin, K., Ruan, H., Wang, R., Wohlleben, W. and Mast, Y. **2014**. Proteomic approach to reveal the regulatory function of aconitase AcnA in oxidative stress response in the antibiotic producer *Streptomyces viridochromogenes* Tu494. PloS one, 9(2): e87905.

Miguelez, E.M., Hardisson, C. and Manzanal, M.B. **1999**. Hyphal death during colony development in *Streptomyces antibioticus*: morphological evidence for the existence of a process of cell deletion in a multicellular prokaryote. J Cell Biol, 145(3): 515-25.

Millan-Oropeza, A., Rebois, R., David, M., Moussa, F., Dazzi, A., Bleton, J., Virolle M.J. and Deniset-Besseau, A. **2017**. Attenuated total reflection fourier transform infrared (ATR FT-IR) for rapid determination of microbial cell lipid content: correlation with gas chromatography-mass spectrometry (GC-MS). Appl Spectrosc, DOI: 10.1177/0003702817709459.

Mohimani, H., Kersten, R.D., Liu, W.T., Wang, M., Purvine, S.O., Wu, S., Brewer, H.M., Pasa-Tolic, L., Bandeira, N., Moore, B.S., Pevzner, P.A. and Dorrestein, P.C. **2014**. Automated genome mining of ribosomal peptide natural products. Chem Biol, 9(7): 1545-51.

Moir, J.W. and Wood, N.J. **2001**. Nitrate and nitrite transport in bacteria. Cell Mol Life sciences : CMLS, 58(2): 215-224.

Mooney, S., Leuendorf, J.E., Hendrickson, C. and Hellmann, H. **2009**. Vitamin B6: a long known compound of surprising complexity. Molecules, 14(1): 329.

Morimoto, T., Loh, P.C., Hirai, T., Asai, K., Kobayashi, K., Moriya, S. and Ogasawara, N. **2002**. Six GTP-binding proteins of the Era/Obg family are essential for cell growth in *Bacillus subtilis*. Microbiol, 148(Pt 11): 3539-52.

Mossoba, M.M., Azizian, H., Tyburczy, C., Kramer, J.K.G., Delmonte, P., Kia, A.R.F. and Rader, J.I. **2013**. Rapid FT-NIR analysis of edible oils for total SFA, MUFA, PUFA, and trans FA with comparison to GC. J Am Oil Chem Soc, 90(6): 757-70.

Nagaraj, N., Kulak, N.A., Cox, J., Neuhauser, N., Mayr, K., Hoerning, O., Vorm, O. and Mann, M. **2012**. System-wide perturbation analysis with nearly complete coverage of the yeast proteome by single-shot ultra HPLC runs on a bench top Orbitrap. Mol Cell Proteomics, 11(3): M111-013722.

Nazari, B., Kobayashi, M., Saito, A., Hassaninasab, A., Miyashita, K. and Fujii, T. **2013**. Chitin-induced gene expression in secondary metabolic pathways of *Streptomyces coelicolor* A3(2) grown in soil. Appl Environ Microbiol, 79(2): 707-13.

Neilson, K.A., Ali, N.A., Muralidharan, S., Mirzaei, M., Mariani, M., Assadourian, G., Lee, A., van Sluyter, S.C. and Haynes, P.A. **2011**. Less label, more free: approaches in label-free quantitative mass spectrometry. Proteomics, 11(4): 535-53.

Nguyen, K.T., Willey, J.M., Nguyen, L.D., Nguyen, L.T., Viollier, P.H. and Thompson, C.J. **2002**. A central regulator of morphological differentiation in the multicellular bacterium *Streptomyces coelicolor*. Mol Microbiol, 46(5): 1223-38.

Nieselt, K., Battke, F., Herbig, A., Bruheim, P., Wentzel, A., Jakobsen, Ø.M., Sletta, H., Alam, M.T., Merlo, M.E., Moore, J., Omara, W.A.M., Morrissey, E.R., Juarez-Hermosillo, M.A., Rodríguez-García, A., Nentwich, M., Thomas, L., Iqbal, M., Legaie, R., Gaze, W.H., Challis, G.L., Jansen, R.C., Dijkhuizen, L., Rand, D.A., Wild, D.L., Bonin, M., Reuther, J., Wohlleben, W., Smith, M.C.M., Burroughs, N.J., Martín, J.F., Hodgson, D.A., Takano, E., Breitling, R., Ellingsen, T.E. and Wellington, E.M.H. **2010**. The dynamic architecture of the metabolic switch in *Streptomyces coelicolor*. BMC Genomics, 11(1): 10.

NIST, 2014. Standard Reference Database 14. Available on: http://www.nist.gov/srd/nist1a.cfm.

Nothaft, H., Parche, S., Kamionka, A. and Titgemeyer, F. **2003**. *In vivo* analysis of HPr reveals a fructose-specific phosphotransferase system that confers high-affinity uptake in *Streptomyces coelicolor*. J Bacteriol, 185(3): 929-37.

Nothaft, H., Rigali, S., Boomsma, B., Swiatek, M., McDowall, K.J., van Wezel, G.P. and Titgemeyer, F. **2010**. The permease gene *nagE2* is the key to N-acetylglucosamine sensing and utilization in *Streptomyces coelicolor* and is subject to multi-level control. Mol Microbiol, 75(5): 1133-44.

Nouws, J., Nijtmans, L., Houten, S.M., van den Brand, M., Huynen, M., Venselaar, H., Hoefs, S., Gloerich, J., Kronick, J., Hutchin, T., Willems, P., Rodenburg, R., Wanders, R., van den Heuvel, L., Smeitink, J. and Vogel, R.O. **2010**. Acyl-CoA dehydrogenase 9 is required for the biogenesis of oxidative phosphorylation complex I. Cell Met, 12(3): 283-94.

O'Connor, T.J. and Nodwell, J.R. **2005**. Pivotal roles for the receiver domain in the mechanism of action of the response regulator RamR of *Streptomyces coelicolor*. J Mol Biol, 351(5): 1030-47.

Obanye, A.I.C., Hobbs, G., Gardner, D.C.J. and Oliver, S.G. **1996**. Correlation between carbon flux through the pentose phosphate pathway and production of the antibiotic methylenomycin in *Streptomyces coelicolor* A3(2). Microbiol, 142(1): 133-7.

Oexle, H., Gnaiger, E. and Weiss, G. **1999**. Iron-dependent changes in cellular energy metabolism: influence on citric acid cycle and oxidative phosphorylation. BBA - Bioenergetics, 1413(3): 99-107.

Ohnishi, Y., Ishikawa, J., Hara, H., Suzuki, H., Ikenoya, M., Ikeda, H., Yamashita, A., Hattori, M. and Horinouchi, S. **2008**. Genome sequence of the streptomycin-producing microorganism *Streptomyces griseus* IFO 13350. J Bacteriol, 190(11): 4050-60.

Okamoto, S., Taguchi, T., Ochi, K. and Ichinose, K. **2009**. Biosynthesis of actinorhodin and related antibiotics: discovery of alternative routes for quinone formation encoded in the *act* gene cluster. Chem Biol, 16(2): 226-36.

Okino, S., Suda, M., Fujikura, K., Inui, M. and Yukawa, H. **2008**. Production of D-lactic acid by *Corynebacterium glutamicum* under oxygen deprivation. Appl Microbiol Biotechnol, 78(3): 449-54.

Olukoshi, E.R. and Packter, N.M. **1994**. Importance of stored triacylglycerols in *Streptomyces*: possible carbon source for antibiotics. Microbiol, 140(Pt 4): 931-43.

Onaka, H., Nakagawa, T. and Horinouchi, S. **1998**. Involvement of two a-factor receptor homologues in *Streptomyces coelicolor* A3(2) in the regulation of secondary metabolism and morphogenesis. Mol Microbiol, 28(4): 743-53.

Ong, S.E., Blagoev, B., Kratchmarova, I., Kristensen, D.B., Steen, H., Pandey, A. and Mann, M. **2002**. Stable isotope labeling by amino acids in cell culture, SILAC, as a simple and accurate approach to expression proteomics. Mol Cell Proteomics, 1(5): 376-86.

Ou, X., Zhang, B., Zhang, L., Zhao, G. and Ding, X. **2009**. Characterization of *rrdA*, a TetR family protein gene involved in the regulation of secondary metabolism in *Streptomyces coelicolor*. Appl Environ Microbiol, 75(7): 2158-65.

Parche, S., Nothaft, H., Kamionka, A. and Titgemeyer, F. **2000**. Sugar uptake and utilisation in *Streptomyces coelicolor*: a PTS view to the genome. Antonie van Leeuwenhoek, 78(3-4): 243-51.

Park, S.S., Yang, Y.H., Song, E., Kim, E.J., Kim, W.S., Sohng, J.K., Lee, H.C., Liou, K.K. and Kim, B.G. **2009**. Mass spectrometric screening of transcriptional regulators involved in antibiotic biosynthesis in *Streptomyces coelicolor* A3(2). J Ind Microbiol Biotechnol, 36(8): 1073-83.

Pawlik, K., Kotowska, M., Chater, K.F., Kuczek, K. and Takano, E. **2006**. A cryptic type I polyketide synthase (*cpk*) gene cluster in *Streptomyces coelicolor* A3(2). Arch Microbiol, 187(2): 87-99.

Pawlik, K., Kotowska, M. and Kolesinski, P. **2010**. *Streptomyces coelicolor* A3(2) produces a new yellow pigment associated with the polyketide synthase Cpk. J Mol Microbiol Biotechnol, 19(3): 147-51.

Perez-Redondo, R., Santamarta, I., Bovenberg, R., Martin, J.F. and Liras, P. **2010**. The enigmatic lack of glucose utilization in *Streptomyces clavuligerus* is due to inefficient expression of the glucose permease gene. Microbiol, 156(Pt 5): 1527-37.

Perkel, J.M. **2012**. Choosing the optimal ionization source for your mass spectrometry needs. Accessed on May 10th, 2017. Available on: http://www.biocompare.com/Editorial-Articles/41599-Choosing-the-Optimal-Ionization-Source-for-Your-Mass-Spectrometry-Needs/

Perkins, D.N., Pappin, D.J., Creasy, D.M. and Cottrell, J.S. **1999**. Probability-based protein identification by searching sequence databases using mass spectrometry data. Electrophoresis, 20(18): 3551-67.

Piette, A., Derouaux, A., Gerkens, P., Noens, E.E.E., Mazzucchelli, G., Vion, S., Koerten, H.K., Titgemeyer, F., De Pauw, E., Leprince, P., van Wezel, G.P., Galleni, M. and Rigali, S. **2005**. From dormant to germinating spores of *Streptomyces coelicolor* A3(2): new perspectives from the *crp* null mutant. J Proteome Res, 4(5): 1699-708.

Pistorius, A.M.A., DeGrip, W.J. and Egorova-Zachernyuk, T.A. **2009**. Monitoring of biomass composition from microbiological sources by means of FT-IR spectroscopy. Biotechnol Bioeng, 103(1): 123-9.

Preiss, J. **2006**. Bacterial glycogen inclusions: enzymology and regulation of synthesis. In: Inclusions in Prokaryotes, Shively, J.M. (Ed.) Springer Berlin Heidelberg, pp: 71-108.

R Core Team. **2015**. R: A language and environment for statistical computing. R Foundation for Statistical Computing.

Ramer, G. and Lendl, B. **2006**. Attenuated total reflection Fourier transform infrared spectroscopy. In: Encyclopedia of analytical chemistry, Meyers, R.A (Ed). John Wiley & Sons Ltd: Chichester.

Reuther, J. and Wohlleben, W. **2007**. Nitrogen metabolism in *Streptomyces coelicolor*: transcriptional and post-translational regulation. J Mol Microbiol Biotechnol, 12(1-2): 139-46.

Rigali, S., Titgemeyer, F., Barends, S., Mulder, S., Thomae, A.W., Hopwood, D.A. and van Wezel, G.P. **2008**. Feast or famine: the global regulator DasR links nutrient stress to antibiotic production by *Streptomyces*. EMBO Rep, 9(7): 670-5.

Rodriguez-Garcia, A., Barreiro, C., Santos-Beneit, F., Sola-Landa, A. and Martin, J.F. **2007**. Genome-wide transcriptomic and proteomic analysis of the primary response to phosphate limitation in *Streptomyces coelicolor* M145 and in a *ΔphoP* mutant. Proteomics, 7(14): 2410-29.

Rodríguez, E., Banchio, C., Diacovich, L., Bibb, M.J. and Gramajo, H. **2001**. Role of an essential acyl Coenzyme A carboxylase in the primary and secondary metabolism of *Streptomyces coelicolor* A3(2). Appl Environ Microbiol, 67(9): 4166-76.

Romero-Rodríguez, A., Rocha, D., Ruiz-Villafan, B., Tierrafría, V., Rodríguez-Sanoja, R., Segura-González, D. and Sánchez, S. **2016**. Transcriptomic analysis of a classical model of carbon catabolite regulation in *Streptomyces coelicolor*. BMC Microbiol, 16(1): 77.

Ross, P.L., Huang, Y.N., Marchese, J.N., Williamson, B., Parker, K., Hattan, S., Khainovski, N., Pillai, S., Dey, S., Daniels, S., Purkayastha, S., Juhasz, P., Martin, S., Bartlet-Jones, M., He, F., Jacobson, A. and Pappin, D.J. **2004**. Multiplexed protein quantitation in *Saccharomyces cerevisiae* using amine-reactive isobaric tagging reagents. Mol Cell Proteomics, 3(12): 1154-69.

Rossa, C.A., White, J., Kuiper, A., Postma, P.W., Bibb, M. and Teixeira de Mattos, M.J. **2002**. Carbon flux distribution in antibiotic-producing chemostat cultures of *Streptomyces lividans*. Met Eng, 4(2): 138-50.

Rottig, A., Hauschild, P., Madkour, M.H., Al-Ansari, A.M., Almakishah, N.H. and Steinbuchel, A. **2016**. Analysis and optimization of triacylglycerol synthesis in novel oleaginous *Rhodococcus* and *Streptomyces* strains isolated from desert soil. J Biotechnol, 225: 48-56.

Ruckert, C., Albersmeier, A., Busche, T., Jaenicke, S., Winkler, A., Friethjonsson, O.H., Hreggviethsson, G.O., Lambert, C., Badcock, D., Bernaerts, K., Anne, J., Economou, A. and Kalinowski, J. **2015**. Complete genome sequence of *Streptomyces lividans* TK24. J Biotechnol, 199: 21-2.

Ryding, N.J., Anderson, T.B. and Champness, W.C. **2002**. Regulation of the *Streptomyces coelicolor* calcium-dependent antibiotic by *absA*, encoding a cluster-linked two-component system. J Bacteriol, 184(3): 794-805.

Ryu, Y.G., Kim, E.S., Kim, D.W., Kim, S.K. and Lee, K.J. **2007**. Differential stringent responses of *Streptomyces coelicolor* M600 to starvation of specific nutrients. J Microbiol Biotechnol, 17(2): 305-12.

Saito, N., Xu, J., Hosaka, T., Okamoto, S., Aoki, H., Bibb, M.J. and Ochi, K. **2006**. EshA accentuates ppGpp accumulation and is conditionally required for antibiotic production in *Streptomyces coelicolor* A3(2). J Bacteriol, 188(13): 4952-61.

Salcedo, E., Cortese, J.F., Plowe, C.V., Sims, P.F. and Hyde, J.E. **2001**. A bifunctional dihydrofolate synthetase-folylpolyglutamate synthetase in *Plasmodium falciparum* identified by functional complementation in yeast and bacteria. Mol Biochem Parasitol, 112(2): 239-52.

Sanchez, S., Chavez, A., Forero, A., Garcia-Huante, Y., Romero, A., Sanchez, M., Rocha, D., Sanchez, B., Avalos, M., Guzman-Trampe, S., Rodriguez-Sanoja, R., Langley, E. and Ruiz, B. **2010**. Carbon source regulation of antibiotic production. J Antibiot, 63(8): 442-59.

Sanssouci, E., Lerat, S., Daigle, F., Grondin, G., Shareck, F. and Beaulieu, C. **2012**. Deletion of TerD-domain-encoding genes: effect on *Streptomyces coelicolor* development. Can J Microbiol, 58(10): 1221-9.

Sanssouci, E., Lerat, S., Grondin, G., Shareck, F. and Beaulieu, C. **2011**. *tdd8*: a TerD domain-encoding gene involved in *Streptomyces coelicolor* differentiation. Antonie van Leeuwenhoek, 100(3): 385-98.

Santos-Beneit, F. **2015**. The Pho regulon: a huge regulatory network in bacteria. Front Microbiol, 6: 402.

Santos-Beneit, F., Rodriguez-Garcia, A., Franco-Dominguez, E. and Martin, J.F. **2008**. Phosphate-dependent regulation of the low- and high-affinity transport systems in the model actinomycete *Streptomyces coelicolor*. Microbiol, 154(Pt 8): 2356-70.

Santos-Beneit, F., Rodriguez-Garcia, A. and Martin, J.F. **2011**. Complex transcriptional control of the antibiotic regulator AfsS in *Streptomyces*: PhoP and AfsR are overlapping, competitive activators. J Bacteriol, 193(9): 2242-51.

Sawai, R., Suzuki, A., Takano, Y., Lee, P.C. and Horinouchi, S. **2004**. Phosphorylation of AfsR by multiple serine/threonine kinases in *Streptomyces coelicolor* A3(2). Gene, 334: 53-61.

Sawers, R.G., Falke, D. and Fischer, M. **2016**. Oxygen and nitrate respiration in *Streptomyces coelicolor* A3(2). In: Advances in microbial physiology, Robert, K.P. (Ed). Academic Press, pp: 1-40.

Scigelova, M. and Makarov, A. **2006**. Orbitrap mass analyzer-overview and applications in proteomics. Proteomics, 6(Suppl 2): 16-21.

Schauner, C., Dary, A., Lebrihi, A., Leblond, P., Decaris, B. and Germain, P. **1999**. Modulation of lipid metabolism and spiramycin biosynthesis in *Streptomyces ambofaciens* unstable mutants. Appl Environ Microbiol, 65(6): 2730-7.

Schneider, D., Bruton, C.J. and Chater, K.F. **2000**. Duplicated gene clusters suggest an interplay of glycogen and trehalose metabolism during sequential stages of aerial mycelium development in *Streptomyces coelicolor* A3(2). Mol Gen Genet, 263(3): 543-53.

Schneider, D., Pohl, T., Walter, J., Dörner, K., Kohlstädt, M., Berger, A., Spehr, V. and Friedrich, T. **2008**. Assembly of the *Escherichia coli* NADH:ubiquinone oxidoreductase (complex I). BBA - Bioenergetics, 1777(7–8): 735-9.

Schreier, H.J. **1993**. Biosynthesis of glutamine and glutamate and the assimilation of ammonia. In: *Bacillus subtilis* and other Gram-positive bacteria, Sonenshein, A.L., Hoch, J.A. and Losick, R.M. (Eds). American Society of Microbiology Press.

Seaver, L.C. and Imlay, J.A. **2004**. Are respiratory enzymes the primary sources of intracellular hydrogen peroxide? J Biol Chem, 279(47): 48742-50.

Seifart Gomes, C., Izar, B., Pazan, F., Mohamed, W., Mraheil, M.A., Mukherjee, K., Billion, A., Aharonowitz, Y., Chakraborty, T. and Hain, T. **2011**. Universal stress proteins are important for oxidative and acid stress resistance and growth of *Listeria monocytogenes* EGD-e *in vitro* and *in vivo*. PloS one, 6(9): e24965.

Selvaraj, S., Sambandam, V., Sardar, D. and Anishetty, S. **2012**. *In silico* analysis of DosR regulon proteins of *Mycobacterium tuberculosis*. Gene, 506(1): 233-41.

Sen, A., Daubin, V., Abrouk, D., Gifford, I., Berry, A.M. and Normand, P. **2014**. Phylogeny of the class Actinobacteria revisited in the light of complete genomes. The orders 'Frankiales' and Micrococcales should be split into coherent entities: proposal of Frankiales ord. nov., Geodermatophilales ord. nov., Acidothermales ord. nov. and Nakamurellales ord. nov. Int J Syst Evol Microbiol, 64(Pt 11): 3821-32.

Senko, M.W., Remes, P.M., Canterbury, J.D., Mathur, R., Song, Q., Eliuk, S.M., Mullen, C., Earley, L., Hardman, M., Blethrow, J.D., Bui, H., Specht, A., Lange, O., Denisov, E., Makarov, A., Horning, S. and Zabrouskov, V. **2013**. Novel parallelized quadrupole/linear ion trap/Orbitrap tribrid mass spectrometer improving proteome coverage and peptide identification rates. Anal Chem, 85(24): 11710-4.

Seno, E.T., Bruton, C.J. and Chater, K.F. **1984**. The glycerol utilization operon of *Streptomyces coelicolor*: genetic mapping of gyl mutations and the analysis of cloned gylDNA. Mol Gen Genet, 193(1): 119-28.

Seno, E.T. and Chater, K.F. **1983**. Glycerol catabolic enzymes and their regulation in wild-type and mutant strains of *Streptomyces coelicolor* A3(2). J Gen Microbiol, 129(5): 1403-13.

Shepherd, M. and Poole, R.K. **2013**. Bacterial respiratory chains. In: Encyclopedia of Biophysics, Roberts, G.C.K. (Ed). Springer Berlin Heidelberg, pp: 172-7.

Sherazi, S.T.H., Arain, S., Mahesar, S.A., Bhanger, M.I. and Khaskheli, A.R. **2013**. Erucic acid evaluation in rapeseed and canola oil by Fourier transform-infrared spectroscopy. Eur J Lip Sci Technol, 115(5): 535-40.

Sherazi, S.T.H., Talpur, M.Y., Mahesar, S.A., Kandhro, A.A. and Arain, S. **2009**. Main fatty acid classes in vegetable oils by SB-ATR-Fourier transform infrared (FTIR) spectroscopy. Talanta, 80(2): 600-6.

Shields-Menard, S.A., Amirsadeghi, M., Sukhbaatar, B., Revellame, E., Hernandez, R., Donaldson, J.R. and French, W.T. **2015**. Lipid accumulation by *Rhodococcus rhodochrous* grown on glucose. J Ind Microbiol Biotechnol, 42(5): 693-9.

Shu, D., Chen, L., Wang, W., Yu, Z., Ren, C., Zhang, W., Yang, S., Lu, Y. and Jiang, W. **2009**. AfsQ1-Q2-sigQ is a pleiotropic but conditionally required signal transduction system for both secondary metabolism and morphological development in *Streptomyces coelicolor*. Appl Microbiol Biotechnol, 81(6): 1149-60.

Siebring, J. **2010**. The phosphofructokinases of *Streptomyces coelicolor*. University of Groningen.

Singh, R. and Reynolds, K.A. **2015**. Characterization of FabG and FabI of the *Streptomyces coelicolor* dissociated fatty acid synthase. Chembiochem, 16(4): 631-40.

Smiatek, J., Harishchandra, R.K., Rubner, O., Galla, H.J. and Heuer, A. **2012**. Properties of compatible solutes in aqueous solution. Biophys Chem, 160(1): 62-8.

Smirnov, A., Esnault, C., Prigent, M., Holland, I.B. and Virolle, M.J. **2015**. Phosphate homeostasis in conditions of phosphate proficiency and limitation in the wild type and the *phoP* mutant of *Streptomyces lividans*. PloS one, 10(5): e0126221.

Smith, C.P. and Chater, K.F. **1988**. Cloning and transcription analysis of the entire glycerol utilization (*gylABX*) operon of *Streptomyces coelicolor* A3(2) and identification of a closely associated transcription unit. Mol Gen Genet, 211(1): 129-37.

Smith, C.P. and Chater, K.F. **1988**. Structure and regulation of controlling sequences for the *Streptomyces coelicolor* glycerol operon. J Mol Biol, 204(3): 569-80.

Sola-Landa, A., Moura, R.S. and Martín, J.F. **2003**. The two-component PhoR-PhoP system controls both primary metabolism and secondary metabolite biosynthesis in *Streptomyces lividans*. Proc Nat Acad Sci, 100(10): 6133-8.

Sola-Landa, A., Rodríguez-García, A., Amin, R., Wohlleben, W. and Martín, J.F. **2013**. Competition between the GlnR and PhoP regulators for the *glnA* and *amtB* promoters in *Streptomyces coelicolor*. Nucleic Acids Res, 41(3): 1767-82.

Sola-Landa, A., Rodríguez-García, A., Apel, A.K. and Martín, J.F. **2008**. Target genes and structure of the direct repeats in the DNA-binding sequences of the response regulator PhoP in *Streptomyces coelicolor*. Nucleic Acids Res, 36(4): 1358-68.

Sola-Landa, A., Rodríguez-García, A., Franco-Domínguez, E. and Martín, J.F. **2005**. Binding of PhoP to promoters of phosphate-regulated genes in *Streptomyces coelicolor*: identification of PHO boxes. Mol Microbiol, 56.

Staunton, J. and Weissman, K.J. **2001**. Polyketide biosynthesis: a millennium review. Nat Prod Rep, 18(4): 380-416.

StrepDB - The Streptomyces annotation server. Accessed on June 2nd, **2017**.Availabe on: http:// http://strepdb.streptomyces.org.uk

Strieker, M., Tanović, A. and Marahiel, M.A. **2010**. Nonribosomal peptide synthetases: structures and dynamics. Curr Opin Struct Biol, 20(2): 234-40.

Takahashi-Iniguez, T., Cruz-Rabadan, S., Burciaga-Cifuentes, L.M. and Flores, M.E. **2014**. Molecular cloning, purification, and biochemical characterization of recombinant isocitrate dehydrogenase from *Streptomyces coelicolor* M145. Biosci Biotechnol Biochem, 78(9): 1490-4.

Takano, E. **2006**. Gamma-butyrolactones: *Streptomyces* signalling molecules regulating antibiotic production and differentiation. Curr Opin Microbiol, 9(3): 287-94.

Takano, E., Chakraburtty, R., Nihira, T., Yamada, Y. and Bibb, M.J. **2001**. A complex role for the gamma-butyrolactone SCB1 in regulating antibiotic production in *Streptomyces coelicolor* A3(2). Mol Microbiol, 41(5): 1015-28.

Takano, E., Gramajo, H.C., Strauch, E., Andres, N., White, J. and Bibb, M.J. **1992**. Transcriptional regulation of the *redD* transcriptional activator gene accounts for growth-phase-dependent production of the antibiotic undecylprodigiosin in *Streptomyces coelicolor* A3(2). Mol Microbiol, 6(19): 2797-804.

Takano, E., Kinoshita, H., Mersinias, V., Bucca, G., Hotchkiss, G., Nihira, T., Smith, C.P., Bibb, M., Wohlleben, W. and Chater, K. **2005**. A bacterial hormone (the SCB1) directly controls the expression of a pathway-specific regulatory gene in the cryptic type I polyketide biosynthetic gene cluster of *Streptomyces coelicolor*. Mol Microbiol, 56(2): 465-79.

Tanne, C., Golovina, E.A., Hoekstra, F.A., Meffert, A. and Galinski, E.A. **2014**. Glass-forming property of hydroxyectoine is the cause of its superior function as a desiccation protectant. Front Microbiol, 5: 150.

Thevenieau, F., Sambou, S., Virolle, M.J. and Dulermo, T. **2014**. Triacylglycerol-based lipid composition. AVRIL, Université Paris-Sud. United States of America Patent 203219.

Thevenieau, F., Virolle, M.J., Dulermo, T. and Vergne, M. **2014**. Method for the production of lipids by microorganisms and use of said lipids. European Patent 202778.

Thomas, L., Hodgson, D.A., Wentzel, A., Nieselt, K., Ellingsen, T.E., Moore, J., Morrissey, E.R., Legaie, R., Wohlleben, W., Rodriguez-Garcia, A., Martin, J.F., Burroughs, N.J., Wellington, E.M. and Smith, M.C. **2012**. Metabolic switches and adaptations deduced from the proteomes of *Streptomyces coelicolor* wild type and *phoP* mutant grown in batch culture. Mol Cell Proteomics, 11(2): M111013797.

Thompson, A., Schafer, J., Kuhn, K., Kienle, S., Schwarz, J., Schmidt, G., Neumann, T., Johnstone, R., Mohammed, A.K. and Hamon, C. **2003**. Tandem mass tags: a novel quantification strategy for comparative analysis of complex protein mixtures by MS/MS. Analyt Chem, 75(8): 1895-904.

Tierrafría, V.H., Cuauhtemoc, L.C., Nidia, M.C., Alba, R.R., Sara, C.L., Esteban, M., Romina, R.S., Ruiz-Villafan, B. and Sanchez, S. **2016**. Deletion of the hypothetical protein SCO2127 of *Streptomyces coelicolor* allowed identification of a new regulator of actinorhodin production. Appl Microbiol Biotechnol, 100(21): 9229-37.

Tiffert, Y., Supra, P., Wurm, R., Wohlleben, W., Wagner, R. and Reuther, J. **2008**. The *Streptomyces coelicolor* GlnR regulon: identification of new GlnR targets and evidence for a central role of GlnR in nitrogen metabolism in actinomycetes. Mol Microbiol, 67(4): 861-80.

Tschowri, N., Schumacher, M.A., Schlimpert, S., Chinnam, N.B., Findlay, K.C., Brennan, R.G. and Buttner, M.J. **2014**. Tetrameric c-di-GMP mediates effective transcription factor dimerization to control *Streptomyces* development. Cell, 158(5): 1136-47.

Tunca, S., Barreiro, C., Coque, J.J. and Martin, J.F. **2009**. Two overlapping antiparallel genes encoding the iron regulator DmdR1 and the Adm proteins control siderophore and antibiotic biosynthesis in *Streptomyces coelicolor* A3(2). FEBS J, 276(17): 4814-27.

Tunca, S., Barreiro, C., Sola-Landa, A., Coque, J.J. and Martin, J.F. **2007**. Transcriptional regulation of the desferrioxamine gene cluster of *Streptomyces coelicolor* is mediated by binding of DmdR1 to an iron box in the promoter of the *desA* gene. FEBS J, 274(4): 1110-1122.

Uguru, G.C., Stephens, K.E., Stead, J.A., Towle, J.E., Baumberg, S. and McDowall, K.J. **2005**. Transcriptional activation of the pathway-specific regulator of the actinorhodin biosynthetic genes in *Streptomyces coelicolor*. Mol Microbiol, 58(1): 131-50.

Umeyama, T., Lee, P.C. and Horinouchi, S. **2002**. Protein serine/threonine kinases in signal transduction for secondary metabolism and morphogenesis in *Streptomyces*. Appl Microbiol Biotechnol, 59(4-5): 419-25.

Urem, M., Swiatek-Polatynska, M.A., Rigali, S. and van Wezel, G.P. **2016**. Intertwining nutrient-sensory networks and the control of antibiotic production in *Streptomyces*. Mol Microbiol, 102(2): 183-95.

Valot, B., Langella, O., Nano, E. and Zivy, M. **2011**. MassChroQ: A versatile tool for mass spectrometry quantification. Proteomics, 11(17): 3572-7.

Van Dien, S.J. and Keasling, J.D. **1999**. Effect of polyphosphate metabolism on the *Escherichia coli* phosphate-starvation response. Biotechnol Prog, 15(4): 587-93.

van Keulen, G., Alderson, J., White, J. and Sawers, R.G. **2005**. Nitrate respiration in the actinomycete *Streptomyces coelicolor*. Biochem Soc Trans, 33(Pt 1): 210-2.

van Keulen, G. and Dyson, P.J. **2014**. Production of specialized metabolites by *Streptomyces coelicolor* A3(2). Adv Appl Microbiol, 89: 217-66.

van Wezel, G.P., Konig, M., Mahr, K., Nothaft, H., Thomae, A.W., Bibb, M. and Titgemeyer, F. **2007**. A new piece of an old jigsaw: glucose kinase is activated posttranslationally in a glucose transport-dependent manner in *Streptomyces coelicolor* A3(2). J Mol Microbiol Biotechnol, 12(1-2): 67-74.

van Wezel, G.P., Krabben, P., Traag, B.A., Keijser, B.J.F., Kerste, R., Vijgenboom, E., Heijnen, J.J. and Kraal, B. **2006**. Unlocking *Streptomyces* spp. for use as sustainable industrial production platforms by morphological engineering. Appl Environ Microbiol, 72(8): 5283-8.

van Wezel, G.P., Mahr, K., Konig, M., Traag, B.A., Pimentel-Schmitt, E.F., Willimek, A. and Titgemeyer, F. **2005**. GlcP constitutes the major glucose uptake system of *Streptomyces coelicolor* A3(2). Mol Microbiol, 55(2): 624-36.

van Wezel, G.P. and McDowall, K.J. **2011**. The regulation of the secondary metabolism of *Streptomyces*: new links and experimental advances. Nat Prod Rep, 28(7): 1311-33.

Viollier, P.H., Minas, W., Dale, G.E., Folcher, M. and Thompson, C.J. **2001**. Role of acid metabolism in *Streptomyces coelicolor* morphological differentiation and antibiotic biosynthesis. J Bacteriol, 183(10): 3184-92.

Viollier, P.H., Nguyen, K.T., Minas, W., Folcher, M., Dale, G.E. and Thompson, C.J. **2001**. Roles of aconitase in growth, metabolism, and morphological differentiation of *Streptomyces coelicolor*. J Bacteriol, 183(10): 3193-203.

Voelker, F. and Altaba, S. **2001**. Nitrogen source governs the patterns of growth and pristinamycin production in *Streptomyces pristinaespiralis*. Microbiol, 147(Pt 9): 2447-59.

Wakil, S.J., Stoops, J.K. and Joshi, V.C. **1983**. Fatty acid synthesis and its regulation. Annu Rev Biochem, 52: 537-79.

Walther, T.C. and Mann, M. **2010**. Mass spectrometry–based proteomics in cell biology. J Cell Biol, 190(4): 491-500.

Wang, C., Ge, H., Dong, H., Zhu, C., Li, Y., Zheng, J. and Cen, P. **2007**. A novel pair of two-component signal transduction system *ecrE1*/*ecrE2* regulating antibiotic biosynthesis in *Streptomyces coelicolor*. Biologia, 62(5): 511-6.

Wang, L., Tian, X., Wang, J., Yang, H., Fan, K., Xu, G., Yang, K. and Tan, H. **2009**. Autoregulation of antibiotic biosynthesis by binding of the end product to an atypical response regulator. Proc Nat Acad Sci USA, 106(21): 8617-22.

Wang, R., Mast, Y., Wang, J., Zhang, W., Zhao, G., Wohlleben, W., Lu, Y. and Jiang, W. **2013**. Identification of two-component system AfsQ1/Q2 regulon and its cross-regulation with GlnR in *Streptomyces coelicolor*. Mol Microbiol, 87(1): 30-48.

Wasylenko, T.M., Ahn, W.S. and Stephanopoulos, G. **2015**. The oxidative pentose phosphate pathway is the primary source of NADPH for lipid overproduction from glucose in *Yarrowia lipolytica*. Met Eng, 30: 27-39.

Weber, T., Blin, K., Duddela, S., Krug, D., Kim, H.U., Bruccoleri, R., Lee, S.Y., Fischbach, M.A., Müller, R., Wohlleben, W., Breitling, R., Takano, E. and Medema, M.H. **2015**. AntiSMASH 3.0 - A comprehensive resource for the genome mining of biosynthetic gene clusters. Nucleic Acids Res, 43: W237-43.

Weissman, K.J. **2009**. Introduction to polyketide biosynthesis. In: Methods in Enzymology, Academic Press: London, pp: 3-16.

Wentzel, A., Bruheim, P., Overby, A., Jakobsen, O.M., Sletta, H., Omara, W.A., Hodgson, D.A. and Ellingsen, T.E. **2012**. Optimized submerged batch fermentation strategy for systems scale studies of metabolic switching in *Streptomyces coelicolor* A3(2). BMC Syst Biol, 6: 59.

Wisniewski, J.R. and Mann, M. **2012**. Consecutive proteolytic digestion in an enzyme reactor increases depth of proteomic and phosphoproteomic analysis. Analyt Chem, 84(6): 2631-7.

Wither, M.J., Hansen, K.C. and Reisz, J.A. **2016**. Mass spectrometry-based bottom-up proteomics: Sample preparation, LC-MS/MS analysis, and database query strategies. Curr Protoc Prot Sci, 86.

Wolanski, M., Donczew, R., Kois-Ostrowska, A., Masiewicz, P., Jakimowicz, D. and Zakrzewska-Czerwinska, J. **2011**. The level of AdpA directly affects expression of developmental genes in *Streptomyces coelicolor*. J Bacteriol, 193(22): 6358-65.

Wong, J.W.H., Sullivan, M.J. and Cagney, G. **2008**. Computational methods for the comparative quantification of proteins in label-free LCn-MS experiments. Brief Bioinform, 9(2): 156-65.

Woodruff, H.B. **1981**. A soil microbiologist's odyssey. Annu Rev Microbiol, 35: 1-28.

Wray, L.V., Atkinson, M.R. and Fisher, S.H. **1991**. Identification and cloning of the *glnR* locus, which is required for transcription of the *glnA* gene in *Streptomyces coelicolor* A3(2). J Bacteriol, 173(22): 7351-60.

Wu, X., Edwards, N. and Tseng, C.W. **2006**. Peptide identification via tandem mass spectrometry. In: Advances in computers, Chau-Wen, T. (Ed). Elsevier, pp: 253-78.

Xu, D., Seghezzi, N., Esnault, C. and Virolle, M.J. **2010**. Repression of antibiotic production and sporulation in *Streptomyces coelicolor* by overexpression of a TetR family transcriptional regulator. Appl Environ Microbiol, 76(23): 7741-53.

Xu, Y., Liao, C.H., Yao, L.L., Ye, X. and Ye, B.C. **2016**. GlnR and PhoP directly regulate the transcription of genes encoding starch-degrading, amylolytic enzymes in *Saccharopolyspora erythraea*. Appl Environ Microbiol.

Xu, Z., Wang, Y., Chater, K.F., Ou, H.Y., Xu, H.H., Deng, Z. and Tao, M. **2017**. Large-scale transposition mutagenesis of *Streptomyces coelicolor* identifies hundreds of genes influencing antibiotic biosynthesis. Appl Environ Microbiol, 83(6).

Yagüe, P., López-García, M.T., Rioseras, B., Sánchez, J. and Manteca, Á. **2013**. Pre-sporulation stages of *Streptomyces* differentiation: state-of-the-art and future perspectives. FEMS Microbiol Lett, 342(2): 79-88.

Yague, P., Willemse, J., Koning, R.I., Rioseras, B., Lopez-Garcia, M.T., Gonzalez-Quinonez, N., Lopez-Iglesias, C., Shliaha, P.V., Rogowska-Wrzesinska, A., Koster, A.J., Jensen, O.N., van Wezel, G.P. and Manteca, A. **2016**. Subcompartmentalization by cross-membranes during early growth of *Streptomyces* hyphae. Nat Commun, 7: 12467.

Yan, L., Zhang, Q., Virolle, M.J. and Xu, D. **2017**. In conditions of over-expression, WblI, a WhiB-like transcriptional regulator, has a positive impact on the weak antibiotic production of *Streptomyces lividans* TK24. PloS one, 12(3): e0174781.

Yang, Y.H., Kim, J.N., Song, E., Kim, E., Oh, M.K. and Kim, B.G. **2008**. Finding new pathway-specific regulators by clustering method using threshold standard deviation based on DNA chip data of *Streptomyces coelicolor*. Appl Microbiol Biotechnol, 80(4): 709-17.

Yang, Y.H., Song, E., Kim, E.J., Lee, K., Kim, W.S., Park, S.S., Hahn, J.S. and Kim, B.G. **2009**. NdgR, an IclR-like regulator involved in amino-acid-dependent growth, quorum sensing, and antibiotic production in *Streptomyces coelicolor*. Appl Microbiol Biotechnol, 82(3): 501-11.

Yang, Y.H., Song, E., Lee, B.R., Kim, E.J., Park, S.H., Kim, Y.G., Lee, C.S. and Kim, B.G. **2010**. Rapid functional screening of *Streptomyces coelicolor* regulators by use of a pH indicator and application to the MarR-like regulator AbsC. Appl Environ Microbiol, 76(11): 3645-56.

Yates, J.R. **2004**. Mass spectral analysis in proteomics. Annu Rev Biophys Biomol Str, 33: 297-316.

Yates, J.R., Ruse, C.I. and Nakorchevsky, A. **2009**. Proteomics by mass spectrometry: approaches, advances, and applications. Annu Rev Biomed Eng, 11: 49-79.

Yeo, M. and Chater, K. **2005**. The interplay of glycogen metabolism and differentiation provides an insight into the developmental biology of *Streptomyces coelicolor*. Microbiol, 151(Pt 3): 855-61.

Yu, T.W., Shen, Y., McDaniel, R., Floss, H.G., Khosla, C., Hopwood, D.A. and Moore, B.S. **1998**. Engineered biosynthesis of novel polyketides from *Streptomyces* spore pigment polyketide synthases. J Am Chem Soc, 120(31): 7749-59.

Yu, Z., Zhu, H., Dang, F., Zhang, W., Qin, Z., Yang, S., Tan, H., Lu, Y. and Jiang, W. **2012**. Differential regulation of antibiotic biosynthesis by DraR-K, a novel two-component system in *Streptomyces coelicolor*. Mol Microbiol, 85(3): 535-56.

Zhang, H., Boghigian, B.A. and Pfeifer, B.A. **2010**. Investigating the role of native propionyl-CoA and methylmalonyl-CoA metabolism on heterologous polyketide production in *Escherichia coli*. Biotechnol Bioeng, 105(3): 567-73.

Zhang, H., Ishige, K. and Kornberg, A. **2002**. A polyphosphate kinase (PPK2) widely conserved in bacteria. Proc Nat Acad Sci USA, 99(26): 16678-83.

Zhang, L., Li, W.C., Zhao, C.H., Chater, K.F. and Tao, M.F. **2007**. NsdB, a TPR-like-domain-containing protein negatively affecting production of antibiotics in *Streptomyces coelicolor* A3 (2). Acta Microbiol Sin, 47(5): 849-54.

Zhang, Y., Fonslow, B.R., Shan, B., Baek, M.C. and Yates, J.R. **2013**. Protein analysis by shotgun/bottom-up proteomics. Chem Rev, 113(4): 2343-94.

Zhou, M., Boekhorst, J., Francke, C. and Siezen, R.J. **2008**. LocateP: genome-scale subcellular-location predictor for bacterial proteins. BMC Bioinformatics, 9: 173.

Zhu, Q. and Jackson, E.N. **2015**. Metabolic engineering of *Yarrowia lipolytica* for industrial applications. Curr Opin Biotechnol, 36: 65-72.

ÉCOLE DOCTORALE
Agriculture, alimentation, biologie, environnement, santé (ABIES)

Titre : Étude comparative du protéome de *S. coelicolor* M145 et *S. lividans* TK24, deux souches phylogénétiquement proches ayant des capacités très différentes à accumuler des TAG et à produire des antibiotiques.

Mots clés : *Streptomyces*, antibiotiques, triacylglycérol (TAG), métabolisme primaire et secondaire, protéomique, biologie de systèmes.

Résumé : Les *Streptomyces* sont des bactéries filamenteuses du sol à Gram +. Elles sont connues pour leur capacité à produire des métabolites secondaires utiles en médecine et en agriculture. *S. coelicolor* et *S. lividans* sont des souches modèles phylogénétiquement proches. Elles ont cependant des capacités contrastées à accumuler des lipides de réserve de la famille des triacylglycérol (TAG) et produire des métabolites secondaires alors qu'elles possèdent des voies de biosynthèse similaires pour ces deux types de molécules.

En présence de glucose, *S. coelicolor* produit des niveaux élevés de métabolites secondaires spécifiques et son contenu en TAG est faible alors que c'est le contraire chez *S. lividans*. En revanche, en présence de glycérol, les deux souches accumulent une quantité de TAG similaire mais *S. coelicolor* produit aussi des métabolites secondaires.

Le but de la présente thèse était de déterminer les caractéristiques métaboliques différentielles qui sous-tendent les différentes capacités biosynthétiques de ces deux souches modèles. Pour ce faire, une analyse protéomique comparative sans marquage des souches cultivées en milieu R2YE liquide ou solide en présence de glucose ou de glycérol comme principales sources de carbone a été réalisée en utilisant la technique de chromatographie liquide couplée à de la Spectrométrie de Masse en tandem (LC-MS / MS). Au total, 2024 et 4372 protéines ont été identifiées à partir des cultures liquides et solides, représentant 24% et 50% du protéome théorique. Les études en liquide ont révélé que le métabolisme de *S. lividans* était principalement glycolytique alors que le métabolisme de *S. coelicolor* était principalement oxydatif. Elles ont également indiqué que ces caractéristiques pourraient être liées au catabolisme préférentiel des acides aminés par rapport au glucose chez *S. coelicolor* par rapport à *S. lividans*. De plus, cette thèse constitue la première analyse protéomique du métabolisme de ces deux souches modèles en présence de glycérol.

Title : Comparative study of the proteome of *S. coelicolor* M145 and *S. lividans* TK24, two phylogenetically closely related strains with very different abilities to accumulate TAG and produce antibiotics.

Keywords : *Streptomyces*, antibiotics, triacylglycerol (TAG), primary and secondary metabolism, proteomics, systems biology.

Abstract : *Streptomyces* are filamentous Gram+ soil bacteria well known for their ability to produce secondary metabolites useful in medicine and agriculture. *S. coelicolor* and *S. lividans* are phylogenetically closely-related model strains but they have contrasted abilities to accumulate storage lipids of the TriAcylGlycerol (TAG) family and to produce secondary metabolites whereas they possess similar pathways for the biosynthesis of these molecules. In the presence of glucose, *S. coelicolor* produces high levels of specific secondary metabolites and its TAG content is low whereas it is the opposite for *S. lividans*. In contrast, in the presence of glycerol, the two strains accumulated similar amount of TAG but *S. coelicolor* still produces secondary metabolites. The aim of the present thesis was to determine the differential metabolic features supporting such different biosynthetic abilities.

To do so, a comparative label-free shotgun proteomic analysis of the strains grown in liquid or solid R2YE media with glucose or glycerol as main carbon sources was carried out using Liquid chromatography−tandem mass spectrometry (LC−MS/MS). A total of 2024 and 4372 proteins were identified in liquid and solid cultures, representing 24% and 50% of the theoretical proteome, respectively.

These studies revealed that *S. lividans* metabolism was mainly glycolytic whereas *S. coelicolor* metabolism was mainly oxidative. They also suggested that these features might be related to the preferential catabolism of amino acids over glucose of *S. coelicolor* compared to *S. lividans*. Furthermore, this thesis constituted the first proteomic analysis of the metabolism of these two model strains in the presence of glycerol.

Université Paris-Saclay
Espace Technologique / Immeuble Discovery
Route de l'Orme aux Merisiers RD 128 / 91190 Saint-Aubin, France